Last Interglacial Iberian Neandertals as fisher-hunter-gatherers

J. Zilhão[1,2,3]*, D. E. Angelucci[4], M. Araújo Igreja[3,5,6], L. J. Arnold[7], E. Badal[8], P. Callapez[9], J. L. Cardoso[3,10], F. d'Errico[11,12], J. Daura[2,3], M. Demuro[7], M. Deschamps[3,13], C. Dupont[14], S. Gabriel[3,5,6], D. L. Hoffmann[15,16], P. Legoinha[17], H. Matias[3], A. M. Monge Soares[18], M. Nabais[3,19], P. Portela[18], A. Queffelec[11], F. Rodrigues[3], P. Souto[20]

[1]Institució Catalana de Recerca i Estudis Avançats (ICREA), Passeig Lluís Companys 23, 08010 Barcelona, Spain.

[2]Universitat de Barcelona, Departament d'Història i Arqueologia, Facultat de Geografia i Història, c/Montalegre 6, 08001 Barcelona, Spain.

[3]Centro de Arqueologia da Universidade de Lisboa (UNIARQ), Faculdade de Letras de Lisboa, Universidade de Lisboa, Alameda da Universidade, 1600-214 Lisboa, Portugal.

[4]Università degli Studi di Trento, Dipartimento di Lettere e Filosofia, via Tommaso Gar 14, 38122 Trento, Italy.

[5]Laboratório de Arqueociências (LARC), Direcção Geral do Património Cultural, Calçada do Mirante à Ajuda 10A, 1300-418 Lisboa, Portugal.

[6]Environmental Archaeology Group, Research Center in Biodiversity and Genetic Resources (ENVARCH, CIBIO/InBIO), University of Oporto, Rua Padre Armando Quintas 7, 4485-661 Vairão, Portugal.

[7]Environment Institute and Institute for Photonics and Advanced Sensing (IPAS), Department of Earth Sciences, School of Physical Sciences, University of Adelaide, North Terrace Campus, Adelaide, South Australia 5005, Australia.

[8]Universitat de València, Departament de Prehistòria, Arqueologia i Història Antiga, Av. Blasco Ibañez 28, 46010 València, Spain.

[9]Departamento de Ciências da Terra (CITEUC), Faculdade de Ciências e Tecnologia, Universidade de Coimbra, Rua Sílvio Lima, 3030-790 Coimbra, Portugal.

[10]Universidade Aberta, Rua da Escola Politécnica 147, 1269-001 Lisboa, Portugal.

[11]CNRS (UMR 5199–PACEA), Université de Bordeaux, Bât. B18, Allée Geoffroy Saint Hilaire, CS 50023, 33615 Pessac Cedex, France.

[12]SFF Centre for Early Sapiens Behaviour (SapienCE), Sydnesplassen 12/13, 4 Etage, Postboks 7805, 5020 University of Bergen, Bergen, Norway.

[13]Centre National de la Recherche Scientifique, UMR 5608–TRACES, Université Toulouse Jean Jaurès, Maison de la Recherche, 5 allées Antonio Machado, 31058 Toulouse cedex 9, France.

[14]Centre National de la Recherche Scientifique, UMR 6566–CReAAH, Laboratoire Archéosciences, Bât. 24-25, Université de Rennes 1-Campus de Beaulieu, 35042 Rennes Cedex, France.

[15]Max Planck Institute for Evolutionary Anthropology, Deutscher Platz 6, 04103 Leipzig, Germany.

[16]Geoscience Center, Isotope Geology Division, University of Göttingen, Goldschmidtstrasse 3, 37077 Göttingen, Germany.

[17]Geobiotec, Departamento de Ciências da Terra, Faculdade de Ciências e Tecnologia, Universidade Nova de Lisboa, 2829-516 Caparica, Portugal.

[18]Centro de Ciências e Tecnologias Nucleares (C2TN), Instituto Superior Técnico, Universidade de Lisboa, Estrada Nacional 10, 2695-066 Bobadela, Portugal.

[19]Institute of Archaeology, University College London, 31-34 Gordon Square, London WC1H 0PY, UK.

[20]Sociedade Torrejana de Espeleologia e Arqueologia, Quinta da Lezíria, 2350-510, Torres Novas, Portugal.

Abstract

Marine food–reliant subsistence systems such as those in the African Middle Stone Age (MSA) were not thought to exist in Europe until the much later Mesolithic. Whether this apparent lag reflects taphonomic biases or behavioral distinctions between archaic and modern humans remains much debated. Figueira Brava cave, in the Arrábida range (Portugal), provides an exceptionally well preserved record of Neandertal coastal resource exploitation on a comparable scale to the MSA and dated to ~86 to 106 thousand years ago. The breadth of the subsistence base—pine nuts, marine invertebrates, fish, marine birds and mammals, tortoises, waterfowl, and hoofed game—exceeds that of regional early Holocene sites. Fisher-hunter-gatherer economies are not the preserve of anatomically modern people; by the Last Interglacial, they were in place across the Old World in the appropriate settings.

Introduction

The major innovations of the Middle Stone Age (MSA) of southern Africa are widely seen as reflecting the emergence of cognitive and behavioral modernity. A feedback loop between the consumption of marine foods and the development of the brain might underpin this process (1,–3). Reliant on dense and predictable resources, the "coastal adaptations" so engendered would represent a late Middle to early Upper Pleistocene "broad-spectrum revolution" (4, 5) that triggered demographic growth, social complexification, and, eventually, the out-of-Africa expansion of modern humans (6, 7). The strong prosocial behavior arising out of such adaptations would have provided the competitive edge that has been postulated to explain the disappearance of Neandertals and other anatomically archaic Eurasian humans (8, 9). It has been proposed that shell middens, defined as shell-supported sediment where shells interfinger with other shells and the matrix fills the voids, are the archeological proxy for such South African coastal adaptations; by contrast—and reflecting a genuine and critical difference in subsistence and behavior— shellfish remains have been found at low density, if they occur at all, in Last Interglacial and later Middle Paleolithic sites of Eurasia (8, 9). An alternative view is that the difference between these two regional records is of degree rather than kind and affected by taphonomic bias (10, 11); therefore, humans might well have foraged for marine foods for much longer and across their entire range, as suggested by skeletal evidence (12). In the Mediterranean basin, bivalve shell was used for functional purposes (13,–15), but low productivity may explain why shellfish consumption did not result in the formation of Middle Paleolithic shell middens; such accumulations are rare even in the regional Holocene, when the isotope evidence corroborates the minor role played by marine foods in hunter-gatherer subsistence (16, 17). Under this productivity explanation, one would expect things to be different in the marine resource‑rich shores of the North Atlantic, as is indeed suggested by the documented consumption of shellfish at a string of Last Interglacial sites in Morocco (18). However,

modern humans are assumed to be behind the formation of the Maghreb's record and so it is the absence of Middle Paleolithic shell middens in the Atlantic coasts of Europe inhabited by Neandertals that is claimed to be of special significance (8). Because of transport costs, shellfish consumption is tightly tethered to the point of acquisition (19, 20). Thus, when the sea level was lower, as it was during most of the Pleistocene, one can expect a marine mollusk‑rich archeological record to be found only where the adjacent continental platform is very steep and extant and past shorelines are not separated by a large stretch of Holocene-submerged land. For peak interglacial periods, when the sea level was as high or higher than today, archeological site preservation necessitates that the original record formed sufficiently above the shore or in particularly shielded environments offering protection against marine erosion. In South Africa, sustained tectonic uplift created the Cape Fold Bel's abrupt coastline, which features caves and rock shelters located well above the present-day tidal range. This geomorphology has favored the preservation of archeological deposits that bear witness to the Last Interglacial exploitation of the seashore below. Such preservation conditions are generally not replicated along Atlantic Europe's coastlines. In Scandinavia and Britain, Last Interglacial shell middens would have been wiped out by the ice caps of subsequent glacial maxima, whereas sea-level rise would have submerged any deposits formed off of the French coast, where the continental shelf is >200 km wide. Along the Cantabrian coast, the shelf is much narrower and, accordingly, marine food remains are found in Middle and Upper Paleolithic sites; none, however, feature accumulations in the shell-midden scale characteristic of the region's later Mesolithic (21). Along the west coast of Portugal, the continental platform is generally wide. However, during low-sea-level periods, a fjord-like landscape formed along the marine canyon off the ~20-km coastline of Arrábida, a mountain range 30 km south of Lisbon. Here, the submerged and extant shorelines are short distances apart, the karst setting provides for erosion-protected accumulation contexts, and coastal upwelling and large tidal amplitudes make for a highly productive littoral where resources were intensively harvested in the Mesolithic, as documented by the nearby shell middens of the Sado estuary (22). Exclusively in Europe, it is along this coastline that sites containing Last Interglacial shell middens stand a good chance of preservation. Gruta da Figueira Brava (38° 28'14''N, 8°59'10''W; WGS84 datum), a cave first explored in the 1980s and the focus of our 2010 to 2013 archeological excavations, is one such site (23) (see the supplementary materials and methods and figs. S1 to S7).

Materials and Methods

Area C, directly accessible through Entrance 1, was the target of the 1986 to 1989 paleontological investigations. Our 2010 to 2013 work concerned Entrance 3 and Area F, which can be accessed from Area C to Areas D and E through narrows of difficult speleological negotiation. In Area F, the upper part of the sedimentary fill was largely unconsolidated and amenable to normal, trowel-aided excavation but the lower part was heavily cemented and had to be excavated with power tools, as was also the case in the Sondagem exterior (SEx) trench opened in Entrance 3. Here, investigation of the deposit was

complemented by soil micromorphological analysis of representative samples spanning the complete stratigraphic sequence. Finds were manually piece plotted against site grid and site datum. The sediment was dry sieved on-site and the residue entirely saved for subsequent wet sieving and floatation. For the sediments containing the remains of phases FB2 and FB3, the sorting of fish bones from the sieved or floated sediment has yet to be carried out; therefore, fish counts are provided for FB4 only. Following established practice in the archeology of Portuguese Mesolithic shell middens, our weight/volume shell density parameter derives from bulk samples of unconsolidated sediment. Radiocarbon dating failed because the age of the samples was beyond the method's limit of applicability. The deposit's Last Interglacial age is demonstrated by the uranium (U)-series and single-grain optically stimulated luminescence (OSL) results for stratigraphically associated speleothems and the sediments themselves. Additional details and an extensive description of the dating work are provided in the supplementary materials and methods. The analytical protocols used in the study of animal and plant remains and of stone tools followed standard practice and are also further explained in the supplementary materials.

Results

Site, stratigraphy, and dating

In its current configuration, Figueira Brava features three entrances (Figs. 1 to 3). The Pleistocene fill has been almost entirely eroded away in Entrance 1 and interior Areas A and B but is preserved under flowstone behind the sediment-cum-speleothem blockages separating Entrances 2 and 3 from, respectively, Areas C and F. The exposed terrace in front is the marine abrasion platform of Marine Isotope Stage (MIS) 5e. Originally, this now-unroofed area was part of the cave and remained sediment filled until after the Last Glacial Maximum (LGM). An erosion-scarred, archeologically rich breccia— the external exposure of the sedimentary fill found interiorly in Areas C to F—is found at the back of the terrace, where preservation is explained by heavy cementation and the protection offered by the extant overhang.
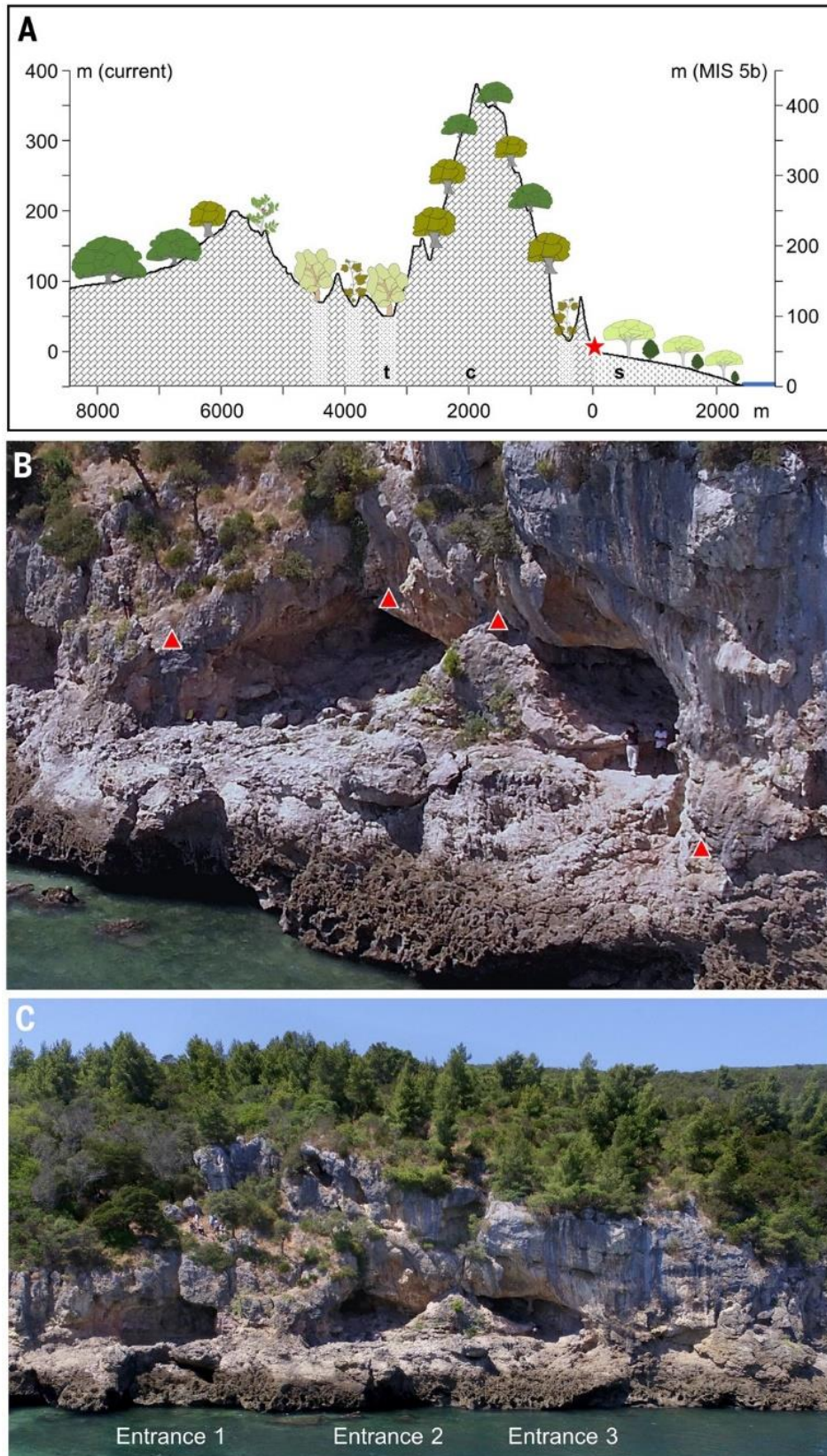
Fig. 1. Setting. (A) North–south transect of the Arrábida range through Figueira Brava, indicated by the red star; the plant cover is reconstructed from the site's paleobotanical data. t, thalweg soil with *Quercus deciduous* and *Vitis*; c, calcareous soil with evergreens, e.g., *Olea*, *Quercus*, and *Pistacia*; s, sandy soil with *P. pinea* and *Juniperus*. (B and C) Oblique (B) and frontal (C) drone views of the marine abrasion platform of MIS 5e and the original, now-unroofed cave space. Note the cemented remnant between Entrances 2 and 3, which preserves a complete stratigraphic sequence. The triangles mark breccia-capping flowstone and other speleothems sampled for U-series dating.

Fig. 2. Excavation. (A and B) Area F trench during the 2012 excavation of square T8 (A) and at the end of the last, 2013 field season (B). Stratigraphic depth reached in each square or quadrate is indicated; note the constrained space between capping flowstone and cave roof. (C and D) Entrance 3 during the initial, 2010 field season; (C) shows cutting of the rock-hard breccia for the extraction of a continuous column of blocks for soil micromorphology analysis spanning the sequence and (D) is a close-up view of Cut B, which samples the base of the UC complex, after extraction.
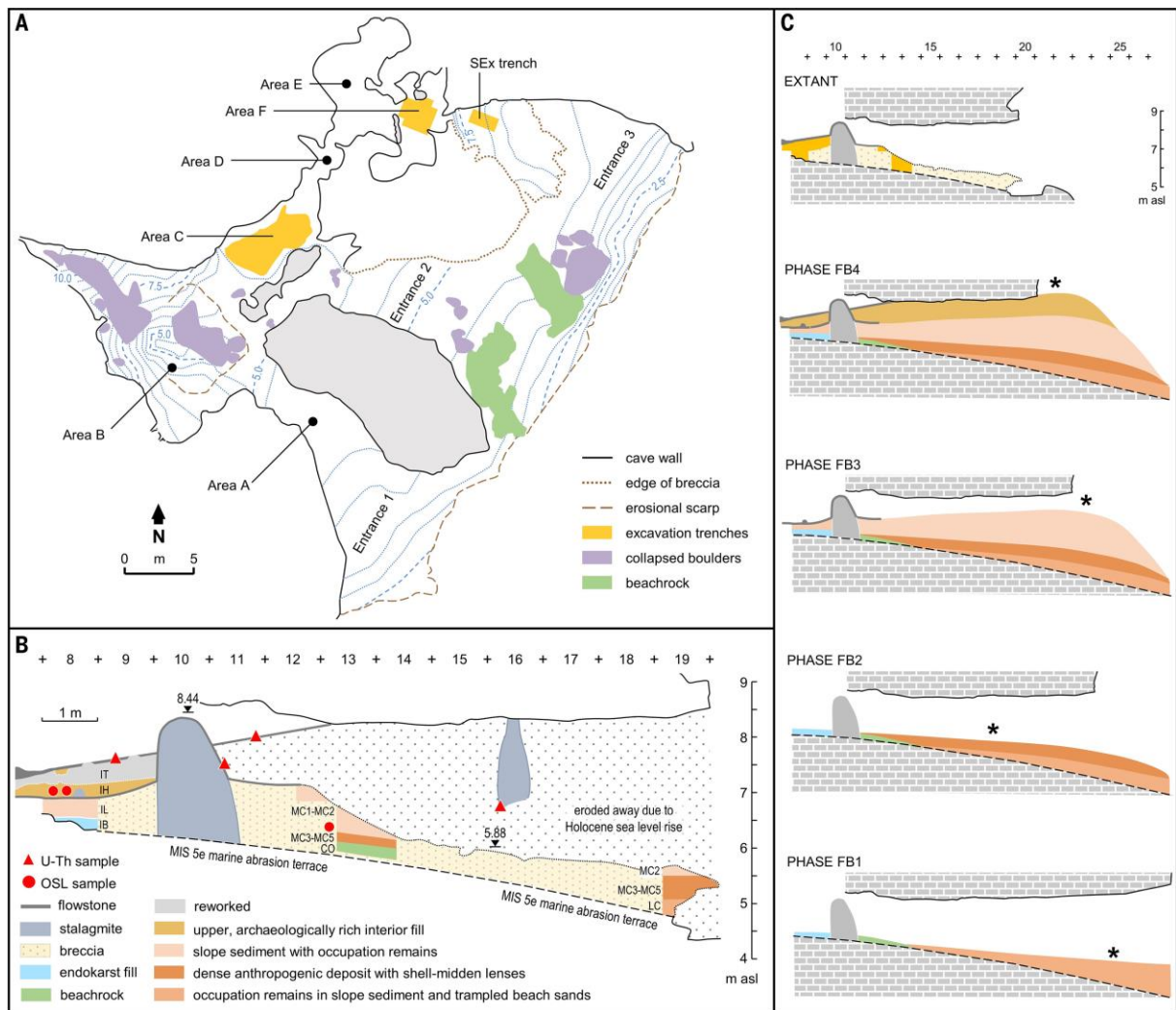
Fig. 3. Site. (A) Plan with position of trenches (Area C, 1986 to 1989 paleontological work; Areas F and SEx, 2010 to 2013 archeological excavation) and indication of main features. (B) Stratigraphic outline along the T > S axis of the 2010 to 2013 grid. (C) Schematic of the evolution of cave and fill through the different occupation phases; note the changing position of the trenches relative to the center of human occupation (indicated by the asterisks). Elevations are shown in meters above sea level (m asl).

We estimate that only ~100m³, or 5% of the original fill, remains. Figure 3 and Table 1 summarize the stratigraphic correlation between the different areas (see also supplementary text S1 and S2, figs. S8 to S21, and tables S1 to S17). The sequence, for which Bayesian modeling of the dating results offers a robust chronology and duration estimates (supplementary text S11 and Fig. 4), can be summarized as follows. Middle Pleistocene: Fine white sands filling depressions in the substrate (unit IB2) accumulated in an endokarst setting before excavation of the cave by the sea, overlain by flowstone (unit IB1). MIS 5e: Beachrock of the Last Interglacial highstand (complex CO). MIS 5c: Trampled, anthropized beach sands exposed by sea-level retreat (unit LC3), overlain by colluvium with aeolian inputs (units LC1 to LC2 and complex MC, Entrance 3; complex IL, Area F; layers 3-4, Area C), in turn capped by flowstone (unit MC0, Entrance 3; unit IL1, Area F). Dating constrains this sedimentary package to between 92.0 and 94.0 ka ago (for the upper limit of the range) and 104.0 and 106.0 ka ago (for the lower limit of the range) and suggests a duration of minimally two millennia for the subsequent interval of sedimentation

arrest and speleothem growth. MIS 5b: Colluvium with aeolian inputs that eventually filled up the remaining cave space (complex UC, Entrance 3; complex IH, Area F; layer 2, Area C). Dating and stratigraphic constraints put this package in the 86.0 to 90.0 ka ago interval. MIS 5a to MIS 2: Flowstone and associated speleothems (unit IH1, Area F; layer 1, Area C), which began to form no later than 76.9 ka ago, underwent continuous growth through MIS 4 to MIS 2 and, before the onset of post- LGM erosion, thoroughly sealed the deposit. Tardiglacial‑Holocene: Post-LGM flowstone and stalagmites (unit IT1, Area F; layer 0, Area C); in places, these speleothems are overlain by a thin, dark lens of fine, very recent organic sediments that also fill voids in their fabric (unit IT2, Area F); unit IT0 of Area F and layer 2a of Area C correspond to sediment reworked by subsurface burrowing and contain Holocene intrusions. The MIS 5b and 5c sediments lack foraminifera tests, corroborating that the sea remained distant (fig. S22 and table S19), and their paleobotanical content (Fig. 1, fig. S23, and table S20) reveals a local vegetation cover of Mediterranean type (with *Pinus pinea*, *Olea europaea*, deciduous and evergreen *Quercus* spp., *Ficus carica*, and *Vitis vinifera*). Thus, local environmental conditions remained broadly like present. The most obvious factor of landscape change was sea-level fluctuation; because of the strict soil requirements of the stone pine and the continuous presence of pinewoods in the site's catchment, we can nonetheless infer that, throughout, the cave's limestone terrain remained separated from the seashore by a dune belt (supplementary text S3 and S4).

AREA C (1986-89)	ENTRANCE 3 (2010-13) (b)	AREA F (2010-13) (c)	HUMAN OCCUPATION	U-Th AGE (ka)	CHRONO-STRATIGRAPHY
2a		IT0 (d)		–	Reworked
0	–	IT2 (e)	–	–	Holocene
		IT1		13.5-16.6	MIS 2 - MIS 5a
1	UC1	IH1		23.4-81.9	
2	UC2-UC6	IH2	Phase FB4	–	MIS 5b
		IH3		–	
		IH4		–	
		IH5		86.9-88.1	
		IH6		–	
		IH7		85.4-89.8	
		IH8		86.7-92.7	
3	MC0	IL1	Phase FB3	90.2-93.2	MIS 5c
	MC1-MC2	IL2		–	
		IL3		–	
	MC3-MC5	–	Phase FB2	–	
4	LC1-LC3		Phase FB1	–	
5	CO	IB1	–	103.5-152.3	MIS 5c - MIS 6
–	–	IB2 (f)		–	MIS 6 or older

Table 1. Stratigraphy. Correlation among the different areas of Figueira Brava, speleothem dating constraints, position of the sequence in the global Pleistocene record, and archeological phasing.
(a) Same color codes as in Fig. 3; the U-Th ages are bracketed by the upper and lower limits of the 95.4% probability intervals of the results obtained,
respectively, for the uppermost and lowermost sample or sub-sample measured in any given stratigraphic unit
(b) UC = Upper Complex; MC = Middle Complex; LC = Lower Complex; CO = Conglomerate
(c) IT = Interior Top; IH = Interior High; IL = Interior Low; IB = Interior Base
(d) The stone tool component of unit IT0 is entirely derived from underlying units IH2-IH3 and, therefore, relates to Phase FB4
(e) Unit IT2 (the surficial "black lens") overlies or abuts unit IT1; in profile views, however, it can be observed in apparently inferior position when filling-in voids that post-Pleistocene processes of differential erosion created at the interface between IT1 and IH1
(f) The archeological content of unit IB2 is intrusive; it relates to human occupation during Phase FB3
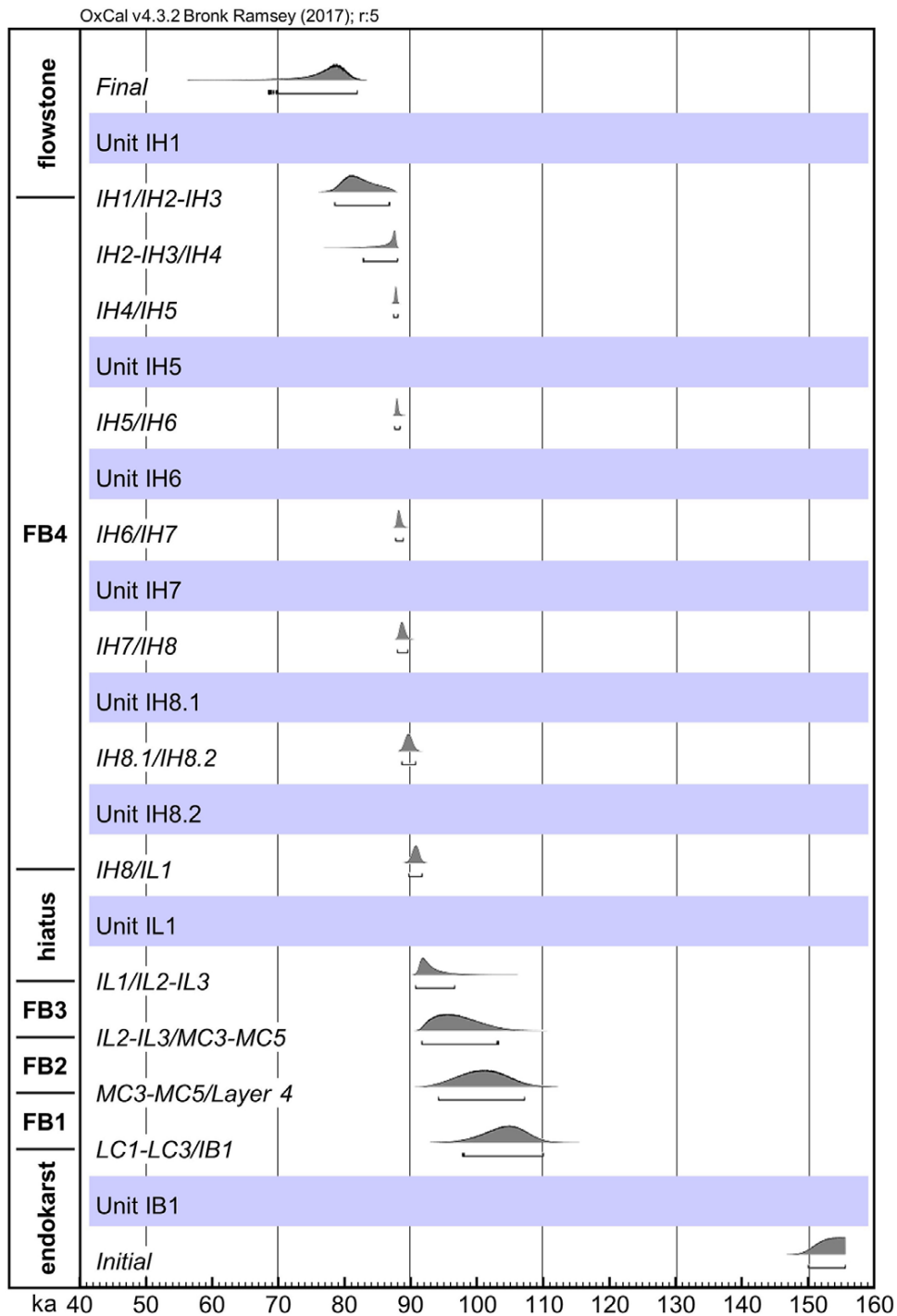
Fig. 4. Chronology. Age boundaries for the different stratigraphic units and human occupation phases calculated by Bayesian modeling of the U-series and OSL results.

Formation process and phases of human occupation

In a stratified cave or rock shelter site with a sequence that spans many millennia, human usage of the place may change as a result of environmentally driven factors (with attendant implications for settlement-subsistence systems) as much as local factors; overhang collapse and sedimentary buildup, for instance, may bring about substantial change to habitability and spatial configuration, whereas variation in accumulation dynamics may cause syndepositional or postdepositional displacements and

affect stratigraphic integrity. Thus, even when the different stratigraphic units exposed by excavation are in the same place relative to the site's extant configuration, they may well correspond to loci of behavior and accumulation that represent quite distinct emplacements relative to the time of occupation. To offset the impact of these factors, we adopted a "phase" framework whereby stratigraphic units formed under conditions that remained similar at all scales (local, regional, and environmental) are grouped for meaningful comparison of change through time (Fig. 3 and fig. S18). PhasesFB1 toFB3 fall within MIS 5c. Dating constraints imply a duration of ~12 ka within the very long Greenland Interstadial (GI) 23 warm period; the three sedimentary packages are of comparable thickness and there is no reason to think that they do not represent broadly similar temporal intervals of about four millennia each. Such is also the span indicated by the much tighter chronological control available for the MIS 5b deposit containing the FB4 archeological remains. Although a shorter duration fully within the 2500 years of GI 22 cannot be excluded, the current arctic distribution of bird (the great auk, *Pinguinus impennis*) and mammal (the ringed seal, *Pusa hispida*) taxa represented in the IH complex of Area F and in Area C (23) (fig. S33) is consistent with FB4 extending into at least the initial stages of the colder phase that followed, Greenland Stadial (GS) 22. Distances to the shoreline, estimated from global sea-level curves and the local, seismically reconstructed bathymetry (24), could have oscillated between 250 and >2000m, but on average were ~750, ~1500, and ~2000 m during phases FB1 to FB2, FB3, and FB4, respectively (see supplementary text S2.4 to S2.6, figs. S1 and S19, and table S18). Phase FB1 is documented by the dense accumulations of mussel shell in the LC complex of Entrance 3 (Fig. 5 and fig. S25). Found along the site's seaward erosional scarp, these exposures represent depositional contexts that, at the time of occupation, were interior and peripheral to the main activity area, which would have been located farther out, in the then-extant cave porch. The subhorizontal, well-layered disposition of the shell lenses is apparent in both field and soil micromorphology thin section (fig. S13); it reflects a largely in situ context and rules out the possibility that the shells are reworked from natural thanatocenoses formed by hydrodynamic processes. Human agency, otherwise demonstrated by the association with quartz artifacts and animal bone remains, is implied by the site-to shore distance and the accumulations' intrinsic features: most shells are broken, the fragments belong to edible-size specimens with valves 7 to 8 cm long or more, small-size specimens and articulated valves are scarce or altogether absent, and many valves lie on their convex side (in a seashore thanatocenosis, wave energy would have inverted most to a more stable position with the concave side facing down). Phase FB2 is represented in Entrance 3 by highly anthropized units MC3 to MC5, which overlie either the LC complex (along the seaward erosional scarp) or the MIS 5e beachrock [6 m inward, at the base of the Sondagem exterior (SEx) trench] (Fig. 5 and fig. S11). Because of the intervening recession of the porch, the location of these remnants then coincided with the main, daylight activity area, which is consistent with the abundant charcoal and burnt food debris that underpin the deposit's dark color. The soil micromorphological thin sections document shell-supported structure in the MC5 unit and show that shell and shell fragments are the dominant component of the groundmass (Fig. 6, figs. S13 and S40, and

tables S14 and S15). Phase FB3 is represented by units MC1 and MC2 of Entrance 3 and the IL complex of Area F. From the marked decrease in the density of charcoal, mollusk shell, bones, and artifacts, we can infer that the site was infrequently visited during this period (Table 2 and tables S20 to S38). Beginning at this time and continuing into FB4, the abundant remains of which are contained in layer 2 (Area C) and the IH complex (Area F), sedimentary buildup pushed occupation outward of the drip line. However, through syndepositional, low-energy displacement mechanisms (mainly gravity and runoff), habitation debris were transported along the interior slope of the talus, eventually accumulating in the site's interior areas, where they form the bulk of the deposit. A caprine scapula and wild cat maxillary cemented together in unit IH6 provide a good illustration of the site formation processes in operation: after the soft tissue decayed, the cat's canine fell from its socket but remained close by, showing how, once its different components were set in place, postdepositional disturbance did not further affect the unstructured comingling of the remains (Fig. 7A). Once postglacial sea-level rise and attendant erosional processes unroofed the terrace in front and removed most of the infill deposit, burrowing animals were able to access the site's interior; therefore, despite the extensive flowstone cap, the unconsolidated portions of the subsurface sediment were affected. This fact hinders the interpretation of Area C's FB4 finds because its layers 2 (in situ) and 2a (reworked) were excavated as a single unit (23). In Area F, however, we carefully separated the disturbed areas (figs. S7 to S9); their Holocene-intruded components could thus be used as a standard of seaside, naturally accumulated faunal and plant remains against which to assess the Pleistocene material.

Fig. 5. Entrance 3. Exposures and extent of the LC and lower MC complexes and their shell-midden lenses. (A and B) The charcoal-, burnt-bone-, and burnt-shellrich deposit (units MC3 to MC5) exposed at the bottom of the SEx trench (A) and along the seaward erosional scarp of the brecciated fill (B), from which a representative soil micromorphology thin section (Cut E, sample 1002) was cut. (C) Horizontal exposure of the mussel shell bed in the upper LC complex from which a representative soil micromorphology thin section (Cut G, sample 1022) was cut. (D and E) Vertical exposures of the LC complex from which a representative soil micromorphology thin section (Cut G, sample 1021) was cut. (D) Before cutting. (E) After cutting. (F) Overview of the sedimentary fill preserved in Entrance 3; the exposures illustrated in (A) to (E) are positioned in the photo and against the excavation grid (inset).
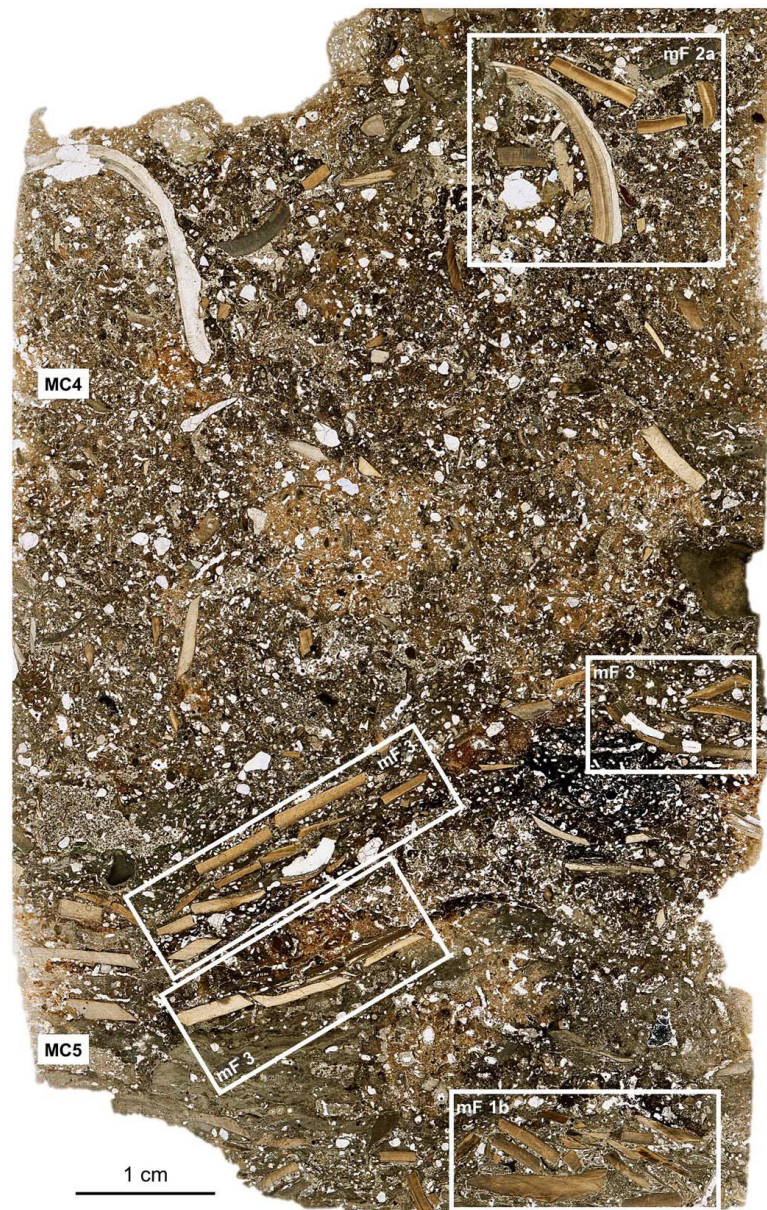
Fig. 6. Micromorphology. Units MC4 and MC5 under the microscope (thin section FB1002; PPL scan). The rectangles highlight areas in which the different microfacies (mF) present are readily apparent: mF1b, interconnected shells with calcitic matrix; mF3, horizontally oriented components; mF2a, heterogeneous coarse sands and shells.

Stone tools

Lithic artifacts are abundant throughout (supplementary text S9, Fig. 7H, figs. S34 to S39, Table 2, and tables S38 to S41). The lithics retrieved in the 0.89m3 of square U8 total 15.3 kg and form a representative sample for phases FB3 and FB4; the total for 0.24 m3 of FB2 excavated in the SEx trench is 1745 g. Quartz is dominant (>90% by specimen counting and >80% by weight in all three phases), features complete reduction sequences, and includes a small number of retouched pieces; most blanks were used without retouch in tasks involving the cutting and scraping of both hard (e.g., wood and bone) and soft (e.g.,meat) materials. Flint and flint-like rocks are rare: there were only 130 pieces in all units of both Entrance 3 and Area F. The inventory includes blanks, exhausted cores, and imported Levallois flakes and blades. Reduction sequences are incomplete and most cores are exhausted; their dorsal,

production side features centripetal, unipolar, bipolar, and multipolar scar patterns. Flake morphology is consistent with reduction by recurrent, centripetal schemes. For both flint and quartz, most retouched tools are denticulates or sidescrapers (figs. S36 and S37); some were resharpened on-site, as shown by characteristic debris. This raw material economy is a direct reflection of availability and remained stable through time, underpinning the absence of appreciable techno-typological change. Quartz could have been procured locally, either from marine deposits or from continental conglomerates and alluvial terraces, where the occasionally knapped cobbles of quartzite, limestone, and lydite can also be found. The flints are allochthonous. Reports that nodules exist in Paleogene formations ~5 km to the northeast could not be confirmed, and the closest sources of the assemblage's Cenomanian varieties are on the right banks of the Tagus, in the Lisbon area, >30 km to the north (supplementary text S9). Plant remains Eighty-seven percent of the identified charcoal is pine. Only *P. pinea*, the stone pine, could be identified to species (supplementary text S4; Fig. 7, I to K; fig. S23; and table S20). The wood was burned at hearth temperatures, indicating use as fuel, but most stone pine remains are bracts and nut shells (90, 77, and 71%, respectively, of the pine material in FB2, FB3, and FB4). Thus, the cones were not collected as fire starters because if they had been so used, they would have been thoroughly consumed. In addition, bracts often preserve anatomical shape, which implies roasting rather than burning. These patterns reflect the exploitation of the stone pine as a fruit tree. The harvest would happen in the autumn or winter of the third year after flowering, when the nuts reach maturity but before the cones open to spread the seeds. The mature cones are always found at the very top of the canopy, which must be climbed for collection. The assemblage's charred needles corroborate that the cones were taken directly from the tree and stored on-site; here, the nuts were extracted by low-temperature heating and then cracked open to get the kernels, whose absence from the record reflects consumption.

Site (a)	Phase (b)	MIS stage	Meters to shore	Volume (m³) (c)	Marine mollusk shell (d)			Lithics (e)			
					(kg/m³)	(MNI)	(MNI/m³)	(N)	(N/m³)	(g)	(kg/m³)
FB	FB4	5b	2000	1.374	128.2	503	366	1087	2588	10,021	23.9
	FB3	5c (late)	1500	3.000	22.6	60	46	434	517	7435	8.9
	FB2	5c (early)	750	0.240	370.7	106	442	599	2496	1745	7.3
CBD	Aterian	5c	1750	7.455	–	1810	243	1595	214	–	–
	Mousterian	5d	2500	8.954	–	176	20	1176	131	–	–
HDP1	AH-1	5e	100	0.672	12.1	333	496	1118	1663	–	–
	AH-II	5e	100	0.253	11.5	179	708	1049	4146	–	–
	AH-III	5e	100	0.479	13.2	328	685	447	933	–	–
BBC	M1	5a	650	–	20.74	3203	2647	28,425	21,348	–	–
	M2	5a	650	–	39.12	3118	5029	2801	2935	–	–
	M3	5a	650	–	86.14	2692	2361	16,736	29,284	–	–
PP13B	SBS	5c	500	0.095	8.7	69	726	394	4147	3243	34.3
	URF	5c	500	0.518	4.5	240	463	1213	2342	11,327	21.9
	LRF	5c	500	0.548	3.8	240	438	41	75	313	0.6
	LC-MSA upper	5d	500	0.047	3.3	37	787	58	1234	415	8.9
	LC-MSA middle	5e	80	0.172	2.3	59	343	179	1041	1508	8.7
KR	MSA II	5c	250	1.580	35.5	4656	2947	–	–	–	–
	MSA II (SMONE)	5c	250	0.224	–	–	–	2671	11,925	–	–
	MSA II (BOS)	5c	250	0.491	–	–	–	4.32	8207	–	–
	MSA I	5e	40	1.170	46.4	6577	5621	–	–	–	–

Table 2. Density. Shown is the intensity of marine resource exploitation versus the intensity of human occupation at Last Interglacial coastal sites of Iberia and Africa using shellfish and stone tools as proxies (19, 33, 34, 43, 49–54).
(a) Site acronyms: FB = Figueira Brava; CBD = Contrebandiers; HDP1 = Hoedjiespunt 1; BBC = Blombos; PP13B = Pinnacle Point 13B; KR = Klasies River
(b) PP13B acronyms: SBS = Shelly Brown Sand; URF = Upper Roof Fall; LRF = Lower Roof Fall; LC-MSA = Lightly Cemented MSA (only the richest stratigraphic aggregates have been considered)
(c) For FB3, lithics density is calculated for the volume that the sample comes from (0.84 m³); for BBC, lithics density derives from the >1 cm fraction in a part of the 1998 and the 1999 field seasons, while shell density derives from the >3 mm fraction in squares F4, F5, E5a and E5b
(d) For FB, the weight/volume data are based on the composition analysis of bulk samples and likely subsume small fragments of crab shell; for the other sites, the weight is of all marine mollusk shell present in the excavated and sieved sediment (table S45); the ranges for individual units are [153-12,404] in N/m³ and [0.3-162.5] in kg/m³ at KR and [<10-163.8] in kg/m³ at BBC
(e) For FB, the counts, weights and density ratios are derived from the SEx trench and square U8 of Area F only; for KR (SMONE and BOS), the density of lithics is calculated from a volume of deposit estimated from the area and thickness of the excavation (the values reported in the source are of the volume of matrix remaining after finds, manuports and larger clasts had been sorted out)
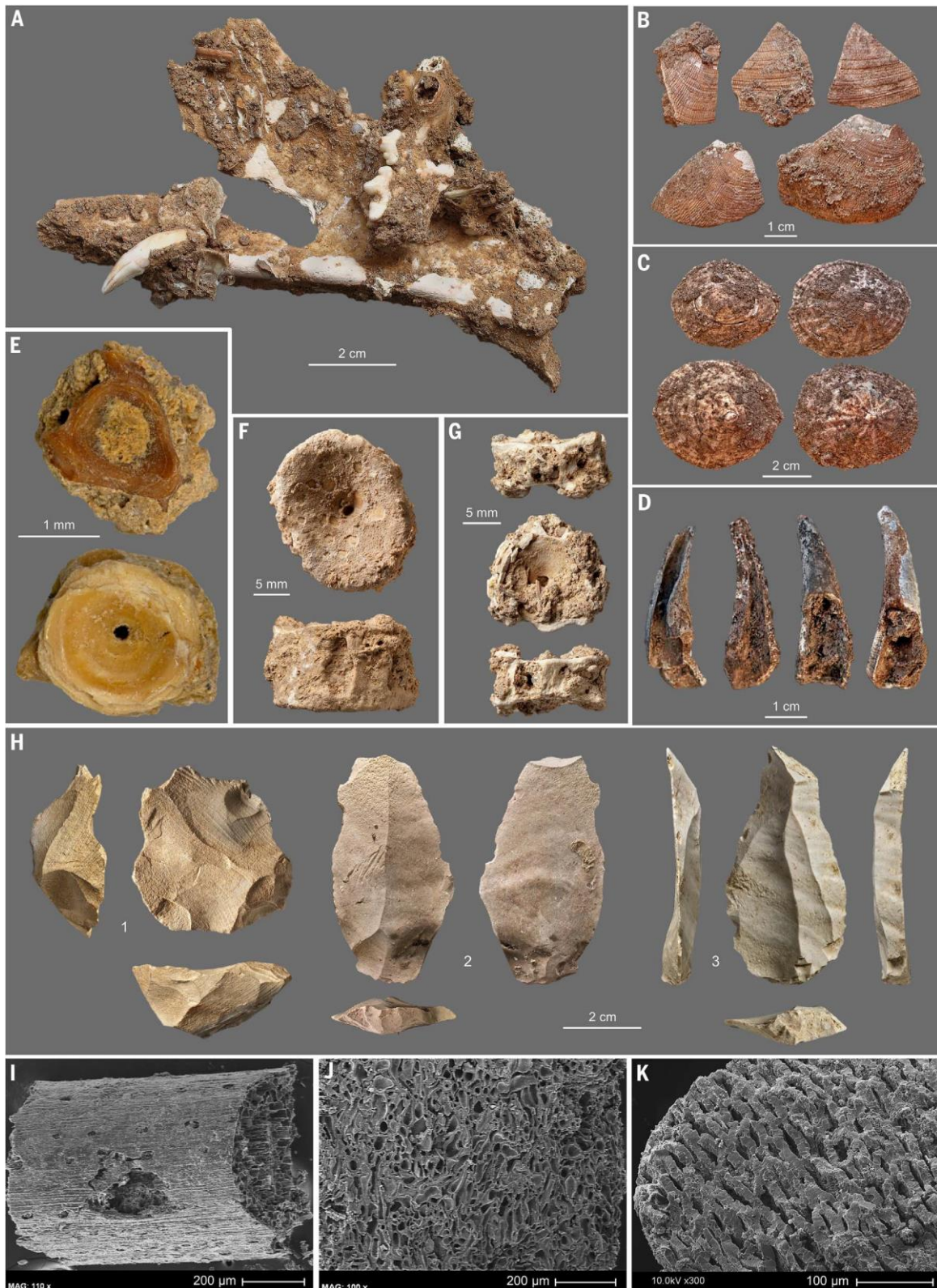
Fig. 7. Finds. (A) Felis sylvestris left maxilla and its loose canine cemented to a caprine scapula from Area F (unit IH6). (B) Ruditapes decussatus shell fragments from the SEx trench (spit A51 of units MC3 to MC5). (C) Patella vulgata shells from Area F (left top and bottom, units IH4 and IH6, respectively; right, unit IH8). (D) Cracked-open and burnt fragments of Cancer pagurus pincers from Area F (left, units IT0 and IH3; right, unit IH8 both). (E to G) Vertebrae of eel (E), one thermo-altered, and shark [(F) and (G)] from Area F (units IH4 to IH6). (H) Stone tools from Area F: 1, Levallois core from unit IH3; 2 and 3, laminary Levallois flakes from, respectively, units IH4 and IH6. [Photos in (F), (G), and (H): J. P. Ruas.] (I to K) Scanning electron microscope images of Pinus pinea charred remains. Shown are a needle (I) and cone bract (J) from Area F (unit IH6) and a nutshell (K) from the SEx trench (spit A52 of units MC3 to MC5).

Shellfish

The marine mollusk assemblage includes specimens of *Steromphala*, *Littorina*, *Bittium*, *Nucella*, and *Tritia*, as well as valves of *Glycymeris*, *Ostrea*, and *Pecten* (supplementary text S5, figs. S26 and S27, and tables S21 to S24). Coeval, personal ornamentation–related use of these or morphologically similar taxa has been documented (25–27), but no traces of anthropogenic modification could be identified in the Figueira Brava specimens. The numbers involved, however, imply routine collection—for purposes that remain elusive to us—of the beached shells of large bivalves: in FB2, for instance, three complete and two large fragments of *Glycymeris* were retrieved in the 0.050-m3 excavation of unit MC5. That such shells cannot represent geologically inherited material is corroborated by the fact that none occur in the substantial beachrock remnants locally exposed across the marine abrasion platform. The smaller gastropods may represent incidental collection. A pierced *Littorina obtusata* was retrieved in reworked unit IT0 (fig. S28); radiocarbon dating of this specimen yielded a mid-Holocene age (tables S1 and S2), corroborating its suspected intrusive status and the natural origin of the perforation. The remains of edible shellfish are ubiquitous (supplementary text S5, figs. S24 and S25, and tables S21 to S24). In FB1 and FB2, the accumulations are similar in structure and density to the shell-midden deposits of the regional Holocene (fig. S40). The variation observed in the bulk samples of unconsolidated sediment collected for composition analysis closely tracks that displayed when using excavated specimen counts instead (fig. S25, Table 2, and table S21). For FB2, the values per cubic meter are 370.7 in kilograms, 2504 in number of identified specimens (NISP), and 442 in minimum number of individuals (MNI); for FB4, they are, respectively, 128.2, 2018, and 366. Mollusk shell abundance, relative to matrix and the other components, is therefore comparable in both phases. However, the preserved FB4 deposit does not display shell-midden structure; this is due to issues of site formation, which favored widespread fragmentation, as illustrated by the size class distribution of the piece-plotted and dry-sieved material used in the NISP and MNI calculations, 59% of which is <2 cm (fig. S24). In the exposures of FB1, mussels are almost exclusive. In the excavated FB2 deposit, mussels are found alongside large numbers of the *Ruditapes decussatus* clams (Fig. 7B), which continues to occur afterward but in much diminished proportion. Limpets, 74% of which are *Patella vulgata*, dominate the mollusk assemblages in FB3 and FB4 (Fig. 7C); in decreasing order of abundance, *Patella depressa*, *Patella ulyssiponensis*, and *Patella rustica* are also represented. Substantial amounts of brown crab (*Cancer pagurus*) and spider crab (*Maja squinada*) remains appear for the first time at this point in the sequence; the finds include carapace fragments but are mostly composed of often burnt, cracked-open pincers with a breakage pattern that mimics present-day consume and- discard patterns (Fig. 7D, fig. S24, and tables S25 and S26). Carapace width, which can be estimated from the length of the pincers to average 162 mm, shows that the large crab catch is entirely made up of sexually mature animals. On average, a 16-cm brown crab weighs 800 g. Thus, the decrease in the density of shellfish remains seen when FB4 is compared with FB2 does not necessarily imply a decrease in the economic importance of marine foods; because an adult brown crab is the clean-meat equivalent of some 30 mussels, a poorer

mollusk harvest would have been more than compensated by the new resource. Like the preference for limpets instead of clams, the addition of crabs to FB4's food basket must reflect sea-level-related differences in the configuration of the shoreline and in the availability of the different species across the closer-by points of procurement.

Fish

The rocky coast where crabs and limpets were harvested during FB4 would also have been rich in fish, the bone and tooth remains of which are indeed abundant (supplementary text S6). Among those identified to family, most are eels, congers, and morays, followed by mullets, sharks, and sea breams (Fig. 7, E to G; figs. S29 and S30; and tables S27 to S29). Compared with specimens of known size, the eel bones correspond to fish that were about 30 cm long. In southern Europe, this size range is consistent with individuals in the so-called silver eel stage, which can be caught in estuaries and adjacent marine shores as they pass through on their way back to the sea for reproduction. With regard to sharks, the taxa that could be tentatively identified to species can be caught in shallow water and when trapped in large rock pools left by ebbing tides. This is not infrequently observed in the present, even in the case of the >1-m-long juvenile porbeagle specimens identified in unit IH6 of Area F. During FB4, the sea was on average ~2 km away. Mammalian predators do not transport fish over such distances. The raptors that would be able to carry prey the size of a juvenile shark are carrion eaters, unrepresented in the faunal assemblage, or not known to nest in caves. Regardless, raptor beak or digestion marks were not observed among the fish remains, and the possibility that they represent stomachal contents can be excluded because there is no evidence that whole carcasses of hunted marine birds were being brought in. The only taxon represented at the site that is known to feed on eels is the cormorant, the remains of which, however, all come from reworked unit IT0, where eels and morays are rare (1.2% of the teleost remains) and may well derive from the Pleistocene deposit (where they represent 65.5% of the teleosts). That said, the fresh appearance of the cormorant material reflects their intrusive nature and recent Holocene age, whereas the representation of all the body parts is consistent with natural deaths in a rocky seashore such as that in existence today at the site; furthermore, no eel remains were found in a study of >400 regurgitations of the Sado estuary's extant cormorant populations. These patterns rule out that the fish remains are incidental, and human agency is otherwise implied by the dark-brown color of several eel bones (Fig. 7E), which is indicative of low temperature heating and thus of cooking or roasting.

Small vertebrates, marine mammals, and game

Both resident and migratory species are found among the fauna's waterfowl component (supplementary text S7, fig. S31, and tables S30 to S34). Among them, auks, gannets, and shags are marine birds that come to shore only to breed in island or rocky cliff colonies. In contrast to the body part representation of the intrusive Holocene cormorants, only the meaty wing bones are represented in the Pleistocene assemblage (mallards and geese included). This pattern suggests human agency, as does

the fact that the remains come from FB4, when the site was ~2 km inland. The same applies to the vertebrae of dolphin and the limb remains of ringed seal retrieved in Area C (fig. S33). Land vertebrates are represented by the skeletal remains of reptiles, birds, and mammals (supplementary text S7 and S8, figs. S31 to S33, and tables S30 to S37). Excluding lagomorphs, 89% of the identified mammals are game taxa (red deer, horse, ibex, and aurochs); the remainder are carnivores, small (cat, fox, and lynx; 4%) and larger (brown bear, hyena, and wolf; 7%). Small-carnivore damage was found among the remains of lagomorphs and terrestrial birds, which may have been accumulated, at least in part, by cat or lynx. Almost all the larger carnivore bones come from the units found either side of the episode of sedimentation arrest and speleothem growth between FB3 and FB4; they reflect use of the cave during a period of human abandonment, whereas the few coprolites found in different units of the IH complex show brief hyena incursions during FB4. The remains are commingled with abundant stone tools in a deposit rich in charcoals produced by human-lit fires. Extensive carbonate incrustation hinders observation of bone surfaces, but butchery and percussion marks could nonetheless be identified on the herbivore bones. Of these, none bears signs of gnawing or digestion by hyenas or wolves and many are burnt (fig. S32 and tables S34 and S37); likewise, the pattern of tortoise shell burning is consistent with the roasting-in-carapace technique (28).

Discussion

The pine nut economy seen through the Figueira Brava sequence is well documented in the Upper Paleolithic and Mesolithic of Iberia (29). Supporting evidence for this economy to be in operation during the Middle Paleolithic comes from the LBS and SSL members of Gorham's Cave (Gibraltar) (30). This site has been assigned to MIS 3 or MIS 4 on the basis of anchoring OSL dating results to radiocarbon chronologies, though the latter must be minimum ages only, meaning those members likely span MIS 5a to MIS 5b, overlapping in age with FB4 (supplementary text S10.3). The tortoise, marine taxa, and ungulate remains are unquestionably anthropogenic. The hunting of aurochs, horses, and deer is an ordinary component of the Middle Paleolithic behavioral repertoire. The acquisition of small prey and marine foods would in most cases have required no more than the simplest of technologies such as low-tide handpicking in sandy bottoms, exposed rock faces, submerged crevices, and shallow waters, plus the means to bag and transport the harvest. The remains of seals and dolphins may reflect scavenging, and the waterfowl's small numbers suggest chance acquisition not systematic procurement with netting or similarly elaborated means. These resources reflect the exploitation of all ecosystems present in the site's catchment among mountain, estuary, and sea: rocky shores, coastal lagoons, alluvial plains, dune pinewoods, and forested slopes. On the basis of their present behavior, the aquatic and marine birds must have been taken in autumn or winter, when mature pinecones were also harvested. Adult brown and spider crabs migrate to shallow waters in summer, so that must have been their season of collection. Thus, the change from an FB2 clam- to an FB4 limpet-plus-crab-dominated marine invertebrate

assemblage possibly reflects a stronger autumn to- winter (in the former) versus a stronger spring-to-summer (in the latter) signal. The seasonality data imply year-round presence, but given the evidence for occasional carnivore presence, in a recurrent, not continuous, manner. The evidence from FB3 suggests sporadic use but most resources are documented in all phases. Therefore, there is no reason to think that the differences seen across the sequence imply fluctuation through time in the economic importance of food resources. When the spatial scale of the adaptive system is considered, such differences need not reflect how intensively each resource was harvested or the extent to which the product of the harvest was transported to home base as opposed to being consumed where procured. Rather, they are best explained as relating to the following: (i) where in the changing landscape the archeological record of resource exploitation formed, (ii) the way such a record formed and was (or was not) preserved in the different sites that remained active as home bases throughout, and (iii) the extent to which archeological trenches provide appropriate sampling of intrasite variation in both the vertical and the horizontal dimensions. Even though documented at a single site, the redundancy seen over the many millennia spanned by the Figueira Brava record suggests a stable settlement-subsistence system, not one-off or idiosyncratic behavior. Based on the Holocene sites of Iberia, distance from the shore is a good predictor of the density of invertebrate shells; the Figueira Brava data fit the kilograms per cubic meter trend line (Fig. 8A), but plot below expectations in rate-of-accumulation terms (MNI per square meter per year) (fig. S42 and tables S42 to S44). This pattern suggests that site use was redundant and/or intensive in Holocene sites located at a comparable distance from the nearest shore but intermittent at Figueira Brava; here, individual occupation events nonetheless resulted in the discard of marine food remains in similar amount and manner, as revealed by the comparable structure identified in the soil micromorphology thin sections (supplementary text S10.1 and fig. S40). Carbon and nitrogen isotope analysis of the humans buried in Portuguese Holocene shell middens shows that aquatic foods may have represented up to 50% of their dietary intake (31, 32). There is no reason to think differently about Figueira Brava's Middle Paleolithic people, the more so because their exploitation of marine birds, large crabs, and marine mammals reveals an aquatic resource base with a breadth that exceeds that of the regional Mesolithic (22). When comparing against Last Interglacial marine exploitation proxies from sites in Iberia, the Maghreb, and South Africa, Figueira Brava plots above expectations (supplementary text S10.2, Fig. 8B, Table 2, and tables S44 and S45). To avoid potential biases introduced by the different approaches to the calculation of the kilograms per cubic meter index, specimen counts can be used instead; doing so changes nothing with regard to fish (Fig. 8C), but for mollusks reveals a noisier exponential trend where Blombos is the outlier (Fig. 8D). The Blombos data, however, are for the richest grid units only; they are unrepresentative of the abundance of remains across the extent of the occupied surface and, for the M2 phase, likely inflated by the differential identifiability of the *Perna perna* mussel. Likewise, interpretation of the high values for Bajondillo must take into consideration that they are based on *Mytilus* fragments counted down tothe0.5-mmfraction, whereas 2- to 10-mm mesh size ranges were used at the other Last Interglacial sites shown in the comparison plot. These examples highlight why, in

addition to distance to shore, the observed variation also depends on preservation, sampling, and counting biases. Within South Africa, Klasies River's MNI per cubic meter values stand out as much higher than at other sites similarly located directly on the beach (e.g., Hoedjiespunt), suggesting that site function also contributes significantly to the variation in the amount of shellfish refuse (33). Indeed, the density of shellfish correlates well with that of lithic artifacts (Fig. 8E and Table 2), and the latter can be taken as a good proxy for the intensity of human occupation. The highest values for both parameters are reached at Blombos, and at Klasies River if we take the SMONE unit (34) as being representative of the MSA II phase. These two sites may have been places of long-term, intense residential activity— in agreement with their abundant fire features, human remains, and number of symbolism-related artifacts (shell beads, pigment containers, and engraved and painted items) (35–39)—whereas the others may have been transiently used or only infrequently reoccupied. Available geological descriptions suggest that some of the Klasies River levels (e.g., the SM5 midden at the base of phase MSA II) are shell supported (40); however, Pinnacle Point 5-6 is the only South African site where soil micromorphological analysis demonstrates that is the case for some levels (41) (fig. S41). On the basis of a scatterplot of piece-plotted shells, shell-midden status has been claimed for the MIS 5c accumulations in the eastern area of Pinnacle Point 13B (units SBS, URF, and LRF); taken a step further, the argument would support a difference in kindwith the Middle Paleolithic of Europe because of the much lower density of the distribution of shells across an area of the same size in Vanguard Cave, Gibraltar (8). However, Pinnacle Point 13B is estimated to span a minimum of 8000 years (42), and the marine mollusk MNI represented in the scatterplot is 549 (Table 2), whereas Vanguard's MNI is 65 and comes from a very thin deposit of high integrity corresponding to a single occupation (43, 44). Thus, the Pinnacle Point 13B record could have been produced by the equivalent of one such Vanguard event occurring at the site only once every thousand years. When all factors that condition the density and structure of archeological deposits rich in marine food remains are duly considered, the variation seen in the Last Interglacial sites of Africa and Iberia is in the same range. Figueira Brava, with its abundance of fish, crab, and mollusk remains and presence of lenses of shell supported matrix, is the best Iberian example so far but it is not alone. The cave sites of Aviones, Bajondillo, and Vanguard are examples that meet expectations when their Mediterranean setting is accounted for. In the Atlantic façade, the Cantabrian site of El Cuco is almost certainly another example; the shellfish-rich lower layers of the sequence (Fig. 8D, fig. S42, and tables S42 and S44) yielded finite radiocarbon ages on limpet shell in excess of 42.5 ka (45, 46), but comparable results were obtained at Aviones and Figueira Brava by the same laboratory using the same methods and the same kinds of samples—ones that were eventually shown to be of Last Interglacial age instead (supplementary text S2.1 and S10.2).
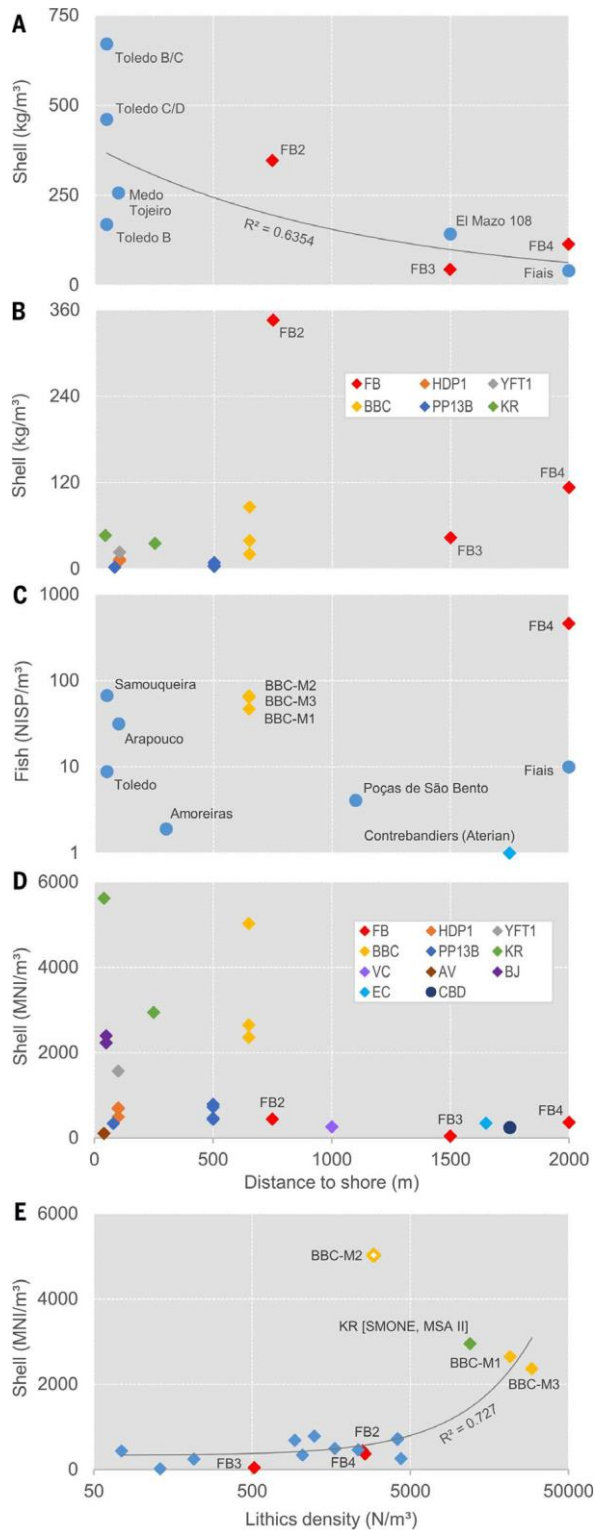
Fig. 8. Significance. Figueira Brava compared with Mesolithic and Last Interglacial sites in Iberia, the Maghreb, and South Africa (data from Table 2 and table S42). Note the logarithmic scale in the y-axis of (C) and the x-axis of (E). Excluding Blombos, the set of sites in (D) fits an exponential trend with R2 = 0.4635. In (E), BBC-M2 is a clear outlier and was excluded from the calculation of linear regression and coefficient of determination. In weight of shell per excavated volume versus distance to shore, Figueira Brava fits the Iberian Holocene trend (A) but falls above expectations derived from the African sites (B). If specimen counts are used instead, Figueira Brava fits the African sites' trend, from which Blombos and Klasies River stand out due to intensive residential use (D and E), but falls well above it for fish (C). FB, Figueira Brava; HDP1, Hoedjiespunt 1; YFT1, Ysterfontein 1; BBC, Blombos; PP13B, Pinnacle Point 13B; KR, Klasies River; VC, Vanguard Cave; AV, Aviones; BJ, Bajondillo; EC, El Cuco; CBD, Contrebandiers.

Conclusions

In littoral areas of Last Interglacial Iberia, Neandertals foraged much like early Holocene humans. Subsistence-wise, Neandertals were therefore geographically as diverse as might be expected, from top-level carnivores in their periglacial range (47) to fisher-hunter-gatherers in the right settings of temperate environments. The routine harvesting of shellfish implies knowledge of tidal regimes and, along the Portuguese littoral, awareness that between late spring and autumn, the consumption of bivalves entails a significant risk of biotoxin poisoning. These cognitive aspects of the Figueira Brava subsistence data are consistent with the rapidly accumulating evidence for jewelry, cave art, and other forms of symbolic material culture in the Middle Paleolithic of Europe (26, 27, 48). The major behavioral gap once thought to separate Neandertals from modern humans would thus seem to be just another example that "absence of evidence is not evidence of absence." A corollary of the Iberian data is that the consumption of aquatic foods is not the *differentia specifica* separating anatomically modern humans in Africa from coeval Eurasians, and ultimately explaining the demise of the latter. Indeed, the possibility must now be entertained that the familiarity with marine resources and seascapes implied by the settlement of Southeast Asia, Sahul (Australia and New Guinea), and the Americas is deeply rooted in the history of our genus.

References

1. S. C. Cunnane, M. A. Crawford, Energetic and nutritional constraints on infant brain development: Implications for brain expansion during human evolution. J. Hum. Evol. 77, 88–98 (2014). doi: 10.1016/j.jhevol.2014.05.001; pmid: 24928072
2. J. C. Joordens, R. S. Kuipers, J. H. Wanink, F. A. Muskiet, A fish is not a fish: Patterns in fatty acid composition of aquatic food may have had implications for hominin evolution. J. Hum. Evol. 77, 107–116 (2014). doi: 10.1016/j.jhevol.2014.04.004; pmid: 25070910
3. K. Kyriacou, J. E. Parkington, A. D. Marais, D. R. Braun, Nutrition, modernity and the archaeological record: Coastal resources and nutrition among Middle Stone Age hunter-gatherers on the Western Cape coast of South Africa. J. Hum. Evol. 77, 64–73 (2014). doi: 10.1016/j.jhevol.2014.02.024; pmid: 25440132
4. M. C. Stiner, Thirty years on the "broad spectrum revolution" and paleolithic demography. Proc. Natl. Acad. Sci. U.S.A. 98, 6993–6996 (2001). doi: 0.1073/pnas.121176198; pmid: 11390968
5. M. A. Zeder, The broad spectrum revolution at 40: Resource diversity, intensification, and an alternative to optimal foraging explanations. J. Anthropol. Archaeol. 31, 241–264 (2012). doi: 10.1016/j.jaa.2012.03.003
6. P. Mellars, K. C. Gori, M. Carr, P. A. Soares, M. B. Richards, Genetic and archaeological perspectives on the initial modern human colonization of southern Asia. Proc. Natl. Acad. Sci. U.S.A. 110, 10699–10704 (2013). doi: 10.1073/pnas.1306043110; pmid: 23754394
7. S. Oppenheimer, The great arc of dispersal of modern humans: Africa to Australia. Quat. Int. 202, 2–13 (2009). doi: 10.1016/j.quaint.2008.05.015
8. C. W. Marean, The origins and significance of coastal resource use in Africa and Western Eurasia. J. Hum. Evol. 77, 17–40 (2014). doi: 10.1016/j.jhevol.2014.02.025; pmid: 25498601
9. C. W. Marean, The transition to foraging for dense and predictable resources and its impact on the evolution of modern humans. Philos. Trans. R. Soc. Lond. B Biol. Sci. 371, 20150239 (2016). doi: 10.1098/rstb.2015.0239; pmid: 27298470
10. R. G. Klein, D. W. Bird, Shellfishing and human evolution. J. Anthropol. Archaeol. 44, 198–205 (2016). doi: 10.1016/j.jaa.2016.07.008

11. M. Will, A. W. Kandel, N. J. Conard, Midden or molehill: The role of coastal adaptations in human evolution and dispersal. J. World Prehist. 32, 33–72 (2019). doi: 10.1007/s10963-018-09127-4

12. E. Trinkaus, M. Samsel, S. Villotte, External auditory exostoses among western Eurasian late Middle and Late Pleistocene humans. PLOS ONE 14, e0220464 (2019). doi: 10.1371/journal.pone.0220464; pmid: 31412053

13. A. C. Colonese et al., Marine mollusc exploitation in Mediterranean prehistory: An overview. Quat. Int. 239, 86–103 (2011). doi: 10.1016/j.quaint.2010.09.001

14. K. Douka, E. E. Spinapolice, Neanderthal shell tool production: Evidence from Middle Palaeolithic Italy and Greece. J. World Prehist. 25, 45–79 (2012). doi: 10.1007/s10963-012-9056-z

15. F. Romagnoli, J. Baena, L. Sarti, Neanderthal retouched shell tools and Quina economic and technical strategies: An integrated behaviour. Quat. Int. 407, 29–44 (2016). doi: 10.1016/j.quaint.2015.07.034

16. M. A. Mannino et al., Upper Palaeolithic hunter-gatherer subsistence in Mediterranean coastal environments: An isotopic study of the diets of the earliest directly-dated humans from Sicily. J. Archaeol. Sci. 38, 3094–3100 (2011). doi: 10.1016/j.jas.2011.07.009

17. M. A. Mannino et al., Origin and diet of the prehistoric huntergatherers on the mediterranean island of Favignana (Ègadi Islands, Sicily). PLOS ONE 7, e49802 (2012). doi: 10.1371/journal.pone.0049802; pmid: 23209602

18. A. Chakroun et al., The Pleistocene of Rabat (Morocco): Mollusks, coastal environments and human behavior. Afr. Archaeol. Rev. 34, 493–510 (2017). doi: 10.1007/s10437-017-9279-6

19. G. L. Dusseldorp, G. H. J. Langejans, Carry that weight: Coastal foraging and transport of marine resources during the South African Middle Stone Age. Southern African Humanities 25, 105–135 (2013). 20. K. Hardy et al., Shellfishing and shell midden construction in the Saloum Delta, Senegal. J. Anthropol. Archaeol. 41, 19–32 (2016). doi: 10.1016/j.jaa.2015.11.001

21. L. G. Straus, Iberia before the Iberians (Univ. of New Mexico Press, 1992).

22. J. E. Arnaud, in The Mesolithic in Europe. Papers presented at the Third International Symposium, C. Bonsall, Ed. (John Donald, Edinburgh, 1989), pp. 614–631.

23. M. T. Antunes, Ed., Últimos Neandertais em Portugal. Evidência, odontológica e outra, (Academia das Ciências, 2000).

24. P. Brito, Thesis, University of Lisbon (2009).

25. D. E. Bar-Yosef Mayer, B. Vandermeersch, O. Bar-Yosef, Shells and ochre in Middle Paleolithic Qafzeh Cave, Israel: Indications for modern behavior. J. Hum. Evol. 56, 307–314 (2009). doi: 10.1016/j.jhevol.2008.10.005; pmid: 19285591

26. D. L. Hoffmann, D. E. Angelucci, V. Villaverde, J. Zapata, J. Zilhão, Symbolic use of marine shells and mineral pigments by Iberian Neandertals 115,000 years ago. Sci. Adv. 4, eaar5255 (2018). doi: 10.1126/sciadv.aar5255; pmid: 29507889

27. J. Zilhão et al., Symbolic use of marine shells and mineral pigments by Iberian Neandertals. Proc. Natl. Acad. Sci. U.S.A. 107, 1023–1028 (2010). doi: 10.1073/pnas.0914088107; pmid: 20080653

28. M. Nabais, J. Zilhão, The consumption of tortoise among Last Interglacial Iberian Neanderthals. Quat. Sci. Rev. 217, 225–246 (2019). doi: 10.1016/j.quascirev.2019.03.024

29. E. Badal, in Las culturas del Pleistoceno superior en Andalucía, J. L. Sanchidrián, M. D. Simón, Eds. (Patronato de la Cueva de Nerja, 1998), pp. 287–300.

30. S. Ward, R. Gale, W. Carruthers, in Neanderthals in Context. A Report of the 1995-1998 Excavations at Gorham's and Vanguard Caves, Gibraltar, R. N. E. Barton, C. B. Stringer, C. Finlayson, Eds. (Institute of Archaeology, Univ. of Oxford, 2012), pp. 89–101.

31. E. J. Guiry, M. Hillier, M. P. Richards, Mesolithic dietary heterogeneity on the European Atlantic coastline: Stable isotope insights into hunter-gatherer diet and subsistence in the Sado Valley, Portugal. Curr. Anthropol. 56, 460–470 (2015). doi: 10.1086/680854

32. D. Lubell, M. Jackes, H. Schwarcz, M. Knyf, C. Meiklejohn, The Mesolithic-Neolithic transition in Portugal: Isotopic and dental evidence of diet. J. Archaeol. Sci. 21, 201–216 (1994). doi: 10.1006/jasc.1994.1022

33. M. Will, A. W. Kandel, N. J. Conard, in Settlement Dynamics of the Middle Paleolithic and Middle Stone Age, N. J. Conard, A. Delagnes, Eds. (Kerns Verlag, 2015), pp. 47–75, vol. IV.

34. M. J. Brenner, S. Wurz, A high-resolution perspective on MIS 5c-d lithic assemblages from Klasies River main site Cave 1. Journal of Archaeological Science: Reports 26, 101891 (2019). doi: 10.1016/j.jasrep.2019.101891

35. F. E. Grine, S. Wurz, C. W. Marean, The Middle Stone Age human fossil record from Klasies River Main Site. J. Hum. Evol. 103, 53–78 (2017). doi: 10.1016/j.jhevol.2016.12.001; pmid: 28166908

36. C. S. Henshilwood et al., Emergence of modern human behavior: Middle Stone Age engravings from South Africa. Science 295, 1278–1280 (2002). doi: 10.1126/science.1067575; pmid: 11786608

37. C. Henshilwood, F. d'Errico, M. Vanhaeren, K. van Niekerk, Z. Jacobs, Middle Stone Age shell beads from South Africa. Science 304, 404 (2004). doi: 10.1126/science.1095905; pmid: 15087540

38. C. S. Henshilwood et al., A 100,000-year-old ochre processing workshop at Blombos Cave, South Africa. Science 334, 219–222 (2011). doi: 10.1126/science.1211535; pmid: 21998386

39. C. S. Henshilwood et al., An abstract drawing from the 73,000-year-old levels at Blombos Cave, South Africa. Nature 562, 115–118 (2018). doi: 10.1038/s41586-018-0514-3; pmid: 30209394

40. H. J. Deacon, V. B. Geleijnse, The stratigraphy and sedimentology of the Main Site Sequence, Klasies River, South Africa. S. Afr. Archaeol. Bull. 43, 5–14 (1988). doi: 10.2307/3887608

41. P. Karkanas, K. S. Brown, E. C. Fisher, Z. Jacobs, C. W. Marean, Interpreting human behavior from depositional rates and combustion features through the study of sedimentary microfacies at site Pinnacle Point 5-6, South Africa. J. Hum. Evol. 85, 1–21 (2015). doi: 10.1016/j.jhevol.2015.04.006; pmid: 26024567

42. C. W. Marean et al., The stratigraphy of the Middle Stone Age sediments at Pinnacle Point Cave 13B (Mossel Bay, Western Cape Province, South Africa). J. Hum. Evol. 59, 234–255 (2010). doi: 10.1016/j.jhevol.2010.07.007; pmid: 20934084

43. N. Barton, in Neanderthals on the Edge: 150th Anniversary Conference of the Forbes' Quarry Discovery, Gibraltar, C. Stringer, R. N. E. Barton, C. Finlayson, Eds. (Oxbow Books, 2000), chap. 23, pp. 211–220.

44. R. I. Macphail, P. Goldberg, in Neanderthals on the Edge: 150th Anniversary Conference of the Forbes' Quarry Discovery, Gibraltar, C. B. Stringer, R. N. E. Barton, C. Finlayson, Eds. (Oxbow Books, 2000), chap. 20, pp. 182–200.

45. I. Gutiérrez-Zugasti et al., The role of shellfish in hunter– gatherer societies during the Early Upper Palaeolithic: A view from El Cuco rockshelter, northern Spain. J. Anthropol. Archaeol. 32, 242–256 (2013). doi: 10.1016/j.jaa.2013.03.001

46. I. Gutiérrez-Zugasti et al., A chrono-cultural reassessment of the levels VI–XIV from El Cuco rock-shelter: A new sequence for the Late Middle Paleolithic in the Cantabrian region (northern Iberia). Quat. Int. 474, 44–55 (2018). doi: 10.1016/j.quaint.2017.06.059

47. K. Jaouen et al., Exceptionally high d15N values in collagen single amino acids confirm Neandertals as high-trophic level carnivores. Proc. Natl. Acad. Sci. U.S.A. 116, 4928–4933 (2019). doi: 10.1073/pnas.1814087116; pmid: 30782806

48. D. L. Hoffmann et al., U-Th dating of carbonate crusts reveals Neandertal origin of Iberian cave art. Science 359, 912–915 (2018). doi: 10.1126/science.aap7778; pmid: 29472483

49. R. N. E. Barton, in Neanderthals in Context. A Report of the 1995-1998 Excavations at Gorham's and Vanguard Caves, Gibraltar, R. N. E. Barton, C. B. Stringer, C. Finlayson, Eds. (Institute of Archaeology, Univ. of Oxford, 2012), chap. 20, pp. 243–252.

50. H. L. Dibble et al., New excavations at the site of Contrebandiers Cave, Morocco. Paleoanthropology 2012, 145–201 (2012).

51. C. S. Henshilwood et al., Blombos Cave, Southern Cape, South Africa: Preliminary report on the 1992–1999 excavations of the Middle Stone Age levels. J. Archaeol. Sci. 28, 421–448 (2001). doi: 10.1006/jasc.2000.0638

52. G. H. J. Langejans, K. L. van Niekerk, G. L. Dusseldorp, J. F. Thackeray, Middle Stone Age shellfish exploitation: Potential indications for mass collecting and resource intensification at Blombos Cave and Klasies River, South Africa. Quat. Int. 270, 80–94 (2012). doi: 10.1016/j.quaint.2011.09.003

53. C. W. Marean, Pinnacle Point Cave 13B (Western Cape Province, South Africa) in context: The Cape Floral kingdom, shellfish, and modern human origins. J. Hum. Evol. 59, 425–443 (2010). doi: 10.1016/j.jhevol.2010.07.011; pmid: 20934095

54. J. F. Thackeray, Molluscan fauna from Klasies River, South Africa. S. Afr. Archaeol. Bull. 43, 27–32 (1988). doi: 10.2307/3887610

ACKNOWLEDGMENTS

Supplementary Materials and Methods

The site

Gruta da Figueira Brava (38°28'14"N, 8°59'10"W, WGS84 datum; Fig. S1) is a cave site located in Serra da Arrábida, 30 km SE of Lisbon. Despite rising to only 501 m asl (above modern sea level), this small, WSW-ENE oriented chain with an uplifted calcareous massif represents the best example of the Alpine orogeny in Portugal (57). The southern flank of the range plunges into the Atlantic through vertical cliffs, while the northern side descends smoothly towards the alluvial plain of the paleo-Tagus river (58). This structural setting underpins the differences between the two slopes in vegetation cover and traditional land use — oak groves are common on the northern ones, while those facing south are dominated by olive and carob (and feature Macaronesian endemisms, e.g., *Euphorbia pedroi*). The climate is Mediterranean but moderated by proximity to the ocean (59). At the nearby city of Setúbal, the average minimum temperature of the coldest month (January) is 4.7 °C, the average maximum temperature of the warmest month (August) is 29.5 °C, and the average mean annual temperature is 17 °. Precipitation, concentrated between October and March, is on average 641 mm/year (it can reach 700 mm/year in the mountain itself).

An almost complete, Lower Jurassic to Pliocene sedimentary succession forms the geological bulk of the chain. The terrain of Paleogene and Miocene age includes shallow transgressive marine deposits as well as alluvial fan conglomerates that reflect the uplift (60). At Figueira Brava, the bedrock, modelled as a sea cliff by Quaternary erosion, belongs to a Lower Miocene formation, the "Azeitão lutites and marls", here overthrusted by Jurassic limestone (61). The cave is excavated in a shallow marine, light-yellow sandstone of fine to medium sand grains and a few pebbles, cemented by calcium carbonate and intercalated with bioclastic sandstone and fossiliferous beds. The cave's sandstone bedrock outcrops in meter-thick layers dipping approximately E/30° and is dissected by sub-vertical fractures running approximately NW-SE. The upper part of the sequence is a paraconglomerate with mm- to cm-sized quartz pebbles and occasional fossils (mostly bivalves).

Typical karst surface features can be observed along this Miocene formation, and an alignment of variably eroded caves exists at the base of the sea cliff. Two of them — Gruta da Figueira Brava and, ~80 m to the west, Lapa de Santa Margarida (Fig. S2) — still preserve an interior, roofed space. Both open onto a beachrock-covered, regularized platform that lies ~5 m asl and, seawards, is cut by a vertical, erosive scarp. This platform corresponds to the Last Interglacial marine terrace observed at the same elevation in different points of the Arrábida coast (61). Beachrock (or isolated cobbles thereof derived) is present at the base of the caves' excavated (at Figueira Brava) or exposed (at Santa Margarida) interior fill, suggesting that speleogenesis involved erosion by the sea, coupled with the action of water running along distension fractures.

Today, Figueira Brava's interior passages connect to the outside via three different "entrances" (Fig. S3). Entrances 2 and 3 are clogged by speleothem-capped breccia. The wild fig offshoot after which the site is named grows in Entrance 1, the largest. This entrance provides access to Area A, which is a ~15 m-long, 3-to-5 m-wide passage developed along one of the NW-SE structural fractures. This passage opens into Area B, a hall whose collapsed bottom opens directly to the sea below, evidencing the ongoing underwater formation of a

new cave. A perpendicular joint running parallel to the seaward edge of the terrace connects Area B to Areas C-F, which are the interior space behind Entrances 2 and 3. The inner side of that joint corresponds to the back wall of the original cave.

Entrances 2 and 3 are physically separated by a large cemented remnant of the sedimentary fill, preserved over its total thickness under a protrusion of the cliff. Originally, both entrances would have formed, together with Areas C-F behind, a single, continuous space. Since, the irregular outline of the roof, the accumulation of sediment, and the growth of large stalagmites divided that space into separate compartments communicated by narrow passages of difficult, often impossible negotiation.

The cluttering-up of Entrances 2-3 explains why a Pleistocene sedimentary fill could survive, largely intact, in the space behind, where a continuous flowstone cap offered additional protection against erosion. In contrast, a few patches of breccia cemented against the floor and walls are all there is to show that, once, Areas A-B were also filled-up. Substantial, heavily indurated, speleothem-capped remnants of a Pleistocene deposit can also be seen along the southern wall of Entrance 2 and the northern wall of Entrance 3, almost all the way to the sea. Flowstone and stalagmites are found as far out as the edge of the marine abrasion platform (Fig. S4).

These observations demonstrate that, when the cave was a functional deposition system in which sediments and archeological remains accumulated, the extant Figueira Brava platform was the basal bedrock of a nowadays-unroofed large cavity; the current entrances correspond to the intersection of that cavity with short, narrow passages leading to the NE-SW joint forming the true back of the cave. Santa Margarida is a better-preserved example of such a morphology and provides a good analogue for the situation in existence at the time of formation of the archeological deposit preserved at Figueira Brava. Why the original setting was significantly altered at one but not at the other can be explained by differential exposure to the littoral erosion processes triggered by Late Glacial and Holocene sea level rise.

Previous work

The existence in this section of the Arrábida littoral of shell-bearing Quaternary deposits in association with caves and a marine terrace assigned to the Tyrrhenian transgression is first mentioned by Breuil and Zbyszewski (*62*). However, it was not until 1978 that cavers and archeologists from the Setúbal Museum (MAEDS; *Museu de Arqueologia e Etnografia do Distrito de Setúbal*) and the Almada Archeological Center (CAA; *Centro de Arqueologia de Almada*) identified Figueira Brava as a site of potential archeological interest.

Subsequent explorations of the cave's interior space resulted in the collection of Pleistocene mammal remains and quartz artefacts (*63*). A date ("16-11-1984") written with yellow chalk on the wall of Area F, just behind the large stalagmitic column separating it from Entrance 3, records one of these early incursions. They were followed by paleontological excavation work, carried out between 1986 and 1989 under the direction of Miguel Telles Antunes and João Luís Cardoso, and eventually published as a monograph (*23*).

This 1980s research (Fig. S5) concerned two areas: a 1 m × 2 m rectangular trench excavated into unconsolidated sands preserved against the west wall of Area B, reported to be very rich in micro-vertebrate remains but whose exact position is uncertain (and, hence, not shown in the Fig. S3 plan); and an 8 m-long

trench across the entire width of Area C where, in 1986, the sedimentary fill was first tested. This initial work concerned a section of the passage in which the capping flowstone was already extensively broken. In the following years, the rest of the flowstone was removed, and the excavation was taken down to bedrock (encountered, on average, at ~1 m below surface); a stratigraphic baulk was left along the SW edge, where the flowstone intersected a lowering cave roof and excavation was impracticable. Along this baulk, from top to bottom, the following succession was recognized (Fig. S5e): layer 0, young, yellowish stalagmites; layer 1, capping stalagmitic crust; layer 2a, coarse red-brownish sands with modern intrusions; layer 2, coarse red-brownish sands rich in Mousterian stone tools and Pleistocene faunal remains; layer 3, grey sands with ash and scattered finds; layer 4, thin red sands with rare finds; layer 5, the marine conglomerate.

Based on published accounts and labelling, we know that some of the Area C finds were logged with the associated information on depth from surface, distance from a horizontal datum, and stratigraphic unit of provenience. We can also tell that the basal units (layers 3-4) of the succession were physically differentiated as such at the time of digging, and that the rare finds made therein were identified accordingly. However, the isolation and separate excavation of the substantial pockets of reworked sediment found under the capping flowstone are reported to have been impracticable in the field. The reddish-brown sands situated between layer 3 and the layer 1 flowstone were therefore excavated as if they were a single, homogeneous fill; the Holocene intrusions therein (e.g., the remains of domesticates, namely sheep/goat) were sorted out post-hoc, following criteria based on taxonomic classification, degree of fossilization and surface condition.

For the stone tools, this procedure poses little problem, as they are homogeneously Middle Paleolithic (among artefacts, the few Holocene intrusions found in the Area C trench were ceramic sherds, including fragments of Roman amphorae). For the larger mammal remains, the monograph's illustration of selected specimens bearing the characteristic incrustation and/or carbonate coating that, at the site, is a secure indication of Pleistocene age, suggests that the 1980s *modus operandi* was effective. However, for small land vertebrates that remain extant in the area and are known cave dwellers (or prey thereof), such criteria can identify the very recent, fresh material but not that potentially intruded in earlier Holocene times. This is even more of a problem when the assemblages subsume material coming from different sectors of Areas A and B (e.g., Area B's rectangular trench) because, at the time of collection, the same reddish-brown sands forming Area C's layer 2 were unconsolidated and surface-exposed, with no flowstone protection. Thus, given the explicit provenience indications provided in the monograph's corresponding chapter, there is no question that this problem affects the insectivores, the bats and the lagomorphs (and, therefore, probably also the small carnivores, the rodents, the reptiles and the amphibians). The other categories of published faunal remains must also be affected, but the extent to which they do include post-Pleistocene intrusions is unclear.

Because of post-Pleistocene sea level rise, which brought the very base of the Figueira Brava cliff back to the edge of the water, potential heterogeneity is an issue of major concern in the case of the marine components of the 1980s faunal assemblage. Even though the bones of marine birds, seal and dolphin illustrated in the monograph are in all aspects taphonomically like those of horse, deer or ibex, the criteria of patina and degree of fossilization used for bone are inapplicable to invertebrate shell. And, indeed, the published mollusks,

crustaceans and echinoderms consist of material submitted for specialist study as if it constituted a single, stratigraphically homogeneous assemblage.

Conventional radiocarbon dating — to 30,930±700 BP (radiocarbon years Before Present) (ICEN-387) — of a bulk sample of limpet shells from layer 2 of the Area C excavation confirmed that the 1980s invertebrate assemblage included specimens of Pleistocene age. That result, however, is at odds with the biostratigraphic significance of *Arvicola cantiana* and the rather evolved form of *Microtus brecciensis* identified among the rodents. These taxa imply a late Middle or early Upper Pleistocene age because *M. brecciensis* is the fossil ancestor of the extant form, *M. cabrerae*, which it replaced at around the time of the Middle/Upper Pleistocene boundary (*64*). A possible explanation for the discrepancy is that the shell sample contained a residual component of Holocene age (even if the rest were of infinite radiocarbon age, 5% of mid-Holocene material would have sufficed to bring the result up to ~31,000 years); if so, the human occupation would be significantly older. Alternatively, the shells of Pleistocene age could have been reworked from earlier, dismantled Quaternary terraces, in which case using the assemblage's marine invertebrates to make inferences about the diet of Middle Paleolithic humans, or about the chronology of the deposit, would be unwarranted.

These areas of uncertainty hindered the significance of Figueira Brava for two much-debated issues in Paleoanthropology — the late persistence of Neandertals in Iberia, and the role of marine foods in the diet of pre-Holocene humans. A quarter of a century after the pioneer work of Antunes and his team, the site therefore needed revisiting for the acquisition of archeological, geological and dating samples that might address the pending issues. In the field, such new work was carried out between 2010 and 2013, under the direction of one of us (JZ), and it has since been followed by the ongoing laboratory processing and study of the finds, as detailed in the following sections.

Field methods

Excavation

The archeological potential of Areas A-C was exhausted by the 1980s project. Therefore, the new work focused on Entrance 3 and the unexplored parts of the site's interior (Figs. S6-S12). Of these, Area D is but a long narrow between flowstone-capped fill and cave roof that only physically fit personnel can pass, while the NW corner of Area E is occupied by a very large disturbance suggestive of burrowing by badger or fox (Figs. S7a-c). Since no excavation was possible in the former and the stratigraphic integrity of the latter was compromised, the *locus* selected for further geological and archeological investigation was Area F (Figs. S7d-g): an elongated, low-roofed compartment separated from Area E by a dense alignment of stalagmites, columns and draperies. A small aperture through this speleothem curtain provided communication with Entrance 1 via Areas A-E and, thereby, an access route for the excavators. Equipment, finds, and the sediment bagged for sieving could in turn be passed back and forth directly via a small window situated between the roof of the cave and the large stalagmitic column plugging the back of Entrance 3.

In the first season of the new excavations (May 2011), a 1 m² trench (square U8) was opened in the center of Area F. This emplacement was selected for two reasons: (a) the geometry of the enclosing walls suggested

that the sedimentary fill would be at its thickest; and (b) a vertical joint in the roof created enough space above the floor for excavation down to arm's depth by a person kneeling or lying prone. The capping flowstone was cut with hammer and chisel to expose the cave earth underneath, and the stalagmites growing from the flowstone were removed and saved for dating and paleoclimate research (Figs. S7d-e, S8c-d). This initial trench was taken down to a depth of ~50 cm. In the second season (May 2012), the U>T8 profile was sampled for OSL dating (Fig. S9f) and grid unit T8 was then taken to the same depth as U8. Once bedrock was reached in both (at a depth of ~1 m), the excavation proceeded to squares U-T/7, whose eastern half was taken down to a depth of ~30 cm. The excavation of these half units was completed during the last season (May 2013), which, in addition, extended the work to grid units U-T/9, S8-SE and S9-SW, and to Entrance 3, where the SEx (*Sondagem Exterior*; Exterior Test) trench was open. The stratigraphic depth eventually reached in each sector is indicated in Fig. S6. Lighting was provided by battery-powered LED panels during the first season; afterwards, electric cable connection to either a generator or the national power grid made it possible to use large fluorescent lamps and machinery (e.g., jackhammers).

Through the excavation of the Area F deposit, the contrasts in texture and color and the recurrence of incrustation patches and flowstone sheets, out of which stalagmites often grew, provided clear stratigraphic markers. Individual décapage units, called "spits," scrupulously respected observed stratigraphic boundaries (inevitably, whenever power tools had to be used, in approximate manner only). The natural topography of the surface of each new unit was carefully exposed and recorded before work proceeded toward the next one down. When thicker than 5 cm, stratigraphic units were split into subdivisions that respected the observed dip of the stratification. Interstratified speleothems were systematically collected for U-series dating (Figs. S8-S10).

In Area F, the first step of the excavation process consisted in cleaning away the burrowed sediments found immediately below the capping flowstone to expose the intact, but deeply scarred, Pleistocene deposit underneath. The latter's compact, often cemented or brecciated surface made for a sharp contact, easily detectable to the touch, with the reworked, very loose, overlying or adjacent parts of the fill. The openings of small, narrow tunnels penetrating further down into the deposit were also identified at this stage; they were eventually emptied, and the finds they contained carefully separated out, prior to subsequent excavation of the surrounding *in situ* sediment (Figs. S7g, S9a-b).

Most stone tools are quartz; of these, only cores and retouched pieces, or their fragments, plus complete and proximal debitage products, were piece-plotted. The small percentage of flint and quartzite artefacts, and the faunal remains identifiable to taxon or body part, including the remains of birds, fishes, mollusks and crustaceans, were systematically plotted. Cut-offs were set at 2.5 cm for lithics and 5 cm for faunal remains (except when diagnostic; among the lithics, e.g., retouched items; among the fauna, e.g., epiphyseal fragments, loose teeth, small but unbroken gastropods, large valve fragments and fragments of rare mollusk taxa). Finds not matching these criteria were bagged together according to their stratigraphic and quarter-square-meter unit of excavation provenience.

The excavated sediment was sieved or floated in its entirety. During the first two seasons, the >3 mm fraction was dry-sieved and sorted at the dig. The residue was collected in large cuts of flexible, <0.5 mm

"mosquito"-mesh, washed in the immediately available seawater to reduce weight, and then transported to the field laboratory where, after thorough fresh-water cleaning, it was left to dry and sort. To avoid unintended contamination related to small mammal burrowing, only those wood charcoal particles collected during excavation in clearly intact areas of the deposit were kept for analysis and potential dating. Given the paleobotanical interest revealed, the procedure was modified for the last season; the residue passing the 3 mm dry-sieve mesh was then bagged and transported to the field laboratory for floatation and a more thorough acquisition of plant remains.

Spits were designated sequentially, top to bottom, from 1 to n, preceded by the letter A (in the interior excavation, spits A0 to A9; in the SEx trench, spits A49 to A53). Finds were also numbered sequentially, 1-to-n, per year of excavation (2011-1 to 2011-n; 2012-1 to 2012-n; 2013-1 to 2013-n), with further sub-numbering of bagged finds when individualization was necessary for description or cataloguing purposes (e.g., 2011-1-1 to 2011-1-n). At the dig, the finds were bagged with pre-printed number labels and their description, coordinates, stratigraphic provenience and associated field number were logged onto a database running on a battery-powered PDA.

Décapage surfaces (Figs. S9-S10) and stratigraphic profiles (Figs. S11-S12) were recorded via digital photography, aided by interpretative, on-site sketching made on prints thereof. Photo mosaics were assembled using PT GUI© or Microsoft ICE©, and orthorectified with the University of Venice's RDF© software. The physical constraints imposed by the cave's internal space (Figs. S7a-b, d-e) prevented the use of a total station, so piece-plotting was carried manually, using rulers and line levels. Elevations and three-dimensional piece-plotting data were recorded to the nearest centimeter, against the excavation grid and an arbitrarily set zero plane; the latter was physically defined on the interior wall of the cave at an elevation of 9.77 m asl. Linking to the national grid and the WGS84 datum was carried out via GPS-aided, total station topography of the accessible areas of the site: Entrances 1-3 and Areas A-C. The previously available compass-and-clinometer speleological survey of Areas D-F was then tied at both ends to the overall site plan.

Despite their variably indurated nature, the upper part of Area F's *in situ* deposit was amenable to excavation with hand tools: archeological trowel, occasionally aided by hammer-and-chisel. The lower part was much poorer in finds, consisted of rock-hard breccia capped by continuous flowstone, and its excavation required the use of jackhammers; and ditto for the SEx trench. Even though we saved and further lab-processed the small blocks into which the cemented portions of the deposit had to be jackhammer-reduced, the difference in recovery technique must be borne in mind when comparing the contents of the upper part of the interior deposit with either its lower part or the SEx trench.

Dating

Radiocarbon dating (Tables S1-S2) used single-shell samples: (a) six from the exterior area of Entrance 3 collected *in situ* while cutting the blocks for soil micromorphological analysis; (b) two from the Area F trench collected in the reworked deposit found immediately under the capping flowstone; and (c) five from the 1980s excavation archive labelled as coming from Area C's Pleistocene deposit.

U-series dating used samples of the flowstone and stalagmites capping the fill and of interstratified speleothems (flowstone sheets or stalagmites buried by subsequent sedimentary build-up). As an aid to the reconstruction of the site's original setting, speleothems from the exterior area of Entrance 3 were also dated; samples were either cut from extant remnants (e.g., of hanging flowstone) or machine-cored from *in situ* stalagmites (Tables S3-S6; Figs. S4-S11).

Single-grain optically stimulated luminescence (OSL) dating was performed on six sediment samples collected at the beginning of the 2012 field season from exposed stratigraphic profiles (Tables S7-S10; Figs. S5-S6, S9f, S11b). Depending on the local hardness of the deposit, the samples were collected using PVC tubes and metal cylinders (samples FB12-1, FB12-2, FB12-5, FB12-6) or extracted as intact blocks of consolidated sediment (samples FB12-3, FB12-4). *In situ* gamma dose rate measurements were performed in the OSL sample holes to assess spatial heterogeneity in the surrounding gamma radiation field of each sample. Approximately 500 g of additional bulk sediment was collected from the surrounding few centimeters of each sample hole for beta dose rate determination and water content analysis. Samples FB12-1, FB12-2 and FB12-4 were collected from layers 2 and 4 of the 1986 excavation trench in Area C (Fig. S5e-f), samples FB12-5 and FB12-6 from the U>T8 profile of Area F (Fig. S9f), and sample FB12- from Cut D of Entrance 3 (subsequently excavation-expanded to form the exterior trench, SEx; Figs. S4d, 11b).

Geoarcheology

For correlation with the sequence observed in the 1980s excavation of Area C, a stratigraphic column of the brecciated deposit preserved in Entrance 3 was drafted during a week-long field season carried out in July of 2010. Given the hardness of the sediment, it was decided that the best approach to its archeological study was via soil micromorphological analysis of representative thin sections. Using an angle grinder, 18 undisturbed samples spanning the entire column, from top to bottom and in continuous manner, were extracted along six exposures, designated Cuts A-F (Table S11; Figs. S4d, S11b-e). Subsequently, two samples from the interior deposit were cut from portions of variably carbonate-encrusted sediment saved for that purpose during the excavation. Eleven of these samples were selected for processing and analysis. In addition, bulk samples of unconsolidated sediment, approximately 1 kg each, were taken in non-brecciated areas of the deposit for an analysis of their composition — six from Area F and one from the SEx trench.

Lab methods

Soil micromorphology

After marking and oven-drying at 60 °C, the samples for soil micromorphological analysis collected in the field were sent to the *Servizi per la Geologia* laboratory (Piombino, Italy). Preparation went through the following stages: impregnation with a mixture of resin, styrene and hardener; curing; cutting into cm-thick slabs; and final preparation of 30 µm-thick sections measuring 95 mm by 55 mm (Fig. S13). The thin sections were analyzed at the University of Trento's *Laboratorio B. Bagolini* using an Olympus BX51P polarizing microscope with magnifications between 20× and 1000×, under plane-polarized light (PPL), crossed-polarized

light (XPL), and incident light (the latter for observation in standard light conditions and for primary fluorescence). Fluorescence observation was performed using two distinct wideband filter combinations: ultraviolet and blue (super wideband), with excitation filters respectively between 330-335 and 420-480 nm, and corresponding suppression filters at 420 and 520 nm. Thin-section description followed Bullock *et al.* (*65*) and Stoops (*66*).

Composition analysis

To assess the relative weight of the deposit's different components (matrix, lithics, bone, shell), ~100 g sub-samples were extracted from the field-collected samples of bulk, unconsolidated sediment. The sub-samples were disaggregated and then passed through a manually shaken sieve column with three mesh sizes: 4 mm, 2 mm, and 1 mm. The material collected in each sieve was then weighed and macroscopically sorted with fine tweezers. This was done by placing the sediment on a white sheet obliquely illuminated by artificial light. After sorting, each category was briefly scanned under a Meiji EM213 TR microscope to decide on instances for which macroscopic examination had been insufficient and to fix any identification errors made during the preceding stage. The sorted assemblages were weighed on a digital scale with centigram precision. The different steps of the process were photo-recorded with a Leica Wild M3C microscope or a Nikon Coolpix E995 camera.

For comparison, the procedure was repeated for bulk samples taken from a Portuguese Mesolithic site, the Toledo shell-midden (*67*). As published analyses of similar deposits use density (e.g., N/m³, or Kg/m³) to quantify the proportion of the different components, the volume of each of our sub-samples had to be derived from the corresponding weight. We calculated using an average density of 1.45, which we have derived from the measurement of the weight and volume of a ~5 kg sample of loose sediment retrieved in a reworked pocket below the capping flowstone and featuring the same mix of components (matrix, shell, bone and lithics). Our value is marginally higher than the standard for dry loose sand (1442 kg/m³) but lower than the standard for packed sand (1682 kg/m³; https://www.vcalc.com/wiki/KurtHeckman/Sand+Density; accessed November 6, 2017). Therefore, in inter-site comparisons, the density numbers provided for Figueira Brava are likely to represent somewhat of an underestimation.

Micropaleontology

Sub-samples of the sediment collected in the field for analysis of the deposit's composition were processed to investigate their micropaleontological component. These sub-samples were washed with mesh diameters of 63 μm, 125 μm, 250 μm, 500 μm and 1 mm. The different fractions were then hand-picked for foraminifera fossils under a Leica MZ8 binocular microscope.

Radiocarbon dating

Shell samples were submitted to AMS (Accelerator Mass Spectrometry) radiocarbon dating at ORAU (Oxford Radiocarbon Accelerator Unit) and the National Ocean Sciences Accelerator Mass Spectrometry (NOSAMS) facility, Woods Hole (MA). For these kinds of samples, ORAU uses a stepped pre-treatment protocol consisting

of cleaning and removal of the outer surface by air abrasion with aluminum oxide powder (or acid-etching with 0.2M hydrochloric acid), followed by rinsing with ultrapure water (using ultrasonication if required), drying, rough crushing, and *in vacuo* phosphoric acid reaction (*68*). At NOSAMS, shell samples are cleaned and then dated with a hydrolysis process — conversion to CO_2 of the carbon in the sample via direct hydrolyzation with strong phosphoric acid (H_3PO_4). The calibration of these results was carried out with the Marine13 curve (*69*).

U-series dating

Sub-samples for U-Th dating were either drilled as powder samples using a handheld microdrill with a tungsten carbide drill bit or cut using a microdrill fitted with a diamond cutting disk. Cut pieces were cleaned in MQ (Milli-Q) water using an ultrasound bath and then dried.

The samples are weighed and transferred into pre-cleaned Savillex PFA containers. MQ water is added and the samples completely dissolved by adding sufficient 7 M HNO_3 (Romil™, supra purity (sp) grade). A mixed ^{229}Th-^{236}U tracer is then added to the solution. The container is tightly closed, and the solution is refluxed on a hotplate at 80 °C for several hours to equilibrate sample and spike and then evaporated to dryness. The sample is dissolved again with 50 μl concentrated HNO_3 (Romil™ sp) plus 50 μl concentrated H_2O_2 (Romil™ sp). The container is tightly closed and placed on a hotplate at 90 °C for a minimum of two hours. Then, 50 μl concentrated HCl (Romil™ sp) is added to the solution, the container is tightly closed and placed again on a hotplate at 90 °C for at least 12 hours. The solution is then dried down and the sample dissolved in 600 μl 6 M HCl for column chemistry. Chemical separation and purification consist of a double resin procedure with AG 1-X8 used to separate U and Th followed by a first Th fraction purification using AG 1-X8 too. The final purification of the U and Th fractions is done using UTEVA resin. Further details can be found in Hoffmann *et al.* (*47, 70*).

U and Th isotopes are measured by multi-collector (MC) inductively coupled plasma mass spectrometry (ICPMS). Samples were analysed in two laboratories, the U-series laboratory of the geochronology section at the National Center for Human Evolution Research in Burgos, Spain (CENIEH; *Centro Nacional de Investigación sobre la Evolución Humana*), and the U-series laboratory of the Department of Human Evolution at the Max Planck Institute for Evolutionary Anthropology (MPI-EVA) in Leipzig, Germany. Identical spike, standard solutions, instrumentation and analytical protocols were used in both laboratories. Mass spectrometry analyses are done following procedures outlined in Hoffmann *et al.* (*71*) using a ThermoFinnigan Neptune MC-ICPMS. The Neptune is equipped with the Neptune plus interface, an energy filter — RPQ (Retarding Potential Quadrupole) lens — for small ion beams measured on the central ion counter (MasCom SEM). For sample introduction, a setup including a Cetac Aridus II with Quickwash and a Savillex PFA nebuliser tip with a 35 μl/min uptake rate is used.

U and Th isotope compositions are separately measured. A sample-standard bracketing protocol is used for both U and Th isotope ratio measurements. Procedural chemistry blank values are typically less than 1 pg ^{238}U, 1 fg ^{235}U, 0.1 fg ^{234}U, 1 pg ^{232}Th and 0.1 fg ^{230}Th, respectively. Activity ratios are calculated from isotope concentration ratios using the following decay constants: $\lambda_{238} = (1.55125 \pm 0.0017) \cdot 10^{-10}$ a^{-1} (*72*), $\lambda_{234} = (2.826 \pm$

0.0056)$\cdot 10^{-6}$ (*73*), λ_{232} = (4.95 ± 0.035)$\cdot 10^{-11}$ (*74*), λ_{230} = (9.1577 ± 0.028)$\cdot 10^{-6}$ (*73*). Analytical errors are quoted at 95 % confidence.

The degree of detrital ^{230}Th is indicated by the measured ^{230}Th/^{232}Th activity ratio and corrections were calculated using the conventional "bulk earth" value, i.e. a detrital ^{238}U/^{232}Th activity ratio (correction factor) of the upper continental crust (*75*) of 0.8 with 50% uncertainty and a ^{238}U decay chain in the detrital component in secular equilibrium. Isochron analyses (Fig. S14) are done using Osmond type five points isochrons (*76*).

Single-grain OSL dating

The six OSL dating samples were processed under safe (dim red) light conditions at the purpose-built CENIEH luminescence dating facility (Burgos, Spain). The ends of the PVC or metal tubes and the exposed outermost layers of the intact blocks were first removed down to a depth of at least 2 cm to ensure that only the un-illuminated centers were isolated for optical dating. Quartz grains of 212-250 µm diameter were prepared for burial dose estimation using standard procedures (e.g., *77*), including heavy liquid density separation at 2.72 g/cm^3 and 2.62 g/cm^3, and a 48% hydrofluoric acid etch (40 minutes) to remove the alpha-irradiated outer layers of the quartz extracts. OSL measurements were made using the experimental apparatus described by Arnold *et al.* (*78, 79*). Samples were irradiated with a Risø TL-DA-20-mounted ^{90}Sr/^{90}Y beta source that had been calibrated to administer known doses to multi-grain aliquots and single-grain discs (average single-grain dose rate at the time of measurement = 0.149 Gy/s). For single-grain measurements, spatial variations in the beta dose rate across the disc plane were considered by undertaking hole-specific calibrations using gamma-irradiated quartz (*80*). Quartz grains with a diameter of 212-250 µm were measured in aluminum discs drilled with an array of 300 × 300 µm holes to ensure true single-grain resolution (*81*).

Equivalent dose (D$_e$) values were determined using the single-aliquot regenerative-dose (SAR) procedures (*82*) shown in Table S7. For the single-grain SAR procedure, sensitivity-corrected dose-response curves were constructed using the first 0.08 s of each green laser stimulation after subtracting a mean background count obtained from the last 0.25 s of the signal. For the multi-grain SAR procedure, sensitivity-corrected dose-response curves were constructed using the first 0.8 s of each blue LED stimulation after subtracting a mean background count obtained from the last 0.10 s of stimulation. The suitability of the SAR D$_e$ determination procedure shown in Table S7 was evaluated by undertaking a series of multi-grain aliquot and single-grain dose-recovery tests on sample FB12-1. Multi-grain aliquot dose-recovery tests were first used to ascertain optimal preheating conditions for bulk grain populations. These tests were performed on ~180-grain aliquots using a series of different regenerative dose preheat (PH$_1$) conditions (ranging between 200 °C for 10 s and 260 °C for 10 s) and two different test-dose preheat (PH$_2$) combinations (160 °C for 10 s or 200 °C for 10 s). A known laboratory dose of 100 Gy was applied to groups of 3-4 aliquots after optically bleaching their natural OSL signals using two 1,000 s blue LED stimulations separated by a 10,000 s pause (to ensure complete decay of any photo-transferred charge in the 110 °C TL trap). The administered dose was treated as a surrogate natural dose and subsequently measured using the multi-grain version of the SAR sequence shown in Table S7. To confirm the suitability of the SAR procedure at the single-grain scale, we repeated the dose-recovery test on 600 individual quartz grains from sample FB12-1 using a subset of the multi-grain preheat conditions. A higher dose

of 150 Gy was administered to these quartz grains after bleaching their natural signals using the same procedure described above. This higher administered dose was chosen as being closer to the expected natural dose of FB12-1, as determined from preliminary D_e measurements made on 100 grains of this sample.

Between 900 and 1900 single-grain D_e measurements were made for each sample. Individual D_e values were only included in the final age calculation if they satisfied a series of standard and widely tested quality-assurance criteria, as detailed in Arnold *et al.* (*78, 79*) (Table S8). Single-grain OSL D_e estimates were rejected from further consideration if they exhibited one or more of the following properties: (i) weak OSL signals (i.e., the net intensity of the natural test-dose signal (T_n) was less than three times the standard deviation of the late-light background signal); (ii) poor recycling ratios (i.e., the ratios of sensitivity-corrected luminescence responses (L_x/T_x) for two identical regenerative doses were not consistent with unity at 2σ); (iii) high levels of signal recuperation/charge transfer between SAR cycles (i.e., the sensitivity-corrected luminescence response of the 0 Gy regenerative dose point amounted to >5% of the sensitivity-corrected natural signal response (L_n/T_n) at 2σ); (iv) anomalous dose-response curves (i.e., those displaying a zero or negative response with increasing dose) or dose-response curves displaying very scattered L_x/T_x values (i.e., those that could not be successfully fitted with the Monte Carlo procedure and, hence, did not yield finite D_e values and uncertainty ranges); (v) saturated or non-intersecting natural OSL signals (i.e., L_n/T_n values equal to, or greater than, the I_{max} saturation limit of the dose-response curve at 2σ); (vi) extrapolated natural signals (i.e. L_n/T_n values lying more than 2σ beyond the L_x/T_x value of the largest regenerative-dose administered in the SAR procedure); (vii) contamination by feldspar grains or inclusions (i.e., the ratio of the L_x/T_x values obtained for two identical regenerative doses measured with and without prior IR stimulation (OSL IR depletion ratio; Duller, 2003) was less than unity at 2σ).

Individual D_e estimates are presented with their 1σ error ranges in Table S9 and Figs. S15-S17, which are derived from three sources of uncertainty: (i) a random uncertainty term arising from photon counting statistics for each OSL or TT-OSL measurement, calculated using Eq. 3 of Galbraith (*83*); (ii) an empirically determined instrument reproducibility uncertainty of 1.6% for each single-grain measurement (calculated for the specific Risø reader used in this study according to the approach outlined in Jacobs *et al.* (*84*)); and (iii) a dose-response curve fitting uncertainty determined using 1000 iterations of the Monte Carlo method described by Duller (*85*) and implemented in Analyst.

Environmental dose rates have been calculated using a combination of *in situ* field gamma-ray spectrometry and low-level beta counting for samples FB12-1, FB12-2, FB12-3, FB12-5 and FB12-6. Time restrictions in the field prevented us from obtaining field gamma-ray spectrometry measurements for FB12-4, and so the environmental dose rate of this sample has been calculated using high-resolution gamma spectrometry (HRGS) (Tables S9-S10). The absence of *in situ* gamma-ray spectrometry measurements is not thought to have caused significant bias in the dose rate evaluation of sample FB12-4 (i.e., not beyond the existing dose rate uncertainty range) because the surrounding sediments were homogeneous silts and sands devoid of large clasts. Further support for the general spatial homogeneity of the deposits sampled in this study comes from comparison of beta dose rates obtained using replicate laboratory and *in situ* measurements for samples FB12-1, FB12-2,

FB12-3, FB12-5 and FB12-6: the weighted mean beta dose rate ratio obtained from beta counting and field gamma spectrometry measurements made on these five samples is 1.01±0.11.

In situ gamma dose rates were determined from measurements made using a Canberra NaI:Tl spectrometer. The 'energy windows' approach (e.g., [86]) was used to derive individual estimates of U, Th and K concentrations from field gamma-ray spectra. Beta counting measurements were made using a Risø GM-25-5 beta counter ([87]) on dried and homogenized, bulk sediments collected directly from the OSL sampling positions. Background-subtracted count rates were measured for three aliquots of each sample and compared with net count rates obtained simultaneously for a loess sediment standard with known U, Th and K concentrations ([88]). Final beta dose rate estimates were calculated after making allowance for beta dose attenuation due to grain-size effects and HF etching ([89]). HRGS measurements were performed on dried and powdered bulk sediments using a high-purity germanium co-axial detector, following the preparation, acquisition and calibration procedures outlined in Lesley ([90]). ~120 g of each sediment sample was sealed in a plastic container for at least 30 days (the equivalent of ~8 half-lives of ^{222}Rn; $t_{1/2}$ = 3.825 days) to enable the post-radon daughters of ^{214}Pb and ^{214}Bi to build up and reach equilibrium with parental ^{226}Ra activities. Following re-establishment of equilibrium in the post-radon nuclides, the sealed samples were counted for 3-4 days. In addition to calculating the environmental dose rate of FB12-4, HRGS was used to assess the present-day state of secular (dis)equilibrium in the ^{238}U and ^{232}Th decay series for a series of representative samples selected from each of the studied stratigraphic units (Table S10). The specific activities of ^{238}U (determined from ^{235}U emissions after correcting for ^{226}Ra interference, and ^{234}Th emissions after correcting for ^{228}Ra interference), ^{226}Ra (derived from ^{214}Pb and ^{214}Bi emissions), ^{210}Pb, ^{228}Ra (derived from ^{228}Ac emissions), ^{228}Th (derived from ^{212}Pb, ^{212}Bi and ^{208}Tl emissions) and ^{40}K were measured for each sediment sample, and used to derive daughter-to-parent isotope ratios for ^{226}Ra:^{238}U, ^{210}Pb:^{226}Ra and ^{228}Th:^{228}Ra.

Cosmic-ray dose rate contributions have been calculated using the equations of Prescott and Hutton ([91]) after taking into consideration site altitude and geomagnetic latitude, as well as density and thickness of sediment and bedrock overburden. A small, assumed internal (alpha plus beta) dose rate of 0.03±0.01 Gy/ka has been included in the final dose rate calculations based on published ^{238}U and ^{232}Th measurements for etched quartz grains from a range of locations (e.g., ([84, 92-94]) and an alpha efficiency factor (a-value) of 0.04±0.01 ([95, 96]). Radionuclide concentrations and specific activities have been converted to dose rates using the conversion factors given in Guérin et al. ([97]), making allowance for beta-dose attenuation ([89, 98]) where applicable. The beta dose rates, gamma dose rates (for samples FB12-1 to FB12-4; see below) and cosmic-ray dose rates have been corrected for estimated long-term water contents ([99]). The long-term water contents of samples FB12-5 and FB12-6 are based on present-day moisture evaluations, since the natural hydrological conditions of these sediments remain largely undisturbed in the closed, interior area of the cave and are representative of those prevailing throughout the sample burial periods. The present-day sediment water contents of the remaining samples collected from the exterior trench (FB12-3) and the 1986 excavation trench (FB12-1, FB12-2, FB12-4) are very low (3-10% dry sediment weight) and are not considered to be representative of the moisture conditions prevailing throughout the sample burial period because the exposures had dried out prior to sampling. The long-term water contents of these four samples are calculated

as being equivalent to 40% of their present-day saturated water values based on comparative proportional saturation assessments made on samples FB12-5 and FB12-6 from the deeper cave interior. A relative uncertainty of 20% has been assigned to the long-term moisture estimates to accommodate any minor variations in hydrologic conditions during burial.

Plant remains

The sediment excavated in 2013 was saved in its entirety for machine floatation in the laboratory. To recover the smallest remains, a 1 mm mesh was used for the heavy residue and a 0.25 mm mesh for the light fraction. The heavy residue was checked with a 10× magnifying glass to recover the archeological and botanical material that had not floated. The fine fraction was divided with a sieve stack (1 to 0.25 mm) and sorted under a Leica M165C low-power stereomicroscope.

Whether hand-picked during excavation or obtained through floatation, the charred plant material was analyzed following the protocol outlined in Badal *et al.* (*100*). Taxonomic identification was based on analysis of freshly cut tissue sections under a Leica DM6000 M with dark/bright field contrast modes and polarized light at 50-500× magnifications, supported by reference to the plant anatomy literature (*101*) and the collection of modern charred woods of the Laboratory of Archeology, University of Valencia. Detailed observation of specific features and of alteration and weathering factors was carried out at the Central Service for Experimental Research Support of the University of Valencia with Hitachi S-4100 and Hitachi S-4800 Field Emission Scanning Electron Microscopes coupled with the digital image acquisition system QUANTAX 200. The SEMs were configured with 10 KV and a 15 mm working distance; the samples were fixed with a carbon tape, metalized with gold-palladium to facilitate conductivity, and analyzed in vacuum conditions.

Zooarcheology

The faunal remains were variably, often extensively covered by calcareous concretions or stalagmitic crust, which were removed to the extent necessary (or possible). Taxonomic identification relied upon the osteological reference collections of the Archeological Science Laboratory (LARC; *Laboratório de Arqueociências*) of the General-Directorate for Cultural Heritage (DGPC; *Direcção-Geral do Património Cultural*), in Lisbon, for mammals, birds and fishes, and the Malacology Laboratory of the French CNRS (*Centre National de la Recherche Scientifique*) in Rennes, for the crabs. The studied sample includes the piece-plotted, the group-bagged and the >3 mm dry-sieve-collected remains of (a) marine invertebrates, (b) fishes, (c) birds, and (d) land vertebrates, except for the microfauna (rodents, insectivores and bats, plus amphibians and the smaller reptiles), the sorting and classification of which has yet to be completed.

The mammal bone material that could not be identified to a specific taxon was assigned to one of the following categories: (1) Very Large Macro-mammals (larger than 1000 kg, e.g., elephant, rhino); (2) Large Macro-mammals (from 300 to 1000 kg, e.g., horse, aurochs, bear); (3) Medium Macro-mammals (from 100 to 300 kg, red deer and other cervids); (4) Small Macro-mammals (from 20 to 100 kg, e.g., chamois, ibex, hyena, wolf); (5) Larger than Very Small Macro-mammals (clearly >20 kg animals that cannot be assigned to a specific

weight group); (6) Very Small Macro-mammals (<20 kg, e.g., lynx, wildcat, fox, rabbit); (7) Indeterminate (mostly, heavily fragmented remains).

Once its most evident lithic and faunal components had been sorted, the sieve and floatation residues were resubmitted to detailed examination for the small-sized remains of fish that might be masked by the sediments' variable but generally high level of incrustation. Fifty-five large bags of sediment (i.e., >1000 kg) have already been thusly processed, but this work has yet to be completed for parts of the *in situ* Pleistocene levels and most of the reworked deposit found below the capping flowstone. When necessary, the sediment was disaggregated in ultrasonic vats using tap water first, and then diluted acetic acid to improve the effect. As fully satisfactory results could not be obtained, 16 bags have been reserved for future disaggregation by other means. The treated sediment was entirely sorted under a modular stereomicroscope customized with light ring (Leica MZ6, 6.3:1 zoom), after which the fish remains identified were further treated to remove the adhering matrix to the extent required for taxonomic identification. Bone surfaces were cleaned with stitching pins, dental scalers and tweezers, which often succeeded in removing the concretions without damaging the bone surface underneath. When these procedures were not effective, selected specimens, namely fish teeth, were cleaned using a buffered solution of acetic acid with a pH of about 3.1 obtained by adding 5 mg of powdered calcium carbonate to 50 ml of acetic acid. After filtering, another 200 ml of fresh acid was added to the solution and the pH checked using suitable indicator paper. Good results could be obtained with no more than 15 minutes of immersion.

Taxonomically identified remains were counted by NISP (Number of Identified Specimens) and MNI (Minimum Number of Individuals). For land vertebrates and mollusks, standard procedures were followed. For the crab remains, the MNI was based on the pincers and corresponds to the highest figure for the left or the right finger — propodus (unmovable finger) or dactylopodus (flexible finger) — in each stratigraphic unit. The carapace width of *Cancer pagurus* individuals was estimated from the length of the pincers using a linear regression derived from measurements made on a sample of 50 individuals from the reference collection (R^2>0.95). For the fish remains, the MNI was estimated using unpaired cranial elements, as well as vertebrae when their features and size permitted assignment to species or location in the vertebral column. To minimize bias, fish MNI estimates also considered intra-species bone size. Taphonomic alterations were noted, as were standard indicators of the remains' natural or anthropogenic accumulation (orientation and type of breaks, occurrence of carnivore- or rodent-gnawing, typology and location of percussion and cut marks).

The taxonomy of mollusks used the Linnaean designation listed as "accepted" in WORMS (World Register of Marine Species; http://www.marinespecies.org/index.php, accessed October 17, 2018). Following Dupont (*102*) and Gutiérrez-Zugasti (*103*), their MNI was calculated as follows. The MNI for gastropods counts fragments where the apex is present. For limpets, this criterion includes body-complete, body-fragment and apical-only specimens. For spiraled gastropods, the MNI adds complete and broken specimens with a complete body whorl to (a) apical-umbilicus fragments and (b) the highest count for either apical, body whorl or umbilicus fragments. The MNI for bivalves adds complete umbones (from fragments or complete valves) to the highest count for either left- or right-side of anterior or posterior umbo fragments.

The large non-food bivalves were manually cleaned from their surface incrustation, to the extent possible, with a tooth pick and under the microscope. The removed sediment and the shell surfaces exposed were examined to check for the presence of pigmentatious materials or other anthropogenic modifications.

Use-wear

Fifty quartz artefacts were selected for examination under an Olympus stereomicroscope (up to 100× magnification) to detect macroscopic use-wear. This was followed by examination with an Olympus metallurgical incident light microscope equipped with Differential Interference Contrast (DIC) (up to 200×), which very effectively detects microscopic use-wear in heterogeneous rocks with highly reflective surfaces (e.g., quartz, quartzite) and allows for three-dimensional views of microtopography (*104*). Photomicrographs were taken with a digital camera Canon EOS 600D. The functional interpretations are based on comparison with a large experimental reference collection housed at LARC. This collection archives quartz, quartzite and rock crystal tool replicas applied by a joint team of zooarcheologists and lithic analysts in projectile throwing, butchery, hide-working and bone-processing tasks. These controlled experiments were designed to test the formation of use-wear on rocks that, in the Paleolithic and Mesolithic of Portugal, were used as frequently as flint (*104-106*).

Supplementary Text

S1. Stratigraphy and site formation

Under the microscope, the bedrock's most common lithotype is biocalcarenite. It is made up of fragments of limestone, shells (often affected by recrystallization or replacement by sparite) and a common silicilastic fraction (quartz and feldspar, as well as occasional muscovite and chert fragments). Grain-size mostly ranges from coarse silt to coarse sand. Micritic limestone and fossiliferous limestone are also present.

The sedimentary fill of Entrance 3 and Area F forms a single body whose excavation had to be carried out separately due to the presence of the massive stalagmitic column separating the two *loci* from roof to bedrock. Stratigraphic correlation is nonetheless possible thanks to the flowstone developing out of that column at approximately mid-elevation. This flowstone "skirt" extends both inward and outward, thereby providing the secure marker upon which the two areas can be linked as proposed in Fig. S6. Table S12 gives the equivalence between excavation spits and stratigraphic units as well as the correlation between the different areas excavated or geologically sampled and studied at the site, including Area C. Table S13 provides estimations of the volume of excavated sediment in the different units and trenches of Area F and Entrance 3 (some 3.5 m³ in total).

The stratigraphic succession studied 2010-13 is described, from top to bottom, in the text that follows. Illustration is provided in Figs. S11-S12, for stratigraphic profiles, and Fig. S13, for soil micromorphology thin sections, detailed description of which is given in Tables S14-S15.

S1.1. The Entrance 3 succession

Four complexes, within which several individual units can be differentiated, have been recognized in this *locus*. **UC** (Upper Complex) is formed of silty loam sediments alternating with flowstone. **MC** (Middle Complex) and **LC** (Lower Complex) are similar in composition but separated by an angular unconformity. Both contain sand grains, some deriving from the bedrock (sub-angular to sub-rounded grains) and others representing aeolian inputs (rounded to well-rounded grains); the noticeable increase in the amount of fine material, organic matter, and anthropic components found as one moves inward is their only, slight measure of lateral variation. **CO** (Conglomerate) is a clast-supported, cemented conglomerate resting on a marine abrasion surface and corresponding to the +5-8 m marine terrace reported in the literature (e.g., *107*).

In the SEx trench, the eroded surface of the fill was formed by sediments belonging to the upper part of the MC complex; a hard, cm-thick and continuous calcareous crust, developed over this surface in post-erosion times, further hardened the exposed Pleistocene breccia. The CO conglomerate was found immediately below the MC sedimentary fill; the stratigraphically intermediate LC complex, identified farther outward, is not represented here.

Complex UC

UC1 is the flowstone sealing the succession. It dips inward, intersecting the cave's roof and thereby contributing to the clog that obstructs communication with Area F.

Unit UC2 is 4YR4/4 silty loam with few angular fragments of limestone from the bedrock, strongly cemented and archeologically sterile. In thin section (Fig. S13, sample FB-1009), it appears as a sort of strongly carbonate-cemented quartzarenite; quartz sand grains are dominant, feldspar and limestone fragments are rare, and there are almost no anthropogenic or biogenic components (only a couple of shell fragments could be identified).

Unit UC3 is the carbonate crust sealing unit UC4.

Unit UC4 is identical to unit UC2 but for the few artefacts it contains at the base. Under the microscope, it displays apedal microstructure with channel and chambers, coarse components mainly in the class of siliciclastic constituents with scarce limestone fragments from the bedrock, burnt and unburnt bone, and a few shell fragments; the fine material is brown to strong brown, speckled, enriched in organic matter. These features indicate that the unit was subject to subaerial exposure and soil formation as an A horizon.

Unit UC5 is flowstone resting on unit UC6.

Unit UC6 is 5YR5/3 sandy silty loam with common sub-angular and sub-rounded fragments of limestone, few fine quartz grains, weakly organic, strongly cemented, with lithic artefacts and bones at its base.

Complex MC

Unit MC0 corresponds to the flowstone capping the underlying sequence.

Unit MC1 is a 5YR5/3 sandy silty loam with common stones (mainly angular and sub-angular fragments of limestone and dolostone, plus a few fine quartz grains), moderately organic, strongly cemented (sheets of flowstone or of secondary, microcrystalline carbonate of variable thickness are present) and with a gradual lower boundary.

Unit MC2 is 7.5YR5/4 silty loam with few stones (small fragments of limestone), moderately organic, and strongly cemented.

Lithic artefacts, bones, shell and charcoal fragments are present in both MC1 and MC2. In thin section (Fig. S13, samples FB-1018, 1019), MC1 shows moderately developed blocky structure and common, sometimes thermo-altered human and biogenic inputs, and microscopic features indicative of bioturbation and slight soil formation. The thin sections from MC2 display a heterogeneous groundmass with both natural constituents (sand grains of mostly quartz, polyquartz and feldspars, fragments of limestone from the bedrock, and reworked fragments of former soils) and anthropogenic or biogenic ones (fragments of shell and bone, sometimes burnt, as well as charcoal). Microstructure is moderately developed, sub-angular and blocky, while fine material is mostly reddish brown, speckled to dusty. In general, unit MC2 looks like an anthropized sediment that underwent slight soil formation, moderate biological activity and, possibly, some trampling.

Units MC3 to MC5 form a very homogeneous, strongly anthropogenic package. Unit MC3 is 7.5YR3/3 sandy loam (the sand is mostly derived from bedrock) with scarce stones (fragments of limestone from a few mm to 3 cm, mainly sub-rounded); it features moderately developed crumb aggregation masked by secondary carbonate accumulation, and is strongly organic, with fine, burnt organic matter. An anthropogenic component is frequent and strongly reduced in size (mm to 1 cm); it comprises fragments of shell and burnt shell, bone fragments (some burnt), and lithic artefacts. Unit MC4 is the strongly cemented MC3-like deposit found, erosion-exposed, at the top of Cut E, in intermediate stratigraphic position between MC3 and MC5. The latter forms the basal part of the MC complex and includes dense lenses of charcoal fragments and burnt shell.

In thin section (Figs. S11d, S13_sample FB-1002), units MC3, MC4 and MC5 are formed of siliciclastic sand grains and scarce to common fragments of Miocene limestone, with common, much broken and variably thermo-altered fragments of shell and (scarce) bones. The fine material is brown and enriched in organic matter. The structure is apedal, with channels, chambers and fine vughs. MC5 contains many sub-horizontally oriented shell fragments, often large and thermo-altered to a varying degree. These features denote an anthropogenic accumulation and may relate to the wasting of hearth residues; the deposit was subsequently modified by biological activity and moderate soil formation (indicated by the well-developed, mm-thick phosphatic rinds of the limestone fragments).

Of those complexes making up the Entrance 3 succession, only MC could be the object of archeological exploration (Figs. S6, S11a-b). Units MC1-MC2 were excavated as a single deposit, spit A49. Due to heavy cementation and the attendant need to use power tools, the interface with unit MC3 was exposed in approximate manner only. Therefore, both the artefact and the ecofact components of spit A50, which corresponds to the first 10 cm of the MC3-MC5 package, are likely to include an undetermined amount of material derived from the base of MC2 (probably negligible, because spit A49 was rather poor in finds). The remainder of the MC3-MC5 package, broadly corresponding to units MC4 and MC5, was excavated down to the beachrock as a single deposit, arbitrarily subdivided into three spits (A51, A52 and A53).

Complex LC

Unit LC1 is a thin layer formed of large, often thermo-altered, sub-horizontal fragments of *Mytilus* sp. shells (no other species were detected) that also contains quartz artefacts; the sediment is locally clast-supported, and the fine material is a scarce, 7.5YR5/4 sandy loam.

Unit LC2 is 7.5YR5/4, well-packed sandy loam, with common stones (heterometric fragments of limestone, sometimes weakly weathered), often lying parallel to the layer's interface; it contains occasional charcoal fragments and lithic artefacts, as well as a few shells. Under the microscope, the siliciclastic components are dominant, the fragments of limestone are subordinate, and shell and bone are common. The sediment is slightly bedded and contains orange-colored and microgranular fine material; the bedding dips ~15°.

Unit LC3 is a thin layer of beach sediment modified by trampling, rich in sub-horizontal *Mytilus* sp. shells (mostly fragments), locally clast-supported. The unit is strongly cemented by calcium carbonate and contains

fine material like that in LC2; the lower boundary is sharp and rests in paraconformity on the marine abrasion platform.

Microscopic observation (Fig. S13, samples FB-1021 and FB-1022) corroborates the field descriptions. Namely, it corroborates that the bulk of unit LC3 is composed of shells and shell fragments embedded in a groundmass showing the same features as overlying unit LC2.

Complex CO

The littoral succession is formed of two elements: conglomerate deposit and abrasion surface.

The conglomerate is a clast-supported (locally sand-supported) beachrock made of pebbles and cobbles (<15 cm, a few cm on average), rounded, mostly (>90%) limestone and dolomite, with occasional sandstone, with no preferred orientation plane; quartz elements are very rare and small. The matrix, strongly cemented by micrite and, locally, sparite, is 7.5YR6/5 sand (gray when weathered), formed of clasts with various shapes (sub-rounded and sub-angular ones prevail), quartz being common; it reaches a maximum thickness of 70 cm.

The abrasion surface is excavated in the Miocene bedrock and dips approximately N150E7S.

S1.2. The Area F succession

The succession exposed in Area F was divided into four complexes: **IT** (Interior Top), **IH** (Interior High), **IL** (Interior Low), and **IB** (Interior Base), with subdivisions, as summarized in Table S12. The different units of complexes IH and IL all dip inwards at a very low angle, contain speleothem fragments, and include variable amounts of often horizontally-lying limestone fragments spalled from the walls and roof of the cave (mostly cm to several cm in size).

Complex IT

Discontinuously distributed on top of the flowstone that, prior to excavation, formed the Area F ground floor, there was a thin scatter of loose, silty, reworked sediment derived from the Pleistocene deposit and brought up by subsurface burrowing: unit IT0. Adjacent to the window communicating Area F with Entrance 3, a thin layer of dark, loose, organic sandy loam, rich in fresh, well-preserved fish bone remains and containing uncharred fig seeds — unit IT2 — covered the capping flowstone. In profile view, this "black lens" could also be observed in intermediate position between two phases of flowstone development (Fig. S12a-b). However, the apparently overlying flowstone unit, IT1, formed in the Late Pleistocene, as shown by the U-series results for sample 1304 (Table S4). Given that the content of the IT2 deposit implies a very recent, probably near-present Holocene age, its position relative to the IT1 flowstone must reflect the filling-in of voids created in the fabric of the speleothem by post-Pleistocene erosional processes. Archeologically, unit IT2 was excavated as spit A0 (if surface) or A0b (the lenses under calcite laminae of the IT1 flowstone).

Complex IH

Unit IH1 is laminar flowstone composed of pure calcite with large, elongated fibrous crystals whose maximum thickness reaches 12 cm and from which several stalagmites and columns grow.

The undisturbed parts of the Pleistocene sediment were separated from the capping IH1 flowstone either by voids or by a layer of irregular thickness made up of very loose organic earth mixing reworked material (fossilized bone remains, Paleolithic stone tools) with Holocene intrusions, some of which very recent (e.g., fragments of the yellow chalk used to inscribe on the wall the previously mentioned 1984 date, or bits of the red tape originally posted by cavers to mark survey points). Such pockets of reworked sediment were archeologically excavated as spits A1 and A2 and, stratigraphically, belong in unit IT0 (Figs. S7g, S9a-b).

Units IH2 and IH3 are described as observed in the U>X8 profile, where, due to heavy cementation, they were least affected by subsurface burrowing. IH2 is well-cemented 7.5YR3/4 silty sand containing dark, organic fine material and scarce cm-sized stones and sand grains that mainly derive from the Miocene bedrock (well-rounded grains of aeolian origin are also present), as well as abundant fragments of digested bone. Unit IH3 is a sort of microconglomerate formed by the fragments of digested bone becoming dominant towards the base of IH2; this microconglomerate also contains some fine sub-angular and sub-rounded fragments derived from the bedrock. Archeologically, units IH2 and IH3 were excavated together as spit A3.

Units IH4 and IH6 are 6.5YR4/4, massive, not cemented, sandy loam with scarce stones; charcoal is apparent in profile view. They are separated by unit IH5, which is a thin, discontinuous calcareous crust featuring a few stalagmitic protuberances (Fig. S9c-e). Another such crust, unit IH7, seals unit IH8, which is a sandy loam whose color varies with the degree of cementation — between 6YR4.5/4 and 7.5YR5/5 — and in which stones (often horizontal) are common and archeological remains are abundant (Fig. S10a-e). Archeologically, units IH4, IH6 and IH8 were excavated separately as spits A4, A5 and A6, respectively.

Complex IL

Unit IL1 is a carbonate crust dipping inward with an angle of ~20-25° and on top of which significant stalagmite growth occurred (Fig. S10f-g). Unit IL2 is a 7.5YR5/4, strongly cemented layer of sandy silt with scarce to common stones, featuring interstratified lenses and other forms of calcite growth. The bottom unit of the complex, unit IL3, is 7.5YR5/6, poorly cemented, silty sand with scarce to common stones. Archeologically, this sequence was excavated as spits A7 (which spanned units IL1-IL2) and A8 (equivalent to IL3).

Complex IB

Unit IB1 is a discontinuous flowstone. Where present, it caps pockets of a variably cemented, 10YR7/2 silty sand, unit IB2, which fills irregularities in the Miocene bedrock. Archeologically, this complex was excavated as spit A9.

S1.3. Dynamics of deposition and erosion

The volume of Figueira Brava's original deposit can be estimated from (a) the width of the marine abrasion platform, ~30 m, (b) the elevation above the platform at which sediment-capping flowstone is found, ~3 m, and (c) the presence of speleothems even along the platform's seaward scarp, which implies a then-extant cave entrance situated farther out, where land has since become sea. These observations indicate that the original cavity was about the same size as Lapa de Santa Margarida, and let us estimate that, at the end of the

accumulation process, the roofed sedimentary fill would have reached a volume of about 2000 m³ — of which probably no more than ~5% survive.

The basal conglomerate is preserved in the Area C and SEx trenches at elevations of +5.2 m and +6 m, respectively, and at progressively lower elevation as one moves south along the exterior platform (+4 m along the southern wall of Entrance 2; Figs. S3, S6). From this evidence we can infer that the surface upon which the overlying archeological succession came to lie dipped to S or SW. In the interior cave, owing to the morphology of the encasing walls, this constraint translated into deposition along a NE-SW axis. As shown by the gradient in the elevation of both capping flowstone and basal bedrock (from +7.5 m and +6.2 m in Area F to +6.4 m and +4.6 m in Area C, respectively), the basal dip was maintained throughout. In the exterior platform, the origin and position of the sediment sources and the mode of sediment introduction also influenced the geometry of the deposit. Given spatial constraints, accumulation must have proceeded along a N-S or NW-SE axis, and in two steps: firstly, abutting the north wall of the cave along the intersection with the marine abrasion surface; secondly, once a near-horizontal plane was reached, which must have been the case at approximately +6.6 m (the elevation of the bedrock floor in Area F), filling-up the space left above, between that plane and the roof.

The observed stratigraphic patterns are consistent with this model, as shown by (a) the preservation in Area F, at the northern end of the site, but nowhere else, of complex IB, a sedimentary remnant predating the Last Interglacial marine erosion processes that eventually exposed the endokarst, (b) the limited spatial distribution of the LC complex along the seaward scarp, (c) the absence in Area F, but presence in Area C, of a lateral equivalent of the MC3-MC5 units of Entrance 3, and (d) the broadly horizontal disposition of the flowstone separating UC from MC. The inward dip of complexes UC (Entrance 3) and IH (Area F) further shows that, at the end of the process, the accumulation formed a cone with apex located outward of the present cave and at higher elevation. This geometry explains the preservation of voids behind the point at which the cone's brim intersected raised areas of the otherwise largely horizontal roof of Entrance 3.

In the now unroofed areas of Entrances 2-3, the cave's fill has since been eroded away. Most likely, slope dynamics, leading to receding of the porch, was involved in the initial stages of the process but, from the onset of the Holocene, the primary role was played by marine erosion.

These dynamics must be borne in mind if we are to understand the position of preserved remnants and excavated trenches relative to the evolving configuration of the inhabited space, with attendant implications for the behavioral interpretation of spatial patterns. Based on the above, our hypothesis regarding how Entrances 2-3 and Areas C-F changed through time is described in the following (Fig. S18).

Complex CO

Once sea level lowered from the interglacial peak and the cave became emersed, the surface revealed was bare rock in the northern, interior parts (Areas D-F). Across Area C and Entrances 2-3, it was a marine abrasion

platform covered by a sand and cobble beach that, at high tide, would have been recurrently inundated (Fig. S18b). During this site formation phase, the cave was not appropriate for human habitation.

Complex LC, Human Occupation Phase FB1

The retreat of the shore line exposed the abrasion platform and its sediment cover, making for a dry cave floor (Fig. S18c). In the northern sector (Entrance 3), such a floor corresponded to beach sands that abutted the north wall, extended at least some 10 m southward and a couple of meters westward, and, beyond, transitioned to beach cobbles. Seaward, this sands-within-the-cave formed a ground floor suitable for human occupation, the focal area of which, however, would have been farther out, in the then-extant cave porch. Therefore, the dense mussel-with-artefacts bed nowadays exposed by the erosional truncation of the site occupied, originally, a peripheral position — at the inner edge of the inhabitable space, several meters away from the main *loci* of human activity.

Complex MC-lower (MC3-MC5), Human Occupation Phase FB2

By this time, slope dynamics would have already cut back the entrance, and colluvial and windblown material would have accumulated fine sediments that covered almost the entire area of the cave, bare rock remaining exposed in Area F only (Fig. S18d). Entrances 2-3 formed an extensive, broadly horizontal sandy platform inward of but adjacent to the drip line — i.e., they were the roofed-but-well-lit interior of a large cave porch. Most of the archeological deposit then formed has since been truncated, or eroded away, but the preserved remnants are in areas that were central to the site and the archeological finds therein are fully representative of coeval human activity.

Complexes MC-upper (MC1-MC2) and IL, Human Occupation Phase FB3

Complexes UC and IH, Human Occupation Phase FB4

With continued accumulation, the sedimentary body's geometry changed to a cone whose apex was located higher-up and out at what is now sea, opposite Entrances 1-2. The inward slope of the cone's northwestern brim explains why, at this time, sediments began to spill all the way to the back of the cave, eventually forming interior complexes IL and IH (Fig. S18e-f). The archeological remains found in such narrow, low-roofed areas, inappropriate for human use, correspond to material syn-depositionally dispersed by low-energy processes (e.g., gravity or run-off) from the *loci* of actual human occupation, which were in the exterior porch. Put another way, the excavated material represents geologically *in situ* but not archeologically in place material — the colluvial scattering, along the surface of a debris cone, of artefacts and ecofacts related to human activities carried out a few meters away from the point of eventual archeological recovery.

S2. Dating

S2.1. Radiocarbon results

As a first step toward the reassessment of the site's chronology, five limpets from the 1986-89 excavation of Area C were dated by radiocarbon at Oxford (Table S1). One yielded an age of 2677±28 BP (OxA-19978;

Table S2). This result confirmed that the shell assemblage provenanced to that area's Pleistocene layer 2 includes material of Holocene age. The other four results fall in the 36.4-44.9 ka BP (thousands of radiocarbon years Before Present) interval. These ages imply that the date previously obtained on a bulk sample of limpets (ICEN-387; 30,930±700 BP) is erroneously young, possibly due to sample heterogeneity (presence of a minor component of recent Holocene age).

A periwinkle and a limpet from the subsurface, disturbed parts of Area F's sedimentary fill were subsequently dated to 7390±25 BP (OS-114170) and 12,880±45 BP (OxA-24055), respectively (Table S2). These additional results show that the reworked Pleistocene sediments also contain shells of mid-Holocene and Tardiglacial age.

During the first millennium cal BC (calibrated years Before Christ), the coastal waters of Portugal featured significant variation in upwelling. For around the time indicated by OxA-19978, the Δr value calculated by Soares and Dias (*108*) is 95±15 years, which translates into an Iron Age date for that sample: 383-203 cal BC. At the time, use of Serra da Arrábida's littoral caves for ritual purposes is documented by artefacts that denote settlement by (or establishment of commercial links with) people of Phoenician or Carthaginian origin (*109*). The sherds of Roman amphorae found in Area C imply that, 2000 years ago, erosional processes had already removed the Pleistocene deposit that once filled Entrance 1 and Area A, making access to Areas B-C of the site practical for humans. If, by then, the configuration of the exterior platform was already broadly like the extant, then such must also have been the case at the slightly earlier time indicated by OxA-19978. Thus, OxA-19978 may well stand for coeval human activity at Figueira Brava.

In the case of OxA-24055 and OS-114170, the dated samples must be washed-ashore, seabed shells of subfossil age. They cannot be anthropogenic because (a) the difficulty of the access route means that no human activity could have taken place in Area F prior to speleological discovery, and (b) we can exclude the possibility that they derive from Upper Paleolithic or Mesolithic deposits once extant in the exterior platform (nowhere at the site have artefacts suggestive of occupations of those periods been identified, and the dating of the capping flowstone remnants in both Entrances 2 and 3 shows that the space had filled-up prior to 50 ka).

These Area F shell samples both come from the SW quadrate of the T9 square, where excavation of the reworked fill revealed a dense midden of marine-eroded mussel shells associated with fresh bird bones, bits of plastic, scraps of cigarette-pack cellophane, and strips of the red tape used to mark survey points when the cave was first mapped in the 1980s (Fig. S7g). This midden must correspond to the nest of a mammal — probably, given the size of the subsurface chambers and tunnels identified at excavation, a rodent (or a very small carnivore, e.g., the weasel, *Mustela nivalis*). As with the other shells of similar surface appearance found therein and otherwise ubiquitously present in the reworked fill, the dated samples are animal-accumulated material brought into the cave for nest-building purposes.

In contrast, the mussel and limpet shells found *in situ* in the Pleistocene deposit show no patina, edge damage, or evidence (e.g., sponge holes) of having laid as empty valves, in the seabed, after the death of the animal. As discussed below, the *in situ* remains reflect the post-consumption discard of the shells of live mollusks harvested for their flesh, i.e., they are direct indicators of human activity at the site. However, the

radiocarbon ages obtained for them are significantly younger than the speleothems sealing the deposit they were found in. For Area C, the oldest shell result (OxA-19982; Table S2) falls in the 46.5-49.1 ka cal BP (thousands of years in the "calibrated Before Present" timescale) range, while the U-series date for the base of the overlying flowstone (sample 1025; Table S4) provides a *terminus ante quem* of 51.6 ka for the accumulation. In Entrance 3, the oldest result (OxA-24051; Table S2) falls in the 45.9-47.9 ka cal BP range, but the U-series dates for the stalagmite atop the remnant of the full sequence preserved between Entrances 2 and 3 provide a *terminus ante quem* of 57.3 ka (sample 1402; Table S6) for the accumulation. In addition, the complete set of Entrance 3 radiocarbon dating results features a fully reversed relationship between age and stratigraphic depth.

There can be little question, therefore, that the radiocarbon results obtained for the shell samples reliably associated with the Middle Paleolithic occupation of Figueira Brava are minimum ages only. Busschers *et al.* (*110*) report a comparable instance of radiocarbon ages in the 30-45 ka range for marine mollusk shells from geological deposits in the Netherlands that stratigraphy and dating by luminescence and U-series securely place in MIS (Marine Isotope Age) 5. An archeological site featuring a similar discrepancy is Cueva de los Aviones (Cartagena, Spain), where dates in the same 30-45 ka range were initially obtained for levels capped by flowstone subsequently dated by U-Th to 115 ka (*27*). In the Dutch case, the addition of younger carbon is thought to relate to bacterial activity, while a continued precipitation of carbonates is more likely to explain the anomaly at Aviones. At Figueira Brava, it may also be that the shells incorporated younger carbon via isotope exchange with water percolating subsurface during the formation of the flowstones that cap the deposit in Area C and Entrance 3. Indeed, given the results for sample 1304 (Table S4), the process remained active in Area C until at least 16.6 ka. In Entrance 3, the calcareous crust formed across the extant, erosion-scarred surface of the fill (Fig. S11a) shows that isotope exchange with environmental water continued through the Holocene (and the more so once the sampled shells became surface-exposed).

S2.2. U-series results

Table S4 lists the results for speleothems capping Areas C and F that provide age boundaries of direct interest for site formation issues and the history of the sedimentary accumulation. The field provenience and the samples themselves, together with details of their sub-sampling, are illustrated in Figs. S5-S8. The dated stalagmites (e.g., sample 1103) show continued growth until the LGM (Last Glacial Maximum). Afterwards, episodic accumulation of additional calcite — at the tip of previously formed stalagmites, or as stalagmite-like protuberances developing out of the flowstone surface — is documented in, respectively, the Holocene (sample 1105) and the Tardiglacial (sample 1304). Sub-samples 1304-3 and 1304-5, for instance, bracket the formation of unit IT1 and, together, provide a maximum age of 16.6 ka for the laterally abutting IT2 black lens.

The composition of the calcite making up the dated speleothems supports the site formation process inferred from the stratigraphic record. Most corrected and uncorrected ages for Area F (Table S4) are statistically the same, illustrating the samples' generally low level of contamination by detrital thorium — with a few exceptions, the ^{230}Th/^{232}Th ratios are high, between 44.9±0.4 and 1859.0±35.6, i.e., well above the threshold of 20 below which the correction for detrital ^{232}Th becomes statistically significant (*111*). The

exceptions concern stalagmite sub-samples taken from the external layers (e.g., 1105-1, 1304-5 to -3) or very close to the base of the flowstone the stalagmite attached to (1207-6). Even in these cases the differences between corrected and uncorrected ages remain minor and the results' chronostratigraphic significance is not impaired.

This pattern corroborates that closed cave conditions prevailed in Area F minimally from 76.9 ka, the younger limit of the probability interval for sub-sample 1207-6. The re-establishment of open cave conditions occurred sometime between 5.3 ka (the latest possible age of sub-sample 1105-1) and 29.7 ka (the earliest possible age of sub-sample 1304-1, the most recent of the U-series dates for Area F's capping speleothems that is associated with a high ^{230}Th/^{232}Th ratio). The low ^{230}Th/^{232}Th ratios found in some sub-samples of Area F's interstratified stalagmites (samples 1106 and 1209; Table S5), which formed in the open cave environment extant during the accumulation of that area's Pleistocene fill, support such a speleogenetic interpretation of the Th content of Area F's samples.

The spread of the results obtained for sub-samples taken closest to the contact between calcite and sediment (i.e., within millimeters of that contact) is significant. In Area C, for instance, flowstone formation did not begin until, at the earliest, ~52.8 ka (based on the 1025-1 result), while, in Area F, the oldest possible ages obtained range between 62.0 ka (based on the 1028-1 result) and 81.9 ka (based on the 1207-6 result). Thus, even though flowstone eventually came to form a continuous crust across Areas C-F, the process must have begun at different moments in different spots of the pre-existing surface, and the accumulation of the archeological deposit most likely ended before the minimum age of 76.9 ka provided by sub-sample 1207-6. The lenses of undated, dirtier calcite separating this sub-sample from the base of the speleothem corroborate the gap (Fig. S8d).

Table S5 provides complete sets of results for interstratified speleothems from the Area F trench. The samples themselves, together with details of their sub-sampling and field provenience, are illustrated in Figs. S8-S10. In general, contamination with detrital thorium is an issue with the upper parts of these samples, implying in some cases corrected ages that are statistically younger than the uncorrected ones (but only slightly so). In the case of sample 1106, a reliable, sufficiently precise isochron age for the speleothem's tip could be derived from five sub-samples taken along a single calcite lamina. The explanation for this moderate contamination problem is likely to reside in that (a) during a hiatus in sedimentation, speleothems developed out of the stabilized ground floor and (b) the precipitation of the last layers of calcite forming their tips and outer rinds happened when deposition of colluvial or windblown material had already resumed.

Sample 1208 is a stalagmite-like protuberance formed at the same elevation as the very thin carbonated crust along which units IH4 and IH6 were stratigraphically differentiated (Fig. S9d-e). This episode of calcite precipitation constitutes unit IH5 of the sequence. The five sub-samples taken along the growth axis of 1208 yielded corrected ages that are statistically the same, suggesting rapid growth during a very short period of marked slowdown — rather than complete interruption — of sediment deposition. This inference is consistent with the thinness of the speleothem and the fact that the stratigraphic units above (IH4) and below (IH6) are geologically and archeologically indistinguishable.

Sample 1106 is a tumbled stalagmite that grew directly atop archeologically rich unit IH8. As clearly seen in the sampled section (Fig. S10b), the base of this speleothem is a mass of stones, bones, shells and quartz artefacts cemented by carbonates precipitated in the voids of the sedimentary matrix — indicating that no hiatus existed between the accumulation of IH8 and the beginning of the phase of speleothem growth (unit IH7 of the sequence) this sample corresponds to.

Samples 1301 and 1302 (Fig. S10c-e) formed during the accumulation of unit IH8, the former adjacent to but at slightly higher elevation than the latter. Both are protuberances of precipitated calcite that dripping "hotspots" created on the surface of the sedimentary fill while deposition of sediments proceeded uninterruptedly. This is reflected in the significant detrital contamination of some sub-samples, which in turn must underpin the occurrence of some outliers (e.g., sub-sample 1301-6). As with 1208, and agreeing with the dating results, the thinness of these protuberances suggests that they represent a narrow time interval.

Sample 1209 (Fig. S10f-g) is a stalagmite whose base documents, as with sample 1106, a phase of flowstone and stalagmite growth (unit IL1) developing without discontinuity as a preceding phase of sediment accumulation, in this case unit IL2, was coming to an end. Sub-sample 1209-4 implies that, ~91.8 ka, the stalagmite was still growing, but sample 1302-1 from overlying unit IH8 implies that, ~88.9 ka, sedimentation had already resumed. Therefore, the hiatus in sedimentation that corresponds to this phase of speleothem growth lasted at most some three millennia (but could have been much shorter because the results for 1209-4 and 1302-1 are statistically indistinguishable).

Sample 1306 (Fig. S8e-g) features a complex fabric and, despite the limited thickness of the speleothem (~6 cm), the dated sub-samples span an interval of about 40,000 years. Under an assumption of continuous, uniform growth, 1.5 mm of calcite would have accumulated at this spot per every millennium of that interval. Such a rate, however, is not consistent with the difference (minimally, five millennia) between the ages for sub-samples 1306-3 (141.5±1.6 ka, 2σ) and 1306-2 (150.2±2.1, 2σ), separated by ~2 mm only. This speleothem is therefore likely to stand for several discrete pulses of calcite formation, of which the most recent, represented by sub-sample 1306-1, provides a *terminus post quem* of 111.3 ka for the overlying archeological deposit.

Table S6 lists complete sets of results for samples taken in the exterior, at present unroofed side of the cave. The samples themselves, their field provenience and details of their sub-sampling are illustrated in Figs. S4, S6-S11. The results obtained corroborate that, until the Tardiglacial, Figueira Brava's marine abrasion platform remained buried under a sedimentary fill that, horizontally, extended to at least the scarp separating the platform from the sea, and, vertically, rose to at least 2-3 m above that platform, often to the roof of the cave.

Entrance 2 samples 1406 and 1407 and Entrance 3 samples 1026, 1402 and 1405 are from flowstone or stalagmite developing atop, or from the surface of, the original fill. Except for sample 1406, detrital contamination is significant, suggesting some degree of exposure to the atmosphere and/or the continued mobility of sediment particles (e.g., via run-off), across the surface of the deposit, through the time of calcite precipitation (note that, outward from the flowstone-cum-breccia barrier that eventually isolated Areas C-F, some amount of empty space remained between the deposit and the cave's irregular roof, as discussed in

section S1.3. above). The result for sub-sample 1406-1 shows that by 45.0 ka flowstone had already begun to form atop the sedimentary fill. This *terminus* is consistent with the chronology obtained for the flowstone capping the cave's interior and supported by the other results: taken together, the interval bracketed by this set of samples is 16.9-70.6 ka, nearly identical to that defined by the results for Areas C and F (Table S4). The results for sample 1026 are especially relevant because (a) the sample corresponds to unit UC1, i.e., the flowstone directly atop the remnant in which Entrance 3's UC complex was described (Fig. S4e) and (b) the chronometric constraint implied is the same as that set for Area F by the cleaner IH1 flowstone (sample 1028) found in correlated stratigraphic position.

Sample 1027 is from an Entrance 3 stalagmite. The isochron age was calculated from five sub-samples taken along a rind that contains charcoal and flint fragments, showing that the calcite precipitated onto archeological sediment in direct contact with the stalagmite's edges (a flint core is found at the same elevation in an adjacent roof-adhering remnant; Fig. S4d). Given the date obtained (81±6 ka, 2 σ; i.e., <87 ka) and that the correlation between the MC0 and IL1 flowstone sheets implies that both formed >88.9 ka (the *terminus ante quem* set by sub-sample 1302-1), sample 1027 must represent a later phase of calcite precipitation: most likely, the beginning of Entrance 3's flowstone capping. This is because the stalagmite the sample comes from belongs in an ensemble of columns attached to a lowered septum of the cave's roof, from which the speleothems now hang (the sedimentary fill from which they originally developed out having since been eroded away; Figs. S4d, S11e).

Sample 1029 is from the rind of the external (Entrance 3) side of the large column beyond which Area F is found. The excavation of the latter showed that the base of the column lies on bedrock, but the sample was collected half-way between the roof above and an exposure of unit MC0 below (Fig. S4e). The column's core formed prior to the accumulation of the sedimentary succession and the external layers sampled represent resumption of dripping and calcite precipitation, eventually covering its upper part with a newer calcite skin formed when the base had already been buried by the IL/MC sediment. This process led to the development of the IL1/MC0 units as the flowstone "skirt" that, all around the column, caps the IL and the MC complexes, thereby providing a backbone for the stratigraphic correlation of Area F and Entrance 3 (Figs. S6, S7f, S11b). Of the two sub-samples measured, the most external (1029-2) is somewhat older, and the difference is statistically significant, but the low ^{230}Th/^{232}Th ratio (13.54±0.11) suggests that the reversal is likely due to detrital contamination issues. The corrected and uncorrected ages for sub-sample 1029-1 are statistically the same, so this result (a) provides a reliable *terminus post quem*, 91.0 ka, for the UC complex, in agreement with its correlation with Area F's IH complex and (b) is consistent with the *terminus ante quem* set by samples 1026, 1402, 1405 for the sediment of the UC complex that once filled the now empty space in front of the sampling point.

S2.3. Single-grain OSL results

Table S9 provides a summary of the environmental dose rates, D_e values and final ages obtained for the six OSL dating samples. The results of HRGS measurements performed on four representative samples from the studied stratigraphic units are shown in Table S10. Daughter-parent isotopic ratios for ^{238}U, ^{226}Ra, ^{210}Pb, ^{228}Ra

and ^{228}Th are consistent with unity at either 1σ or 2σ, indicating that the ^{238}U and ^{232}Th chains exhibit present-day secular equilibrium. The grain-size-attenuated and moisture-corrected beta dose rates calculated using the HRGS results (Table S10) are consistent with those determined for each sample using low-level beta counting (Table S9), confirming the reproducibility of our dose rate estimates.

Fig. S15a summarizes the results of the multi-grain aliquot dose-recovery tests performed on sample FB12-1. The most accurate dose-recovery results were obtained using a PH_1 of 200 °C for 10 s and a PH_2 of 160 °C for 10 s. This preheat combination yielded a weighted mean measured-to-given dose ratio of 0.99±0.03, low inter-aliquot D_e scatter, low-dose and high-dose mean recycling ratios in agreement with unity at 1σ (1.00±0.01 and 0.99±0.01, respectively), and a mean recuperation ratio of less than 2%. Accurate multi-grain aliquot dose-recovery test ratios were also observed for preheat conditions of PH_1 = 200 °C for 10 s and PH_2 = 200 °C for 10 s, PH_1 = 200 °C for 10 s and PH_2 = 180 °C for 10 s, and all PH_1 combinations using a PH_2 of 160 °C for 10 s. However, these alternative preheat combinations all exhibited inferior mean recycling ratios and/or increased inter-aliquot D_e scatter.

The single-grain dose-recovery test performed on sample FB12-1 using the optimum multi-grain preheat conditions (PH_1 of 200 °C for 10 s and a PH_2 of 160 °C for 10 s) yielded an inaccurate weighted mean measured-to-given dose ratio of 0.92±0.02 and an overdispersion of 7±3% (Fig. S15b). The optimum multi-grain preheat combination is therefore sub-optimally suited to the grain populations targeted by our single-grain D_e determination procedures. This disparity potentially reflects the influence of compensatory averaging effects at the multi-grain aliquot scale, which might arise when simultaneously measuring grains that exhibit contrasting responses to the chosen SAR conditions (e.g., *77, 81, 112*). The single-grain dose-recovery test was repeated using the alternative preheat combinations identified as being potentially suitable from the initial multi-grain dose-recovery evaluations. The most suitable single-grain dose-recovery test results were obtained using a PH_1 of 240 °C for 10 s and a PH_2 of 160 °C for 10 s (Fig. S15c), which yielded a weighted mean measured-to-given dose ratio in agreement with unity at 2σ (1.03±0.02), weighted mean low-dose and high-dose recycling ratios of 0.98±0.01 and 1.00±0.01, respectively, and an overdispersion value of 4±3%. These single-grain dose-recovery results demonstrate a minimum level of reliability for natural D_e determination, and hence a preheat combination of PH_1 = 240 °C for 10 s and PH_2 = 160 °C for 10 s has been adopted for single-grain D_e estimation at Figueira Brava.

The OSL grain classification statistics obtained for each sample after applying the SAR quality assurance criteria are summarized in Table S8: 6-18% of the quartz grains measured for D_e determination were considered suitable for OSL dating purposes. The proportions of grains rejected during the single-grain dose recovery test for failing the various SAR quality-assurance criteria are consistent with the corresponding proportions shown for the natural D_e measurements of FB12-1. The similarity of these grain classification statistics provides assurances that the dose recovery D_e datasets are sufficiently representative of the natural D_e datasets for this sample.

Representative OSL dose-response and decay curve for grains that passed the quality assurance criteria are shown in Fig. S16. The majority of accepted grains display rapidly decaying OSL curves (reaching background

levels within 0.5 s), which are characteristic of quartz signals dominated by the most readily bleached (so-called 'fast') OSL component (compare with the OSL decay curve shape for a fast-dominated Risø calibration quartz grain; Hansen *et al.*) (*80*). The single-grain OSL dose-response curves are generally well-represented by either a single saturating exponential function or a saturating exponential plus linear function, as has been widely reported for quartz grains with fast-dominated OSL signals (e.g., (*79, 113-115*) On average, 42% of accepted grains per sample display moderately bright T_n (20 Gy) OSL signals of 100-1000 cts/0.08 s (e.g., Fig. S16a), and 18% of accepted grains per sample have relatively bright T_n OSL signals of >1000 cts/0.08 s (e.g., Fig. S16b). Four of the six OSL samples also contain a small number (<1-5%) of very bright accepted grains displaying T_n OSL signal intensities >10,000 counts/0.08 s (e.g., Fig. S16c). The average T_n OSL signal intensities range between 500 and 1800 counts/0.08 s for each sample.

The single-grain D_e distribution of each sample is shown as a radial plot in Fig. S17. Samples FB12-5 and FB12-6, collected from unit IH6 of Area F exhibit relatively homogenous D_e distributions, low overdispersion values of 14±2% and 17±2% (Table S9), and the majority of individual D_e values lie within two standardized estimates of the weighted mean D_e value (denoted by the dark grey shaded band on Fig. S17a-b). The overdispersion values for these samples are consistent with those typically reported for ideal (well-bleached and unmixed) single-grain D_e datasets at 2σ (global average reported by Arnold and Roberts = 20±1%) (*116*). These D_e distribution characteristics suggest that insufficient bleaching prior to burial (e.g., (*117-119*), post-depositional sediment mixing (e.g., *81, 116, 120*) and beta-dose heterogeneity (e.g., (*121-123*) have not contributed significantly to the D_e scatter of these samples. The interpretation that samples FB12-5 and FB12-6 were well-bleached prior to deposition is consistent with the presence of windblown material in the UC/IH complexes and suggests the potential for sufficient daylight exposure of similar allochthonous deposits prior to their entry into the interior cave chamber. The final D_e values of samples FB12-5 and FB12-6 have therefore been derived using weighted mean D_e estimates, calculated using the central age model (CAM) of Galbraith *et al.* (*124*) (Table S9).

Samples FB12-1, FB12-2, FB12-3 and FB12-4, collected from the 1986 excavation trench in Area C and the Exterior trench in Entrance 3 (the SEx trench), display heterogeneous OSL D_e distributions (e.g., Fig. S17c-f) and higher overdispersion values of 28-39% (Table S9). These overdispersion values do not overlap at 2σ with those of the well-bleached and unmixed samples (FB12-5 and FB12-6) obtained from Area F, suggesting more significant influences of extrinsic D_e scatter. A large proportion of the measured D_e values from these four samples lie outside of their weighted mean (CAM) burial dose 2σ range, and the radial plots show a distinct leading-edge of low D_e values and/or a clustering of higher D_e values. Application of the maximum log likelihood test (*118*) indicates that either the three- or four-parameter minimum age model (MAM-3 or MAM-4) of Galbraith *et al.* (*124*) is statistically favored over the CAM for all four D_e datasets. These D_e distribution characteristics are consistent with those reported elsewhere for heterogeneously bleached single-grain OSL samples (e.g., (*117-119, 125-127*), which can be common in cave environments (e.g., (*128-130*). Post-depositional mixing or bioturbation is not thought to have contributed significantly to the heterogeneous D_e datasets observed in Area C and the SEx trench given the preservation of clear stratigraphic layering at these sample localities. Spatial variations in beta dose rates experienced by individual grains may additionally explain

some of the scatter observed with these samples. However, it seems unlikely that beta heterogeneity could alone account for the very broad range of D_e values for FB12-1, FB12-2, FB12-3 and FB12-4 (D_e range for the four samples = 221-431 Gy; relative D_e range = 2-2.9), especially as the samples were collected from relatively homogeneous sand and silt horizons and care was taken to avoid roof fall materials, clasts and speleothems that could have acted as radioactivity 'cold spots' or 'hotspots'.

The contrasting bleaching characteristics of the samples collected from Area F (FB12-5 and FB12-6) and those collected from Area C (FB12-1, FB12-2 and FB12-4) and the SEx trench (FB12-3) likely reflect spatial (and temporal) heterogeneities in sediment transportation and deposition dynamics within the karst cavities (e.g., *131*). The MC2 unit of the SEx trench contains material that was syn-depositionally dispersed by low-energy gravity or run-off processes. This locally derived colluvial material may have experienced limited daylight exposure prior to entering the cavity, which could explain the heterogeneous D_e dataset of sample FB12-3. The scattered D_e distributions of samples FB12-1, FB12-2 and FB12-4 may similarly reflect the localized introduction of heterogeneously bleached grains into the Area C chamber. However, these complex D_e datasets may equally reflect internal reworking of pre-existing (older) generations of cave sediments and their subsequent incorporation in the layer 2 and layer 4 deposits alongside externally derived, well-bleached grains (see below).

Taking into consideration the complex geomorphic settings of samples FB-1, FB-2, FB3 and FB-4 (shallow cave infill deposits, presence of older generations of grains in the cave chamber), and their seemingly heterogeneously bleached D_e distributions, we have opted to use the MAM to derive the final burial dose estimates. The decision of whether to use the MAM-3 or MAM-4 for final age calculation has been made on statistical grounds using the maximum log likelihood score outlined by Arnold *et al.* (*118*). The MAM D_e estimates have been calculated after adding, in quadrature, a relative error of 15% to each individual D_e measurement uncertainty. This step was added to provide a minimum estimate of the underlying dose overdispersion observed in the well-bleached and unmixed samples from this cave system (FB12-5, FB12-6), following the justification outlined in Arnold and Roberts (*116*) and Arnold *et al.* (*115*).

The two OSL ages for unit IH6 are statistically indistinguishable; 95.0±5.3 and 93.9±5.6 ka (1σ) for samples 12-5 and 12-6, respectively (Table S9). The D_e distributions of these samples are very homogeneous, reflecting the dominance of aeolian particles in the sedimentary matrix of the MC/IL and UC/IH complexes, and justifying calculation of the final OSL ages with the CAM. Based on the 2σ uncertainty range of these results, the *terminus ante quem* for unit IH6 is 83.6 ka, which is in full agreement with the U-series date for overlying unit IH5 (Table S5). OSL samples 12-1 and 12-2 (86.1±6.8 and 89.3±6.4 ka, 1σ) are also, within uncertainty, consistent with this time frame, supporting the correlation of layer 2 of Area C with complex IH of Area F (Table S12). Likewise, the age provided for unit MC2 of Entrance 3 by sample 12-3 (97.8±6.0 ka, 1σ) is fully consistent with the constraints provided by U-series for the accumulation of Area F's IL complex (between 111.3 ka, at the earliest, and 92.0 ka, at the latest), supporting its correlation with units MC1-MC2 of Entrance 3.

On the strength of the 110.2±8.3 ka (1σ) result for OSL sample 12-4 one would not be able to exclude the possibility that the archeology in layer 4 of Area C and in the correlated LC complex of Area F dated significantly beyond 110 ka; if so, the *terminus post quem* of 111.3 ka provided for the accumulation of the Figueira Brava

archeological sequence by U-series sub-sample 1306-1 would be valid for Area F only. Recall that (a) layer 4 of Area C could not be internally differentiated, (b) in Entrance 3, the body of LC3, the lowermost unit of the LC complex, is made up of trampled beach sands that remained exposed once sea level descended from the MIS 5e highstand, and (c) the basal CO complex, absent in Area F, is present in Area C, where, therefore, the sampled layer 4 sands are likely to include an older LC3-like component. This context is reflected in the fact that sample 12-4 features the highest overdispersion of the whole set of OSL ages (Table S7) and reinforces the choice of the MAM for the final age calculation (since this age model has the potential to isolate the well-bleached grains and eliminate grain populations that relate to older generations of LC3-like material). Thus, the 2σ (95.4% probability) interval of OSL sample 12-4 (93.6-126.8 ka) is a reliable, if imprecise measure of the time when, once the sea retreated and the previously accumulated marine sands became exposed as cave floor, the human occupation documented in layer 4 and the LC complex began.

Even though, along available exposures, an angular unconformity separates LC from the overlying MC complex, no evidence exists that the intervening hiatus was long-lasted; namely, no flowstone or carbonate crust formation is observed at their interface. These observations concur to suggest that the two complexes must be close in age and, thus, support consideration of the IB1 flowstone as the base level for the archeological deposit across the whole site. This consideration implies a maximum age for units LC1-LC2 in the range of 111 ka, which is consistent with the OSL date for layer 4.

Further support for this thinking comes from two different lines of evidence. On one hand, the Last Interglacial global sea-level data (*132*) show that it is only by 115-110 ka that we can be certain that sea level had descended below -5 m. Above that threshold, as we know from present evidence, the cave would have been subject to inundation and erosion, preventing human use of the site atop the marine sands forming the base of the LC complex, exposed as the water retreated to a far-away, lower elevation. On the other hand, the purity of the calcite making-up sub-sample 1306-1, reflected in its high ^{230}Th/^{232}Th ratio (66.938±1.258; Table S5), is a good indicator of formation in a clean atmosphere distant from potential sources of detrital accumulation. These chemistry data thus suggest that no significant sedimentary build-up was taking place inside the cave at the time; put another away, they suggest that the accumulation of Area C's layer 4 — and of the upper units (LC1 and LC2) of the LC complex to which it has been correlated — are indeed likely to post-date the time of precipitation of the calcite in sub-sample 1306-1.

S2.4. Correlation with global records

Combined, the OSL results for the sediments themselves (Table S9) and the U-series results for overlying, underlying, and interstratified speleothems (Tables S4-S6) provide well-defined age constraints, as summarized in Fig. S19. Compared against global records (*132-134*), the dating results support the following conclusions:

- The phase of sea level retreat that exposed the marine-accumulated sands of unit LC3, at the base of the LC complex, correlates with MIS 5d.
- The initial stages of the site's human occupation represented in complexes IL (Area F), MC and LC (Entrance 3) — Phases FB1, FB2 and FB3 (Fig. S18) — took place during MIS 5c. When compared with the

Greenland ice record, the dates suggest that at least Phases FB2 and FB3, recorded in the sediments of the MC complex, fall in the long GI (Greenland Interstadial) 23 interval, and that such may also be the case with Phase FB1, recorded in the underlying LC complex. However, an earlier age for the latter — in GS (Greenland Stadial) 24 — cannot be excluded.

- A major sedimentation hiatus occurred at the beginning of MIS 5b, towards the end of GI 23; the IL1/MC0 flowstone sheet, the external rind of the column separating Entrance 3 from Area F (sample 1029), and Area F's stalagmite sample 1209 formed during this hiatus.

- Phase FB4, the last human occupation phase, recorded in complexes IH (Area F) and UC (Entrance 3), took place during MIS 5b. The humid climate reflected in the rhythmic alternation between sediment build-up and flowstone or stalagmite formation agrees with the dates in correlating at least the basal part (units IH4-IH8) with GI 22; it remains possible, however, that the upper part (units IH2-IH3) formed during the following stadial, GS 22.

- The precipitation of the oldest clean calcite found at the base of stalagmite sample 1207 (sub-sample 1207-6) occurred during GI 21. That calcite, however, formed atop dirtier flowstone that itself directly capped the underlying IH2-IH8 sedimentary sequence. This pattern implies a lag between the end of sedimentation and the precipitation event dated by sub-sample 1207-6. We can therefore infer that the process by which calcite precipitation eventually sealed the site's sedimentary fill began earlier than the range indicated by the 1207-6 result (76.9-81.9 ka). This inference agrees with the evidence provided by sample 1027, which shows that precipitation of calcite onto the roof-adhering, unconsolidated sediments of Entrance 3's UC complex could have begun as early as 87 ka. A reasonable interpretation of these dates is that the capping of the archeological deposit by the IH1 flowstone is a process that began at the onset of GI 21, which broadly coincides with the beginning of MIS 5a, ~85.1 ka.

S2.5. Bayesian modelling of the dating results

To gain additional precision, and especially to obtain estimates of duration for the better constrained individual accumulation events within the upper part of the succession, we used OxCal (*135*) to model the dating results within a Bayesian framework. Given the nature of the samples, post-depositional disturbance is not an issue, and the samples' stratigraphic position within the individual sedimentary columns or the individual sub-sampled speleothems is known and unambiguous. Thus, the stratigraphy-derived time ordering of the different results can be taken as a given that provides secure anchoring for the mathematical calculation of uncertainty intervals narrower than those provided by the raw, unmodelled results. In this context, any anomalies in the expected age/depth relationship can be attributed to issues related to either dating (e.g., with regards to U-Th, detrital contamination) or algorithm design.

Besides observed order, the construction of the model also assumed: (a) the validity of the correlation between the different areas of the site (which the unmodelled results corroborate); (b) the precedence of unit IB1 relative to the deposition of layer 4 and units LC1-LC2, as argued above; and (c) the precedence of sample 1027 relative to sample 1207 within an "IH1 Sequence" whose initial and final boundaries concern the beginning of the process of flowstone formation that eventually sealed the site (not the full interval

represented by IH1 as a stratigraphic unit, which spans all of MIS 5a, MIS 4 and MIS 3, plus the early part of MIS 2). This latter constraint finds justification in the fact that the 1027 calcite precipitated directly onto archeological sediment, while the basal 1207 sub-sample (1207-6) formed when — presumably, later — the correlated Area F unit (basal IH1) had already become stabilized by the previous precipitation of carbonates (and, thus, clean calcite could begin to develop into the thick, massive stalagmite that yielded the sample).

The Outlier Analysis carried out on the thusly ordered results flagged a small number of U-Th results with an Agreement Index ≤58 (Table S16; Fig. S20): those for sub-samples 1208.2, 1208.4, 1301.7, 1301.6, 1301.5, 1301.2, 1301.1 and 1209.3. Except for 1208.2, which was found not to affect the outcome, these results were excluded from a second-generation model built with the "Sequence" command as a sequence of nested sequences within which (a) only OSL samples 12-6 and 12-5, whose relative stratigraphic ordering cannot be determined, were defined as a "Phase," and (b) an age estimate for undated unit IH4 was introduced to make it possible that a boundary between IH3 and IH4 be calculated. Based on the observation that IH4 and IH6 are of identical thickness and two halves of a homogeneous deposit separated by the very minor hiatus represented by IH5, we assumed that IH4 and IH6 represented similar spans, and the assumption was validated by the Agreement Index >60 calculated by OxCal for the thusly derived IH4 age.

The second-generation model yielded agreement values in OxCal's accepted range, and produced modelled results that, for the entire sequence, are given in Table S17, and for the IH complex, are plotted in Fig. S21. To make sure that, other than allowing the model to calculate an additional boundary, the IH4 estimate did not unintentionally bias the outcome, we also ran a model without it. The results were similar, with only minor differences (of no more than a few years or decades).

The modelled results constrain the initial formation of IL1 to the 90.7-93.5 ka interval. Note, however, that this constraint is dependent on the age obtained for sub-sample 1209-5, which comes from a few cm above the base of the 1209 stalagmite, itself developed out of the flowstone sheet that constitutes IL1 *sensu stricto*. These observations imply that the formation of the IL1 flowstone is very likely to have started by 93.5 ka at the latest and, by the same token, that the duration of the hiatus represented by the IL1/MC0 flowstone-cum-stalagmite could well have been close to the upper limit of the span calculated by OxCal, i.e., some 2500 years, if not a bit longer.

Whichever the case may be, it was by 90.3 ka, at the latest, that the last calcite precipitated on stalagmite 1209, while the earliest that stalagmite sample 1106 could have begun to form is 89.3 ka. Minimally, therefore the modelled time span represented by unit IH8, which those two stalagmite samples sandwich, is 1000 years, while the combined span of IH8 derived from samples 1301 and 1302 is, maximally, 2132 years. These limits are consistent with the 1500 years of duration obtained, considering the medians of the probability intervals, from the difference between the IH7/IH8 boundary and the initial boundary of IH8. One and half millennium would therefore seem to be the best estimate for the time span represented by the IH8 deposit.

With regards to the overlying units, the medians for the IH2-IH3/IH4 boundary and for the initial boundary of IH8 suggest accumulation of the IH4-IH8 sequence over a 2500-year span (Fig. S21). So, 1500 years for IH8 imply a one millennium duration for the IH4-IH6 package, and, in keeping with the model's assumption that IH4

and IH6 are of equal length, a duration of 500 years for each. These estimates are consistent with the maximum span of 1004 years derived from the upper limits of the spans calculated for IH6 (382 years) and for IH5 (the speleothem separating IH4 from IH6; 240 years). Based on this reasoning, we can further estimate at no more than 1500 years the time interval represented by the poorly constrained IH2-IH3 units, which are some 50% thicker than IH4-IH6 combined (Fig. S12). Indeed, in such a restricted space, over such a short period of time, and under similar global climactic conditions, sedimentation rates cannot have varied significantly and so it is legitimate to posit that span estimates be positively correlated with deposit thickness.

In all, therefore, the IH complex of Area F, corresponding to Phase FB4 of the site's human occupation, would represent an interval of four millennia fully within the time span, ~85-93 ka, of MIS 5b (*134*). Within that interval, the different IH units would date as follows (Figs. S19d, S21): (a) basal IH7-IH8, to between 90.0 and 88.5 ka, i.e., the first, warmer half of the GI 22 interstadial; (b) intermediate IH4-IH6, to between 88.5 ka and 87.5 ka, i.e., the second, cooler half of the GI 22 interstadial (see the $\delta^{18}O$ curve in Fig. S19d); and (c) uppermost IH2-IH3 to between 87.5 and 86.0 ka, the first part of the GS 22 stadial, which begins 87.6 ka and ends 85.1 ka. Even though these chronological estimates could be inferred from the unmodelled results, the modelling exercise provides additional robustness; however, a shorter chronology — accumulation of all IH in about half the time (2500 years) and fully within GI 22 (87,600 to 90,040 years ago) — remains possible.

The modelled constraints for the lower part of the succession, represented by complexes IL, in Area F, MC and LC, Entrance 3, are significantly more imprecise. Assuming a similar sedimentation rate, a duration of some 12,000 years can be derived from (a) MC and LC being, together, about three times the thickness of UC, (b) the correlation of UC with IH, and (c) IH's duration of ~4000 years. Using ~92.0-94.0 ka as the date for the beginning of the formation of the IL1/MC0 flowstone (for which sample 1209-5 provides a *terminus ante quem* of 90.7- 93.5 ka), the accumulation of LC2 atop the trampled marine sands of LC3 would therefore have begun no earlier than ~104.0-106.0 ka. This reasoning supports that the MC-LC sediment package and the FB3, FB2 and FB1 human occupation phases recorded therein reflect sediment deposition and human use of the place through the very long GI 23 interstadial (which lasted from 104.0 to 90.1 ka) and fully within MIS 5c (~93-106 ka), as inferred from the unmodelled results. Given that nothing suggests otherwise, an equal duration, ~4000 years, for each of those three initial phases, is a reasonable inference.

S2.6. Site-to-shore distances

Given the chronological constraints determined for the occupation of Figueira Brava and the curve of global sea level change (*132*), the off-site bathymetric evidence can be translated into distances to the coast line once corrected for the post-Pleistocene accumulation of estuary-related sediments (*24*) (Figs. S1, S19c; Table S18). Using the mean for global sea level values, the nearest shore would have been found ~750 m away during early MIS 5c, ~1500 m away during late MIS 5c, and ~2000 m away during MIS 5b.

Considering the extremes of the band of uncertainty surrounding global mean values, shorter site-to-shore distances can be contemplated. For MIS 5b, the minimum would have been ~750 m, but for MIS 5c it would have been only ~250 m (the distance corresponding to a sea level of -8 m, i.e., -11 m relative to the abrasion

platform). It is unlikely, however, that the site ever featured such an on- or near-beach location during the period represented by the archeological sequence. Given the steep local topography (Fig. S1b), such a short distance would imply that, during equinoctial tides (which, along the Portuguese coast, reach amplitudes of up to 4 m), the intervening terrain would have been within the reach of storm waves, i.e., regularly exposed to erosional processes affecting the stability of land forms. In addition, (a) the fact that no foraminifera are found among the wind-blown material present through the sequence shows aeolian inputs deriving not from an adjacent beach but from a dune belt separating the site from the sea, and (b) the abundant charred remains of the stone pine demonstrate that such a belt was there indeed (see below).

Based on evidence from Mallorca, Dorale *et al.* have proposed that, in the western Mediterranean, sea level reached +1-2 m during MIS 5a (*136*). Along the Arrábida coast, such a MIS 5a highstand would be only some 2 m below that of MIS 5e. Since the edge of the vertical scarp linking the abrasion platform to the sea below lies at +2.5 m (Fig. S3), a +1-2 m sea level means implies that, relative to the shore, the site had in MIS 5a the same position as nowadays. Thus, if, at current elevation (+3-5 m), the Figueira Brava platform is subject to active marine erosion, we can be certain that the same would have been true at the slightly lower, +1-3 m elevation implied by a MIS 5a rise of the scale hypothesized for Mallorca. If such a rise had occurred, the deposit formed during MIS 5c and MIS 5b would have been eroded away, but it was not: as shown by the dates obtained for the associated flowstone samples, the exterior platform remained a roofed, uneroded, sediment-filled cave space until MIS 2.

For Figueira Brava, a Mallorca-scale MIS 5a sea-level rise can only be contemplated if we hypothesize that the Arrábida coast was uplifted by several meters over the very short time span, five millennia, separating such a high from the lowest MIS 5b stand. The annual uplift rate implied by this scenario is, however, one order of magnitude higher than the range (0.11±0.01 mm) estimated for the Cape Saint Vincent area, which is 150 km to the south and in which the marine terrace assigned to MIS 5e lies at +20 m, not +5 m. A Mallorca scenario also implies that such a short uplift burst would have been fully reversed after the end of MIS 5a, which is geologically implausible. Indeed, the Sado basin is characterized by "low vertical motions, subsidence or low rates of coastal retreat," with no uplift or with annual uplift rates below 0.03 mm (*137*).

The minimum site-to-shore distance estimates in Table S18 are therefore unrealistic. It is the distances derived from the mean of the sea level variation curve that are robust and provide a reliable basis to assess the subsistence behavior of the site's human inhabitants, namely with regards to the use of coastal and marine resources. Based on this reasoning, the procurement distances implied are in the range of 750 to 1500 m for Phases FB1, FB2 and FB3, and of 2000 m for Phase FB4.

S3. Foraminifera

Whether foraminifera occurred in the deposit was investigated to assess the potential contributions to the build-up of the archeological succession of the bedrock, as parent material, and of marine accumulation processes. The yield of the analyzed samples is described in Table S19 and illustrated in Fig. S22.

The few specimens found form two groups: (a) yellowish, heavily eroded, and (b) whitish, relatively fresh. The former group probably consists of material derived from the local bedrock, as otherwise suggested by the presence of the fossil species *Orbulina suturalis*. The FAD (First Appearance Datum) of this taxon is some 15 Ma (million years), in the Langhian Stage of the Miocene, in good agreement with previous assessments of the age of the geological formation into which the Figueira Brava caves have been excavated (*107*). The taxonomic composition of the relatively fresh group is suggestive of brackish, marsh, lagoon or shallow inner shelf depositional environments and, hence, of accumulation by sea water penetrating the cave at high tide; alternatively, it could represent tests windblown from such nearby deposition environments, or material accidentally introduced by humans with algae or mollusk shells that the foraminifera attached to.

Accumulation of the whitish, fresh material by human agency is excluded by its stratigraphic distribution. Among the archeologically fertile units, only spit A53, which corresponds to unit MC5 yielded some; none was found in the different units of Area F's IH complex. In the case of the MC5 sample, however, we are dealing with a provenience — the base of the archeological deposit excavated in SEx trench — that was cemented together, in continuous manner, with the uppermost part of the beachrock. As power tools had to be used in the excavation, accurate décapage of the contact surface was not possible; thus, some beachrock sediment made its way into the material excavated as spit A53. Given the complete absence of foraminifera in the samples from the overlying, archeologically fertile units, and bearing in mind that none were identified in the soil micromorphology thin sections either, we must conclude that the fresh tests found in the A53/MC5 sample come from the beachrock.

The other foraminifera, all whitish/fresh, come from unit IB2 of Area F. This unit is made up of homogeneous silty sands that, though derived from the local bedrock in an endokarst context, nonetheless contained a few shells and artefacts. These remains reflect post-depositional introduction by trampling or burrowing across an exposed, unconsolidated sedimentary surface, which would have occurred once this part of the site became the interior area of an open cave. As with the fresh foraminifera present in the MC5 sample, such remains must reflect the temporary inundation of the marine terrace and the cave behind, with attendant pool formation, prior to the retreat of the shore line to a lower level and the subsequent accumulation of the continental sediments making up the archeological succession. The very small shells of marine gastropods found in the MC5 sample (Fig. S22e) further support this interpretation.

The time of introduction into the Figueira Brava deposit of foraminifera that are not bedrock-derived can thus be constrained to the interval between (a) the highstand during which the ocean excavated the cave system (MIS 5e, peaking above +5 m around 120 ka) and (b) the descent of sea level to well below present (beginning in early MIS 5d, around 115 ka). The absence of foraminifera in all the samples dated to the MIS 5c-MIS 5b interval further shows that, through the accumulation of the archeological deposit, the shore line was never close enough to Figueira Brava for their tests to enter the site via the operation of geological processes (e.g., marine inundation, or aeolian transport). This evidence is consistent with the notion that, along the Arrábida coast, the sea levels of MIS 5c and 5a were never high enough to bring Figueira Brava back to an on-the-beach position or to erode the accumulated archeological succession.

S4. Plant remains

Results from the floatation, sorting and classification of the plant remains are summarized in Table S20 and Fig. S23, which includes a frequency diagram (Fig. S23a) and data on the material's stone pine component (Fig. S23b-e). It should be borne in mind that, due to the heavy cementation, which hindered recovery and analysis, the numbers for the basal levels of Area F (units IL1-IL3) and for the SEx trench must somewhat underestimate the abundance of the remains. Note also that, as with the foraminifera, the lower boundaries of the SEx spits that reached the MC2/MC3 and MC5/CO interfaces could be defined in approximate manner only. Much as the MC5 foraminifera sample (spit A53) contains specimens derived from the CO conglomerate, so the charcoal sample from unit MC3, excavated as spit A50, may well include some material derived from MC1-MC2, excavated as spit A49.

Stone pine (*Pinus pinea*) is the dominant taxon. The diagnostic anatomical features used in the identification are: in the wood, axial intercellular resin canals present in latewood, growth-ring boundaries distinct in transverse section, ray parenchyma with pinoid to taxodioid pits visible in radial section, and cross-field with one to four pits; in the cone bract, an obtuse visible part; in the nut, the thick and woody shell. When the small size of fragments or their degree of alteration prevented certainty, pine remains were classified as *Pinus* sp. However, whenever determination to species was possible — which was the case with 46% of the wood fragments, 100% of the nut shell fragments, and all the sufficiently large cone bracts — only *P. pinea* was identified. As no evidence of other pine species was found, Fig. S23b assumes that all the remains of wood and cone bract are of the stone pine.

S4.1. Taphonomy

In the IT2 sample (N = 154), the charcoal fragments are large (>4 mm) and plant tissue is well preserved; thus, 77% could be identified to at least genus level. However, the external morphology of the wood is lost; only the anatomy is preserved. This pattern implies that the charcoal originated in fires that burned at temperatures of 280-500 °C (the pyrolysis stage of the combustion process, during which the surface of branches and logs is fully consumed).

In the Pleistocene samples (N = 1274), cell fusion, microorganism infestation and carbonate precipitates are the most frequently observed types of post-depositional alteration. These alterations hinder the botanical classification, even though carbonatation may have favored the preservation of the more fragile plant parts (such as pine needles, a truly exceptional finding). The fragments are also much smaller (mostly, <2 mm). However, the frequency of specimens identified to genus level, 90%, is higher than in the Holocene sample. The reason is threefold: (a) the Pleistocene assemblage is overwhelmingly dominated by pines; (b) besides wood, it includes *Pinus pinea* needles, cone bracts (some, >2 mm), and nut shell, all of which are entirely absent from the recent, naturally accumulated IT2 material; and, (c) these stone pine parts preserve the original shape, which facilitates the identification and implies that combustion stopped at the roasting stage, below 280 °C (Fig. S23d). By these features, the pine charcoal from the Pleistocene levels of Figueira Brava is unambiguously anthropogenic.

S4.2. Ecology

The IT2 assemblage stands for a vegetation of *Olea*, *Quercus* sp., *Rhamnus*, *Phillyrea*, *Arbutus unedo*, *Pistacia*, *Pinus pinea* and other woody plants. This composition is very much like the extant Serra da Arrábida's — a Mediterranean sclerophyll woodland that, on limestone soils, may grow to 15-20 m because many shrub taxa (*Quercus coccifera*, *Rhamnus alaternus*, *Phillyrea latifolia*) develop as trees. Deciduous taxa (*Quercus faginea*, *Acer monspesullanum*) are found on deeper, more humid soils, while *Arbutus unedo*, which also reaches tree size, thrives in areas with less calcareous soils.

Pinus pinea, however, is absent from the natural vegetation of the southern slope of the mountain, immediately around the site. This taxon tends to thrive on the sandy soils of maritime or continental dunes; thus, its presence in the IT2 assemblage must reflect a regional component, in keeping with the notion that the unit's sediment originated in a (tsunami-like?) event that dredged onto the Figueira Brava platform the content of adjacent sea bottoms. As Figueira Brava is just outside the mouth of River Sado, the Holocene build-up of such bottoms is largely the result of fluvial discharges. Therefore, it is to be expected that their content — including charcoal particles generated by natural fires —will reflect a catchment that extends upriver, where open woodlands of stone pine cover the land over a considerable extension.

The IT2 sample also contained 20 seeds. However, they are non-carbonized, which means that, though possibly accumulated by the same recent Holocene event, they could also represent post-depositional intrusion, if not unintended contamination. Whichever, their source must be local, as implied by the taxonomic composition of this small assemblage: the seeds belong to trees (fig and olive) and shrubs (white goosefoot, blackberry) that can be found in the site's immediate vicinity.

At present, the stone pine occurs between sea level and elevations of up to 1000 m, mostly in the thermo- and meso-mediterranean vegetation belts. In its normal range, average annual temperatures are between 13 and 18 °C, the average temperature of the coldest month is above zero, and cold spells below 5 °C are of very short duration. Humidity-wise, the species is very tolerant, and will thrive through summer droughts as much as six months long (*138*). Its coexistence with *Olea europaea* implies climatic conditions very much like those of the present across the MIS 5b-MIS 5c climatic oscillations under which the site's Pleistocene deposit accumulated.

The Angiosperm taxa found in IT2 are also those present in the Pleistocene deposit, reflecting a similar low-elevation, Mediterranean, limestone bedrock ecosystem. From the stone pine's rather strict soil requirements, and the abundance and anthropogenic nature of its remains, we can infer the proximity of a dune belt through the site's Middle Paleolithic occupation. Such a landscape form would have existed in the now submerged coastal platform, sandwiched between the paleo-mouth of the Sado and adjacent beaches, to the south, and the steep slopes of the southern flank of Serra da Arrábida, to the north.

S4.3. Economy

Preservation/classification issues cannot explain why the distribution of the MIS 5 charcoals is clearly skewed in favor of the stone pine, as the pattern remains clear at the higher level of Gymnosperm vs.

Angiosperm frequency. Indeed, Gymnosperms are 93% of the MIS 5 remains but only 18% in Holocene unit IT2 (Table S20). In addition, cone bracts and nut shell stand for 86% of the MIS 5 pine material, while none were found in IT2, where the taxon is represented by wood only (Table S20; Fig. S23b).

By comparison with a natural assemblage accumulated under similar climatic conditions, the Middle Paleolithic anthropogenic remains thus represent a doubly biased sample of the local vegetation. The nature of these biases informs us on economic choice. The fact that the stone pine assemblage retains a similar composition across the sequence tells us that these choices reflect long-term adaptation, not one-off idiosyncrasy. The variation in the relative frequency of plant parts (nut shell and cone bract vs. wood) bespeaks of activity patterns related to the changing position of the excavation trenches relative to the center of the human occupation. Most of the nut shell remains, 88%, relate to Phase FB2, where, together with cone bracts, they represent 90% of the pine and 74% of all charcoal (Table S20). Knowing that the volume of excavated FB2 sediments is less than one tenth of FB3 and FB4 combined (Table S13), these numbers are even more impressive and support that the SEx trench sampled the core area of the FB2 occupation (Fig. S18), where the fire-aided processing and consumption of food, and the discard of the corresponding remains, took place.

As shown by the fact that they burned to >280-300 °C, the wood remains of pine imply collection for fuel. This cannot be the case, however, with the cones, needles and seeds. The cone is highly resin-rich and will therefore be quickly consumed; dry pine cones are ideal to start a fire but not to maintain one. Thus, at Figueira Brava, use of pine cones as a fire starter is contradicted by (a) the presence of seeds and needles (by definition, a dry cone will have none), (b) the abundant bract remains, which far outnumber the wood remains, whereas use as fuel would lead to bracts being in much lower numbers because of how more rapidly they would have been consumed, and (c) the larger size and better preservation of the original morphology apparent in the bract remains, which implies that they were roasted rather than burnt.

Pine nuts reach maturity two and half years after fecundation, that is, in the third autumn after the flowering. When the following summer comes, the heat will naturally open the cone and gravity will disperse the seeds around the tree. With a controlled use of fire these features of the stone pine's reproductive behavior can be used to obtain the food source (the nut's kernel) prior to it being lost on the ground. The unchanging pattern of stone pine nut consumption seen across the thousands of years represented by the Figueira Brava sequence implies such a control and such a knowledge. The presence of needles further corroborates collection of whole, closed cones directly from tree branches, not from the ground, and their on-site storage prior to consumption.

Based on this evidence, the parsimonious explanation of the Figueira Brava data is that stone pine cones were collected whole, prior to opening, in autumn and winter. They were transported to the site, where extraction of the ripe nuts was done by heating the cones over the embers of an open fire. Note that, with a single blow inflicted upon moderate heating, a single ripe cone will yield up to 100 seeds. This *modus operandi* explains why the tree's only missing part is the nut's kernel: it was eaten (stone pine kernels are among the most nutrient-rich food sources known) (*139*), the shells left behind bearing witness to the consumption.

S5. Marine invertebrates

Complete limpets were frequent in Area F's *in situ* deposit, but most shell found during its excavation was fragmentary, and the same can be seen in Entrance 3's soil thin sections. NISP and MNI counts were consequently expected to underestimate the abundance of marine invertebrates. To control for this preservation bias, abundance was also assessed in terms of density (i.e., shell weight relative to other anthropogenic components and the sedimentary matrix), based on bulk samples of unconsolidated sediment collected for the purpose and analyzed, for comparison, alongside similar samples from the Mesolithic site of Toledo (Table S21; Fig. S25). Bear in mind that (a) in these analyses, the "shell" class subsumes both mollusk shell and crustacean carapace, as distinguishing between the two was hindered by the fragmentary condition of the material, and (b) the indurated nature of the deposit precluded sampling of units IL2 (Area F) and MC2-MC4 (SEx trench; quantitative abundance data for these units are provided in Table S22).

The deposit contained a few shells of land snails, among which *Oxychilus cellarius*, *Rumina decollata*, *Cochlicella barbara*, *Helicella conspurcata* and *Cepaea nemoralis* could be identified. These remains are part of the environmental background noise and were not systematically collected. Indeed, except for the one *Cochlicella*, all come from the reworked sediment of Area F and are likely to be intrusive and of Holocene age. The other mollusk taxa identified are all marine, as are the crustaceans; their taxonomic composition is given in Tables S22-S25 and illustrated in Fig. S24.

S5.1. Taphonomy

The matrix of the basal unit of the LC complex (LC3) is composed of beach sands. However, the deposit lost its original structure to trampling and contains anthropogenic components (lithics and bone). In addition, the sub-horizontal, well-layered disposition of the mollusk shell implies a largely *in situ* context: if the shells stood for post-depositionally redistributed inheritance, a random orientation within the sedimentary matrix would be expected (as indeed seen in thin sections representing colluvial accumulations found higher-up in the sequence, e.g., in units MC2-MC4; Figs. S11c-d and S13_sample FB-1002). These facts exclude the possibility that the LC3 mussel shell lenses are natural thanatocenoses formed by hydrodynamic processes; they are not a pre-existing component of the marine beach upon which the earliest human occupations of the site took place, they are refuse reflecting the on-site consumption of foods harvested elsewhere in the landscape.

The anthropogenic nature of the mussel accumulations found in the LC and basal MC complexes is further supported by their intrinsic features: (a) most shells are broken, not complete, and many are burnt (Fig. S13_sample FB-1002); (b) the fragments belong to edible-size specimens with valves 7-8 cm long or more; (c) small-size specimens are scarce if not altogether absent, as are articulated valves (both being common occurrences in beach-facies biostratonomic concentrations of *Mytilus*); (d) many fragments and valves lie on their convex side, whereas, in a seashore thanatocenosis, wave energy would have inverted most to a more stable position with the concave side facing down (*140, 141*); and (e) foraminifera are not observed in the soil micromorphology thin sections (their residual presence in the MC5 foraminifera sample being due to the fact that, as discussed above, spit A53 includes material derived from the underlying CO complex).

The intrusive, Holocene-age component of the reworked sediment found atop the Area F sequence provides a standard against which to assess what a natural, seashore-accumulated, interglacial marine invertebrate assemblage should be expected to look like. Mussel shells are abundant in that fill, especially in and around the small-mammal nest identified in T9-SW — but they are for the most part complete, slightly patinated and eroded, presenting dulled or damaged edges, and often featuring clionid holes and perforations made by the gastropod *Nucella lapillus*, a natural predator of mussels (Fig. S24a). In contrast, the mussel shell material retrieved *in situ* is fragmentary and fresh — the surfaces are unpatinated and lack clionid or predator holes, and the edges, when preserved, are sharp (Fig. S24b). The fragmentary condition of the Pleistocene assemblage is well apparent in the distribution of size classes, given in Fig. S24c for the mollusk shell and shell fragments accumulated during Phase FB4 (piece-plotted plus dry sieve-collected specimens): 59% are smaller than 2 cm. Such a fragmentary condition is otherwise well apparent in the relative decrease in mussel abundance observed when the proxy used is the MNI instead of the NISP. This decrease is especially marked in the assemblages from Phase FB4 (Fig. S24d), reflecting the lesser sturdiness, relative to the limpet's, of the shell of the mussel (and, hence, its greater susceptibility to post-depositional breakage).

These contrasts in the taphonomy of the mussels are matched by the contrasts in the taxonomic composition of the *in situ* and reworked assemblages of other marine invertebrates. For instance, Echinoderms (in total, five fragments of *Paracentrotus lividus*) were only found in the reworked sediment — suggesting that they correspond to Holocene intrusions and that the same is likely to apply to all those retrieved in the 1986-89 excavation of Area C. With regards to crabs (Fig. S24e-f), the *in situ* deposit is overwhelmingly dominated by remains of *Cancer pagurus* (brown crab). Their carapace width, estimated from the length of the pincers to average 162 mm and range between 111 and 223 mm, shows that the remains all belong to sexually mature animals (*142*). *Cancer pagurus* is also represented in the reworked sediment, in which, however, the remains are derived from the Pleistocene deposit — most specimens feature the diagnostic concretions coating the *in situ* finds. In contrast, *Pachygrapsus marmoratus* — the marbled rock crab, a small crab (carapace width <36 mm) that inhabits rocky shores, where it procures its prey — is entirely absent from the *in situ* Pleistocene assemblage even though it is dominant among the non-concreted crustacean remains of the reworked deposit (Table S25).

Marbled rock crabs are a common occurrence in the present-day inter-tidal pools of the Figueira Brava platform itself and, as such, it is to be expected that their carapace and claw remains would have made their way, entirely through natural agency, into the parts of the Pleistocene fill of the adjacent caves that underwent Holocene reworking. *Cancer pagurus*, however, is a sublittoral species that, in the adult age indicated by the Figueira Brava size data, most of the time lives in the sea floor and does not form natural seashore thanatocenoses. In addition, the animals caught were transported for deferred consumption some 2000 m inland — the site-to-shore distance estimated for MIS 5b (Table S18), during which 99% of the brown crab and spider crab remains retrieved in the excavation entered the cave (Table S26). The types of fracture breaks observed on the claws and the fact that many remains are burnt (Fig. S24g-h) further corroborate the anthropogenic nature of Figueira Brava's remains of *Cancer* and *Maja*.

A 16 cm adult brown crab male weighs about 800 g (*143*). Apart from humans, the other agents capable of moving such large crabs over the distances involved are the aquatic eagle and other birds of prey of similar size (*144*). Figueira Brava, however, is a cave, and hence not an appropriate place for such large birds of prey to nest in, and even less so given the evidence for continued human occupation through the accumulation of the IH complex. Both factors — distance to the shore line, and human presence — also preclude that the scale of Figueira Brava's accumulation of marine invertebrate remains be related to the activity of other avian (e.g., seagulls) or mammalian (e.g., otters) agents.

Several long stretches of the coast of central and southern Portugal feature large caves located directly adjacent to the seashore or no further inland than Figueira Brava was during its Middle Paleolithic occupation. Were the activity of non-human agents susceptible of producing marine invertebrate accumulations akin to Figueira Brava's, the corresponding evidence would no doubt have been noticed and reported; it hasn't. By its intrinsic characteristics and association with wood charcoal, stone tools and animal bones, there can be no question that Figueira Brava's Middle Paleolithic marine invertebrate assemblage was accumulated by humans.

S5.2. Economy

Even though the extreme cementation of the deposit did not allow sampling for composition analysis, the soil micromorphology thin sections show that marine invertebrate remains are at least as abundant in units LC1 and LC3 as in the shell-rich lenses of unit MC5, as otherwise corroborated by inspection of extant exposures (Figs. S11d, S13, S25c-e). With regards to the parts of the sequence that could be excavated and sampled, the relative importance and stratigraphic variation in the composition of the deposit's marine invertebrate material is illustrated in Fig. S25a-b.

In Fig. S25b, the density of shell in the bulk sediment samples is compared with the excavated material's NISP values (normalized; the raw NISP count divided by each unit's excavated volume). Both measures display the same overall pattern: the density of marine mollusk and crab remains is comparable in the stratigraphic units that correspond to Phases FB2 (unit MC5) and FB4 (units IH2-IH8) of the site's human occupation, but much lower in those that correspond to Phase FB3 (units IL3-IB2). However, (a) from IH4 to IH6, the NISP/m³ ratio increases while the bulk density value decreases, and (b) even though the NISP/m³ of unit MC5 is well below that for units IH4 and IH6, its bulk sample yielded more than twice the amount of shell than any of the others (as indeed might be expected based on the soil micromorphological data). These discrepancies must reflect the impact of differential fragmentation. For the MC deposit specifically, heavy cementation and the attendant higher level of excavation-induced breakage cannot but have negatively biased the NISP counts. This factor may also underpin to some extent the NISP/m³ decrease seen in IH8 relative to IH4 and IH6, as, in parts, IH8 was significantly indurated.

All mesh sizes combined, shell represents 25.6% of the deposit in the MC5 bulk sample, but between only 5% and 11% in the bulk samples from IH2-IH8 (Fig. S25a). This difference can be explained by reference to site formation history and with due consideration of site plan and location of sampling windows (Fig. S18). In the case of the lowermost units of the MC complex of Entrance 3, we are dealing with Phase FB2. Thus, our view of

the relative importance of shell is based on areas of the site located at or near the core *loci* of human activity and in which the occupation debris are largely *in situ*. In the case of complex IH of Area F, we are dealing with Phase FB4. Thus, our view of the relative importance of shell is based on samples from areas peripheral to the actual activity *loci* and containing occupation debris syn-depositionally derived from a primary source located outward and upslope. Consequently, less break-up and damage but more scattering are to be expected in the material from Phase FB4, resulting, by comparison with Phase FB2, in higher NISP/m³ ratios for the excavated material but lower g/l ratios for the bulk samples, as indeed observed.

Such site formation processes cannot explain, however, the marked decrease in both ratios seen in the units that correspond to Phase FB3: in Entrance 3, the marine invertebrate NISP/m³ ratio of units MC3-MC5 (Phase FB2) varies between 1380 and 3600, while that for overlying units MC1-MC2 (Phase FB3) is 146 (Table S22). The latter is comparable to the values for the units of the same phase excavated in Area F (Fig. S25b). The soil micromorphology thin sections display the same pattern of mollusk shell decreasing as one moves up from units MC3-MC5 to units MC1-MC2. This marked decrease in the amount of marine invertebrate remains is therefore a site-wide phenomenon that must result from the properties of Phase FB3's uses of the site, not from sampling or excavation bias.

Comparison with the Toledo data supports the inferences above. Sample B of Toledo comes from layer B, a colluvial deposit. Samples B/C and C/D come from dense, localized midden accumulations: B/C from the interface between layer B and the fluvial sands of layer C, which is a terrace of River Alcabrichel, on the right margin of whose estuary the site is located; C/D from the interface with the sands of the Jurassic bedrock, layer D, in parts of the site where layer C is missing. The occupation took place over a ground surface where the layer B colluvium was found in lateral continuity with the layer C fluvial sands, and post-depositional processes redistributed the finds across the site, both horizontally and vertically (*67*). In this scenario, sample B represents the end term of the process, in which the density of finds is impacted by attritional loss and post-depositional scattering, while samples B/C and C/D represent preserved remnants of the original contexts of deposition (explaining well why, as shown in Table S21 and Fig. S25a, shell stands for 14.6% of the total in sample B but for between 45.0% and 62.2% in the other two). Therefore, sample B represents a contextual analogue for the units making up Phase FB4 of Figueira Brava. Samples B/C and C/D, in turn, may well represent better contextual analogues for the units making up Phase FB2, but with a caveat — the constrained space, a cave, in which the occupation of Figueira Brava took place implies that, owing to trampling and repeated use, attritional loss must have impacted the shell component more significantly than they did the more intact depositional environments that samples B/C and C/D of Toledo stand for.

Bearing these considerations in mind, two conclusions can be drawn. Firstly: in terms of the weight of their marine invertebrate remains, Figueira Brava's Last Interglacial cave deposit is fully comparable to Toledo's Holocene open-air deposit. Secondly: the different position of our excavation trenches relative to the focal areas of human activity suffices to explain why our samples from Phase FB4 (which come from Area F) have less shell than those from Phase FB2 (which come from Entrance 3). If a dramatic increase in the rate of sedimentary accumulation is postulated, these conclusions could also hold with regards to Phase FB3, as the

same amount of time would then be represented by a much thicker deposit and, thus, a much higher proportion of matrix relative to the remains of human activity. But the chronometric data at hand provide no support for such a postulate, and so the amount of marine invertebrate remains consumed and discarded at Figueira Brava during Phase FB3 does seem to have genuinely decreased.

Variation in the distance to procurement areas must also contribute to explain these differences. The higher density of marine invertebrate remains seen during Phase FB2/Entrance 3 coincides with a time, MIS 5c, when sea level was higher and the coastline closer, while the lowered density of such remains seen during Phase FB4/Area F coincides with a time, MIS 5b, when sea level was lower and the coastline farther away (Table S18; Fig. S19c). Such a variation would not necessarily mean, however, that, during Phase FB4, marine invertebrates were being harvested less intensively than during Phases FB1 and FB2; it could simply mean that they were being discarded at this locality less often than before because the role played by Figueira Brava in the overall settlement-subsistence system changed as a result of the changes in the site's environmental setting. Indeed, it is likely that the role played by Figueira Brava in Phase FB2, when the shoreline was <1000 m away, was in Phase FB4 played by sites located at a similar distance, ones that, given the lowered stand of MIS 5b, have since become buried in the seabed, if not altogether obliterated.

Factors related to site function probably also underpin the marked decrease in shellfish remains that characterizes Phase FB3. Such a decrease needs not reflect that marine foods were economically less important during that phase than before or after. It may simply indicate that Figueira Brava was at that time less intensively used by humans, as one can otherwise infer from the variation in the vertical distribution of the deposit's other anthropogenic components: the cones and the nut shells of the stone pine (see above; Fig. S23b), and the stone tools (see below).

The role played by situational factors is otherwise well illustrated by the variation in the taxonomic composition of the marine invertebrate assemblages (Fig. S24d). For instance, clams make a much more significant contribution to the marine invertebrate basket during Phase FB2. This difference is likely to reflect changes in the site's environmental setting, with attendant implications for the access to resources. From the importance of clams in Phase FB2 we can infer the proximity of the habitats preferred by the species — estuarine and lagoon areas with shallow, clean, sandy bottoms, and the intertidal zone of sandy beaches.

By the same token, the importance of crabs during Phase FB4 likely reflects changes in the configuration of the adjacent band of littoral terrain; transporting back to site the product of crab harvests made economic sense if, at that time, a rocky coast line was present nearby. Note also that the material from Phase FB2 comes from a deposit excavated over a reduced area in which cementation was extreme. Therefore, it cannot be excluded that the absence of crabs seen among the remains from that phase is an artefact of sample bias. In any case, if large crab procurement represents indeed a MIS 5b subsistence novelty, then it is best seen as a broadening of the exploitation of the coastal ecosystem in which humans had been procuring limpets and mussels since millennia before. It certainly would have required no more than the simplest of technologies — low-tide handpicking in rock crevices or in the shallow waters around reefs colonized by mussels, coupled with

the means to bag and transport the prey, and perhaps also the knowledge of how to disarm the claws by nicking the activating tendon.

On average, one brown crab is the clean meat-equivalent of some 30 mussels. Given the difference in meat yield between crabs and the harvested species of mollusks, the apparent decrease in the values of the shell density parameter seen during Phase FB4 (Fig. S25a-b) could also reflect the opposite of what it apparently suggests, i.e., it could reflect an increased reliance on marine foods, only ones that were more productive.

From the behavior of brown crabs (*142, 143*) we can also make some informed speculations on the mode and seasonality of their acquisition. Adult brown crabs live in deep water during the winter but, in the summer season, they migrate to shallower bottoms; as night falls, these nocturnal animals approach the shore during the flood tide to forage on mussels and barnacles, but, during low-tide daytime, they can also be caught on exposed surfaces of the lower shore (*145*). Much the same applies to the spider crab. Thus, while foraging for limpets and mussels during the summer months, people would also have been able to catch both these large crabs, and so the contrast in crab numbers between Phases FB4 and FB2 may also owe, at least to some extent, to the seasonality of the occupations: spanning summer during Phase FB4, perhaps mostly either side of summer during Phase FB2.

The variation seen across the sequence in both parameters — shell density, and composition of the marine invertebrate food basket — is consistent with the notion that the overall settlement-subsistence system remained stable throughout. What that variation reflects are not economic or dietary shifts but factors that are (a) local, namely, the changing dynamics of the sedimentary build-up, the position of the sampling windows relative to the core areas of the inhabited space, and the seasonality of the occupations, (b) global, namely, sea level change and consequent variation in site-to-shore distances, and (c) regional, namely, relative weight, within the site's economic catchment, of estuarine, lagoon, or sandy beach shores versus rocky coast lines.

S5.3. Non-food taxa

A small number of other taxa are present alongside the overwhelmingly dominant mussels, limpets and clams (Figs. S26-S27). Among the gastropods, those other taxa are a significant proportion in Phase FB2 (33%), but only about 1% in FB3 and FB4 (NISP values; Table S23). Among the bivalves, and assuming the Veneridae that could not be classified beyond family level are edible clam fragments, the non-food taxa are around 4% in all three phases (NISP values; Table S24).

Some of these remains, such as the shells of *Phorcus lineatus* and *Littorina littorea*, are also of edible mollusks that can be found in the same rocky habitats as the targeted mussels and limpets, so their presence may well reflect no more than incidental collection. The same probably applies to such bivalves as the cockles and the razor shell genus *Solen*, which are found in the same habitat as the economically targeted clams.

Most of the other, rarer gastropods, are not edible. *Nucella lapillus* predates on mussels, while the different species of *Steromphala*, *Littorina, Bittium and Tritia* are all rather small. The use of their shells for personal ornamentation is well attested in the Upper Paleolithic, but, with two possible exceptions (see below), the Figueira Brava specimens bear no anthropogenic modification. Their presence in the deposit is therefore likely

to be accidental, and an indirect reflection of the introduction of the algae they live or feed on. This is the hypothesis put forward for a similar component of the coeval, limpet-dominated marine mollusk assemblage from Cueva de los Aviones (Murcia, Spain) (*27, 28*). Here, the algae were interpreted as the packaging used to transport the edible species from the point of collection to the point of consumption. In Holocene contexts, other authors have suggested that algae may have been procured as food, and that the presence in shell-middens of small, <2 cm non-dietary gastropods such as Figueira Brava's *Bittium* and *Tritia* specimens is a proxy for the on-site consumption of seaweeds and seagrasses (*146*).

The interpretation of the other bivalve taxa is less straightforward. The oyster shells may reflect subsistence behavior, but in at least one case the valve is a fossil, as shown by the fact that the carbonate crust adhering to the inner side of the shell is itself clionid-holed (Fig. S27, no. 1). As large oyster shell fragments are occasionally present in the local bedrock, and oyster lumachellas of Miocene age are exposed adjacent to the site, this specimen is at best a manuport, and possibly no more than a natural clast component of the deposit.

The Pectinidae that could be identified to species are not locally available fossils. All belong to *Pecten maximus*, which implies a Pleistocene age, and the condition of the finds shows they are beach-collected shells; deliberate acquisition and intentional transport to the point of eventual discard are therefore implied. Cleaning of the specimens yielded no evidence of the kinds of anthropogenic modification (e.g., ochre painting, pigment staining) documented in other Iberian Middle Paleolithic contexts (*28*). However, the degree of chemical weathering at the interface between the shell surface and the adhering sediment precludes taking such absence of evidence as evidence of absence. Much the same applies to the *Glycymeris* material. In contrast with the *Pecten*'s mostly calcitic structure, *Glycymeris* shells are rich in aragonite and organic compounds and, therefore, even more susceptible to diagenetic degradation of the surfaces.

Six *Glycymeris* and one *Pecten* are intact or only bear minor excavation breaks, and none of the *Glycymeris* is perforated at the umbo. The other *Glycymeris*, the *Callista*, and one of the *Pecten* are fragments but, where the breaks are available for examination, the edges are not rounded. These observations suggest collection of beached shells targeting complete specimens that broke (or were discarded) on site, whether after use or owing to post-depositional processes. The only exception is a *Pecten* whose edges are erosion-smoothed (Fig. S27, no. 4) indicating that, at the time of collection, the specimen already consisted of no more than part, even though a large one, of the valve.

Given the small size of the excavation, the numbers involved — at least eight complete or near-complete valves of *Glycymeris* and *Pecten* — are significant, especially with regards to Phase FB2: three complete and two large fragments of *Glycymeris* come from the 0.050 m³ of unit MC5's excavated volume (Tables S22, S24). We can exclude that those shells derive from the underlying beachrock because (a) the sediment attached to them corresponds to the matrix of the MC complex (Fig. S27, nos. 3, 5), not to the marine sands of the CO complex, and (b) no *Glycymeris* shells have been observed in any of the substantial exposures of the CO complex preserved all over Figueira Brava's marine abrasion platform.

These observations suffice to show that the beach collection of large bivalve shells was a routine practice of the site's Last Interglacial inhabitants. However, in the absence of direct evidence, the purpose of the collection — for use as tools (e.g., spoons), containers, raw-material, ornamentation, or other — remains elusive to us.

S5.4. Perforated shells

Two of the gastropods bore perforations of the body whorl (Fig. S28). The position and type of the perforations are akin to those commonly seen on specimens of the same taxa, or of similar taxa of identical size that, when found in Iberian Upper Paleolithic contexts, are interpreted as shell beads by default.

However, one of these gastropod shells — the *Euspira guilleminii* in Fig. S28f —was retrieved in the floatation of the sediment sample from unit IT2 of square T9. As this unit accumulated in post-Pleistocene, recent times, this specimen clearly cannot be an artefact; like the very small *Littorina obtusata* with a perforated body whorl from the SEx trench's foraminifera sample (Fig. S22e), it shows that gastropod shell is susceptible of bearing perforations that mimic anthropogenic ones but are caused by natural agents. In and of themselves, therefore, perforation of such shells is insufficient to establish a link with human behavior.

The other perforated shell is a *Littorina obtusata* (Fig. S28a-d) also retrieved in square T9 but in the IT0 sediment, in association with the midden of disparate composition found therein that we have interpreted as the nest of a small mammal (see above; Fig. S7g). As the IT0 unit features a mix of reworked Pleistocene and intrusive Holocene material, interpretation of the specimen as a Middle Paleolithic shell bead could not be excluded. The shell was therefore subject to microscopic examination and Raman spectroscopy to investigate the presence of anthropogenic modifications. None was found. The dark speckles found on the surface are manganese oxide; they could easily have been acquired from the original burial environment. The purple staining distributed along the edges is an oil-based ink, not a dye (Fig. S28e), and it probably is an artefact of smudging by the ballpoint-pen-written label the specimen was packed with at the time of collection. Finally, the pitting and smoothing of the surface, coupled with the rounding of the perforation's edges, show the shell underwent abrasion in a sandy sea-bottom after the perforation was produced. The culprit probably was a crab, e.g., *Carcinus maenas* (the green crab), which is represented in the reworked IT0 assemblage (Table S24) and is a known predator of periwinkles.

Coupled with the relatively fresh condition displayed by the *Littorina* shell when compared to the gastropods retrieved in the *in situ* Pleistocene deposit, these negative results indicated that the specimen was unlikely to represent a reworked Middle Paleolithic bead burrowed out of the IH2-IH3 unit. To obtain independent corroboration, the shell was submitted to radiocarbon dating. As mentioned above, the result obtained (OS-114170, 7390±25 BP) confirmed it to be a Holocene intrusion indeed (Tables S1-S2). However, the associated δ^{13}C value of -6.9‰ indicates that the dated specimen developed its shell in brackish waters, which, at first glance, is inconsistent with the marine environment one would tend to assume for the taxon. Therefore, to reject the possibility of analytical error, the shell's δ^{13}C was remeasured at the Sac radiocarbon laboratory in Lisbon. The result obtained, -7.8‰, accords with the original determination; thus, the specimen did develop in a brackish water environment, e.g., an estuary. This conclusion is consistent with accumulation

by natural agency and with the Holocene age determined by radiocarbon because the dating result places the specimen at a time when Sado estuary discharges accumulated along the sea bottom adjacent to the cave. That, at present, the taxon can be found in brackish waters, e.g. in the inner parts of the Ria de Vigo, in southern Galicia, is something that we have been able to establish through our own field observations.

Examination of Upper Paleolithic shell beads has shown that, in a significant number of specimens, perforation pre-existed human collection and modification or use (*147, 148*); put another way, they were collected for body ornamentation because of the perforation they already bore. When diagnostic use-wear is not present around the edges of the hole, or the shell is not additionally modified (e.g., via ochre-painting), the interpretation of such specimens thus rests solely on their context. Interpreting them as beads is legitimate only if they are found in an anthropogenic deposit located away from the seashore and it can be excluded that they represent fossil or subfossil material inherited from the primary source of the sediment (as is potentially the case when the site is a cave or rock-shelter whose fill includes material derived from nearby marine deposits). This conclusion applies to Middle Paleolithic sites as well, and especially so to those of Last Interglacial age located at the edge of the sea, either then or now — as is the case with Figueira Brava as much as with some of the African sites of the Middle Stone Age (MSA) that have yielded perforated gastropod shells (*149, 150*).

S6. Fishes

Except for a shark vertebra identified and piece-plotted during excavation, the fish remains were all retrieved via lab-sorting of the bulk sediment removed from the different trenches. Owing to the small size and fragility of the material, and the high level of induration of the sediment in the IL complex and across the SEx trench, only the samples from Area F's IT and IH complexes have so far been dealt with. The work process and the results obtained are presented and illustrated in Tables S27-S29 and Figs. S29-S30.

Even though the reworked sediments of unit IT0 may contain some Pleistocene material in derived position, most of the fish bones therein are fresh, unpatinated, and well preserved; they present clean surfaces devoid of carbonate coatings. A few cleaner fish bones were found in sediment that was considered *in situ* at the time of excavation, and it cannot be excluded that such specimens represent incomplete "decontamination" at the interface with disturbance pockets. However, almost all the fish remains in units IH2-IH8 were found in cemented sandy aggregates from which they had to be micro-excavated (Fig. S29a-e). There can be no question, therefore, that the IH fish are (a) coeval with the sediments that packaged them, and (b) stratigraphically associated with the lithics and the avian, marine invertebrate, and vertebrate remains found alongside.

Unit IT2 is the small pocket of black silty sands that blanketed the Pleistocene flowstone in the eastern, outward parts of the Area F trench, where it abutted the most recent stalagmites formed atop that flowstone (Fig. S12a-b). The bones in the IT2 fish assemblage retain their natural whitish coloration and include even the most fragile parts of the skeleton, which is consistent with the notion that a single and quite recent, natural deposition event was responsible for the accumulation.

Where taxonomic composition is concerned, the IT2 assemblage stands in marked contrast with that of the *in situ* Pleistocene deposit. Shads (*Alosa* sp.) and the gilthead bream (*Sparus aurata*) make up 93% of the IT2 fish remains, but these and other taxa of the same families (Clupeidae and Sparidae, respectively) represent some 10% only of the remains in IH2-IH8, which are mostly of eels and congers, followed by mullets and sharks. Predictably, given its mixed, but predominantly recent Holocene composition, the fish remains from reworked unit IT0 follow the IT2 pattern closely, even if they also feature some remains belonging to the taxonomic groups that overwhelmingly dominate the *in situ* Pleistocene assemblage (Fig. S29f).

These contrasts cannot be explained by classification-related issues. The skeletal part representation data for the IH2-IH8 remains show that taxonomic assignment is largely based on vertebrae and teeth. Reflecting their higher diagnostic power, which holds across the range of taxonomic groups represented in the three fish assemblages under comparison, these bones represent 61.7% of identified anatomical elements but account for 97.4% of the remains that could be classified to family level (Fig. S29g-h). If anything, classification biases would favor the representation of the Sparidae, whose hard teeth are among the fish remains more often seen among the range of species listed in zooarcheological reports (*151*). Thus, if, in the Figueira Brava case, such classification biases have any effect at all, it is that of nuancing, rather than enhancing, the contrast between the Holocene or mixed assemblages, on one hand, and the *in situ* Pleistocene assemblage, on the other.

Classification issues do play a role with regards to a better understanding of shark remains and their significance. This is because of the incomplete representation of sharks in the reference collections available to us and the heavy incrustation of bone surfaces. Often, the carbonate coatings cannot be completely removed, and important morphological features thereby remain hidden from observation; hence, the conservative approach used in the taxonomic assignment of sharks. Based on the teeth, three different species could be tentatively identified (Fig. S30c-e): *Prionace glauca* (blue shark), *Lamna nasus* (porbeagle) and *Isurus oxyrinchus* (shortfin mako). Several factors allow us to exclude collection of these elements as objects of beauty, or that they derive, via degradation of the cave walls, from the local Miocene bedrock (from where not even a foraminifera contribution has been detected, and in which no shark teeth have ever been observed) (*61*) (*23*): (a) surface appearance, identical to that seen among the deposit's mammal remains and, like these, featuring some manganese staining; (b) association with other skeletal parts (e.g., vertebrae); (c) tight stratigraphic clustering (most remains come from units IH4 and IH6); and (d) morphological contrast with related fossil taxa (see Fig. S30c, which compares a tooth tentatively identified as blue shark from Figueira Brava with a tooth from the Miocene taxon *Hemipristis serra*, a weasel shark, illustrated by Carrillo-Briceño *et al.* (*152*).

As with the crab assemblage, the IT0 and IT2 fish finds reflect what a naturally accumulated fish assemblage might be expected to look like at such a seaside locality. In the case of unit IT2, recall that the sedimentary matrix of the deposit suggests that the finds therein were thrown ashore by a tsunami-like event that dredged adjacent sea bottoms. This depositional dynamic implies an assemblage made up of small size fishes and reflecting local availability. Indeed, most IT2 fish are shads and seabreams, which are among the more abundant fish found in the Mesolithic shell-midden sites of the Sado estuary, and, nowadays, are one of the estuary's main fisheries. In contrast, eels and congers, which make up 59% of the NISP in IH2-IH8, are

represented at those Mesolithic sites by, in all, a single eel vertebra, found at Arapouco, where that vertebra stands for 0.09% of the 1161 identified fish remains (*151*).

The different composition of the two assemblages clearly reflects, therefore, two different catchments. The IT2 and IT0 assemblages reflect primarily, if not completely, the Sado estuary and adjacent shallow, sandy sea bottoms, i.e., the mid-Holocene and present setting of Figueira Brava (Fig. S1). The Pleistocene assemblage in IH2-IH8 reflects a steep coastline with rocky bottoms — the habitat also indicated by the abundant brown crab remains found alongside in the same levels. Compared to specimens of known size, the Figueira Brava eel bones correspond to fish that were about 30 cm long. Based on the metric data reported by Jacoby and Gollock (*153*), i.e., this catch is consistent with mature fish already in the so-called silver-eel stage, reached when ready to migrate back for reproduction. Eels in that stage are found in estuaries and the adjacent sea. Therefore, the Figueira Brava specimens are unlikely to represent freshwater, inland river prey; if not caught in the same rocky shore settings as the conger, they must have come from the kinds of coastal lagoons in which one finds another resource well documented in the site's Pleistocene deposit, the clams (or from adjacent terrain, as, to move between pools and streams, eels are capable of snaking overland for periods of up to several hours).

The mullets and the seabreams that make up most of the other teleosts identified in the IH2-IH8 fish assemblage are often found in shallow, <1 m-deep waters near beaches, which they approach to feed on crustaceans, mollusks and algae. Therefore, they could have been caught in the context of the procurement of crabs and mollusks, with no need for special-purpose boating or fishing technologies. The remaining taxa correspond to a single specimen of Scombridae and six of Clupeidae, all of which come from the uppermost IH unit (IH2-IH3) and look rather fresh by comparison with the other identified remains from the *in situ* Pleistocene deposit; this material may reflect the "incomplete decontamination" issues mentioned above.

Most of the Figueira Brava shark teeth compare well to the lateral upper teeth of juvenile blue sharks. The tentatively identified porbeagle tooth stands for a >1 m-long specimen because it features the secondary cusps that are usually absent in younger individuals. Newborn porbeagles are 58-67 cm long and then grow at an annual rate of 16-20 cm during the first four years of life; therefore, the Figueira Brava specimen was at least 3 years old — minimally, it was a late juvenile, if not already an adult. Whether such sharks were caught at sea or represent the scavenging of beach-stranded individuals cannot be ascertained. Juveniles, and even adults of the identified taxa are not an infrequent observation in shallow coastal waters of the Atlantic, and >1 m-long juvenile specimens can easily be caught in such waters, or when the ebbing tide traps them in rocky pools. That carcasses of marine vertebrates of even larger size were on occasion brought back to the site is otherwise shown by the dolphin remains excavated 1986-89 in Area C (*23*).

The contrasting composition of the Pleistocene *in* situ and the naturally accumulated Holocene fish assemblages argues for different origins. The kinds of coastal ecosystems reflected by the Pleistocene assemblage are the same in which the marine invertebrates found alongside were harvested. Therefore, there is no reason to question that the same agent is involved in the acquisition and transport of both resources and in the accumulation of the remains of their consumption. Human agency is further supported by the fish vertebrae with a dark-brown color indicative of heating or burning found in units IH2-IH3 (N= 1), IH4 (N= 11),

and IH6 (N= 1) (no similarly colored fish bones were observed in either the IT2 or the IT0 mixed/reworked provenience units).

Alternative modes of accumulation are a difficult case to argue. Phalacrocoracidae are present in the *in situ* avian assemblage (see below), but distance to the shore (during the accumulation of unit IH8, ~2000 m; Table S18) precludes the involvement of shags (*Phalacrocorax aristotelis*), which are exclusively marine. In addition, eel, conger and mullet, the main taxa represented in the IH assemblage, are not known to be part of the shags' diet, so the Figueira Brava fish remains cannot have come from the stomach content of hunted specimens. Cormorants (*Phalacrocorax carbo*) can be found in inland waters, the prey size they feed on is consistent with the average 30 cm-length of the Figueira Brava eels, and they have been observed fishing for eels. However, cormorants do not nest in caves, and not a single remain of eel was found among the 2053 fish bones identified among the 411 regurgitations examined to assess the feeding behavior of the cormorant population of the estuary of the Sado and adjacent coast (*154*). In any case, the only *Phalacrocorax* remains in the Figueira Brava Pleistocene assemblage that could be tentatively identified to species would have belonged to a shag, not a cormorant.

Mammals that are regular fish-eaters, such as bears, consume their prey by the water, as they catch it; they do not transport fish back to the den, much less over the distances involved in the Figueira Brava case. With regards to birds of prey, if, today, most of Figueira Brava is an unroofed space, at the time the deposit accumulated it was a cave; therefore, only the eagle owl (*Bubo bubo*) could conceivably have been involved in the accumulation of the smaller fish (but not the sharks). However, in Iberia, eagle owls focus on lagomorphs, and, in Middle Paleolithic contexts, large accumulations of rabbit bones are a well-known signature of their use of a cave for nesting purposes (*155*); that signature is not present at Figueira Brava (see below). In addition, the fish bones bear no diagnostic bone-damage features implicating large birds of prey in the accumulation (beak marks, breakage, etching by digestive acids, etc.), while the other avian predators represented in IH2-IH8 are (a) small ones that hunt similar-sized birds but do not take fish (namely, the sparrowhawk, *Accipiter nisus*, and the little owl, *Athene noctua*), (b) middle-size predators (e.g., the black kite, *Milvus migrans*) that will catch dead or sick fish, or snatch them from other birds, but do not prey on eels, or (c) vultures (namely, *Gyps* sp.), which feed on carrion.

Due to the lack of human skeletal remains and the fact that the site is too old for collagen to preserve, isotope-derived paleonutritional data are unavailable. Thus, the economic and dietary importance of fish can only be indirectly assessed via comparison with specimen counts for more recent sites (see below). However, because of the cementation of the deposit (and the inherent difficulty in teasing the fish out of their sedimentary matrix), one will need to bear in mind that such comparisons are always bound to underestimate the relative importance of fishing in the subsistence economy of Figueira Brava's Middle Paleolithic human inhabitants. Bearing this caveat in mind, it is worth noting that the 5 m² of the IH complex have yielded 562 fish remains (Table S28; and recall that the sorting work has yet to be completed). The total for the Sado estuary Mesolithic shell-midden site of Arapouco, excavated over 60 m², is 1895, and in sites more recently excavated with careful, total recovery of the marine fauna, such as Toledo, the count is 143 (for an area of 27 m²) (*67,*

151). The numbers therefore suggest fishing on a scale minimally like that documented in the mid-Holocene Mesolithic of Portugal, even if not necessarily with the same targets — which may be due to differences in catching technology, if not simply the paleoenvironmental setting.

S7. Birds

A total of 191 bird bones were retrieved in the 2010-13 excavations, all in the Area F trench. Of these, 80 could not be classified any further. Two elements of *Larus* sp. (gull) and *Gavia stellata* (red-throated diver) came from deposits belonging in Phase FB3; the remainder came from deposits belonging in Phase FB4 (N=26) or from reworked units of provenience (N=83) (Tables S30-S31; Fig. S31). A significant number belong to aquatic or marine migratory species (*156*); information on their habitat, behavior and extant presence in Portugal is given in Table S32. As with the crabs and fishes, surface appearance, degree of fossilization and presence of carbonate concretions allow us to sort the Pleistocene-derived material found in the reworked sediment from the Holocene intrusions present alongside.

Once the small proportion (ten out of 83, or 12%) of Pleistocene-derived specimens is removed from consideration, the birds from reworked contexts form a homogenous assemblage whose taxonomic composition is amenable to comparison with Phase FB4's. The contrast is clear (Fig. S31a): marine and aquatic birds represent 87.5% of the Holocene assemblage but only 38.5% of Phase FB4's (and only 19.2% if mallards and divers, mostly found in inland waters, are excluded from the comparison). A similar contrast in taxonomic composition between "with" and "without" concretion specimens is also apparent in the avian assemblage excavated 1986-89 in Area C (*23*). As with the crabs, this contrast reflects the changing position of the cave relative to the shore line. Nowadays, Figueira Brava's Entrances 2-3 are a seaside, unroofed platform that can be used by seabirds and probably was already so used ever since it was exposed by early Holocene marine erosion; thus, it is hardly surprising that, accumulated by natural death and predator kills, or thrown ashore by the waves, Holocene seabird carcasses, or elements thereof, eventually would have found their way into the adjacent cave spaces.

In Iberia, today, cormorants (*Phalacrocorax carbo*) can be seen wherever fish-rich, extensive water bodies exist, along the coast as much as in interior wetlands and dam lakes. They are a common sight on the Arrábida coast, resting or nesting on the rocky shores, on isolated rocks in the middle of the water but close to the coast, or, looking out for the opportunity to scavenge for leftovers, in fishing harbors; their predominance in the Holocene assemblage, where they stand for 47.9% of all the birds and for 54.7% of all the seabirds, is not unexpected. However, the *Phalacrocorax* remains from Phase FB4 are significantly smaller than the *Phalacrocorax carbo* females in the reference material used and, hence, have been assigned to shag (*Phalacrocorax aristotelis*). As shags are exclusively marine, their presence at Figueira Brava, which, during Phase FB4, was a roofed, subterranean and inland environment implies transport from the extant coast line, i.e., over distances of ~2000 m and, hence, human agency — none of the alternative predators that might conceivably be involved is known to take preyed birds to dens located at such a distance.

Other aquatic birds whose preferred habitat are sea shores, estuaries and coastal lagoons are represented in the assemblage from Phase FB4 and among the Pleistocene-derived material found in the reworked sediment: mallards (*Anas* cf. *platyrhynchos*; Fig. S31f), geese (*Anser*), gannets (*Morus bassanus*), sandpipers (*Calidris*), the great auk (*Pinguinus impennis*; Fig. S31c), razorbills (*Alca torda*), guillemots (*Cepphus*) or puffins (*Fratercula*), and divers (*Gavia*). As with shags, the accumulation at Figueira Brava of the remains of these species implies human agency, in at least the case of the seabirds, and quite likely also with regards to divers, geese and mallards. Indeed, the steepness of the Arrábida coast means that the lakes, ponds, marshes and river margins that are the habitat of divers and mallards could only have existed away from the cave, in the flat land of the nowadays-submerged terminal section of the Sado alluvial plain, to south and southeast.

The body part representation and carnivore damage data (Tables S33-S34; Fig. S31a-b) are also consistent with an anthropogenic origin for Figueira Brava's Pleistocene birds. Carbonate accretions were found in none of the Phalacrocoracidae from the reworked sediment. In this homogeneous Holocene assemblage, all body parts are represented, which suggests that the individual bones retrieved come from the disintegration of whole carcasses. Taking the Holocene Phalacrocoracidae as a standard for what a naturally accumulated Pleistocene assemblage of seabirds ought to look like, we see that the assemblage formed combining the marine and aquatic bird remains from the IH complex with those from reworked proveniences that bear cemented accretions deviates significantly from expectation: such remains consist entirely of proximal, meat-bearing wing bones (coracoid, scapula, humerus, ulna and radius). Thus, even though, when looking at individual taxa in isolation, the numbers are too small to allow certainty, the overall pattern suggests that these birds were procured for food, not plumage. Their human consumption is abundantly documented in the archeological, ethnographical and historical records (*157*), and the likely anthropogenic squashing and notching seen in the right distal humerus of a mallard from unit IH8, consistent with mastication-induced damage, may well represent direct evidence to that effect (Fig. S31f).

Interpreting the Pleistocene terrestrial bird assemblage is a more complex task. The skeletal part information is consistent with the introduction of complete bird carcasses because both wings and legs (and even a mandible) are represented, and they are so in approximately the same proportion as among the Holocene, naturally accumulated Phalacrocoracidae. A raven shaft fragment is possibly cut-marked (Fig. S31g), but a distal femur that could not be taxonomically identified bears punctures that are consistent with carnivore-induced damage (even though weathering or corrosion cannot be completely excluded; Fig. S31h). Thus, it is entirely plausible that the assemblage is of mixed origin. The wild fowl species — partridge (*Alectoris rufa*) and woodpecker (*Scolopax rusticola*) — may well have been hunted for food. Sparrowhawks (*Accipiter nisus*) and black kites (*Milvus migrans*) do not nest in caves, so their bones may reflect procurement for plumage, as reported from several Middle Paleolithic sites (*158, 159*). Vultures, represented by a quadrate assigned to *Gyps* sp., and the little owl *Athene noctua*, represented by a left carpometacarpus (Fig. S31e), could be the non-human agents involved in the accumulation of the other terrestrial birds, as both are known to use caves for shelter.

In addition, note that, in the IH complex, carnivore damage was anecdotical and observed only on rabbit and terrestrial or indeterminate birds — none was found on aquatic birds or larger mammals (Table S34). In contrast, crenulated edges, pits and punctures indicative of carnivore involvement in the acquisition or eventual discard of the remains were found on 15.6% (ten out of 64) of the marine birds without concretion retrieved in reworked sediment, and all but one of the carnivore-damaged rabbit bones come from reworked contexts. The taphonomic evidence is therefore fully consistent with the notion that, even though the Holocene-intruded small prey elements were accumulated by non-human agency, the aquatic birds from the *in situ* deposit are anthropogenic.

Until it went extinct, the great auk ranged the cold waters of the North Atlantic, coming to land only to breed in remote, predator-free rocky islands. Occasional Holocene finds document the presence of these large, flightless swimming birds in the Mediterranean. These remains may represent stranded individuals, or else imply that the species once had a more extensive distribution (*160*). The existence of breeding colonies that far south during glacial periods is supported by the representation of the great auk in the Paleolithic rock art of Grotte Cosquer, in Mediterranean France (*161*). Thus, the Figueira Brava remains may well signify that resident populations existed off the Portuguese coast during the colder stadials of the Last Interglacial (recall that, as discussed above, units IH2-IH3 likely accumulated during GS 22).

The vegetation cover indicated by the Figueira Brava charcoal data suggests that, most of the time, the climatic conditions pertaining through the accumulation of the IH complex were not significantly distinct from present ones. Based on this evidence, one can legitimately extrapolate to the MIS 5b time frame the observed migratory behavior of most if not all of Phase FB4's aquatic and marine seabirds (Table S32). Of these, only the shag and the common murre *Uria aalge* (if the bone listed in Table S30 belongs to this species and not to a razorbill) are resident or have been documented to breed along the Portuguese coast in recent times. All the other (the red-throated diver identified from the IL complex, the grey goose, the gannet, and the sandpipers) occur as wintering or migrating-through individuals that can only be observed between October and March. It is likely, therefore, that the acquisition of most of Figueira Brava's aquatic and marine birds took place in autumn or winter.

S8. Mammals and tortoise

The total number of counted remains is 91 for tortoise and 5223 for mammals (Table S35). Of the latter, 470 are teeth or tooth fragments. For the Area F finds that could be identified to at least family level, and excluding the material found in reworked sediment units, taxonomic composition and vertical distribution are given in Table S36 and Fig. S32a-b; anthropogenic modification data and observations are listed in Table S37 and illustrated in Fig. S32c-e.

Rhino, a common occurrence in coeval Iberian assemblages, is absent from Figueira Brava's fauna, but the very large mammal size category is represented in the 1986-89 excavation of Area C by a molar fragment of elephant (*162*). Based on the supposed mid-MIS 3 chronology of the deposit, this remain was originally classified as mammoth but, with current knowledge, *Elephas antiquus* is the correct assignment (*163*). This

earlier work at the site also yielded a few remains of marine mammals: ringed seal (*Pusa hispida*) and short-beaked common dolphin (*Delphinus delphis*) (Fig. S33b-c). The sediment cemented to these bones shows that they originated in the Pleistocene deposit, which, given site-to-shore distances, implies human agency; clearly, the remains are not recent Holocene intrusions derived from natural deaths (e.g., beach-stranded dolphins, a resident population of which nowadays lives in the Sado estuary). In addition, note that the ringed seal is an arctic species closely associated with pack ice; the sporadic occurrence of single individuals has been recorded in the Azores archipelago but, in mainland Portugal, the taxon has never been identified in archeological or paleontological sites of Holocene age.

Whether counted by NISP or MNI, prey ungulates dominate the Figueira Brava fauna. Next come lagomorphs, in Phase FB4, and tortoise, in Phase FB3. The largest species represented in the Area F assemblage is the aurochs. Deer, among which only *Cervus elaphus* could be identified to species, are the most abundant game. Based on dentition and long bone fusion, all age classes are represented, and the same applies to caprines and equids (among which *Equus caballus* could be identified to species).

Human involvement in the accumulation is shown by the percussion and butchery marks observed on specimens that could be identified as horse or deer. Most burnt fragments are too small to allow identification, except with regards to tortoise, owing to the characteristic morphology of the shell. A brown, black or grey color indicative of exposure to heat was recorded in 13 out of the 74 (18%) tortoise remains; this pattern denotes use of a roasting-in-the carapace technique of cooking, as suggested for similar finds from coeval contexts (*29, 164*).

No anthropogenic marks were identified on the carnivore bones, so natural accumulation, implying use of the cave as a carnivore den, is the parsimonious explanation for this material. With regards to bear, hyena and wolf, note that (a) most remains were found in units IH8 and IL2, at the interface between the IH and IL complexes, and (b) the single remains of both lynx and porcupine come from unit IH8, i.e., essentially the same stratigraphic position (for illustration of this material, see Fig. S33). Such a vertical distribution is at odds with the general pattern displayed by all other taxonomic groups, for which the mode is found higher-up in the sequence (Fig. S32b).

To interpret these carnivore remains in terms of site formation process we need to bear in mind that the interface between the IH and IL complexes corresponds to a hiatus in sedimentary deposition. During this hiatus, extensive flowstone formation and stalagmite growth, forming unit IL1 in Area F and unit MC0 in Entrance 3, occurred at the site (Table S12; Fig. S6). Given that the ungulate bones in IH8 and IL2 show no evidence of either gnawing or carnivore modification, this stratigraphic pattern suggests that the remains of porcupine, bear, hyena, wolf and lynx stand for death-at-den events occurring during that hiatus. Eventually, those remains became commingled with the bones of the prey animals brought in by humans once deposition of the IH8 (Area F) and basal UC (Entrance 3) sediment began.

The fact that more than 70% of the larger carnivore remains belong to bear, not to such bone accumulators as the hyena or the wolf (Table S36), is consistent with this interpretation. By the same token, the hyena coprolites found across the IH complex (for complete or near-complete specimens, the counts are six in IH2-

IH3, six in IH4, eleven in IH6, and ten in IH8) must reflect the occasional return of carnivores to the cave, and the same applies to the few remains of hyena and leopard from the 1986-89 excavation of Area C (*162*). Wherever cementation spared the deposit from recent or sub-recent burrowing (namely, in the SW corner of the Area F trench), scatters of nodules and particles of digested bone resulting from the disaggregation of coprolites can be seen under the capping flowstone. These scatters probably reflect reuse of the site as a hyena den once the deposit's build-up brought the cave floor so close to the roof that human use of the space became impossible.

Following this line of reasoning, we also need to note that (a) the vertical distribution of the caprine remains follows the larger carnivore, not the general ungulate pattern (Table S36), and (b) those remains display no anthropogenic modification marks. Notwithstanding that no carnivore modification marks were found either, the concentration of caprines in unit IH8 could therefore reflect predation (by, e.g., the wolf). The lack of anthropogenic modification marks, however, is parsimoniously explained by the taxon's skeletal part representation: the remains are mostly teeth, which make up 67 out of the 72 (i.e., 93%) identified specimens, so it is especially relevant that none bear signs of damage by digestive acids, which would at least seem to exclude hyena involvement. Because no diagnostic elements permitting discrimination were found, the caprine category subsumes both ibex and chamois, but the mountain setting of the site and the Mediterranean paleoenvironmental context suggest that most (if not all) of the IH8 caprines are ibex hunted in cliffs-with-matorral habitat, which would then be found in the higher reaches of Serra da Arrábida. In short: even though it cannot be excluded that carnivores played some role in the accumulation of the caprine remains, there is no positive evidence that they did.

In contrast with the larger carnivore pattern, most of the wild cat remains were found in units IH2-IH3 and IH6. Recall that a rabbit bone from unit IH4 is the single instance of carnivore damage documented in the mammal bone assemblage, and that possible carnivore punctures were observed on some of the terrestrial birds from the IH complex (Table S34; Fig. S31h); as it preys on rabbits and birds, it is therefore entirely plausible that the wild cat is the species responsible for those marks. Such a conclusion does not necessarily entail, however, that wild cat (and perhaps lynx too) are to be held responsible for the accumulation of the smaller prey assemblage in its entirety. Even though the Figueira Brava rabbit assemblage lacks the typical long bone cylinders (diaphysis from which the ends were chewed- or cut-off to access the marrow) that are diagnostic of human consumption, some terrestrial bird bones display modifications that are likely anthropogenic. Therefore, there is no reason to think that the rabbits could not have been brought in by humans too, at least in part; the tortoise most certainly were.

S9. Stone tools

The post-excavation processing of the lithic artefact component of the deposit excavated 2011-13 — cleaning, removal of adhering concretion, sorting of the sieve and floatation samples — has already been completed for square U8. Quartz overwhelmingly dominates the assemblage, but quartzite, flint and other flint-like rocks, limestone and other, rare, lithic raw-materials (e.g., lydite), are also represented (Tables S38-S39). Quartz is locally abundant (e.g., as cobbles, in both marine deposits and continental conglomerates).

Quartzite cobbles are ubiquitous in the fluvial terraces of the Sado and, hence, at the time of occupation, would have been found in the now submerged terminal part of the river valley, southward of the cave. Flint-like rocks can be found ~50 km upstream in conglomerates of Paleogene age, and there are unconfirmed reports of flint being present in conglomerate formations of the same age found ~5 km to the northeast; however, the closest sources of the Cenomanian flints identified in the assemblage are on the right banks of the Tagus, in the Lisbon area, >30 km to the north (*165-167*).

To advance sourcing and define the site's territorial catchment, the siliceous component of the lithic assemblage was fully sorted out early in the post-excavation, finds-processing stage. It was therefore possible to analyzed it in totality (Table S40). A sample of 50 quartz specimens — selected across a range of technological categories based on the presence of suggestive macroscopic modification (e.g., edge scarring, impact fractures) — was also examined for use-wear evidence (Table S41). Illustration of the results obtained and of a small selection of the stone tool assemblage is provided in Figs. S34-S39.

The 2011-13 inventory numbers compare relatively well with those published for the 1986-89 excavation (*23*). The volume of sediment excavated in Area C can be estimated at ~5 m³. Excluding debris to avoid biases related to recovery technique that volume of sediment yielded 3948 lithic artefacts, i.e., some 790/m³. The equivalent ratio for square U8, where the volume of excavated sediment can be estimated at just under 1 m³, is 954 (Table S38). Quartz overwhelmingly dominates both assemblages (it represents 90% of the lithics in Area C and 92% in square U8), and it is represented by all steps of the reduction sequence. For this raw-material, items with a "partial, atypical retouch" were included among the retouched tools only in a very few, unambiguous cases because, with quartz, such types of edge modification are difficult to tease apart from among the irregular, often jagged edges produced at knapping.

Both excavations also yielded similar amounts of retouched tools. All raw-materials combined, the numbers are, per m³, 83 in U8 and 72 in Area C. However, while notches and denticulates represent 66% of the retouched tools in the U8 sample, the corresponding figure for Area C is 23% only; conversely, sidescrapers are 57% of the retouched tools in Area C as opposed to 16% in U8 (Table S39). If this contrast is not simply an artefact of differences in the classification criteria used, it may hint at all of Area C's layer 2 being the lateral equivalent of only Area F's units IH4-H8 because (a) that is where most U8 sidescrapers were found (Fig. S34f) and (b) in the U8 assemblage , the frequency of sidescrapers increases significantly from IT0-IH3 (6%) to IH4-IH6 (17%) and IH8 (40%) (Table S39).

S9.1. Stratigraphic variation

The archeological content of Area F's sedimentary fill is made up of remains displaced from activity areas located a short distance outwards and upslope. Therefore, such remains provide a geologically homogenized sample that is (a) unaffected by clustering biases (i.e., ones resulting from the spatial segregation of certain behaviors or certain tasks) and (b) appropriate for use in analyses of the diachronic variation in the intensity of human activity. However, that variation can be affected by other biases. Namely, with regards to stone tools, those resulting from (a) the excavation breakage of larger pieces, or (b) the loss of smaller pieces that, at

sieving, may have gone unnoticed and ended-up discarded with the cemented sediment chunks they could have been present in.

To assess the potential impact of such biases, Fig. S34a measures the variation in the lithic artefact content per volume unit, using the numbers for square U8 given in Table S13 and two different types of ratios: raw counts per volume, "N/m³" (with reworked unit IT0, whose lithics are entirely Middle Paleolithic, having been considered together with units IH2-IH3 , those most affected by subsurface tunneling); and weight per volume, where "g/l (1)" uses total weight and "g/l (2)" excludes manuports, hammerstones and chunks. In Fig. S34b, the "g/l (2)" indicator is additionally compared with the results for the bulk samples used in the sediment composition analysis. In agreement with expectations based on the geologically homogenized nature of the deposit, the lithics indicators behave in similar manner, and the bulk samples' shell curve tracks the same trend. These observations support that the site was less intensively occupied during the time window corresponding to the upper MC and IL complexes of, respectively, Entrance 3 and Area F (Phase FB3 of the site's human occupation), as concluded above on the strength of the marine invertebrate data alone.

From a methodological standpoint, we can also conclude that (a) the three indicators derived from the excavated lithics are equally reliable for the assessment of intra-site diachronic variation in the intensity of human activity, and (b) the lithics and shell density data derived from the bulk samples are reliable proxies for assessments of variation in the importance of the deposit's anthropogenic components as a whole. For each unit, however, the weight/volume ratios returned by the excavated lithics indicator are up to five times higher than the bulk sediment values. This difference is explained by their different nature: the "excavated lithics" sample represents almost 1 m³ of "all-particle-sizes-included" sediment, while the "bulk lithics" samples represent less than a thousandth of that (just over 0.5 dm³) and lack the larger, bulkier material making up most of the stone tool assemblage (among which the smaller, lighter chippage and debris account for <10% of the total weight; Table S38). That is why the "excavated lithics" sample yields higher weight/volume ratios even when the larger finds are excluded.

S9.2. The flint assemblage

The flint items retrieved in the 2011-13 excavations are counted in Table S40 per techno-economic and technology-of-debitage categories. To increase sample size, the analyses use the "Phase" framework. The assemblage from Phase FB4 is characteristically Middle Paleolithic. Those from Phases FB3 and FB2 are too small for statistical comparison, but their qualitative assessment found no evidence that they might be technologically distinct.

The study of these flints is hindered by extensive burning. Thermal alteration has been observed to a varying degree in 44% of the finds, and it is likely a key factor in the fragmentation of the material (48% of the sample is made up of broken pieces, even though in most cases diagnostic traits remained and assignment to a given technological category was possible).

From the presence/absence of cortex we can infer that, for siliceous rocks, the reduction sequences are incompletely represented at the site. Indeed, 59% of the remains have no cortex at all, while only 8% display a

dorsal side that is >50% cortical. The notion that, with regards to flint, the site is primarily a *locus* of consumption and discard is further supported by several indications of the introduced volumes' intensive reduction and recycling. Abandoned cores are largely exhausted and small (Fig. S34c), one third are broken, and there is evidence that core fragments were reused as blanks for the on-site extraction of small flakes (Fig. S35, nos. 1-2). The latter were also produced from flake blanks, as documented by three such cores and by the Kombewa-type flakes found among the debitage products. Conversely, Levallois cores are present (Fig. S35, nos. 3-4), even though none was found that could have produced the assemblage's larger Levallois products (Fig. S36, nos. 4-5). These are up to 6 cm in length, well above the average for all blanks combined (Fig. S34c).

Most cores feature the reduction of two sides, each playing a different role in the process. The dorsal, production side features centripetal (N = 5), unipolar (N = 3), bipolar (N = 2), and multipolar (N = 1) scar patterns. Accordingly, most flakes present the peripherally arranged type of cutting edge that is so characteristic of the recurrent, centripetal reduction schemes well documented among the cores. Most platforms are unfaceted; dihedral and cortical platforms come next in frequency. None of the imported Levallois blanks, among which most of the assemblage's rare facetted platforms are found, is retouch-modified. Formal tools are 14 (Table S40; Fig. S36, nos. 1-3, 6). Most (N = 6) feature partially or atypically retouched (or worn) edges. The remaining flint tools are denticulates and sidescrapers. Overall, most retouched tools (9 out of 14, or 64%) were made on cortical or part-cortical debitage products, which indicates that they were imported — either as finished implements or as blanks that, prior to discard, were used or re-sharpened at the site. The latter is indicated by a couple of retouch flakes (Table S40).

S9.3. Use-wear on quartz artefacts

All use-wear evidence was found on items made on fine-grained, milky or translucent quartz varieties. None was found, so far, on the coarser-grained varieties that were also flaked at the site (Fig. S37, nos. 1-2). It remains to be investigated whether this pattern reflects a wear-preservation bias or that coarser-grained quartz was more expediently used, leaving no detectable microwear, in the context of short-duration activities.

Post-depositional damage was observed in some cases, along edges as well as surfaces, mostly in the form of flat bright polishes (N = 11) that, owing to their aspect and random distribution across the microtopography of the piece, are distinct from those produced by use. It is only along the worked edges that characteristic use-wear was observed. Such traces consist of (a) polishes that vary in aspect, density and texture according to the nature of the material and the gestures of the worker, and (b) striations associated with those polishes whose distribution, length and orientation are a reliable indicator of motion. In the sample that we analyzed, the preservation of these kinds of traces is quite good and allows some degree of functional inference.

In the 22 pieces that preserved use-wear (Table S41), a single edge was used in all cases. The traces (Figs. S37-S39) indicate the processing of organic, e.g., animal-soft materials (N = 2), and of wood (N = 8). Use on hard materials in the context of cutting and scraping motions is documented in 12 cases, but the exact nature of the contact material remains uncertain.

Wood processing is indicated by the typical polish found in three unretouched flakes (Fig. S38, nos. 2-4), in which it is associated with parallel micro-striations whose orientation and length are characteristic of cutting tasks; the morphology of the impact scars and their distribution on both sides of the used edge are consistent with this functional interpretation. Four denticulates (Fig. S39, nos. 3-4) and one scraper (Fig. S38, no. 1) were also used on wood, but for scraping, not cutting. The processing of hard materials is documented on laminary products (Fig. S37, no. 4), nucleiform pieces (Fig. S39, no. 1), and denticulates (Fig. S39, no. 2). Evidence of involvement with animal-soft material was found on an elongated bladelet-like product (Fig. S37, no. 3), and on a denticulate.

This pilot study shows that the different kinds of domestic activities one might expect in the context of a residential occupation are indeed documented at the site. So far, no evidence has been found for the use of stone tips or stone inserts in either thrusting or throwing weapons, but the sample analyzed is small and did not include the siliceous raw-materials. Therefore, this absence of evidence cannot be taken as evidence of absence.

S10. Comparative framework

Current debates on how adaptation and subsistence changed in the course of human evolution have focused on the origins of so-called "broad spectrum" economies. Traditionally, most accounts emphasized the contrast between the big-game focus thought to characterize the Paleolithic, on one hand, and the major role played by plant foods and small prey animals among the hunter-gatherers of the Late Glacial and the Early Holocene, on the other hand. Recently, the application of appropriate dating techniques has shown that the systematic gathering of shellfish, fish and tortoise was a key feature of human subsistence at several South African sites of much earlier, Last Interglacial age. This evidence has been related to the region-specific emergence of innovative behaviors, in tandem with the emergence of anatomical modernity (*8, 9*). Others, however, have argued that the geographic exclusiveness of the South African pattern is apparent and underpinned by preservation and research biases (*11*).

Due to the shortcomings of the available corpus, putting Figueira Brava in the context of these debates is not an easy task. For instance, quantitative information on the Last Interglacial exploitation of marine mammals is lacking in Iberia, while Figueira Brava is the only site of the period, whether in Europe or Africa, to have yielded such information for plant foods and large crabs. Nevertheless, it has been proposed that fishing and shellfishing represent good proxies for the exploitation of the whole range of resources offered by coastal ecosystems (*8*). Under this premise, Figueira Brava can be compared with relevant instances of broad spectrum foraging: the Last Interglacial littoral sites of Africa and Iberia, because they are of the same age; and the littoral sites of the Iberian Mesolithic, namely the mid-Holocene shell-middens of the Sado valley, because they are located upriver from Figueira Brava, at the bottom end of the paleo-estuary, and had access to a similar range of animal and plant resources, both terrestrial and aquatic.

Compilation and illustration of the data is provided, alongside an explanation of the sources and calculation methods used, in Tables S42-S45 and Figs. S40-S42. Holocene shell-midden sites are normally found on, or

close to the beach or the margins of the coastal lagoons and estuaries in which the aquatic resources were acquired, while coeval inland localities feature amounts of marine or estuarine shells that decrease as the distance to the procurement source increases (*20*). That distance to the shoreline is a key factor in the explanation of inter-site variation in the amount and density of fish and shellfish remains is also agreed upon by most reviews of the South African MSA evidence (*19*). For this reason, in Fig. S42, the density proxies are plotted against the distance between the site and the nearest point of procurement (i.e., the nearest seashore or the nearest estuary margin).

S10.1. Comparison with Holocene shell-middens

The up to 5 m-high shell-mounds of the inner paleo-estuary of the Tagus, near Muge, are a well-known example of the site type. They date from the Late Mesolithic and underwent several spells of excavation between the mid-19th century and the 1960s. Such past work focused on the human burials and used standards of recovery that are insufficient for a meaningful quantitative understanding of the abundance and density of the associated material culture and faunal remains. However, over the last 20 years, one of the mounds, Cabeço da Amoreira, has been re-excavated. Besides a more detailed radiocarbon chronology, the new work produced a geoarcheological interpretation of the deposit based on the analysis of soil micromorphology thin sections (*168-170*); since, the several microfacies (mF) differentiated at Cabeço da Amoreira have also been recognized at the Sado shell-midden site of Poças de São Bento (*171*). As illustrated in Fig. S40, the defining characteristics of the mF types recognized in the shell-middens of the Tagus and the Sado can also be observed in the basal units of Figueira Brava's MC complex (Phase FB2).

At Cabeço da Amoreira, mF Type 1 (dominant interconnected shells) is interpreted as the outcome of tossing and, as such, to reflect very fast deposition events; the presence of a calcitic matrix defines mF Type 1b, which occurs exclusively towards the base of the profiles and relates to the secondary deposition of calcium carbonate derived from the partial dissolution of shells higher up in the sequence. At Figueira Brava, mF Type 1b also appears in a basal position; higher-up in unit MC5, one sees mF Type 3 (horizontally oriented components within microcharcoal-rich, compact and somewhat laminated lenses that, in places, appear post-depositionally tilted). At Cabeço da Amoreira, the interpretation offered for mF Type 3 is that it stands for true occupation surfaces, ones where crushing and trampling, resulting in the *in situ* breakage of shells, are the main post-depositional processes (for an instance of such shell fragmentation in unit MC5 of Figueira Brava, see FB1002-06 in Fig. S13). Unit MC4 of Figueira Brava fits the definition of mF Type 2a (heterogeneous coarse sands and shells, rich in anthropogenic components), which, at Cabeço da Amoreira, is interpreted as the reworking of occupation-derived material accumulated close by the *locus* of original deposition.

The specimen count and the density data provided in Table S42 and plotted in Fig. S42a-f are consistent with the structural similarities highlighted by the soil micromorphological evidence. Regardless of which proxy is used, the general rules that one can infer from the Holocene data are that (a) as expected, the density of the remains decreases as distance to the source increases, (b) the trend is most apparent when the proxy used is the abundance of shell in bulk samples collected for composition analysis (Fig. S42a), and (c) an exponential line fits that trend better than a linear one (the coefficients of determination, R^2, are, respectively, 0.711 and

0.4584). The main phases of Figueira Brava's occupation, FB2 and FB4, plot above the weight/volume trend line, but not much, while FB3 plots below; overall, Figueira Brava fits the trend rather well and, when its values are considered alongside those for the Holocene sites to calculate the regression, the R^2 remains high (0.6354).

Those instances where the weight/volume values deviate more significantly from the regression's prediction can be explained by site-specific sampling and averaging factors. For instance, one might expect a higher density at Medo Tojeiro — and that would indeed be the case if the published data allowed one to exclude the uppermost, post-depositionally disturbed layer 1, where, according to Lubell *et al.* (*49*), shell density was half that observed in the intact deposit. Likewise, the low value for sample B of Toledo reflects the impact of post-depositional scattering, as discussed above. One would expect this factor also to have impacted the Figueira Brava deposit, but it does not seem to. The reason must lie in the properties of the depositional contexts: open-air, across an unconstrained area, favoring spatial scattering, at Toledo; inside a cave, forming a distribution where the bounding walls tightly constrain spatial scattering, at Figueira Brava.

When the abundance of shell is measured in terms of NISP or MNI per unit of volume (Fig. S42b-c), distance to shore still retains some predictive value. However, significant variation can occur even when the comparison is restricted to sites located <1000 m from the nearest point of procurement. That variation must relate to preservation, recovery and analysis issues (Table S43). For instance, Toledo plots below expectations probably because the specimen counts include the sieve fraction of only seven of the 24 square-meter units of Areas A and B. In contrast, the sieve fraction from all excavated grid units is included in the counts for Barranco das Quebradas and Figueira Brava. In the latter, the indurated if not heavily brecciated deposit is responsible for much excavation-induced fragmentation, which hinders the identification of specimens. This factor, negligible in the case of the sandy, largely unconsolidated Holocene middens, inevitably downplays the importance of shellfish at Figueira Brava in comparisons that use MNI-based measures of density.

Factors of site function, site structure and sample representativeness can also have a significant impact on density numbers and need to be born in mind when interpreting them. Density primarily depends on the rate of deposition of the geogenic components (the sedimentary matrix) and the frequency of accumulation of the anthropogenic components (artefacts and ecofacts). For instance, a very dense deposit may result from the repeated discard of small amounts of shell over a long period of time during which sedimentation rates were low. Conversely, a deposit containing interstratified, very rapidly accumulated sterile lenses may appear as low density in kg/m³ terms but in truth result from the discard of larger amounts over shorter intervals. And, in lag deposits where the fine fraction underwent significant post-depositional loss to erosion, the density of shells, whether measured by weight or counts, will represent an overestimated proxy of the importance of shellfish consumption and discard.

To control for sedimentation rates and post-depositional compaction, shell abundance can be assessed in terms of specimen counts per length of time, normalized by the size of the excavated area. At Figueira Brava, this approach remains consistent with expectations derived from the weight/volume trend, but the density of shellfish relative to the Holocene sites is downplayed (Fig. S42d) and remains so even if we double the duration estimates for the Holocene sites and halve those for Figueira Brava. For fish (Fig. S42e-f), however, the fact that

Phase FB4 is a significant outlier does not change, thereby highlighting the extent to which fishing was indeed a significant economic activity at that time.

The following thought experiment helps to shed light on how these and related site formation processes may impact the density data. For 500 m² Site A, let it be visited every 50 years, let each occupation involve that 10,000 shells be discarded in a dedicated 4 m² area located at the edge of the site, let the rate of sediment accumulation be nil or very low, and let the shell heap in said dedicated area raise to 20 cm after ten occupation events (500 years). For 500 m² Site B, let it be visited on an annual basis, let each occupation result in the same 10,000 shells be discarded and scattered across the inhabited space, let the focal point of said space change from one visit to the next, let trampling, surface run-off and gravity redistribute the shells across the whole of the site, and let the occupation debris be buried by sedimentary inputs, eventually forming a deposit that, after the same 500 years, raises to the same 20 cm. A trench through the refuse dump in Site A would return a shell density of 125,000/m³ and a shell accumulation rate of 50/m²/year, while anywhere in Site B a trench through its homogenized deposit would return values of 50,000/m³ and 20/m²/year, respectively. Based on these values alone one might think that shellfishing was more important in Site A than in Site B, but adequate consideration of the geoarcheological context would show the opposite to be the correct conclusion.

Thus, (a) spatial structure and the position of the archeological trenches may condition the abundance of remains, and (b) site function and type of occupation (e.g., transient or prolonged, logistical or residential) may underpin differences in shell density between sites where the importance of the resource was in fact broadly the same. The different *loci* of Barranco das Quebradas provide empirical illustration of the impact that such factors may have on intra- as much as inter-site variability. For instance, the MNI/m³ is highest in localities 1 and 3, excavated over 2-5 m², and lowest in localities 4 and 5, excavated over 9-11 m². This difference illustrates how representativeness may be of special importance when the excavated areas are small. Locality 3 further shows how significant intra-site differences can be: in the four squares of the main trench, the NISP/m³ is 13,362 and the MNI/m³ is 4220, but, in the one square excavated 14 m to the north, they are one order of magnitude lower (1032 and 358, respectively) (*172*).

At Figueira Brava, functional factors suffice to explain the variability observed between the different phases, namely the lower density of shell in the deposit accumulated during Phase FB3. Spatial structure, however, is not so much of an issue because (a) site formation processes spatially homogenized the content of the IH deposit (Phase FB4), and (b) the sample used to assess weight-based density in Phase FB2 is representative of the variation seen across the internal stratigraphy of units MC3-MC5 (Table S22). These Phase FB2 numbers, derived from the excavation of the SEx trench, are also fully consistent with the information provided by the soil micromorphology thin sections obtained 6 m seaward, in the erosional exposure of units MC3-MC5; here, the shell-, burnt shell-, burnt bone- and charcoal-rich deposit can also be laterally followed by the naked eye, along the other axis of the excavation grid, over several meters (Figs. S4, S6, S11c).

These considerations help us understand why the data from unit 108 of the Cantabrian site of El Mazo fit the trend for kg/m³ but deviate hugely for NISP/m³ and MNI/m³ (for this reason, they fail to appear in the

Fig. S42b-d plots). Two immediately overlying units of statistically indistinguishable age, sampled at the same time in the same area but lacking published weight/volume information, have even higher MNI/m³ values: 194,500 (unit 114) and 184,900 (unit 115), more than twice the 91,636 found in unit 108 (*173, 174*). Site structure may explain the deviation, at least in part, as the samples come from a peripheral area of the site and reflect how dense shell can be in well-preserved refuse dumps; if post-depositional processes had resulted in their scattering across the 100 m² of El Mazo's sheltered area, the overall density of the remains would have been averaged out and, at any given point of sampling, much lower (and the attendant breakage would make for significantly diminished specimen counts).

Other factors further contribute to explain why El Mazo appears as an outlier in density estimates based on counts. Note that, given the average density of marine mollusk shell (~2.7 g/cm³) (*175*), the 3133 g yielded by the >2 mm fraction of unit 108's sample correspond to ~1160 cm³. A somewhat lower density may be assumed for the remaining 451 g of other shell material, 96% of which are of echinoderms; even so, shell cannot have represented more than ~1.5 l, i.e., some 7% of the sample's total volume of 22 l. This percentage falls in the range of the values seen at Toledo (14.6% to 62.2%), Figueira Brava (2.7% to 7.2% in Phase FB4, 24.9% in Phase FB2), Medo Tojeiro (7949 g of shell in samples totaling 21.4 kg, i.e., 37.1%) and Fiais (1608 g of shell in samples totaling 27.6 kg, i.e., 5.8%), even though these were calculated on weight, not volume (for Medo Tojeiro and Fiais, the weights were derived from the volume data using the same 1.45 density value for a deposit of mixed composition used in the context of the composition analysis carried out for Figueira Brava and Toledo; see above). Yet, the NISP/m³ counts are three orders of magnitude higher in El Mazo unit 108: 2,786,136 (all shell considered, including land snails, crustaceans and echinoderms; 876,318 for marine mollusk shell only) versus 1624 at Toledo and 2018 to 2504 at Figueira Brava (Table S42).

When, in a comparison, one side shows a proportion of shell relative to matrix and the other components that is smaller but NISP values that are much higher, it can only be because identification was either much more intensively pursued on that side of the equation or much hindered by fragmentation on the other. The weight/specimen ratio for El Mazo unit 108 is 164 mg; as limpets are 82% of the NISP and the average weight of a limpet shell is ~2 g, such ratio translates into an average specimen weight of 80 mg, which is less than the twentieth of an unbroken limpet shell and implies that many of the counted fragments were even smaller. The impact that mesh size and determination criteria can have on count-based density measures is further highlighted by García-Escarzaga *et al.*'s Table 3 (*173*): for the same sample volume, the MNI for *Patella* sp. and *Mytilus* sp. were, respectively, 633 and 9 in the >4 mm fraction, but, after adding the material in the [2-4] mm fraction, the MNI values were raised to 853 (35% more) and 14 (56% more). This example corroborates that, in inter-site comparisons, weight per unit of volume should be preferred over indicators based on specimen counts.

Site-to-source distances remained broadly stable during the accumulation of the Holocene sites reviewed here but underwent major fluctuation through Figueira Brava's sequence. Thus, even if each individual occupation event had produced the on-site discard of the same number and kinds of aquatic food refuse at all the sites, that difference alone would predict that, all other things being equal, the amount of remains

discarded per unit of time would be lower at Figueira Brava. Overall, thus, the data suggest that Figueira Brava functioned just like the home bases of the Iberian Mesolithic, but in more intermittent manner. Its record reflects events of occupation, consumption and discard that are structurally and economically similar but more spaced, both in terms of (a) how frequently people included the site in their year-round itinerary, and (b) how often the seashore was close enough to make it economical that fish, crabs, clams, limpets and mussels be transported to the site.

S10.2. Comparison with Last Interglacial coastal sites

The exploitation of marine mollusks is documented at several Last Interglacial sites of the Maghreb and South Africa, but little quantitative information is available for the former: the Contrebandiers cave excepted (*50*), the published North African data consist of species lists, specimen counts lacking the necessary volume information, or density values deemed "indicative" or "preliminary" only (*18*). In Iberia, besides Figueira Brava, such quantitative data exist for two Mediterranean cave sites, Aviones and Bajondillo, and a third, El Cuco, in Cantabria, whose basal layers are probably of Last Interglacial age. The sampling and counting methods used at the sites for which published information exists are described in Tables S44-S45. Since they are quite diverse, uncritical use of the raw numbers would bias conclusions in several ways and so inter-site comparison requires some discussion of data significance.

The Aviones numbers derive from total excavation samples but specimen counts have not been exhaustive, and the cementation of the deposit entailed significant excavation breakage; thus, specimen counts, whether by NISP or MNI, underestimate shellfish abundance. At Bajondillo, the material comes from the cutting back of a few centimeters of a profile, and it is unclear whether the samples are representative of the situation across the occupation surface or reflect localized concentrations (e.g., refuse dumps, as in the case of El Mazo). From the excavator's account — in personal communication to Curtis Marean (*8*) — we at least know that the Bajondillo accumulation is not shell-supported and cannot be described as a shell-midden. The Bajondillo samples are also small (7.5 l only for level 18), and they include all fragments collected down to the 0.5 mm mesh of the sieve column. In inter-site comparisons, these differences imply a significant bias in favor of Bajondillo, especially when using NISP/m³ values, as indeed revealed by the NISP/MNI ratio of 28.8 and 34.6 that can be derived from the data in Table S42. Those values are up to six-fold Figueira Brava's (5.5 to 5.7), where a 3 mm mesh was used and where the smaller fragments found in the floated and water-sieved residue were not counted. MNI/m³ is therefore the only Bajondillo proxy that can be meaningfully used, though bearing in mind that, in a comparative context, it too will overestimate the abundance of shell at the site.

The basal layers of El Cuco (layers VII-XIII) are separated from the overlying Gravettian by a thick carbonate crust (layer VI). This pattern implies a major hiatus, and the 42.4-46.5 ka radiocarbon dates obtained for shells from layers VII-XIII are in the same age range as those for Aviones and Figueira Brava that were dated by the same laboratory and turned out to be vast underestimates of the samples' true ages (*27*) (see above). One is therefore led to suspect that El Cuco's Middle Paleolithic is also an early, Last Interglacial manifestation of the technocomplex; for this reason, it has been considered here. The shell assemblage derives from the modern excavation of a 2×1 m trench (*176*) and was counted like at Figueira Brava (*44*).

To avoid the biases introduced by fragmentation and recovery, most South African researchers use MNI and weight per volume as proxies for density (*53, 55, 177*). In each of the contexts dated to the Last Interglacial for which data are available (Tables S42, S45), both ratios are computed from the same sample, one that is made up of all identified shell, either excavated- or sieve-collected. The samples are 20 to 200 times larger than at Bajondillo and were sieved using mesh sizes of 3 mm (at Blombos, Pinnacle Point 13B, and Klasies River), 2 mm (at Hoedjiespunt 1), and 1.5 mm (at Ysterfontein). The shell assemblage is weighed, each taxon's MNI is calculated, and volumes are either measured directly (from buckets of excavated sediment) or estimated from the area of the excavation and the thickness of the deposit. At Figueira Brava, due to the constraints imposed by cementation, excavated volumes are estimates based on trench size, and specimen counts are from all the excavated- and sieve-collected shell; the weight per volume data, however, are derived from ~100 g sub-samples of liter-size bulk samples studied with the methods of particle size analysis.

The volumes involved in the MNI comparisons fall for the most part in the 1¼-2¾ m³ range; the exceptions are Bajondillo (less), Aviones and Contrebandiers (more). The samples used represent the totality of the excavated deposit and the totality of its shell content, but, again, with exceptions; in this case, Klasies River and Blombos. At Klasies River, we know that the grid units the sample derives from represent <10% of the area excavated by Deacon in Cave 1A and were selected with no control for lateral variation (*55*); but we have no information on their relative richness. At Blombos, we know that only the three richest square-meter units were used, representing 13% of the trench's 22.5 m² and one fifth (~3 m³) of the excavated volume — 15 m³, as implied by a fish NISP of 860 and a fish NISP/m³ of 58 [(*53*) (Table 8), (*178*) (Table 6.9)] — of MSA sediments. In addition, we also know that, in the selected squares of Blombos, shellfish density (a) varies by a factor of 20 when individual layers are compared separately (e.g., between 163.8 kg/m³ in layer CI and <10 kg/m³ in layers CK, CM, CN, CO and CP below) (*52*), (b) decreases by a factor of two from one phase to the next as we go up in the sequence (in kg/m³, from 86.14 in M3, to 39.12 in M2, and to 20.74 in M1), and (c) if measured by MNI, is lowest in M3 (2361/m³), and more than double in M2 (5029/m³) (Table S42). As the brown mussel, *Perna*, increases dramatically from M3 to M2, the reversal of the kg/m³ trend seen when MNI is used may relate to differential identifiability (e.g., of even rather small mussel shell fragments). Whichever the case may be, these observations carry two implications: firstly, at Blombos as much as elsewhere, weight is a more reliable measure of shellfish abundance per unit of volume; secondly, even Langejans *et al.*'s kg/m³ values (*53*) are overestimates of the situation pertaining across the excavated area as a whole.

These sampling and analysis issues suffice to explain why, in Fig. S42g-h, some of the Blombos values plot above expectations. It is also possible, however, that the anomaly mostly resides in how site-to-shore distances have been estimated. Fisher *et al.*'s (*51*) model returns a minimum distance of 1450 m (corresponding to sea levels off Mossel Bay between -5.70 and -14.85 m) for 56% of the 75.5-102.5 ka interval during which the site would have been occupied. However, two more recent studies have produced evidence strongly suggestive of the distances involved being significantly shorter. Cawthra *et al.* (*56*) found that a depth of 8 to 12 m can be reached within only 650-810 m (a paleoshoreline assigned to MIS 7 would be present at that elevation), and that a large outcrop of foreshore deposits — Unit 18, OSL-dated to 93.9±5 ka and therefore representing a stillstand-to-regressive phase towards the end of MIS 5c — is found at a depth of 24 m and only ~1 km from

the extant shoreline. Jacobs *et al.* (*179*) produced a Bayesian model of the sequence that puts phases M1 and M2 in MIS 5a, to which must also belong the upper, shellfish-rich parts of M3, layers CH-CI, bracketed as they are by dates of 77.4±6.5 ka for layer CH, at the top, and 83.4±3.8 ka for layer CIBh1, at the bottom. As, in immediately underlying layer CK, shellfish density decreases by one-order-of-magnitude, this dating evidence suggests that (a) layers CH-CI accumulated in early MIS 5a, within the 78.5-84.5 ka interval for which Fisher *et al.*'s (*51*) model returns sea levels of -5 to -10 m, and (b) layer CK and the layers under it date to late MIS 5b, when sea level was much lower and the shore much farther out. As both global sea level curves and the local Mossel Bay data and models show that sea level in MIS 5a peaked well above the elevation reached in MIS 5c, it follows that the MIS 5a shoreline must have been much closer than the ~1 km at which we now find the submerged MIS 5c foreshore deposit. Based on this reasoning, Table S42 and Figs. S42g-h posit that most marine food remains from the Blombos layers that have been included in the M3 phase also relate to occupation of the site during MIS 5a, and therefore assume for all three phases a site-to-shore distance of 650 m (which, however, may still represent somewhat of an overestimation).

Klasies River's MNI/m³ values are much higher than at other sites similarly located directly on or adjacent to the beach (e.g., Hoedjiespunt, Ysterfontein). Although we cannot exclude that, as in previous examples, the cause lies in site structure and sampling bias, it is necessary to bear in mind that, as pointed out by Will *et al.* (*32*) and supported by the evidence from the Holocene contexts discussed here, site function may also make a significant contribution to the variability in shellfish abundance. Thus, it may well be that the other South African onshore sites in Table S42 were only transiently used, or infrequently reoccupied, while Klasies River was a place of long-term residential activity — in agreement with the abundant stone tools and fire features, and the recovery of human remains (*34*). The same may apply to Blombos, given the number and relevance of symbolism-related artefacts (shell beads, pigment containers, engraved and painted items) (*35-38*); if dating, sampling and analysis biases are eventually shown not to be an issue, major-home-base status is an alternative explanation for the higher-than-expected density of marine foods seen in some of this site's layers.

Bearing these caveats in mind, Fig. S42g shows that, by density measured in weight/volume, Figueira Brava plots well above expectations. This observation is the more significant because, in the comparison, Figueira Brava is biased against, not for. As discussed above for the lithics component, density values derived from the weight of total excavation samples that include the bulkier remains (the South African sites' case) are bound to be higher than those derived from small samples collected for composition analysis (the Figueira Brava case). Fig. S34b makes this clear for the lithics of Figueira Brava, and it must be the same for shells whenever one side of the comparison is an assemblage entirely made up of centimeter and sub-centimeter fragments while the other side is an assemblage that includes all the excavation-collected finds (e.g., complete specimens). In addition, while fragmentation hinders specimen identification and, hence, the counting of individuals, it has little impact on weight/volume ratios (together, the fragments of a shell will weigh as much as it did when unbroken). The presence of carbonate accretions (to be expected in heavily cemented deposits such as those from Phase FB2) would have the opposite effect because the chemical process used for their ready removal from the Figueira Brava stone tools (washing with diluted acetic acid prior to weighing) is not appropriate for shell. However, that is why the decision was made to derive the site's weight/volume ratios from small bulk

samples of loose sediment, disaggregated and processed with the standard methods of particle size analysis, not from the totality of the excavated-and-sieved shell assemblage that the MNI derives from.

The crab and fish data support that the density of marine food remains be higher at Figueira Brava than at coeval South African sites, and especially so considering distance to shore. Crabs represent significantly more meat than the mollusks found alongside in Figueira Brava's Phase FB4 (see above), but none have been reported from the South African sites. And, at 458, the NISP/m³ of the fish from Phase FB4 multiplies almost tenfold the values for the only Last Interglacial site with which the comparison is possible: Blombos (where the corresponding values range between 47 and 67) (Table S42).

Despite ranking higher than the South African sites in shell weight/volume, Figueira Brava plots at the bottom of their distribution in mollusk MNI/m³ (Fig. S42h). The cause for this contrast probably lies in the amount of fragmentation. This factor works against MNI counts and impacts the Figueira Brava numbers because of the significant excavation breakage entailed by the cementation of the deposit. On the other hand, significant breakage can also result from low sedimentation, slow accumulation and attendant compaction; if so, shell density, however measured, would always be comparatively overestimated. That is not the case at Figueira Brava, however, as the IH complex (Phase FB4) includes levels whose deposition lasted 240 years at the most (e.g., unit IH5; Table S17), while the Mf Type 1b structures seen at the base of the MC complex (Phase FB2) stands for short-lived accumulation events. The intactness of such structures rejects that these be lag deposits and shows that, besides excavation damage, fragmentation results from syn-depositional trampling, i.e., the intensity of short-term human activity, not from post-depositional, long-term diagenesis.

Of the South African sites, only Pinnacle Point 13B has both soil micromorphological analyses and estimates of density enabling direct comparison with Figueira Brava. Even though the microphotographs used in the Pinnacle Point 13B study may have been selected primarily for the illustration of other aspects of site structure and site formation, the fact remains that shell is seen in few: from the Rear/Western area, in MB-03-4B, which represents the 5 cm-thick, recently reworked surface material forming Unit 5; from the Entrance/Eastern area, in MB-04-3A, which shows the site's most recent MSA unit, the Truncation Fill, of MIS 3 age (<39 ka), and in MB-04-03B, which shows the upper part of the underlying Shelly Brown Sand unit, of MIS 5c age [(*180*) (Figs. 6d, 15b-d)]. The visual comparison (Fig. S41) suggests that shell would indeed seem to represent at Pinnacle Point 13B a significantly smaller proportion of the units' groundmass than it does at Figueira Brava, and the published profile photography (*41, 180*) includes not a single example of shell-supported lenses; even if, based on MNI/m³, the values for Figueira Brava and Pinnacle Point 13B are similar (Fig. S42h), the imagery suggest that the significant difference displayed by the weight/m³ plot (Fig. S42g) is truer-to-life.

Despite the evidence reviewed above showing otherwise, it has been argued, based on scatter plots of the piece-plotted shell, that the SBS/URS/LRS package of the Eastern Area of Pinnacle Point 13B represents a true shell-midden accumulation. At the same time, taking the argument one step further, the importance of mollusk gathering in the Mousterian of Vanguard Cave (Gibraltar) was questioned because the distribution of shells (mostly mussel) around a hearth in the Upper Area of the 1995-98 excavations produced a plot much thinner than the dense point clouds formed by the Pinnacle Point 13B data in both the vertical (across a thickness of

~30 cm) and the horizontal (over an area of 2.5×1.5 m) dimensions. With regards to the economic role played by marine foods, the conclusion was that the contrast between the two sites supported that a difference in kind existed between the MSA of South Africa and the Middle Paleolithic of Europe (*8*).

This line of reasoning is flawed at several levels. Firstly, direct comparison between the two plots is meaningless because of how differently each was generated: the Pinnacle Point 13B graphs stem from a protocol requiring total-station piece-plotting of "all finds that were seen by the excavator" (*41*); the Vanguard graphs stem from the scanning of Barton's (2002) Fig. 23.2 (*42*), and this figure is based on a field map hand-drawn at 1:10, meaning that only the material visible at that scale could have been noted. Secondly, the "mollusk" symbols in the scanned Vanguard distribution map represent small groups as much as individual finds. Thirdly, SBS/URS/LRS is a thick package estimated to represent a span of, minimally, 8000 years (*41*), while the Vanguard context is a very thin deposit of high integrity likely to represent a single occupation event (*43*). Bearing in mind that the combined MNI for the SBS/URS/LRS package is 549 (Table S42) and that the MNI for Vanguard's mussel hearth context is 73 (*42*), it is easy to see that the amount of shell discarded in the SBS/URS/LRS package is the equivalent of eight of Vanguard's events. In short, the SBS/URS/LRS accumulation could have been the result of the shells of seventy-odd mollusks having been discarded at Pinnacle Point 13B once every thousand years — hardly a good case for the importance of marine foods in the site's MSA.

From a methodological perspective, what the Pinnacle Point/Vanguard comparison highlights is why scatterplots of piece-plotted shell cannot be used to demonstrate that a given stratigraphic unit is shell-supported. In such plots, the density of point clouds obviously depends primarily on the number of items present in the deposit. However, the actual density of those items in the deposit, not in the plot, depends on factors other than the intensity and redundancy of the human behaviors involved; as pointed out above, rates of sedimentation and post-depositional compaction need to be considered. How an excavation was carried out, namely, which cut-off criteria were used, also matters; for instance, the same amount of material in the same volume of sediment will make for much denser point clouds with piece-plotting of "all finds that were seen by the excavator" (the Pinnacle Point protocol) than with piece-plotting of "all finds that are complete, rare or >5 cm fragments" (the Figueira Brava protocol). Ultimately, the problem is that, in a shell-supported deposit, shell is so abundant, and often so broken, that piece-plotting is simply impracticable: one cannot remove a shell without disturbing the position of those that support it, and the introduction of a digging tool inevitably results in the lifting of shells and sediment matrix in bulk. In such circumstances, precise plotting is a meaningless exercise. Thus, whenever systematic piece-plotting of individual shells is practicable in a given deposit, it can be safely inferred that said deposit is not shell-supported — precisely the opposite of what has been claimed (*8*).

Soil micromorphological analyses, but no specimen counts, are available for Pinnacle Point 5-6 (*8, 40*). The examples used to support the notion that some of this site's shell accumulations meet the criteria for shell-midden status do not differ from Figueira Brava's comparable imagery (Fig. S41). The Pinnacle Point 5-6 visuals come from the SADBS (Shelly Ashy Brown Sand) stratigraphic aggregate, which immediately post-dates the ~74 ka Toba eruption and features a dense distribution of shell; lenses that qualify as shell-middens are said to

also exist in the sequence's basal stratigraphic aggregates, YBSR (Yellowish Brown Sand and Roofspall) and LBSR (Light Brown Sand and Roofspall), which date to the ~79-86 ka interval (*8, 181*). Therefore, these shell-rich deposits all belong in MIS 5a, a period of significant sea level rise that put the Pinnacle Point cliff much closer to the source of marine foods than when site 13B was occupied. As both sites, 13B and 5-6, are adjacent, underwent similar site formation processes, and were excavated and analyzed by the same team with the same methods, the soil micromorphological evidence supports that distance to shore does predict shell abundance rather well, in the Last Interglacial of South Africa as much as in the Holocene of Iberia. Indeed, when Blombos is excluded from the regression, the exponential trend revealed by the distribution of the other values in Fig. S42h has an R² of 0.4595, only slightly lower than the distribution in Fig. S41a.

S10.3. Conclusions

As in the Holocene cases, weight per unit of volume would seem to be the density proxy that best reflects shellfish abundance in the Last Interglacial sites considered here. However, site formation processes, differential preservation, and variation in the methods of recovery and analysis introduce biases whose direction and strength are not always easy to grasp. Consequently, in inter-site comparisons, whether based on weight or specimen counts, only the differences of an order of magnitude or higher are likely to be behaviorally significant.

Applying this rule, there can be little question that the shellfish evidence for "coastal adaptation" is as compelling at Figueira Brava as in the Maghreb or South Africa, to say the least, and the more so if crabs, fishes, and site-to-shore distances are brought to bear on the equation. This conclusion is corroborated by the remains of pine nuts, tortoise, aquatic birds and mammals (both terrestrial and marine) found alongside, and by the long-term stability of the system through more than 15,000 years and two MIS 5 sub-stages.

Available shellfishing data from two coeval sites in Mediterranean Spain, Aviones and Bajondillo, are consistent with the pattern, and the probability is strong that the comparable data from the basal levels of El Cuco, on the Cantabrian coast, bespeak of their being of Last Interglacial age too. Under the premise that shellfishing is a valid proxy for the complete coastal resource package, the conclusion that the settlement-subsistence system of the Last Interglacial people of Arrábida represents an instance of "coastal adaptation" must apply to the Last Interglacial settlement of littoral Iberia as a whole.

Phenotypically, these Arrábida people were Neandertal, like their Eurasian contemporaries, for whom there is skeletal evidence (high frequency of external auditory exostoses) suggestive of significant exposure to cold water and damp wind chill, an etiology that implies routine aquatic resource exploitation (*12*). There is therefore little reason to doubt that Neandertals would have exploited marine resources also in those other coastal areas of their past range that have become inaccessible to archeological inquiry.

Added to the evidence for jewelry, cave art and other forms of symbolic material culture and advances technology in the Middle Paleolithic of Europe (*27, 28, 47, 182-187*), these data suggest that the major cognitive and behavioral gap once thought to separate Neandertals from modern humans is just another example that "absence of evidence is not evidence of absence."

S11. OxCal Code

```
Plot()
{
 Sequence()
{
 Boundary("Final");
 Sequence("Unit IH1 - UTh")
{
 Boundary("Final IH1");
 Span();
 C_Date("1207.6", 79400, 1256);
 C_Date("1027 isochron.", 81000, 3000);
 Boundary("Initial IH1");
 };
 Boundary("IH1/IH2-IH3");
 Boundary("IH2-IH3/IH4");
 C_Date("Unit IH4 - Estimated", 88000, 250);
 Boundary("IH4/IH5");
 Sequence("Unit IH5 - UTh")
{
 Boundary("Final IH5");
 Span();
 C_Date("1208.5", 87693, 381);
 C_Date("1208.4", 88137, 371);
 C_Date("1208.3", 87797, 325);
 C_Date("1208.1", 87559, 313);
 Boundary("Initial IH5");
 };
 Boundary("IH5/IH6");
 Phase("Unit IH6 - OSL")
{
 Span();
 C_Date("12-6", 93900, 5600);
 C_Date("12-5", 95000, 5300);
 };
 Boundary("IH6/IH7");
 Sequence("Unit IH7 - UTh")
{
 Boundary("Final IH7");
 Span();
 C_Date("Unit IH7 - 1106 isochron", 87000, 800);
 C_Date("Unit IH7 - 1106.1", 88670, 581);
 Boundary("Initial IH7");
 };
 Boundary("IH7/IH8");
 Sequence("Unit IH8.1 - UTh")
{
```

```
Boundary("Final IH8.1");
Span();
C_Date("1301.4", 89641, 796);
C_Date("1301.3", 88475, 729);
Boundary("Initial IH8.1");
};
Boundary("IH8.1/IH8.2");
Sequence("Unit IH8.2 - UTh")
{
Boundary("Final IH8.2");
Span();
C_Date("1302.2.3", 90343, 716);
C_Date("1302.2"2., 90818, 813);
C_Date("1302.1", 89260, 1730);
Boundary("Initial IH8.2");
};
Boundary("IH8/IL1");
Sequence("Unit IL1 - UTh")
{
Boundary("Final IL1");
Span();
C_Date("1209.4", 90875, 484);
C_Date("1209.5", 92113, 567);
Boundary("Initial IL1");
};
Boundary("IL1/IL3");
C_Date("IL3 - 12-3", 97800, 6000);
Boundary("IL3/MC3-MC5");
Boundary("MC3-MC5/Layer 4");
C_Date("Layer 4 - 12-4", 110200, 8300);
Boundary("LC1-LC3/IB1");
Sequence("IB1 - UTh")
{
Boundary("Final IB1");
Span();
C_Date("1306.1", 107361, 1965);
C_Date("1306.3", 141513, 794);
C_Date("1306.2", 150169, 1036);
Boundary("Initial IB1");
};
Boundary("Initial");
};
};
```

Supplementary Figures
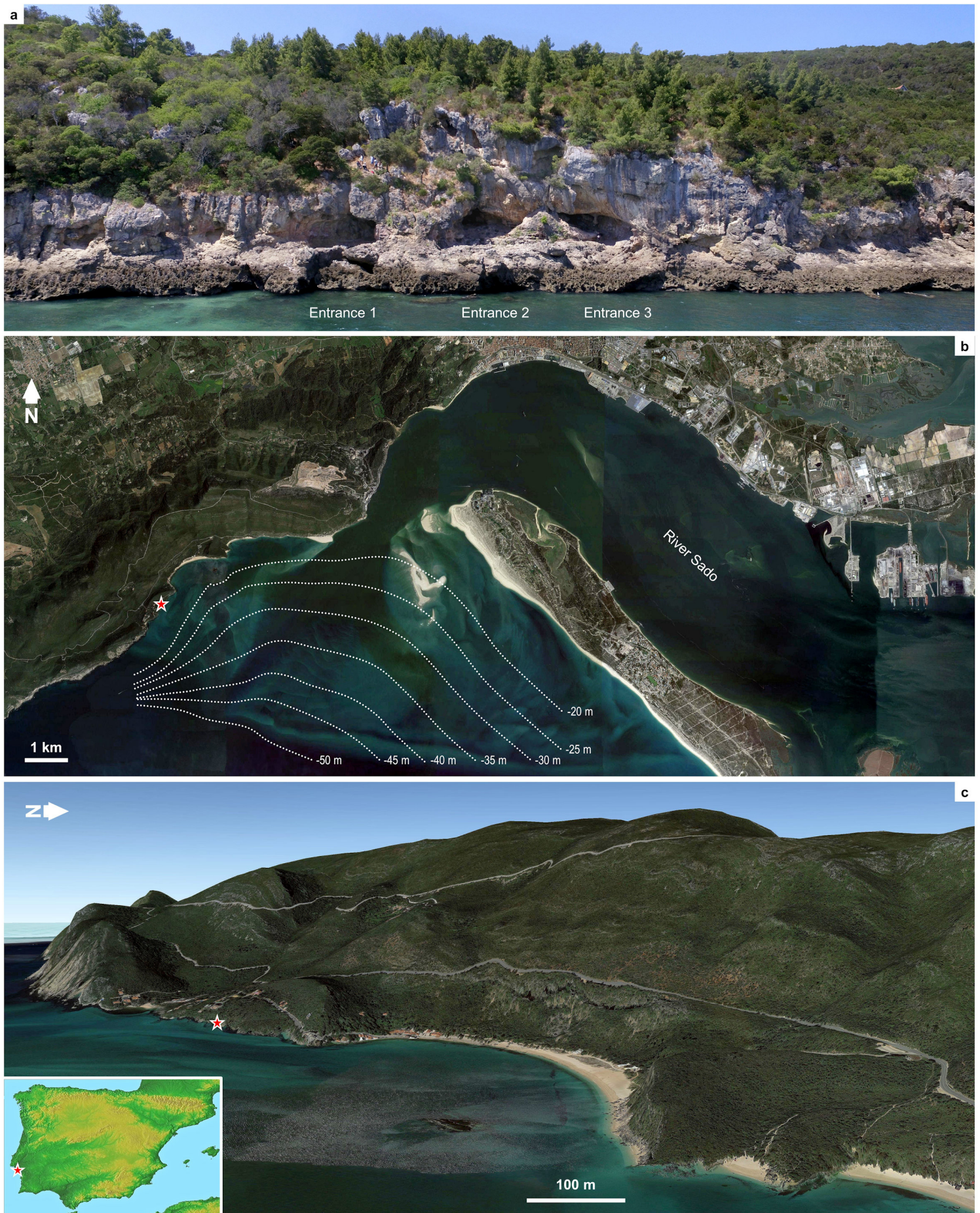
Fig. S1. Site setting. a. The Figueira Brava caves seen from the sea (drone view, August 22, 2016); the cone of cemented deposits between Entrances 2 and 3 preserves the complete Pleistocene sequence, from roof above to marine abrasion terrace below. **b-c.** Zenithal and oblique (1.5× elevation) views (Landsat 2016 images; the site is indicated by the star); to eliminate the bias introduced by the Holocene, estuary-related sedimentary accumulation, the contour lines for the submerged continental platform are derived from seismic profiles. The inset shows the location of the site in Iberia.
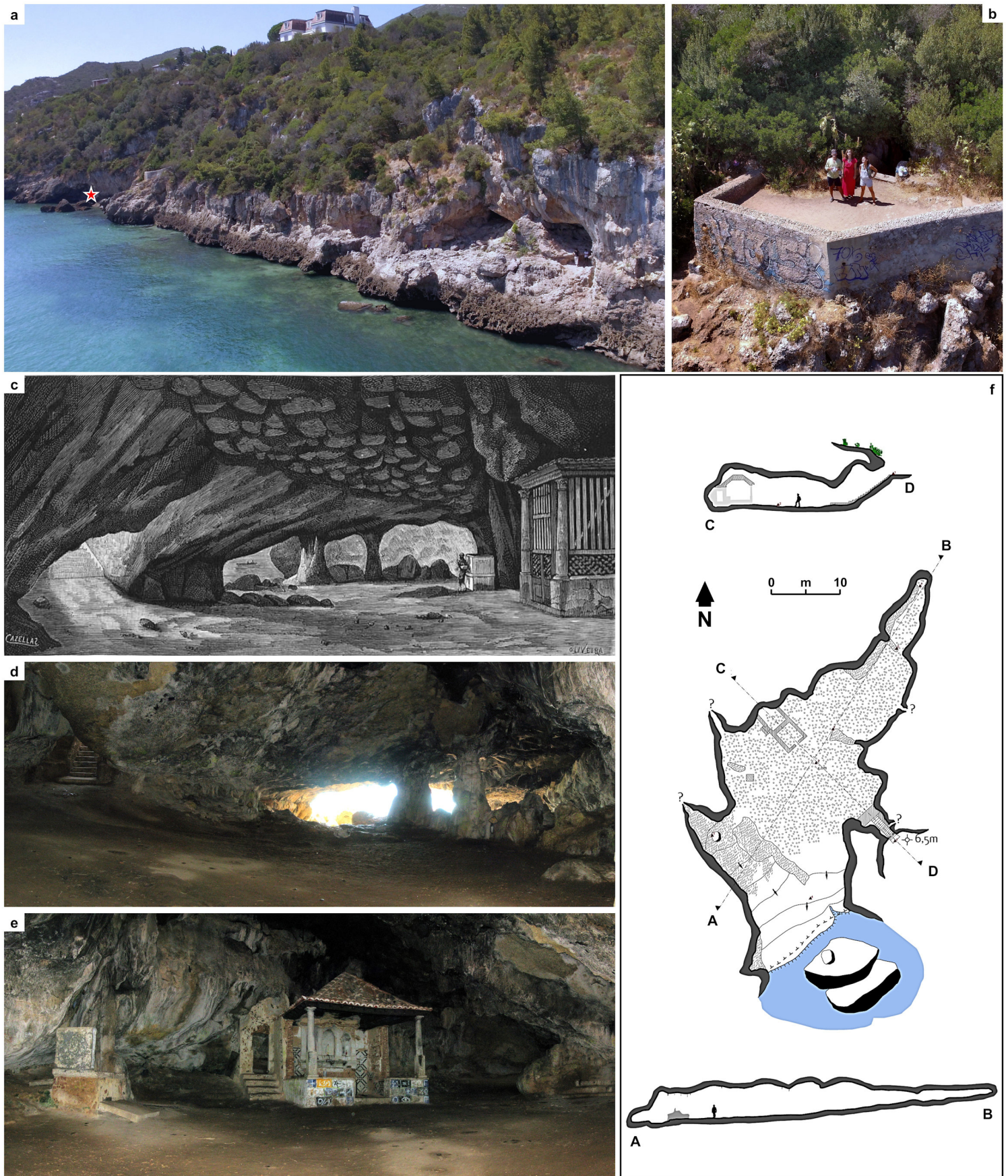
Fig. S2. Lapa de Santa Margarida. a. Location of the sea entrance (indicated by a star) as seen from Figueira Brava (drone view, August 22, 2016). **b.** The land entrance (drone view, August 22, 2016). **c-e.** The cave's interior in a 19th-century illustration (*Occidente*, vol. IX, no. 277, September 1, 1886), and as photographed July 15, 2009. **f.** Topographic plan and cross-sections (2011 survey; courtesy of Rui Francisco, originally prepared for the Archeological Map of the Municipality of Setúbal).
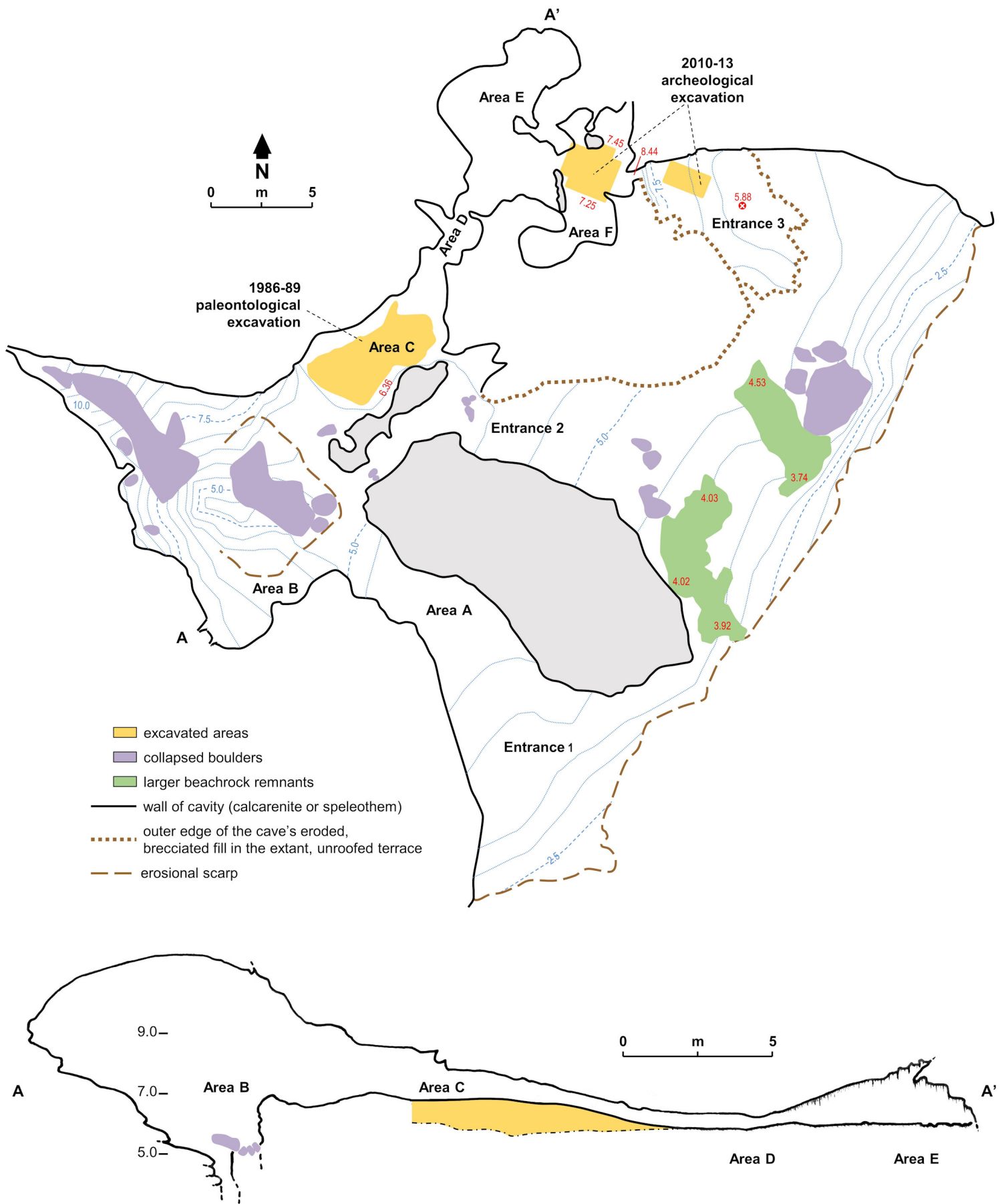
Fig. S3. The Figueira Brava cavities. Plan and long section drawn from topographic surveys by AESDA [*Associação de Estudos Subterrâneos e Defesa do Ambiente*; 2006] and CRIVARQUE, Lda. [*Estudos de Impacto e Trabalhos Geo-arqueológicos*; 2010]. Elevations are in m above sea level.
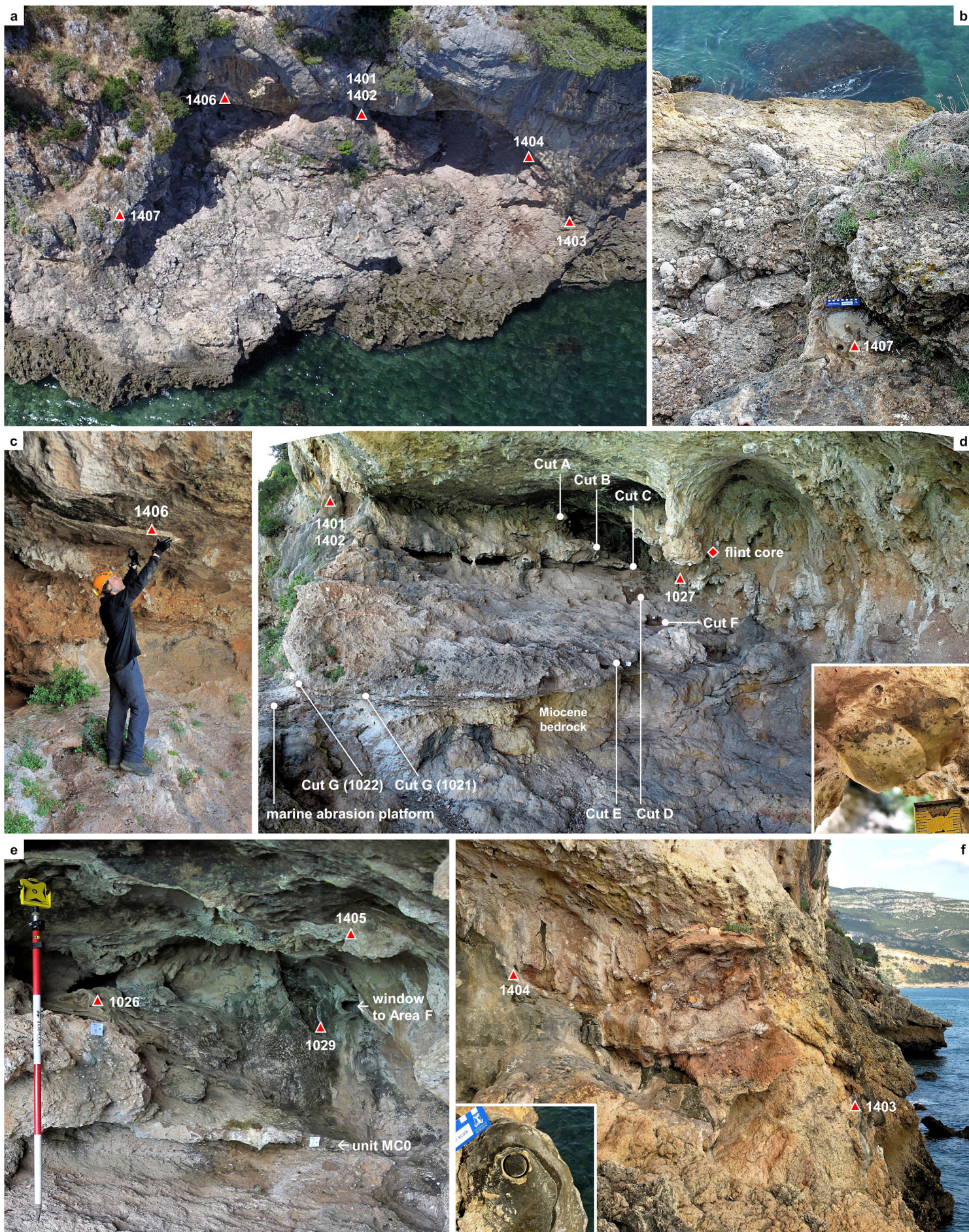
Fig. S4. The Santa Margarida-like, nowadays unroofed space in front of Figueira Brava's Entrances 2-3. a. Drone view (August 22, 2016). **b-f.** Different views (**d.** July 22, 2010; **b-c, e-f.** November 1, 2014) of speleothem and sediment remnants. The position of the samples taken for U-series dating or cut for soil micromorphology analysis is indicated. The insets are close-ups of: a flint core in roof-adhering breccia (**d**); cored U-series sample 1403 (**f**).
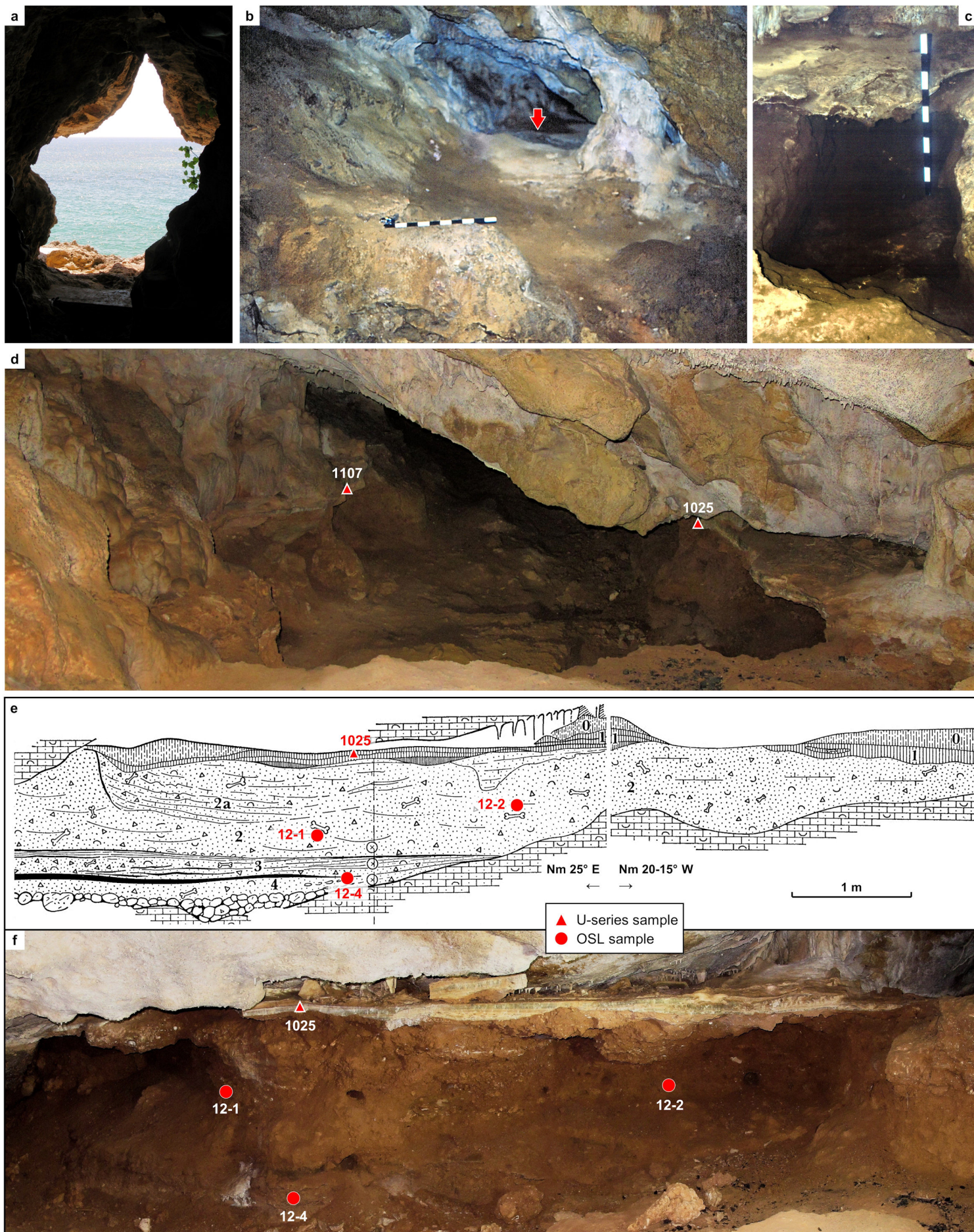
Fig. S5. The 1980s excavation, and position of Area C's OSL and U-series samples. a. Entrance 1 from the inside (July 15, 2009). **b-c.** 1986 view of Area C, seen from Area B, and initial test trench, open in a section of the passage, indicated by the arrow, where the capping flowstone was already broken. **d.** Post-excavation view over Area C (May 3, 2011). **e-f.** Area C stratigraphic profiles (1989 drawing and May 3, 2011 photo).
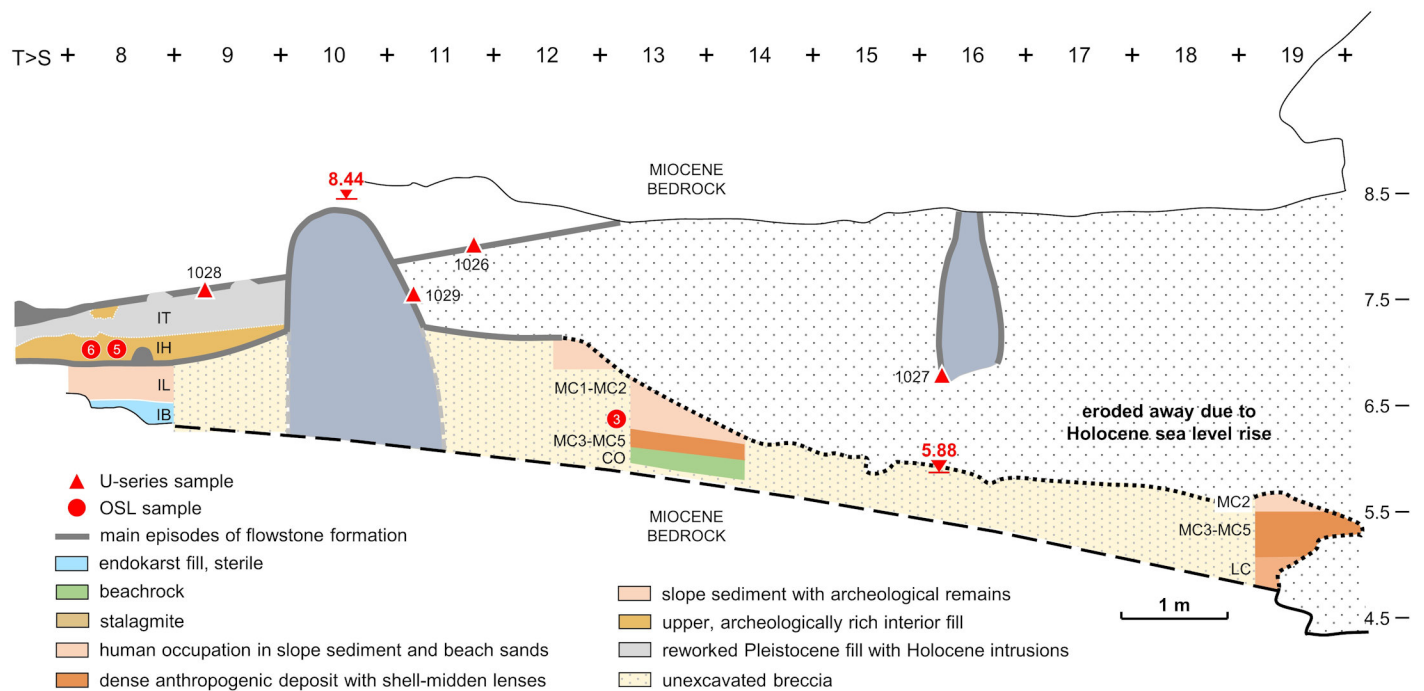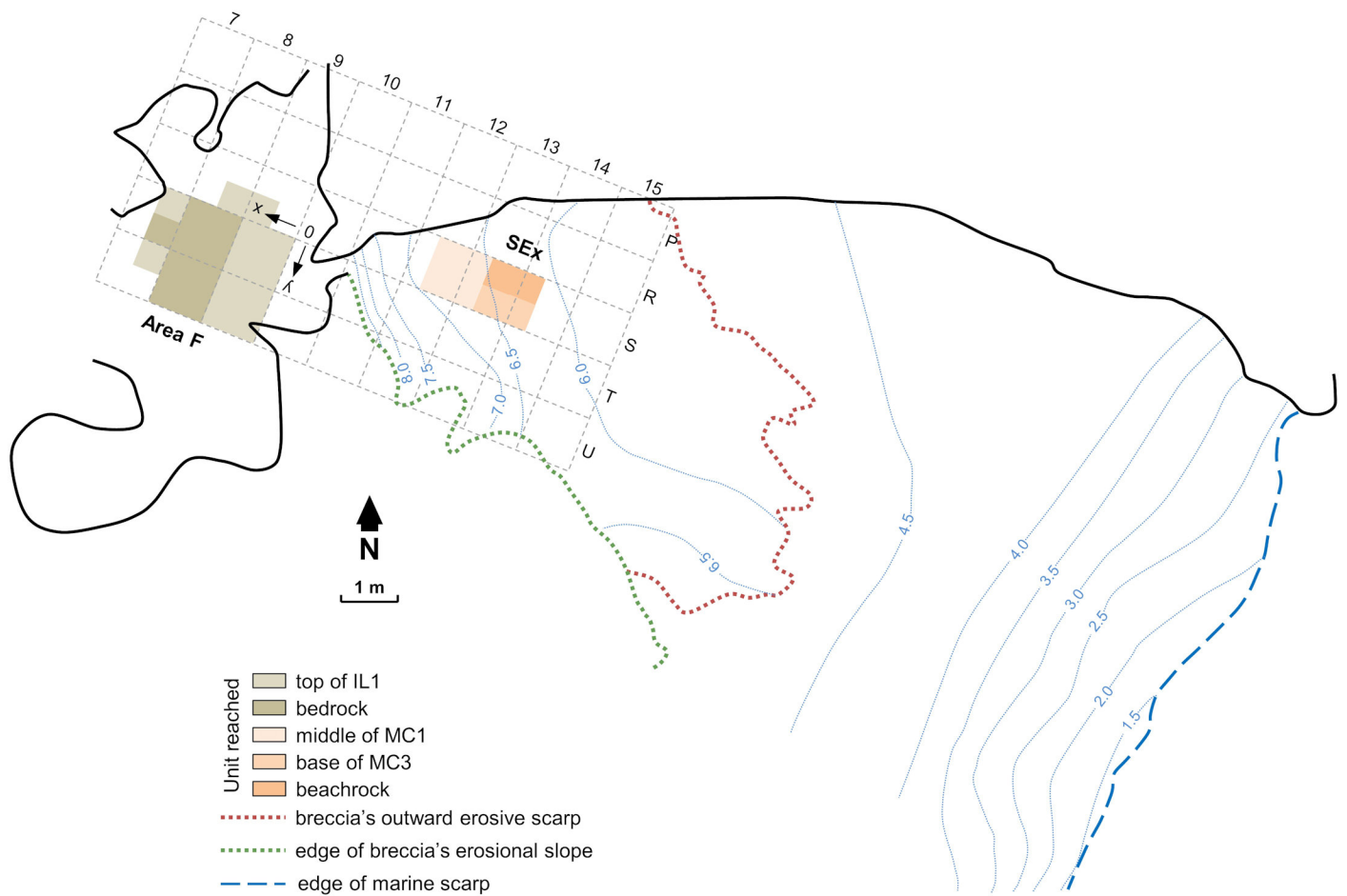
Fig. S6. Area F and Entrance 3: plan, 2010-13 excavation grid, and schematic stratigraphic outline. The position of the 2010 U-series and 2012 OSL samples framing the correlation between the two areas is indicated. The sedimentary succession was archeologically excavated, except for the seaward exposures of the UC and LC complexes, which were studied through field description and micromorphological observation (their thickness and boundaries have been estimated from stratigraphic observations and thin-section data). Across most of Entrance 3, the sequence was eroded down to the elevation of unit MC2. U-series sample 1027 is from the outer skin of a column uniting the fill with a lowered septum of the cave's roof running parallel to, and ~2 m north of the site grid's T>S projection plan (cf. Fig. S4d); this geometry explains why, on elevation grounds, this sample might appear related to the phase of flowstone development atop complex IL while, in fact, it relates to the last stage of the site's sedimentary build-up that samples 1026 and 1028, taken from the flowstone capping the sequence in Entrance 3 and Area F (units UC1 and IH1, respectively), also represent. Elevations are in m above sea level.
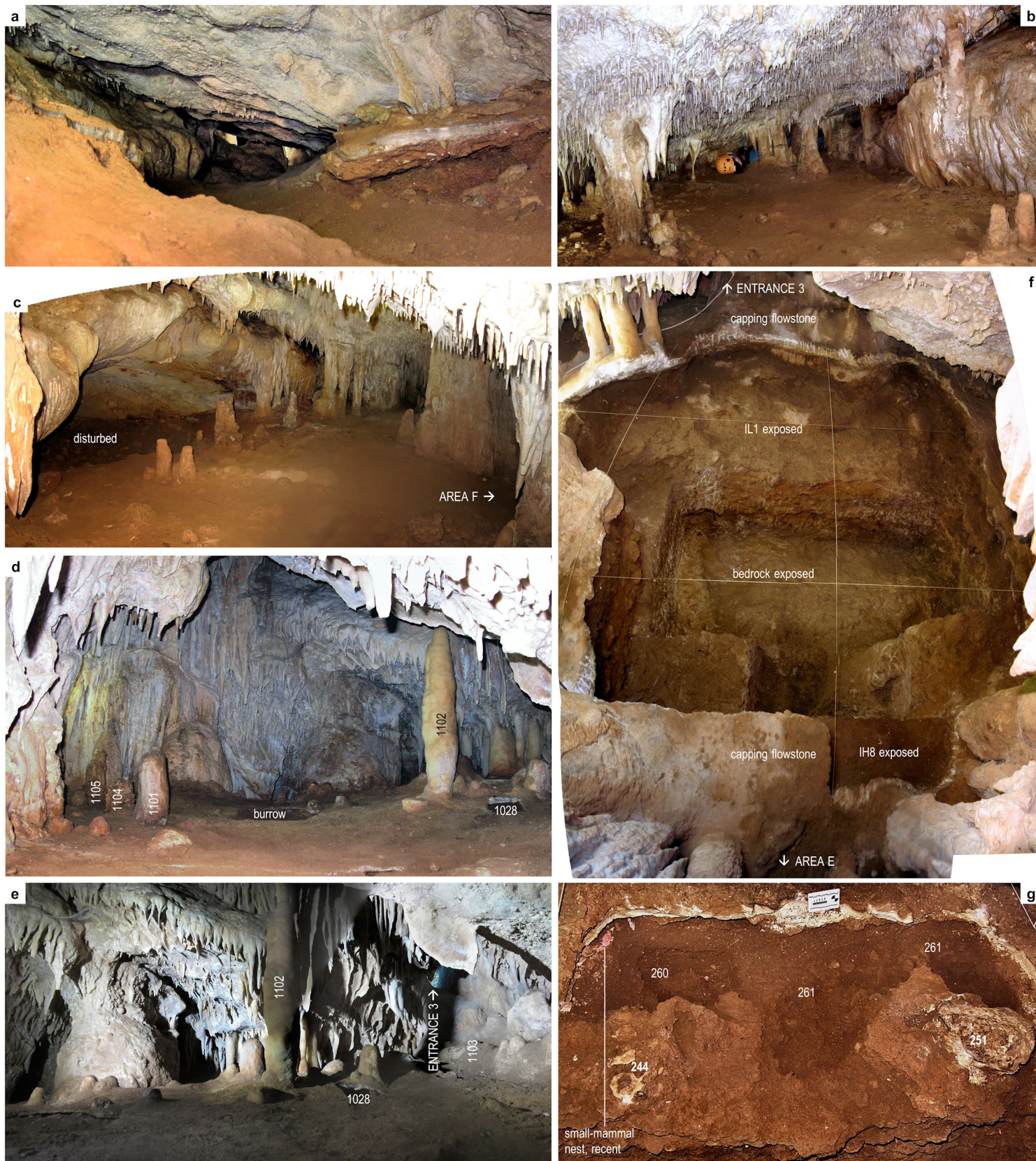
Fig. S7. Area F: access and interior aspect, before and after the 2010-13 work. a. The Area D narrow seen from Area C (May 27, 2011). **b.** The exit of the Area D narrow seen from Area E (May 27, 2011). **c.** Area E; note the large disturbance found against its NW corner (May 26, 2011). **d-e.** South-to-north views of Area F prior to the beginning of the work (May 3, 2011); the position of the stalagmites removed to allow for excavation and kept for dating and paleoclimate analysis, denoted by their sample numbers, is indicated, as is the position of the flowstone sample taken on July 2010; for scale, note that the height of sample 1105 is 32 cm; sample 1103, removed prior to photography to allow for access to the window linking Area F with Entrance 3, is indicated by the position of its stump; the initial 1 m² test in square U8 occupied the space south of the burrowed area revealed by the break in the capping flowstone seen between samples 1101 and 1102. **f.** The Area F trench at the end of the excavation work (May 28, 2013). **g.** Base of spit A1 (reworked unit IT0), in the western half of square U9 (oblique view taken from the previously excavated T-U/8 trench, May 8, 2013; elevations are in cm below datum); note the fragments of red tape visible under the flowstone, denoting the position of a small-mammal nest that also contained plastic, cigarette-pack cellophane, bird bones, and beach-washed, sea-eroded limpet and mussel shells.

81
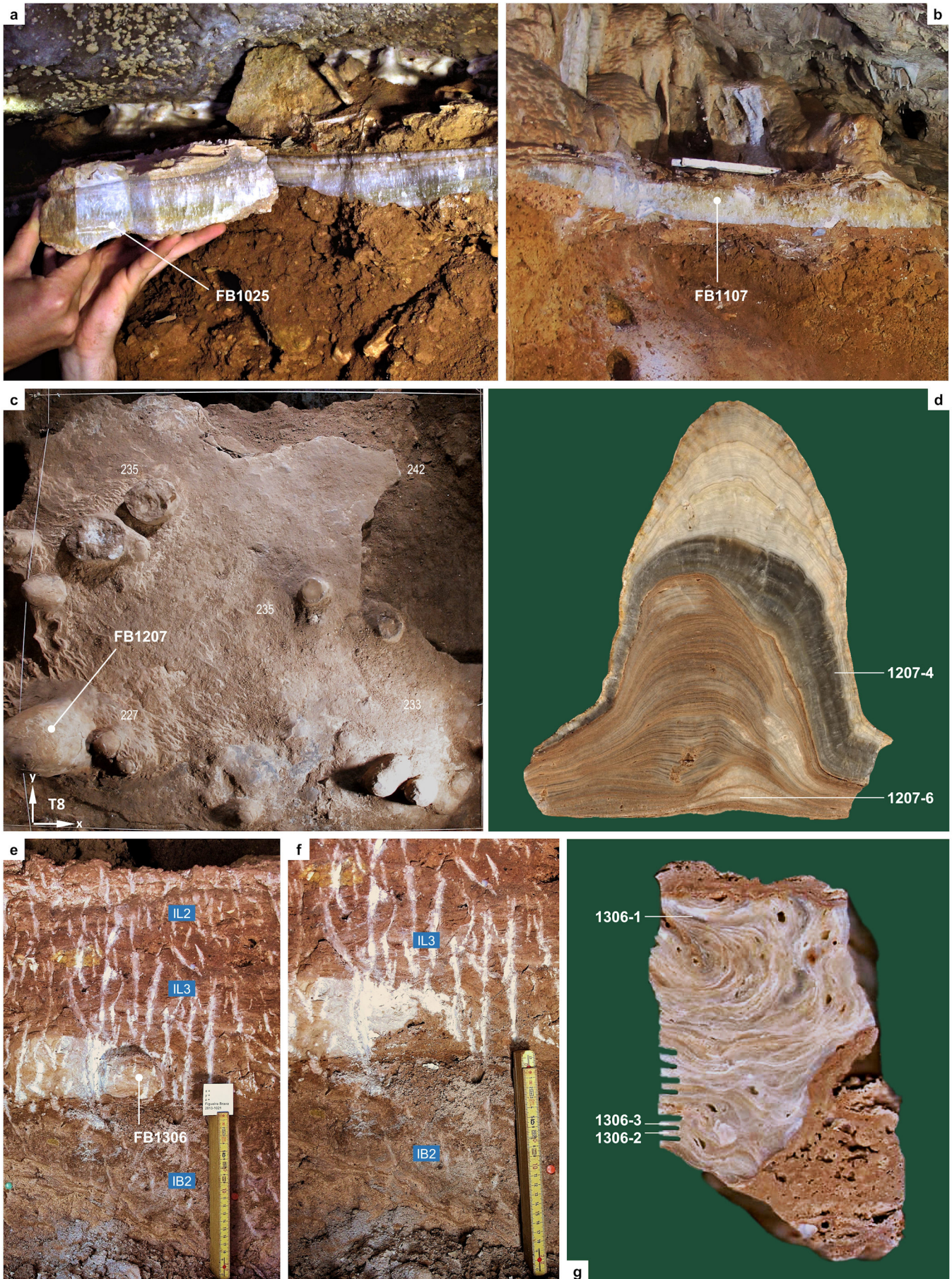
Fig. S8. U-series samples constraining the accumulation of the archeological deposit. a. FB1025 (flowstone capping the SE side of the Area C deposit) repositioned at collection locality. **b.** Sample FB1107 (flowstone capping the NW side of the Area C deposit). **c-d.** FB1027 (stalagmite grown from the flowstone capping the Area F deposit): zenithal view prior to collection (May 10, 2012), and section with position of dated sub-samples. **e-g.** FB1306 (flowstone formed at the interface between over-bedrock unit IB2 and basal archeologically fertile unit IL3): exposed in profile prior to (**e**) and after (**f**) collection, and section with position of dated sub-samples (**g**).
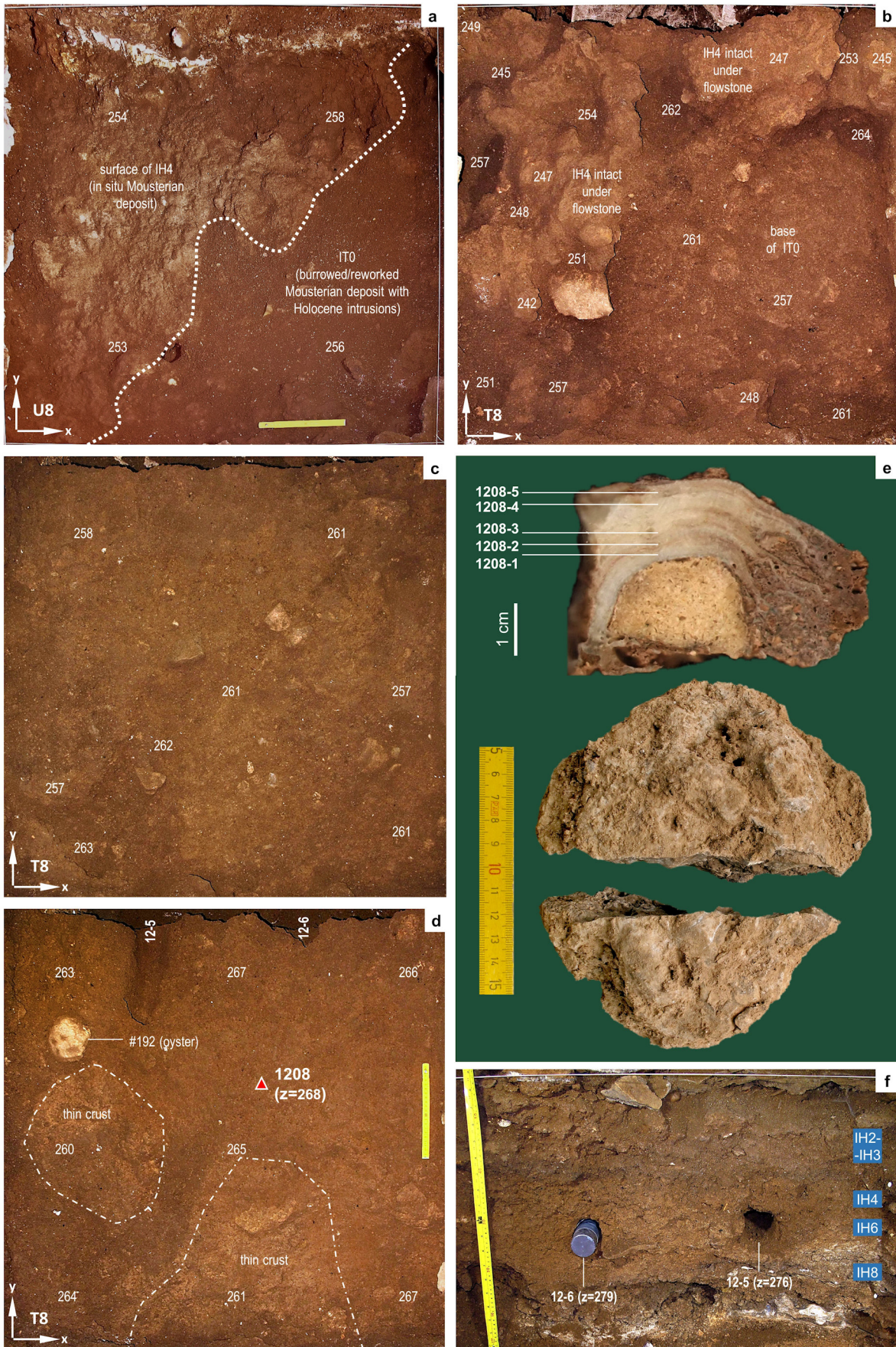
Fig. S9. Area F: excavation and dating. a-b. Reworked unit IT0; during excavation, in square U8 (May 10, 2011) and fully excavated, in square T8 (May 10, 2012). **c.** The interface between units IH2-IH3 and IH4 in square T8 (May 11, 2012). **d.** Base of unit IH4 in square T8, exposing the OSL bore holes into IH6 (samples 12-5 and 12-6) (May 14, 2012); note the discontinuous calcareous incrustation (unit IH5), in places forming true stalagmitic protuberances; the position of FB1208 is indicated. **e.** U-series sample FB1208: after collection, and sectioned with position of dated sub-samples. **f.** Oblique view over the OSL sampling of unit IH6 in the U>T8 cross-section (May 8, 2012). All décapage photos are zenithal views. Elevations are in cm below datum.

Fig. S10. Area F: interstratified speleothems dated by U-series. a-b. Base of unit IH6 in square U8, and sample FB1106 (unit IH7): tumbled at the interface with IH8 (May 19, 2011) (**a**) and cut for dating (**b**). **c-d.** Base of units IH6 (May 30, 2012) (**c**) and IH8 (May 10, 2013) (**d**) in square T7East. (**e**) unit IH8 samples FB1301 and FB1302 (after collection, and cut for dating). **f-g.** FB1209 (unit IL1): standing at the IH8/IL2 interface (May 18, 2012) (**f**), and cut for dating (**g**). All décapage views are zenithal. Dated sub-samples are indicated. Elevations are in cm below datum.
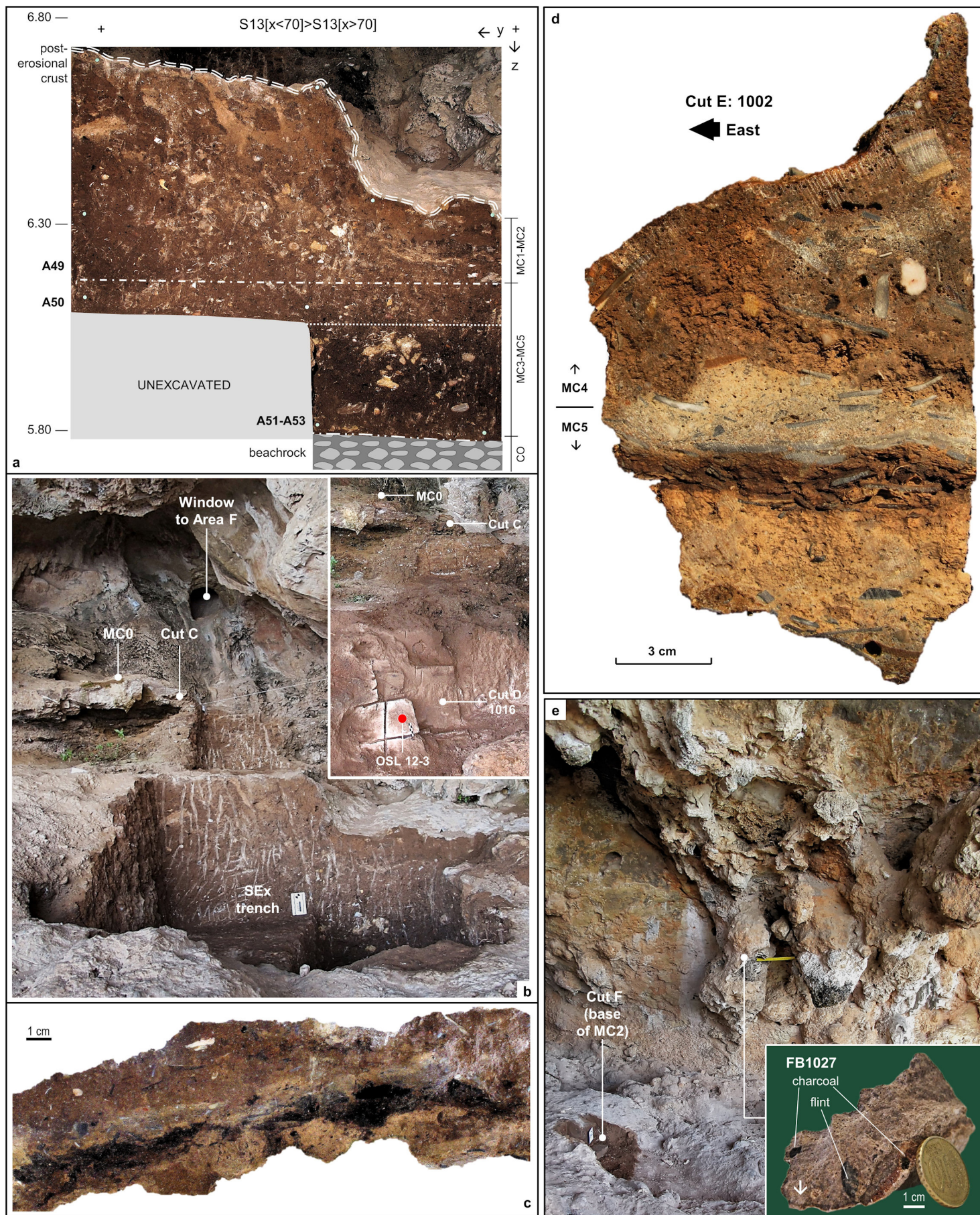
Fig. S11. The Entrance 3 work. a. Orthorectified stratigraphic profile (west wall of the SEx trench, an expansion of Cuts C-D (May 31, 2013); spits and their correspondence with the units of the 2010 stratigraphic column are indicated; elevations are in m above sea level. **b.** The SEx trench (May 30, 2013); the inset (May 8, 2012) shows the position of OSL sample 12-3, taken prior to the excavation of the trench. **c.** The face of units MC4-MC5, as exposed 6 m seaward of the SEx profile, after preparation for removal of micromorphology sample 1002. **d.** Field photo of micromorphology sample 1002; the viewed cut is perpendicular to the exposure's face. **e.** Stratigraphic position, above Cut F, of U-series sample FB1027 (July 23, 2010; a 20 cm yellow ruler is used for scale); the inset shows the sample prior to cutting (the arrow marks the external rind inward of and along which U-series isochron dating was carried out).
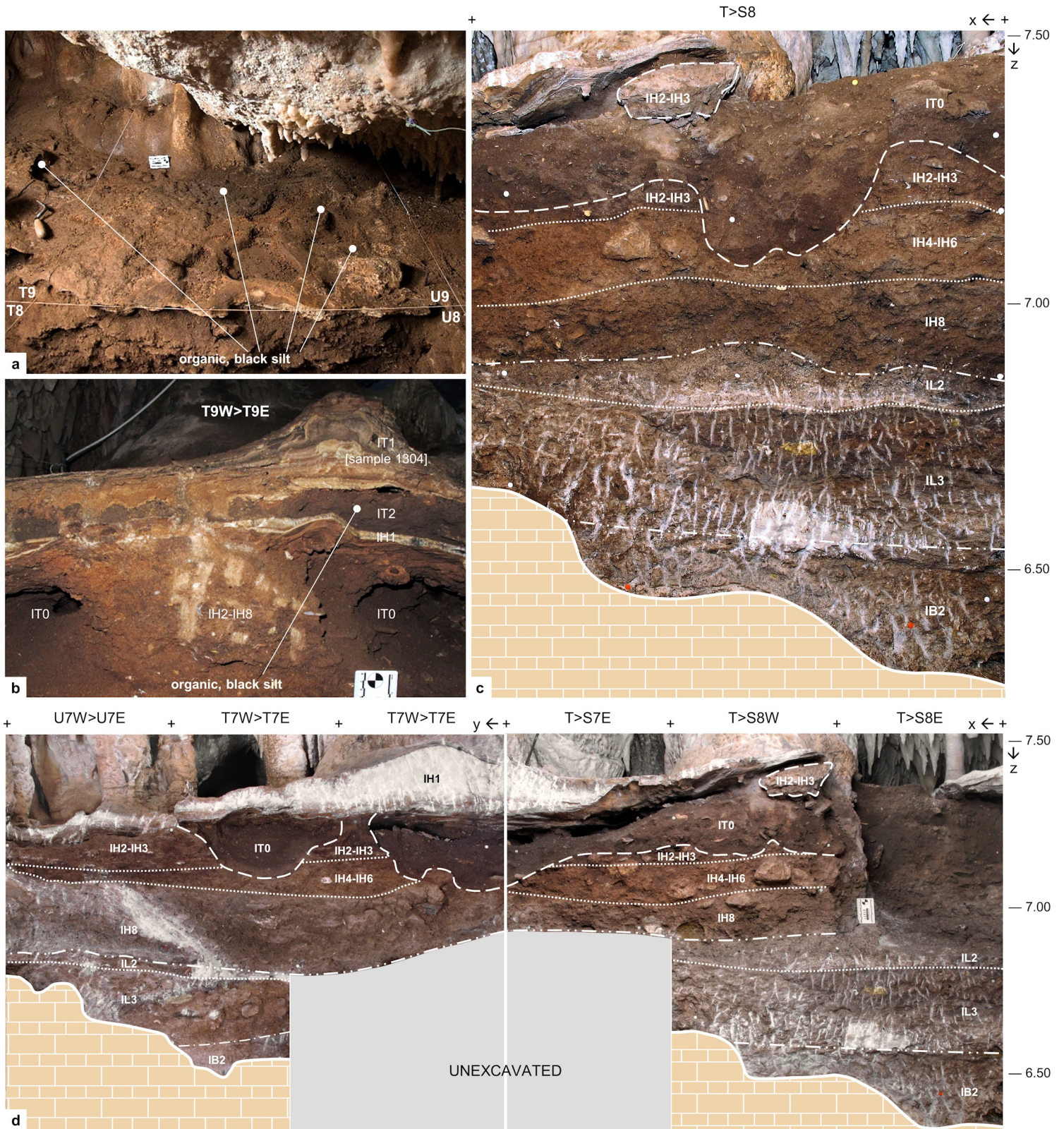
Fig. S12. Area F: the stratigraphic succession. a. Oblique view over the floor of the cave, adjacent to the window that communicates Area F with Entrance 3; note the surficial position, above the capping flowstone, of the dark sediment forming the IT2 "black lens." **b.** Close-up view of the T9West>T9East cross-section during excavation (May 17, 2013); here, the IT2 sediment can be observed in apparently intermediate stratigraphic position; of recent Holocene age, this sediment filled-in the cracks and voids found in the fabric of the flowstone-cum-stalagmite deposit capping Area F at the interface between the initial (unit IH1) and final (unit IT1) phases of Pleistocene speleothem growth. **c.** Orthorectified stratigraphic profile along the north wall of the trench at the end of the 2012 field season (May 31). **d.** Orthorectified stratigraphic profiles along the west (May 24) and north (May 28) walls of the trench at the end of the 2013 field season (after minor straightening of the T>S8W wall and excavation of the IT-IH sequence in the SE quadrate of square S8). Elevations are in m above sea level.
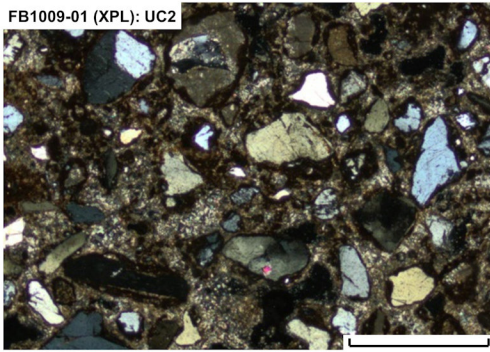
FB1009-01 (XPL): UC2
Unit's groundmass; note the micrite and the limestone and siliciclastic grains
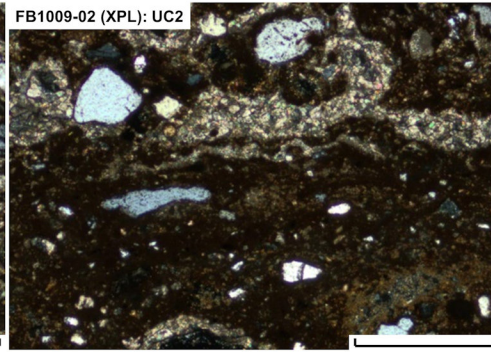
FB1009-02 (XPL): UC2
Laminated intercalation of micrite enriched with organic matter
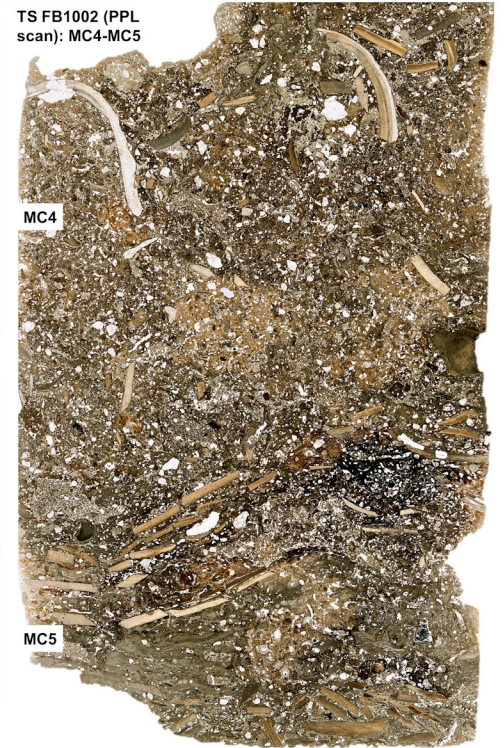
TS FB1002 (PPL scan): MC4-MC5
MC4
MC5

FB1018-08 (XPL): MC1
Charcoal fragment

FB1019-02 (PPL): MC2
Burnt bone fragment
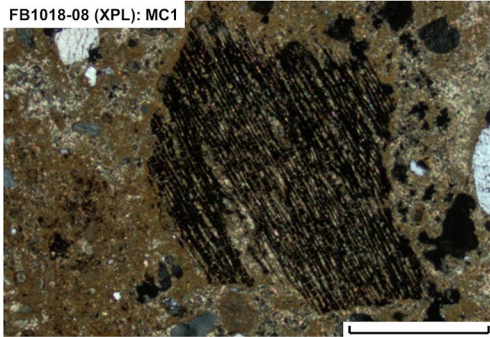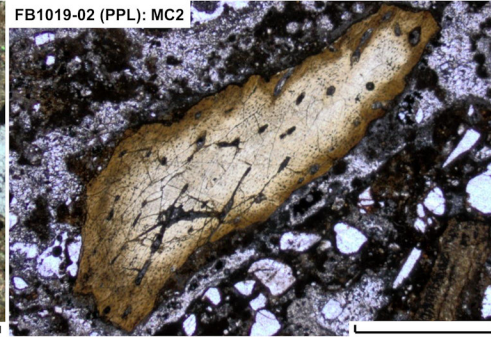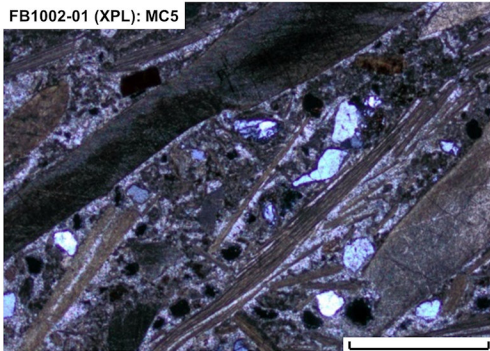
FB1002-01 (XPL): MC5
Unit's groundmass; note the abundant shell fragments
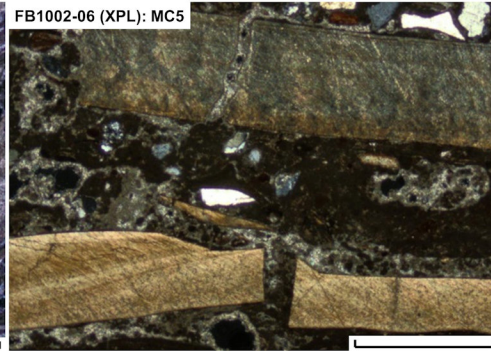
FB1002-06 (XPL): MC5
Shell fragments, probably broken in situ
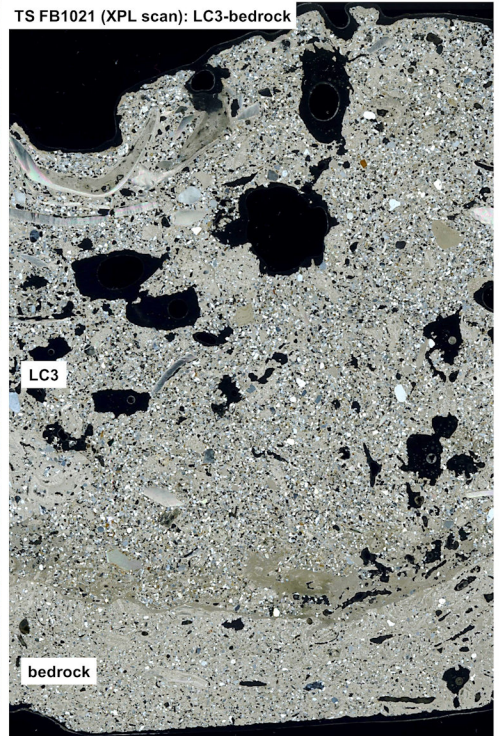
TS FB1021 (XPL scan): LC3-bedrock
LC3
bedrock
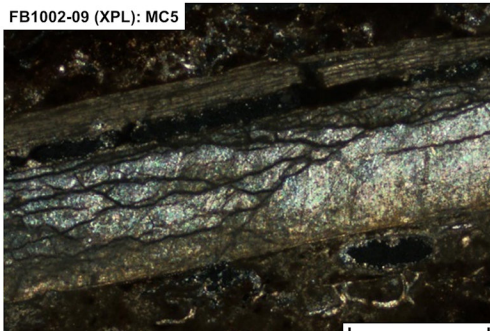
FB1002-09 (XPL): MC5
Burnt mussel shell; note detachment of inner layer and the latter's microcracks
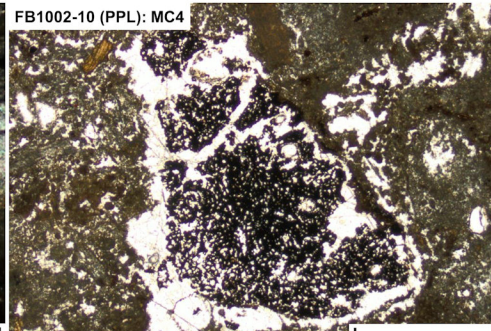
FB1002-10 (PPL): MC4
Fragment of burnt organic matter
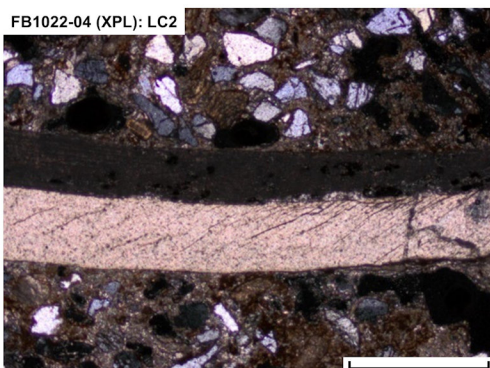
FB1022-04 (XPL): LC2
Well-preserved *Mytilus* sp. shell, with inner and outer layers clearly visible
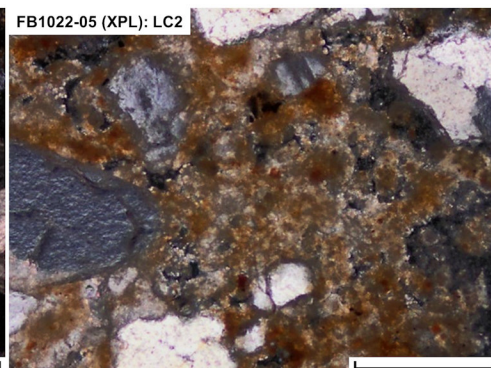
FB1022-05 (XPL): LC2
Groundmass and fine material with clay and iron oxides
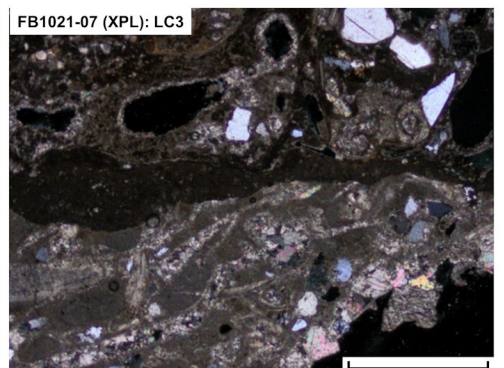
FB1021-07 (XPL): LC3
Detail of micrite crust between bedrock and unit LC3

Fig. S13. Entrance 3 soil micromorphological thin sections. PPL: plane polarized light; XPL: crossed polarized light; scale bars are 1 mm, except for FB1002-09 (bar = 0.5 mm) and FB1022-05 (bar = 0.2 mm). The scans of the FB1002 and FB1021 thin sections span a width of 9.5 cm.

87
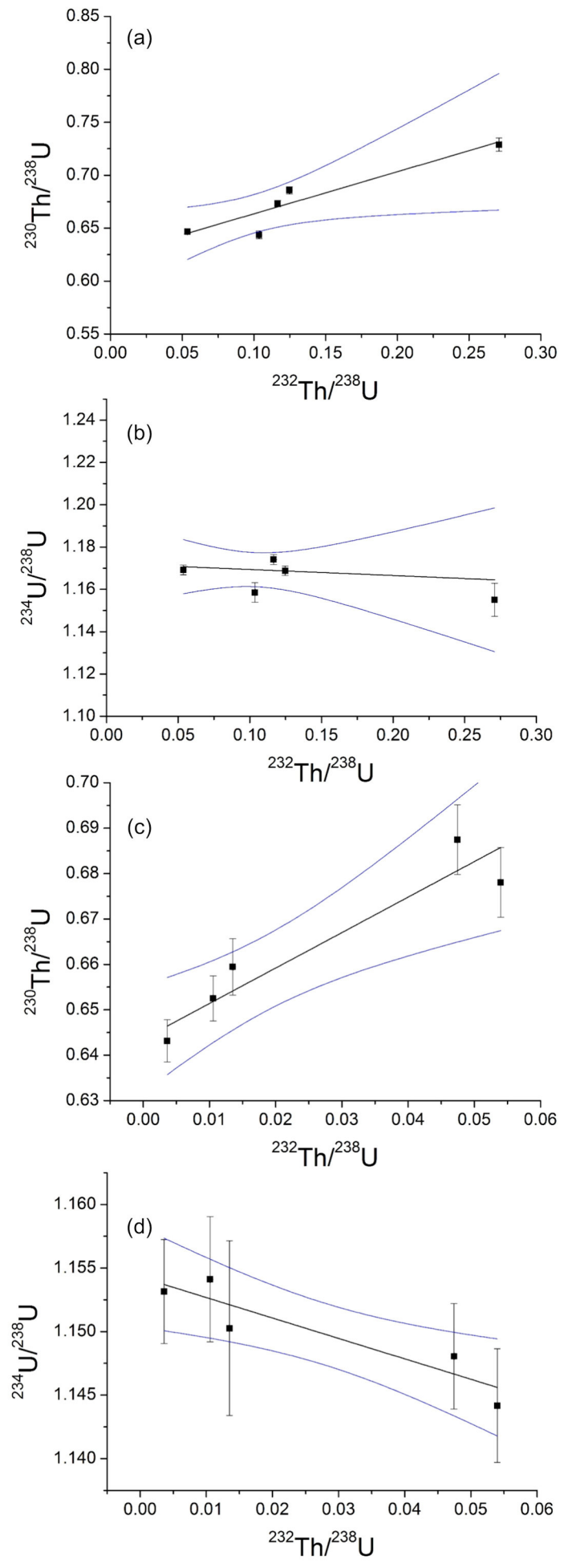
Fig. S14. Isochron plots. a-b. U-Th sample 1027 (age, 81.0±6.0 ka, 2σ). **c-d.** U-Th sub-sample 1106-2 (age, 87.0±1.6 ka, 2σ).
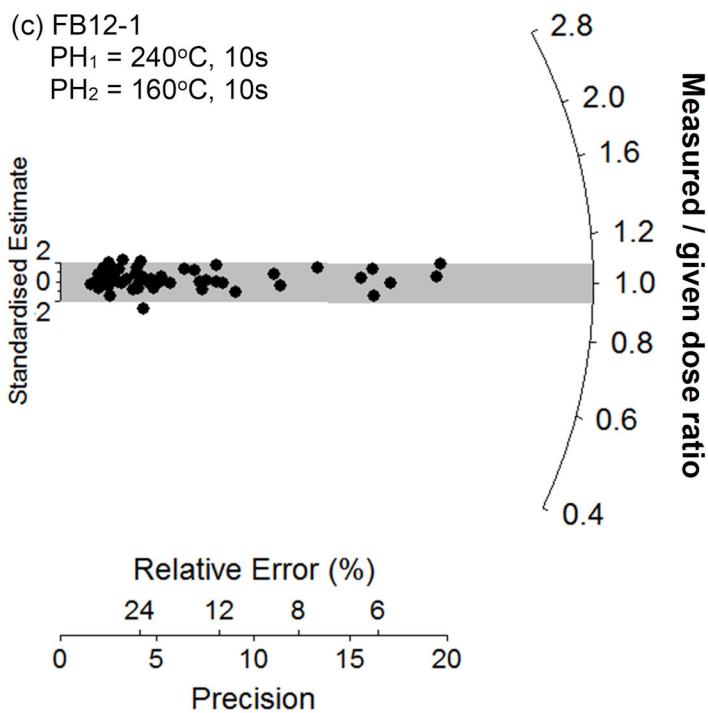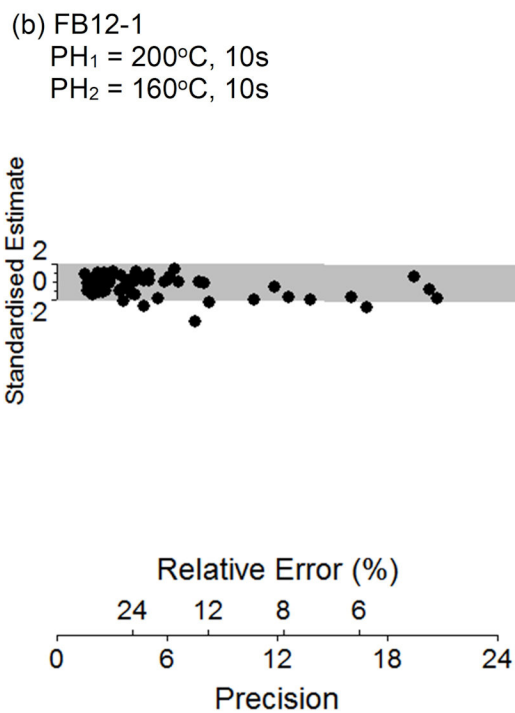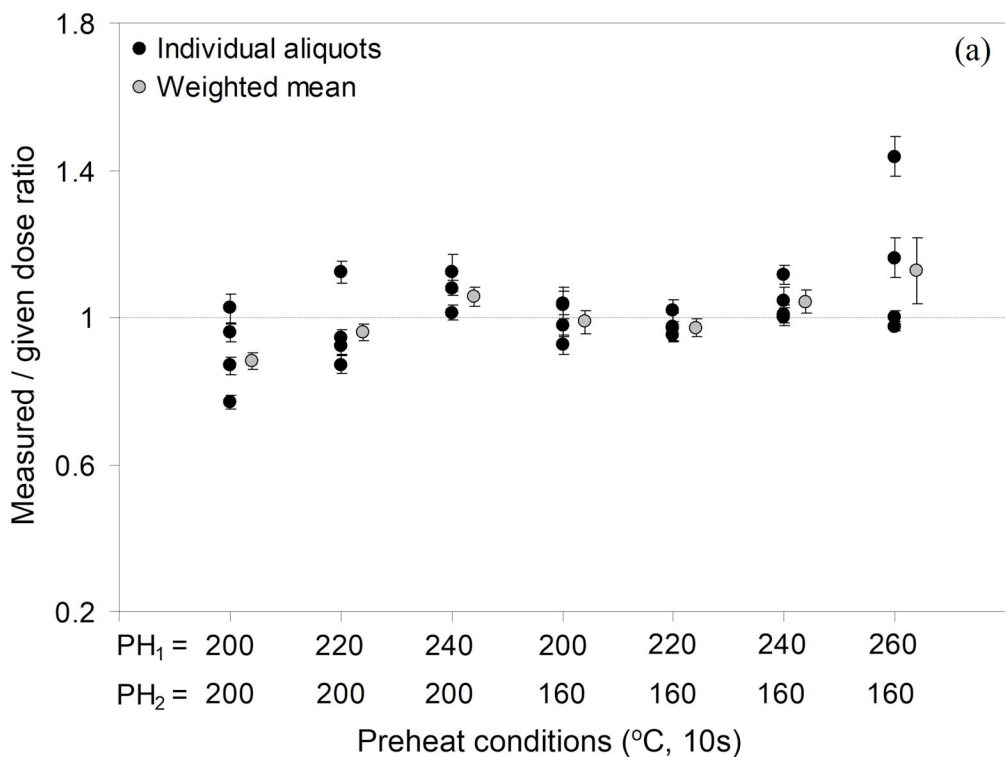
Fig. S15. OSL dose-recovery test results for sample FB12-1. a. Recovered-to-given dose ratios versus PH_1 temperature (held for 10 s) for ~180-grain aliquots. The natural OSL signals of the multi-grain aliquots were optically bleached with two 1000 s blue LED illuminations at ambient temperature, each separated by a 10,000 s pause. A known dose of 100 Gy was then administered to each aliquot and the multi-grain aliquot SAR procedure shown in Table S7 was subsequently used to estimate this dose. Two different test-dose preheat (PH_1 and PH_2) conditions were applied in the dose-recovery SAR procedure (160°C for 10 s or 200°C for 10 s). b-c. Radial plots showing the recovered-to-given dose ratios obtained for individual quartz grains, using a regenerative-dose preheat (PH_1) of 200°C for 10 s and a PH_2 of 160°C for 10 s (b), and a PH_1 of 240°C for 10 s and a PH_2 of 160°C for 10 s (c). The single-grain natural OSL signals were bleached using the same procedure outlined above and the administered doses were subsequently recovered using the single-grain SAR procedure shown in Table S7. The grey-shaded regions on the radial plot are centered on the administered dose for each grain (sample average = 150 Gy; though this amount varied for individual grains, owing to spatial variations in the dose rate of the beta source). Individual D_e values that fall within the shaded region are consistent with the administered dose at 2σ.
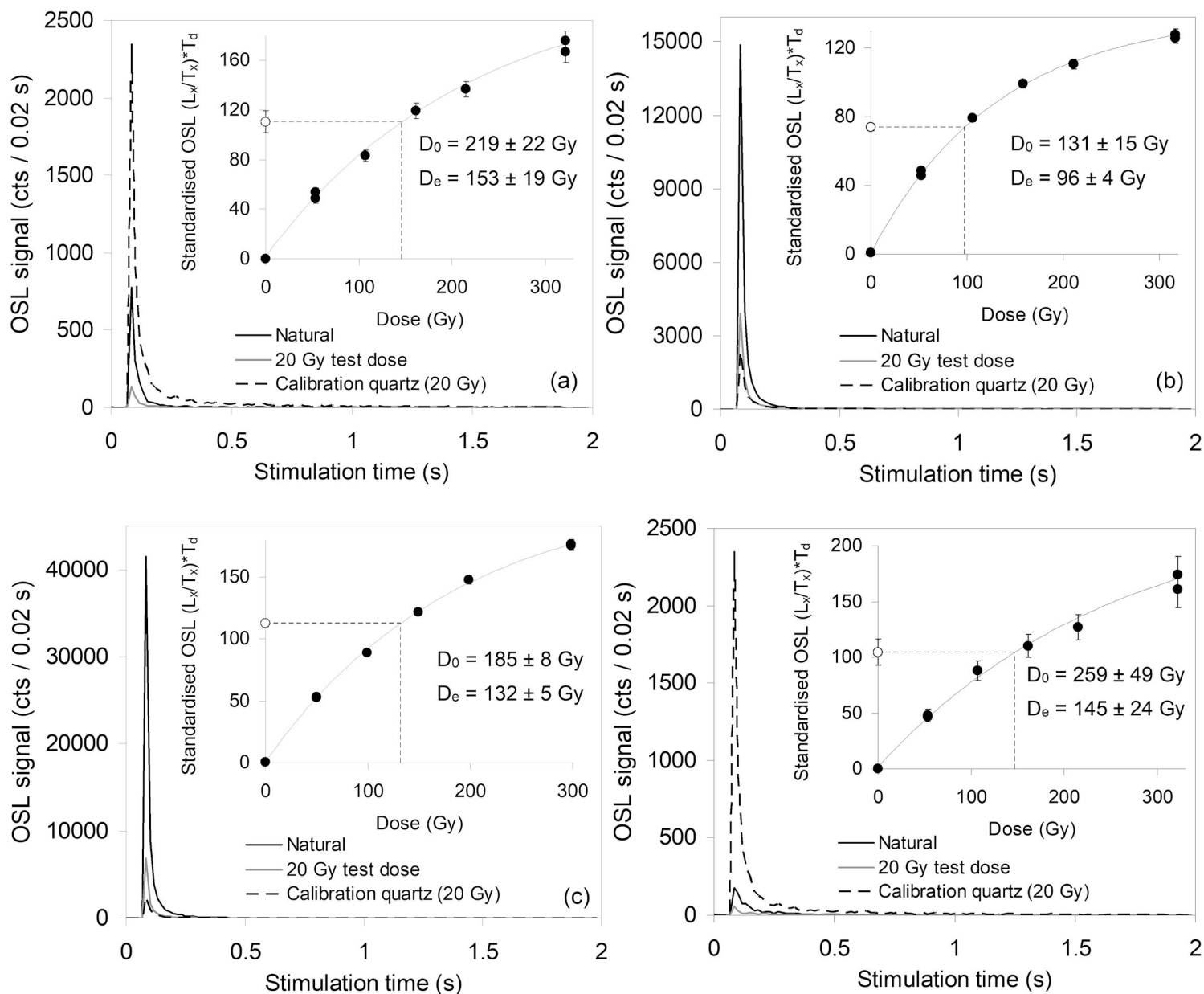
Fig. S16. Representative single-grain OSL decay and dose-response curves for quartz grains from sample FB12-1. The decay curve of a fast-component dominated calibration quartz grain is shown for comparison (Risø calibration quartz standard from Rømø, batch #98; Hansen et al., 2015). In the insets, the open circle denotes the sensitivity-corrected natural OSL signal, and filled circles denote the sensitivity-corrected regenerated OSL signals. The D_0 value characterizes the rate of signal saturation with respect to administered dose and equates to the dose value for which the saturating exponential dose-response curve slope is $1/e$ (or ~0.37) of its initial value. **a.** grain with moderate OSL signal brightness (T_n intensity = 100-1,000 counts / 0.08 s). **b.** grain with bright OSL signal (T_n intensity = ~1,000-10,000 counts / 0.08 s). **c.** grain with very bright OSL signal (T_n intensity = >10,000 counts / 0.08 s). **d.** grain with relatively dim OSL signal (T_n intensity = <100 counts / 0.08 s).
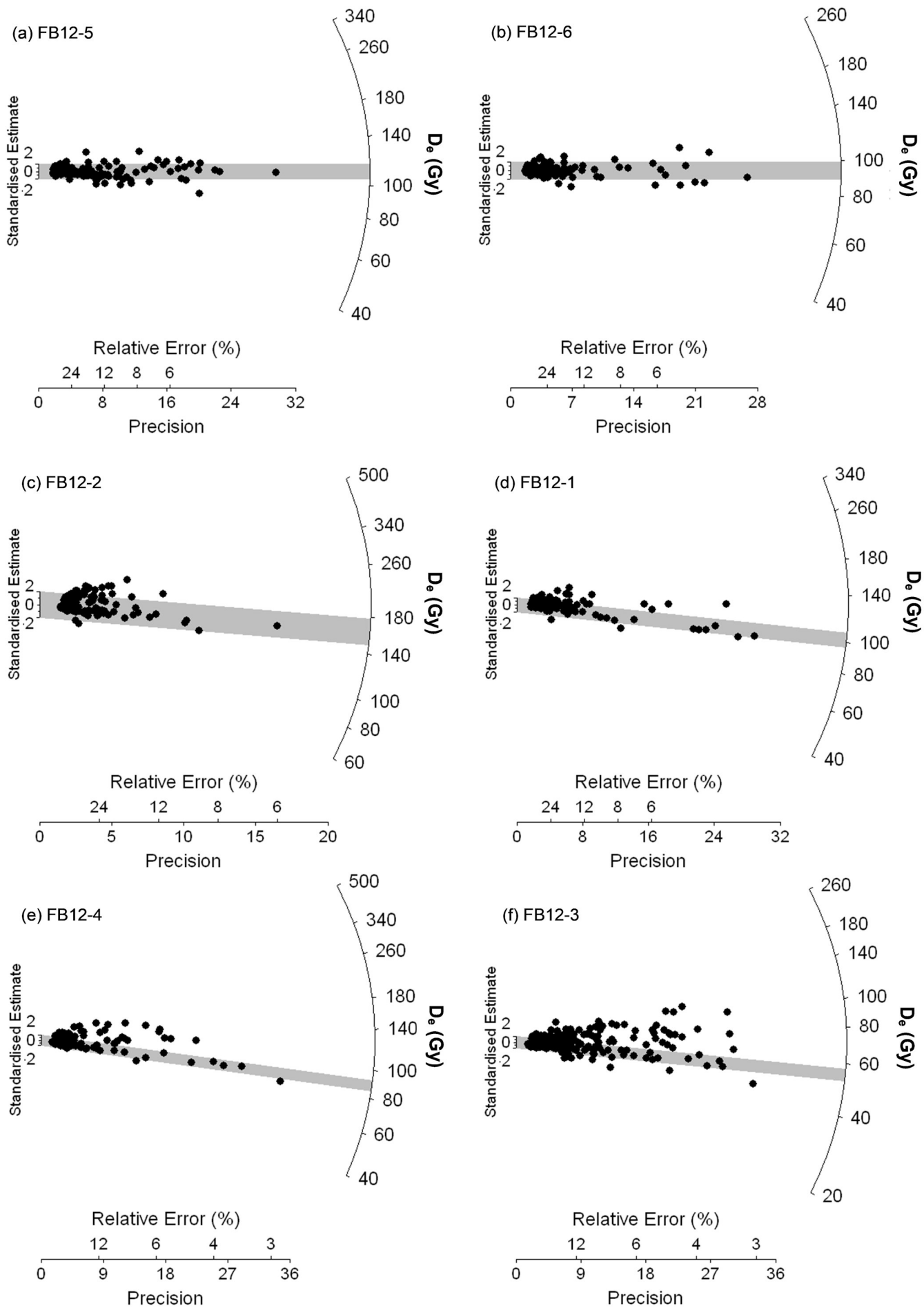
Fig. S17. OSL dating results. The single-grain OSL D_e distributions for the Figueira Brava samples, shown as radial plots. The grey bands are centered on the D_e values used for the age calculations, which were derived using either the central age model (samples FB12-5 and FB12-6), the 3-parameter minimum age model (samples FB12-1 and FB12-4), or the 4-parameter minimum age model (samples FB12-2 and FB12-3).
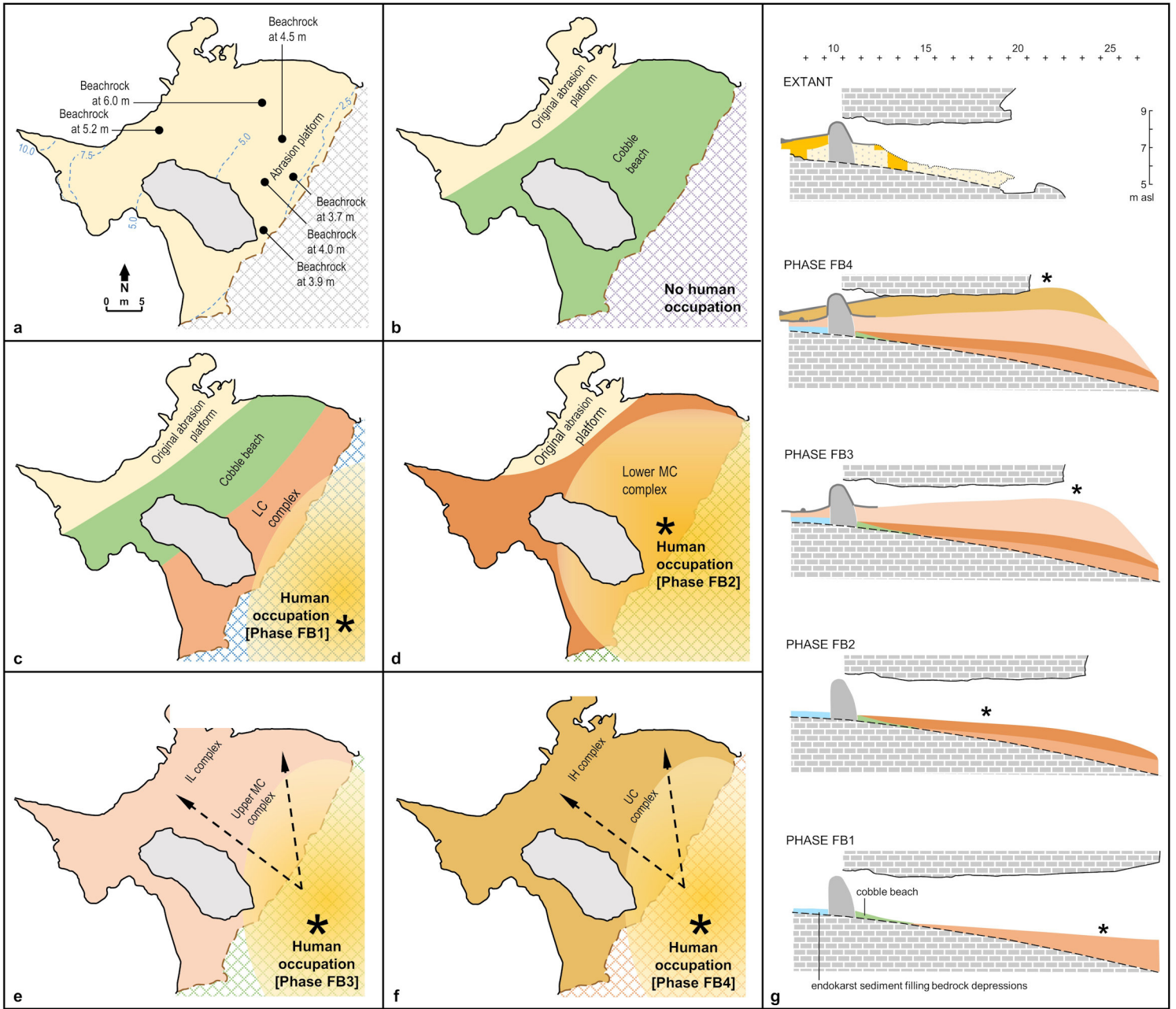
Fig. S18. Figueira Brava site formation and human occupation phases. a. Elevation data (m asl) for the marine abrasion platform (dashed contour lines) and individual beachrock remnants. **b.** During the MIS 5e highstand, the abrasion platform below +5.0-6.0 m asl was covered by a cobble beach. **c.** The retreat of the shore line exposed a sand beach abutting the cobble beach along the +5 m contour line; the preserved LC sediment remnants containing the remains of Phase FB1 correspond to the innermost periphery of the inhabited space. **d.** Slope dynamics cut back the entrance, and colluvial and aeolian sediments accumulated atop the previous fill; the preserved remnants of the lower MC complex (units MC3-MC5) containing the remains of phase FB2 correspond to the main habitation area. **e-f.** With continued accumulation, the cave filled-up, human occupation had to move outward, and the archeology in the preserved remnants of the upper MC (units MC1-MC2), UC and IL complexes (phases FB3 and FB4) corresponds to material syn-depositionally dispersed to the back of the cave by low-energy surface dynamics (indicated by the dashed black arrows). **g.** Schematic of the evolution of cave and fill through the different occupation phase to present-day, in profile view, along the T>S plane of the excavation grid.
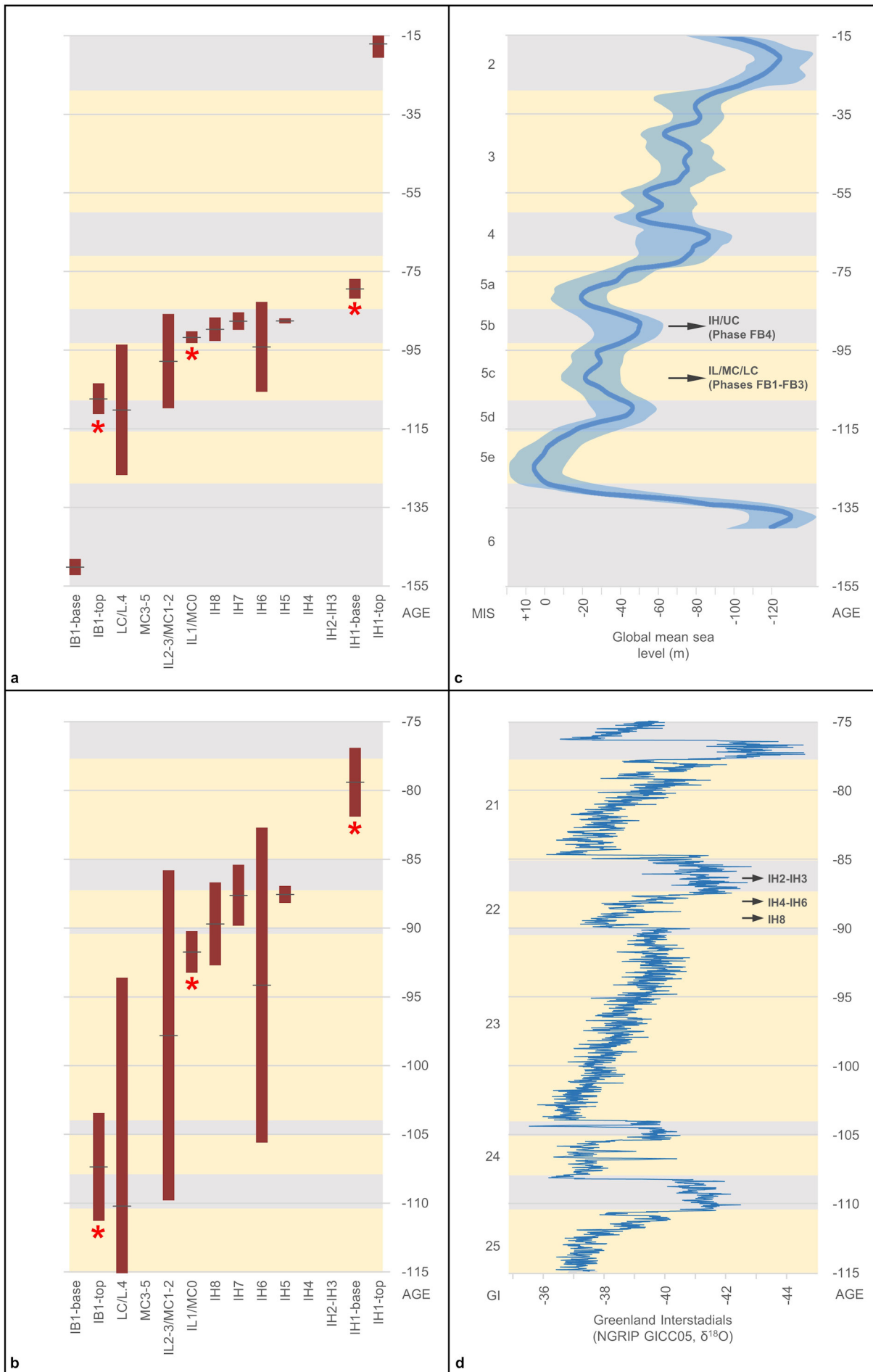
Fig. S19. Dating constraints and correlation with global records. a-b. 95.4% probability intervals for key events of sediment deposition and speleothem formation derived from the OSL and U-series dating of Figueira Brava; for interstratified speleothems with more than one dated sub-sample, the younger limit of the uppermost one and the older limit of the lowermost one have been used; the asterisks denote the samples providing an age for the key events of flowstone formation constraining the chronology of the archeological deposit. **c.** Marine Isotope Stages and sea level change (global mean and uncertainty band) during the last 140,000 years; the extremes in sea-level variation that occurred during the deposition of the Area F/Entrance 3 succession are indicated; the start dates used for MIS sub-stages are 130 ka (5e), 116 ka (5d), 108 ka (5c), 93 ka (5b), and 85 ka (5a). **d.** Greenland Interstadials; the IL/MC complexes formed during GI 23, the IH/UC complexes formed during GI 22 and, possibly, the subsequent stadial (GS 22) as well.

93
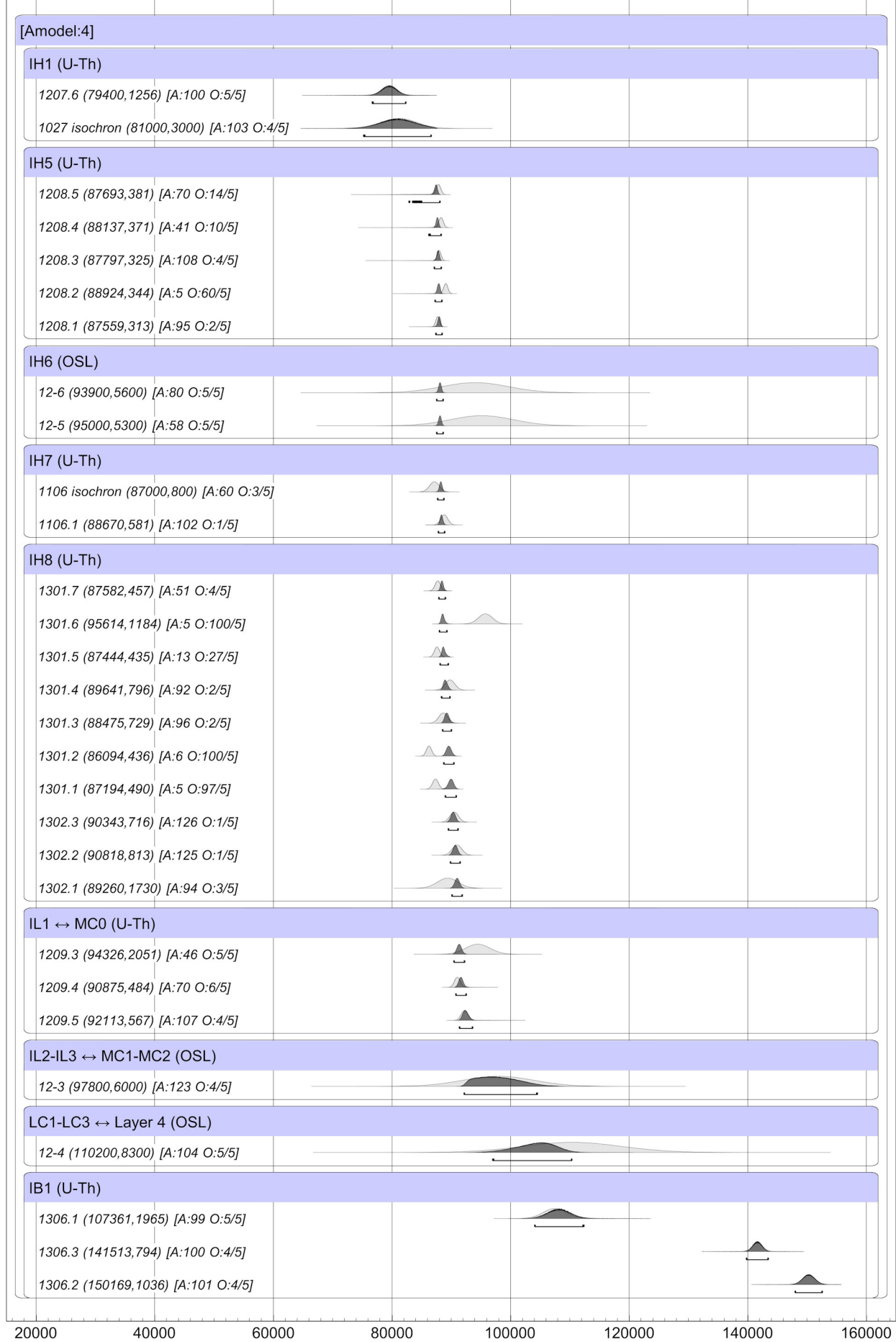
Fig. S20. Bayesian modelling of the Figueira Brava dating results. Outlier analysis. Modelled results in dark grey, unmodelled results in light grey. A: Agreement Index. O: posterior/prior outlier probabilities.
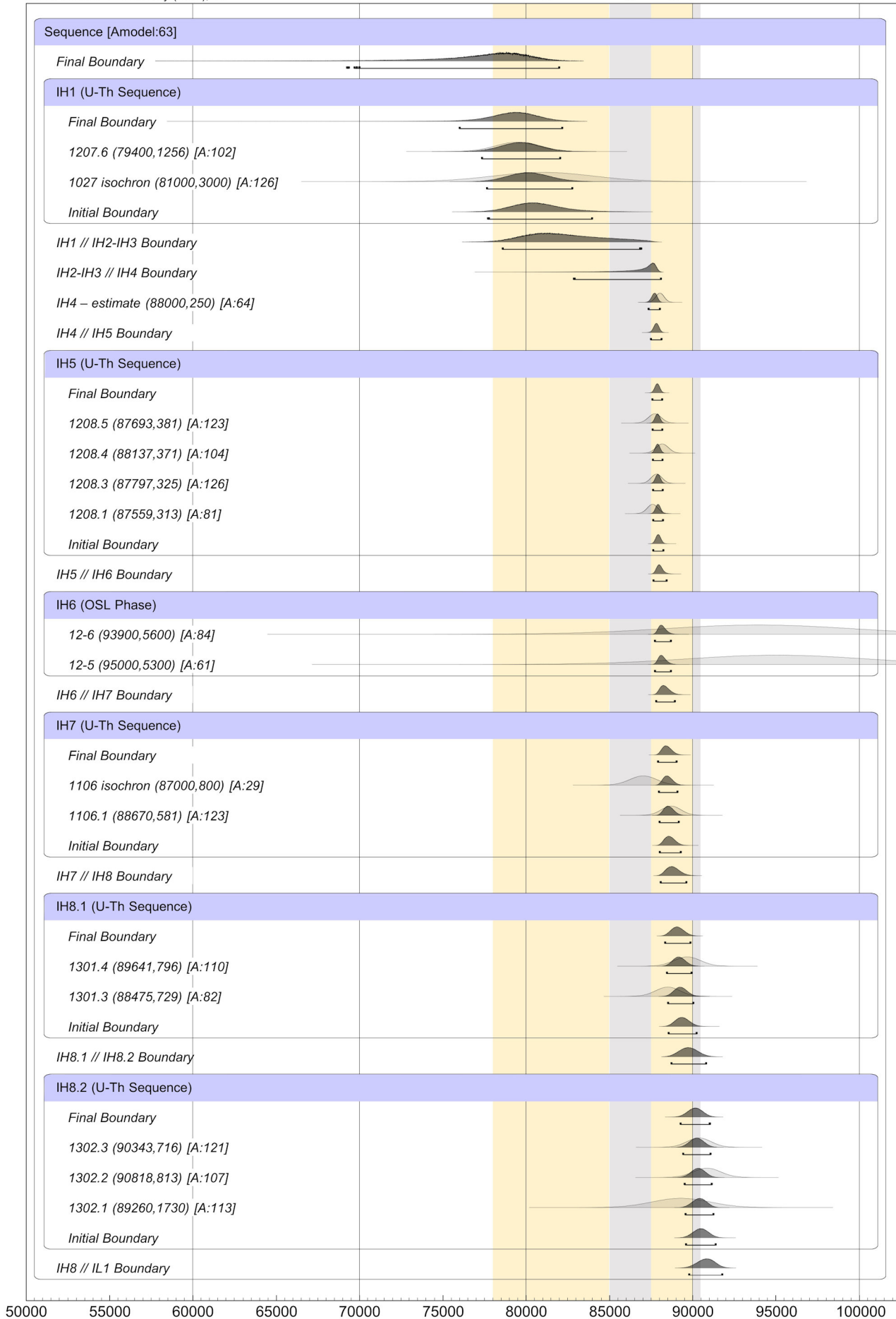
Fig. S21. Bayesian model of the Figueira Brava dating results. Modelled results for Area F's IH complex. A: Agreement Index.
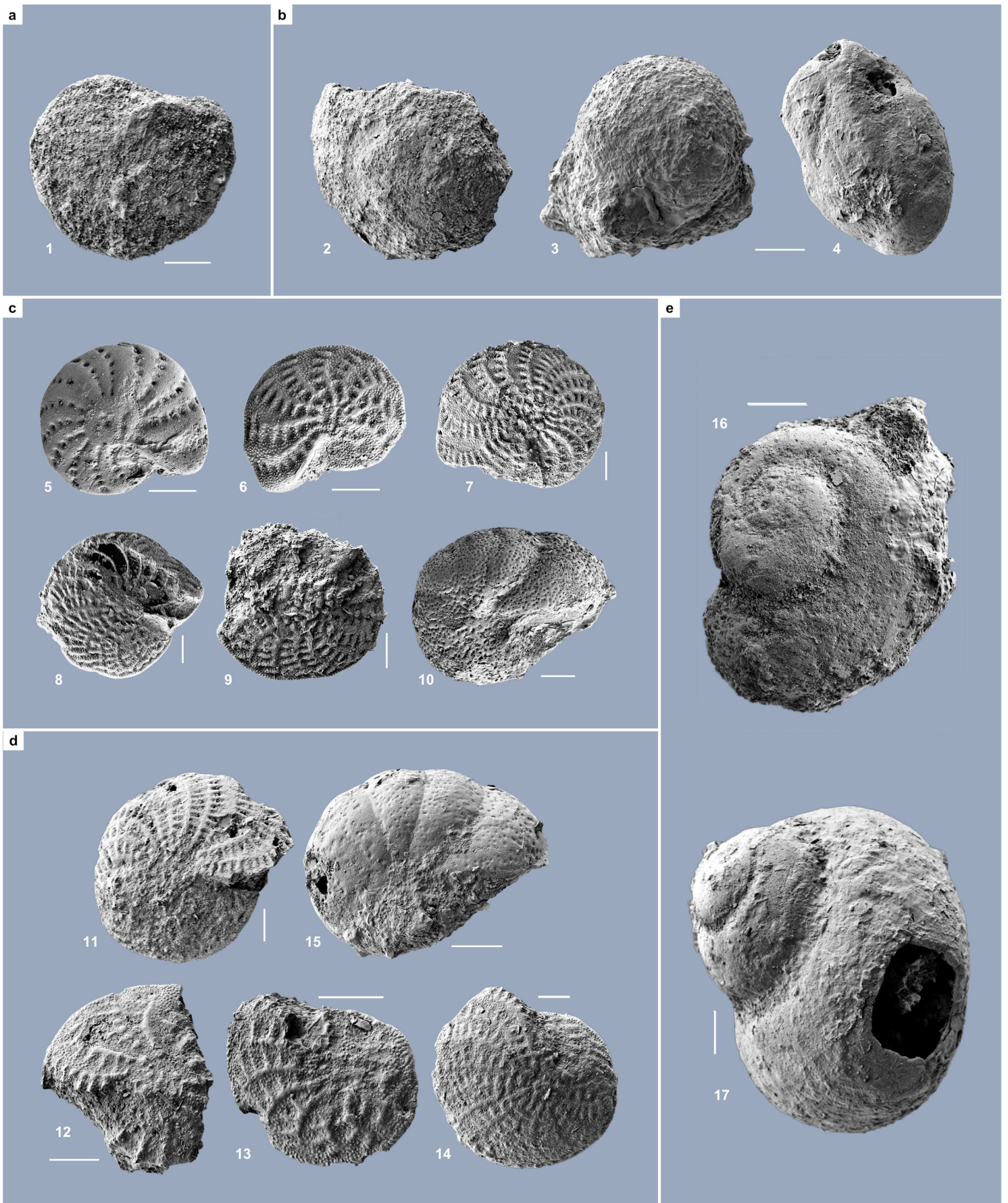
Fig. S22. Microfossils: SEM (Scanning Electron Microscope) photos of the taxa represented in the samples. a-b. Yellowish, heavily eroded foraminifera tests in the samples from the IT2 (**a**) and MC5 (**b**) units. **c-d.** Whitish, relatively fresh foraminifera tests in the samples from the IB2 (**c**) and MC5 (**d**) units. **e.** Gastropod shells in the sample from MC5. **1,5-9, 11-14.** *Elphidium* spp.; **2.** *Ammonia* (?) sp.; **3.** *Orbulina suturalis*; **4.** *Quinqueloculina* sp.; **10,15.** *Cibicides refulgens*; **16.** undetermined gastropod; **17.** *Littorina obtusata*. Each white bar used for scale represents 100 μm .

Fig. S23. Carbonized plant remains. a. Frequency diagram. **b.** Distribution of pine plant parts across the Holocene, naturally accumulated IT2 deposit, and the Middle Paleolithic occupation phases. **c.** *P. pinea* nuts: shell present, kernel absent. **d-e.** *P. pinea* from FB4: cone bract (**d**) and sections under SEM (**e**).

97
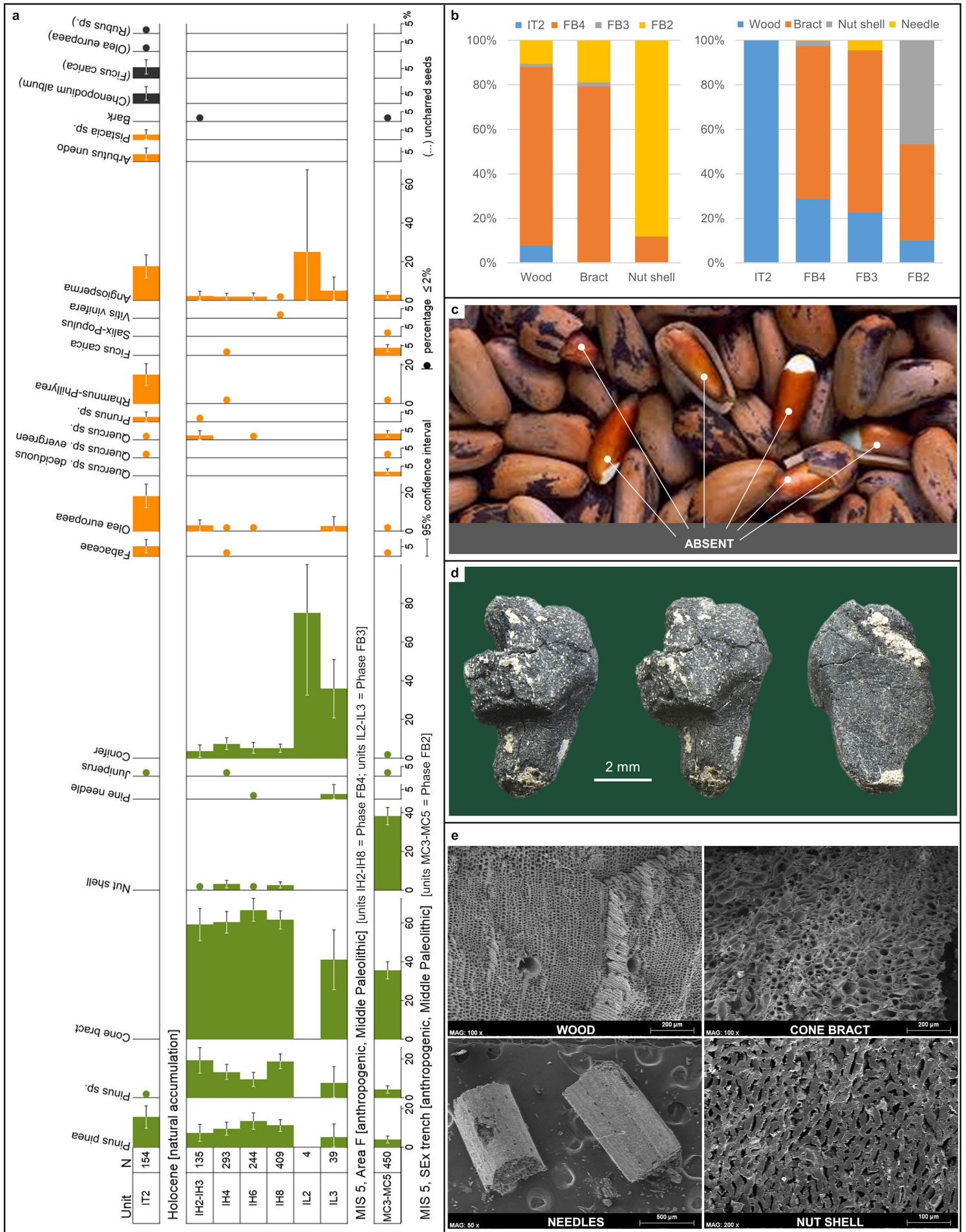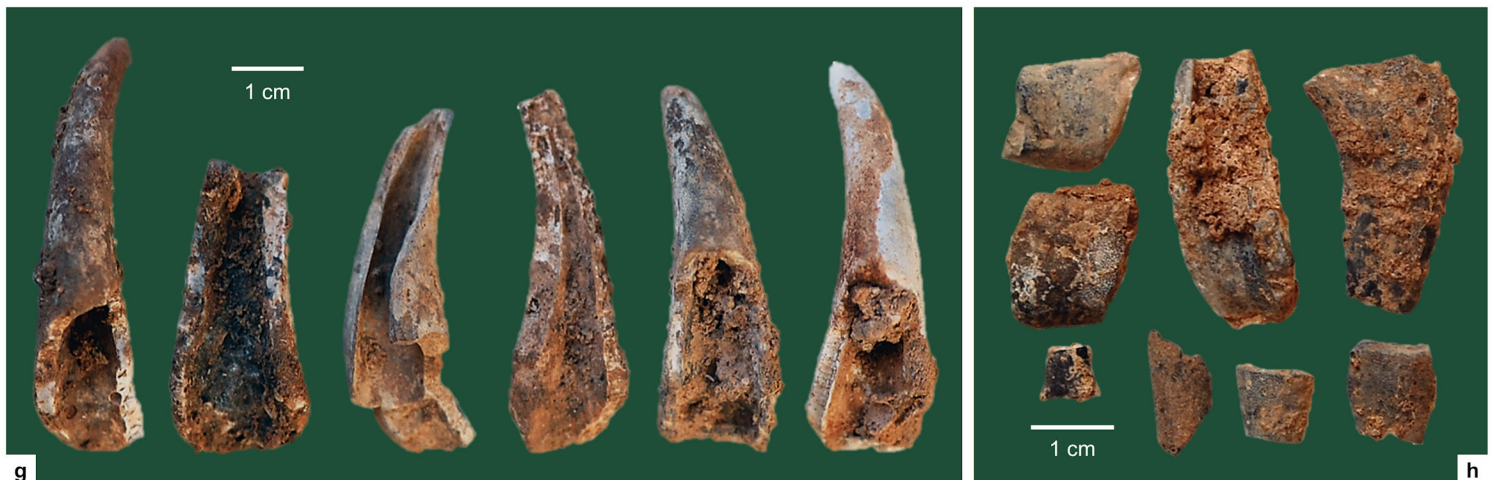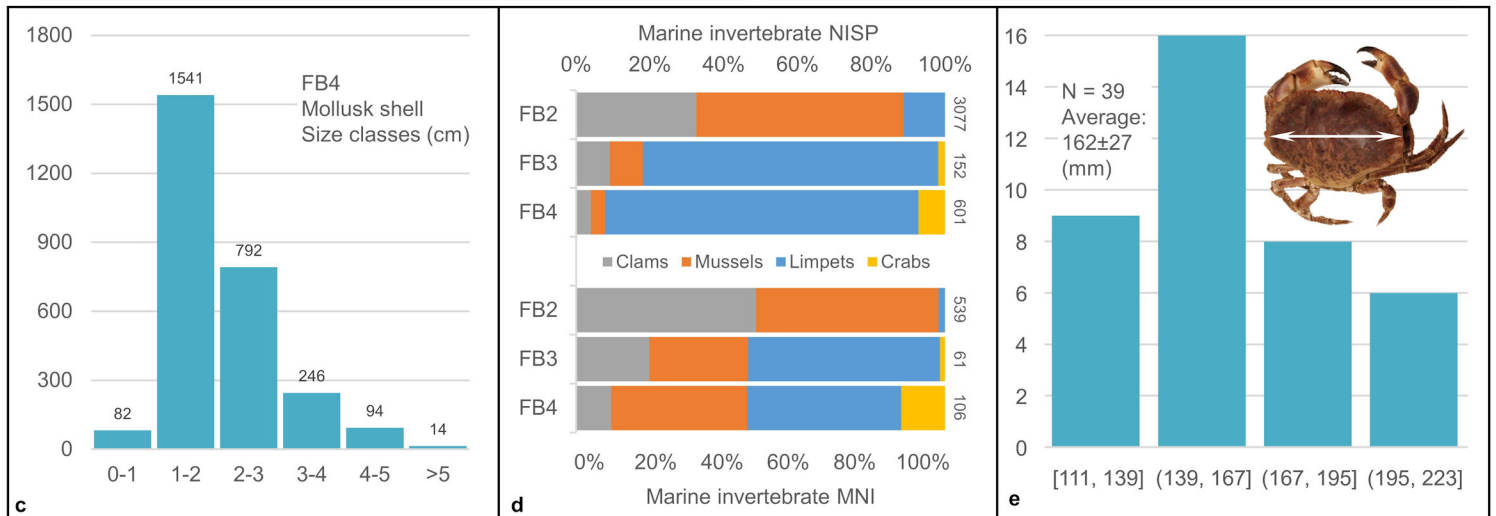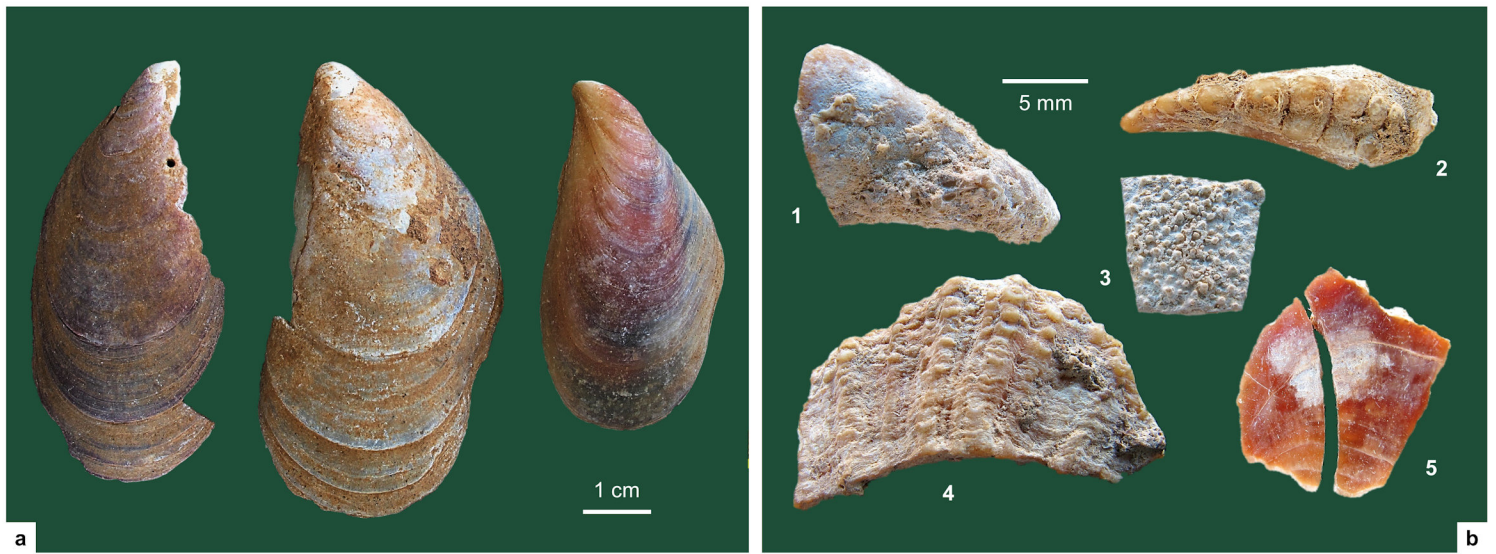
Fig. S24. Marine invertebrate taphonomy. a. Intrusive mussel shells in the small mammal burrow of T9SW (unit IT0). **b.** Crab claw (1-2), crab carapace (3), limpet (4) and mussel (5) shell fragments sorted from wet-sieved *in situ* deposit (unit IH8). **c.** Mollusk shell breakage in the IH complex (units IH2-IH8), Phase FB4. **d.** Chronological variation in the frequency of the main marine invertebrates across human occupation phases. **e.** Histogram of brown crab carapace width (mm; *in situ* units only). **f.** Taxonomic composition (by NISP) of the *in situ* and reworked crab assemblages. **g.** Brown crab pincers with anthropogenic breaks; **h.** Brown crab carapace and pincer fragments, burnt.

98
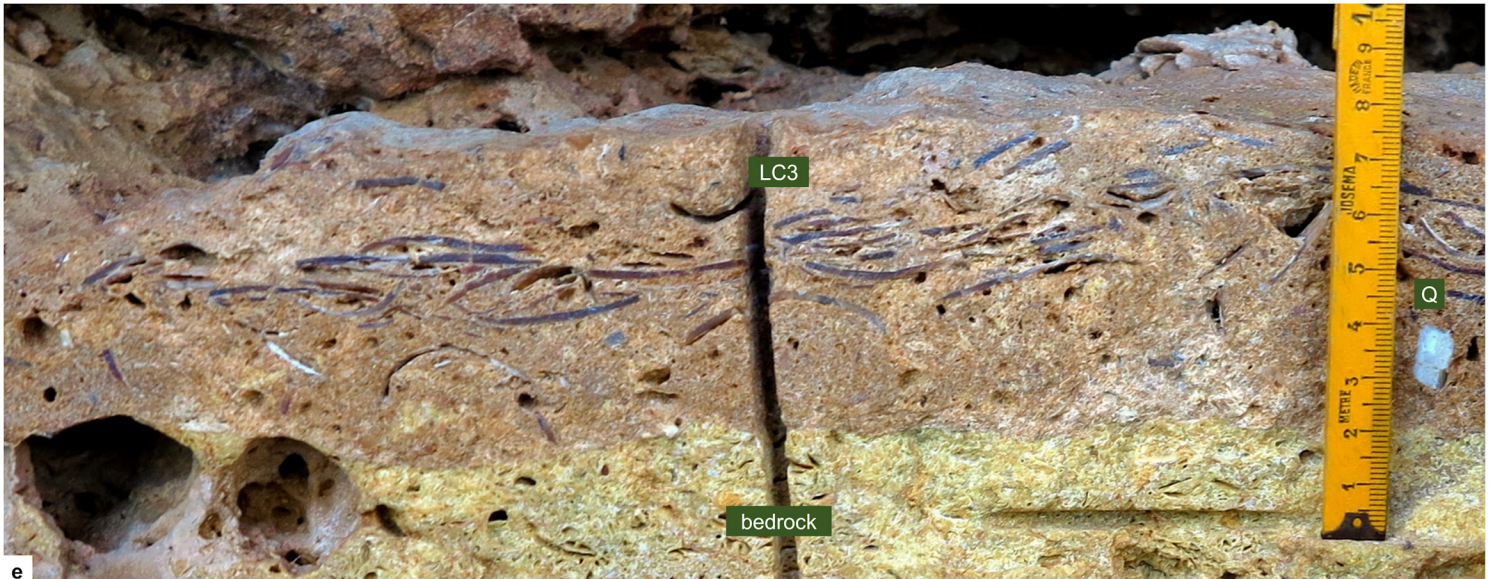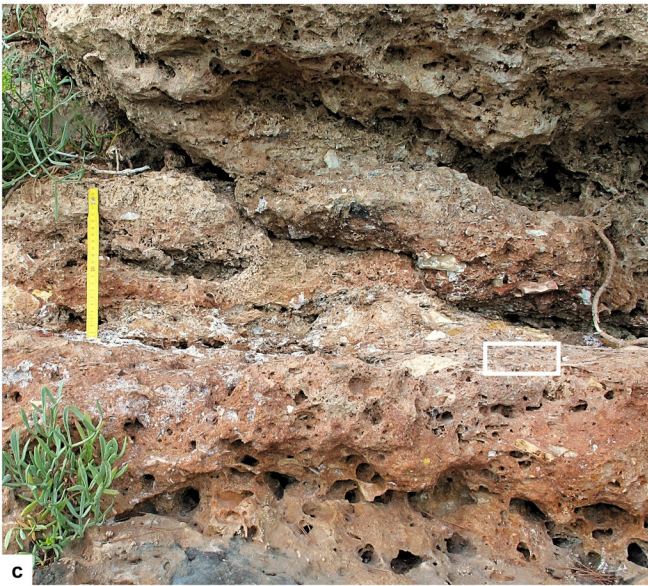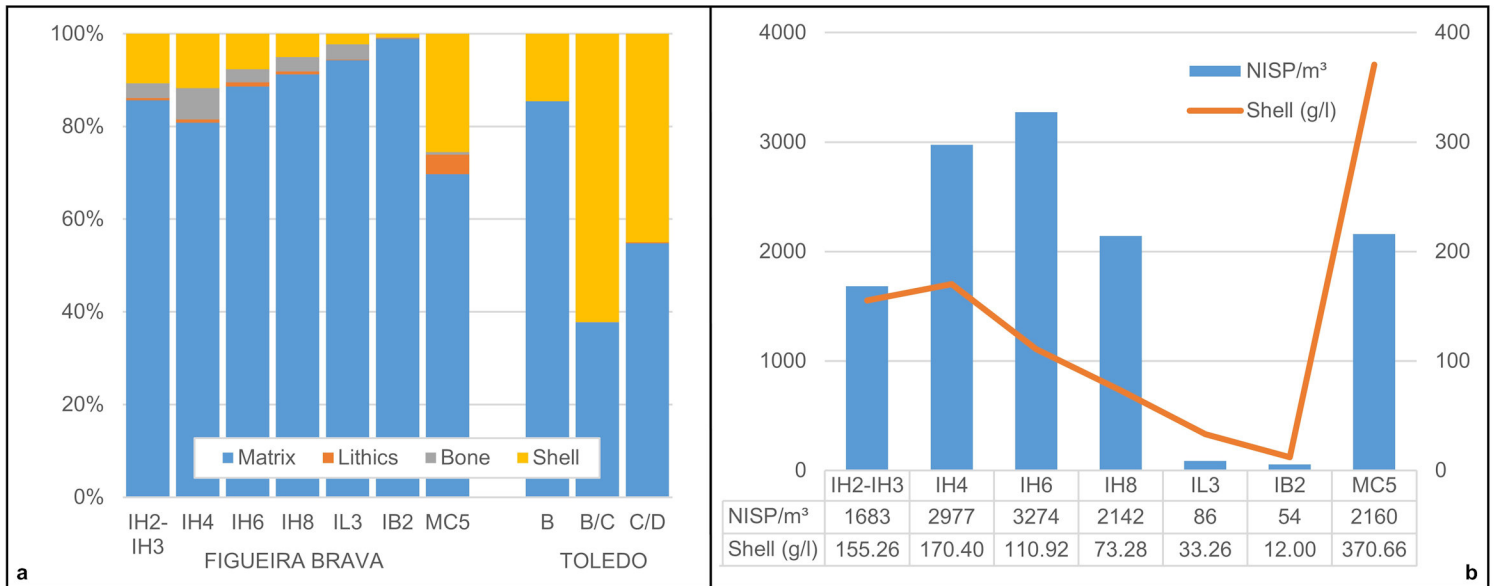
Fig. S25. The density of marine invertebrate remains (mollusk and crab). a-b. Stratigraphic variation at Figueira Brava and Toledo; for bulk samples, all mesh sizes (>4 mm, 2-4 mm, 1 mm) were combined, and the sample's weight was translated into volume using 1.45 for the density of loose sand. c-d. Exposure of the LC complex, prior to the cutting of sample 1022, and close-up of the LC1 mussel-shell surface in the area indicated by the white rectangle; a 20 cm yellow ruler was used for scale (July 20, 2010). e. Section view (November 21, 2017) of the LC3 mussel bed after the cutting of sample 1021; note the presence of quartz artefacts (Q) all the way down to the contact with bedrock.

99
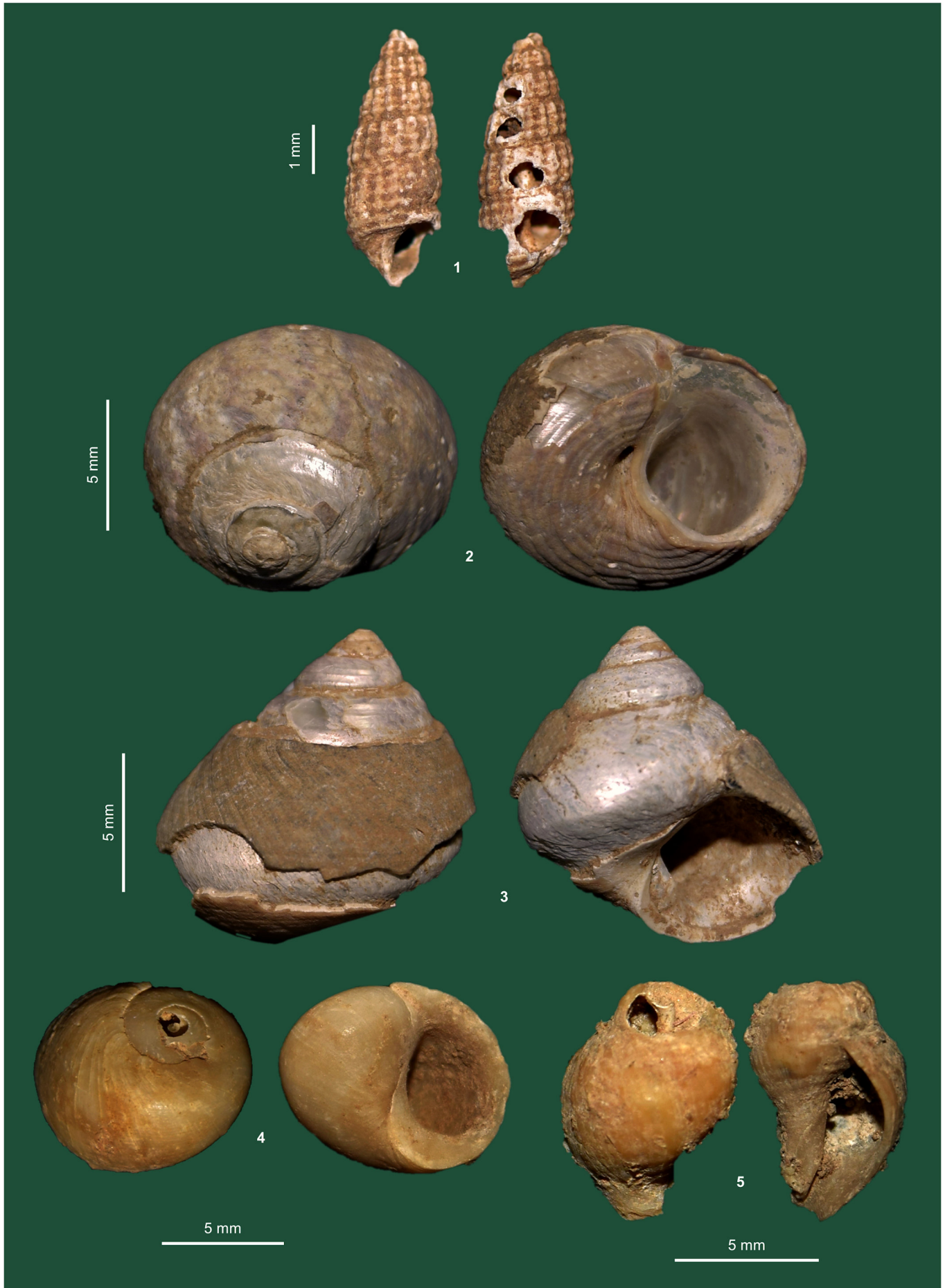
Fig. S26. Non-food gastropods from the *in situ* MIS 5 deposit. 1. *Bittium reticulatum* (square S9, unit IH4). **2.** *Steromphala umbilicalis* (square U8, unit IH2-IH3). **3.** *Phorcus lineatus* (square U8, unit A3). **4.** *Littorina obtusata* (square T8, unit IH8). **5.** *Nucella lapillus* (square S9, unit IH6).

Fig. S27. Non-food bivalves from the *in situ* MIS 5 deposit. 1. *Ostrea* sp. fragment (right valve; manuported Miocene fossil? square U9, unit IH8) .
2. *Callista chione* fragment (square S8, unit IH6). **3.** *Glycymeris* sp. fragment (SEx trench, unit MC5). **4.** *Pecten maximus* fragment (left valve; square U8, unit IL2). **5.** *Glycymeris glycymeris* (SEx trench, unit MC5). **6.** *Pecten maximus* (left valve; square U9, unit IH2-IH3). Each white bar used for scale represents 1 cm.
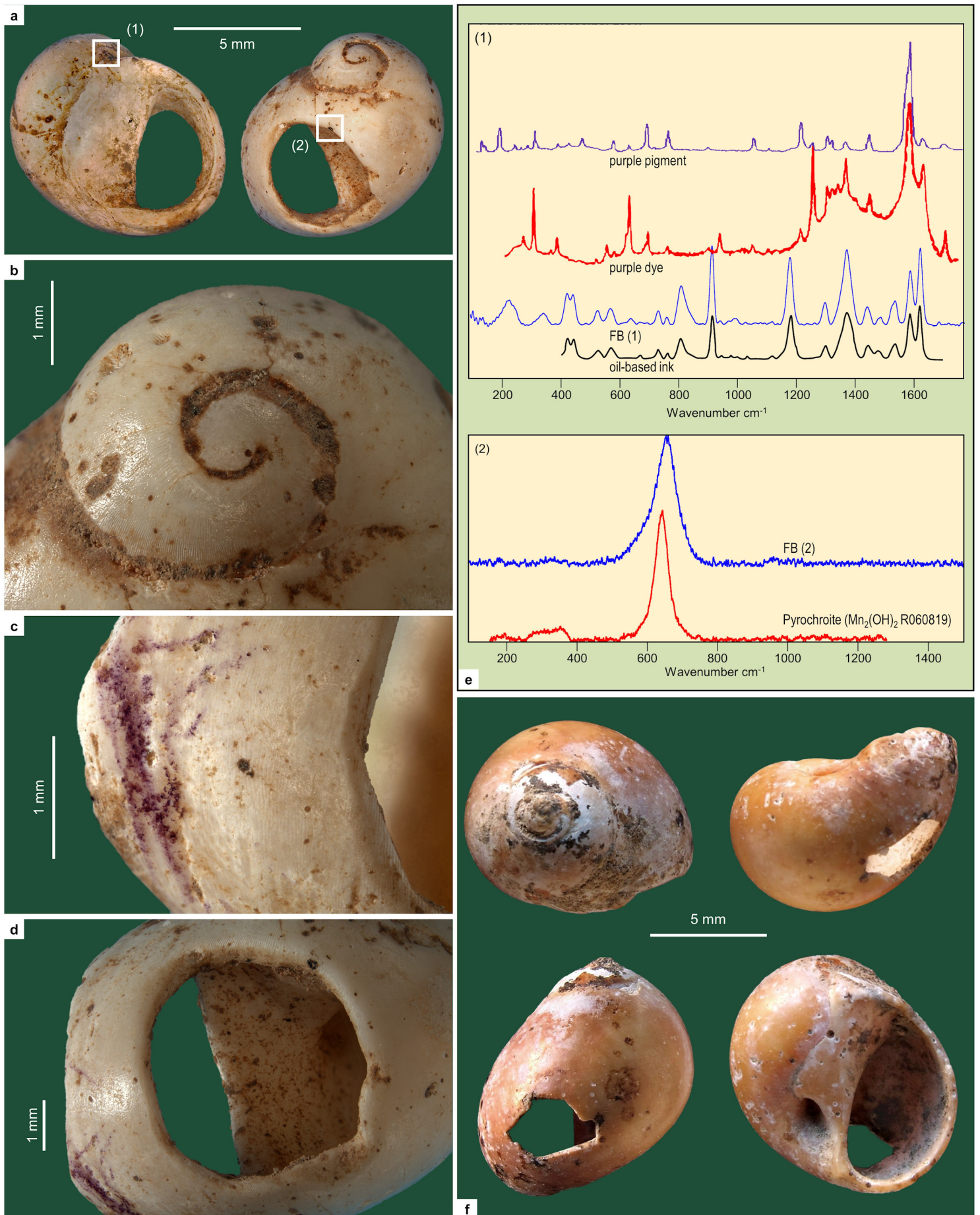
Fig. S28. The perforated gastropod shells. a. *Littorina obtusata* from the small mammal nest in T9-SW, reworked unit IT0, directly radiocarbon-dated to 7390±25 BP (OS-114170); the location of the two accretions analyzed by micro-Raman spectroscopy is indicated. **b-d.** close-up views of the *L. obtusata* shell; note the pitting of the surface and the well-rounded edges of the perforation. **e.** micro-Raman spectra (arbitrary units) of the purple (1) and black (2) accretions, which match, respectively, to a manganese mineral and an oil-based ink. **f.** *Euspira guilleminii* in the floatation sample from T9-East, unit IT2.
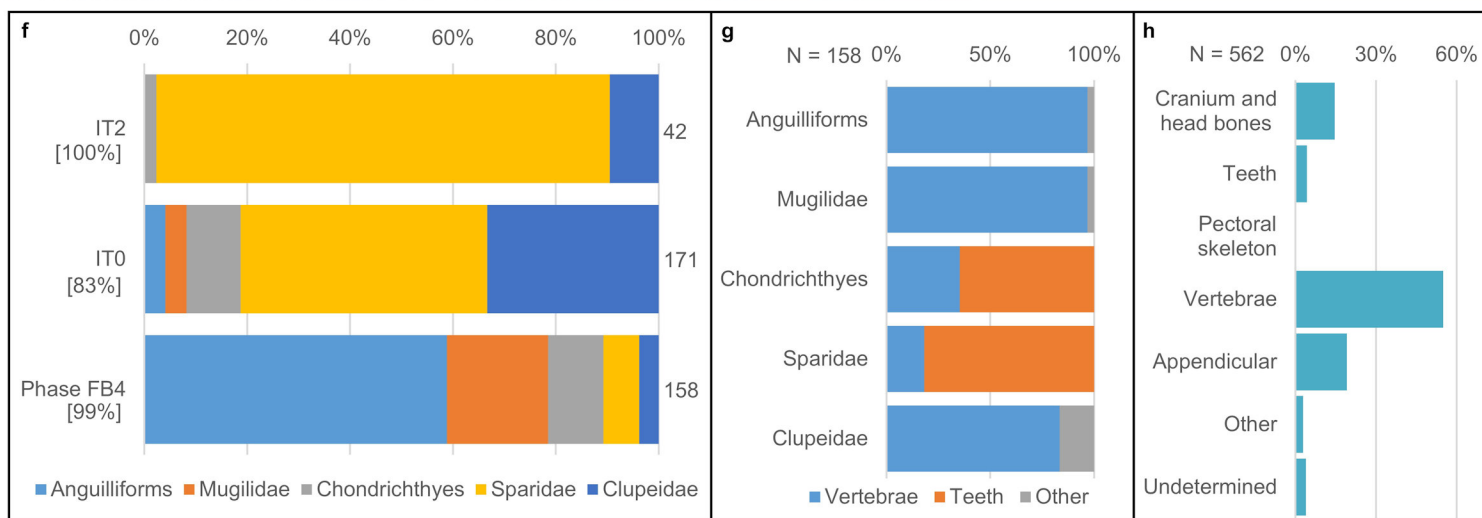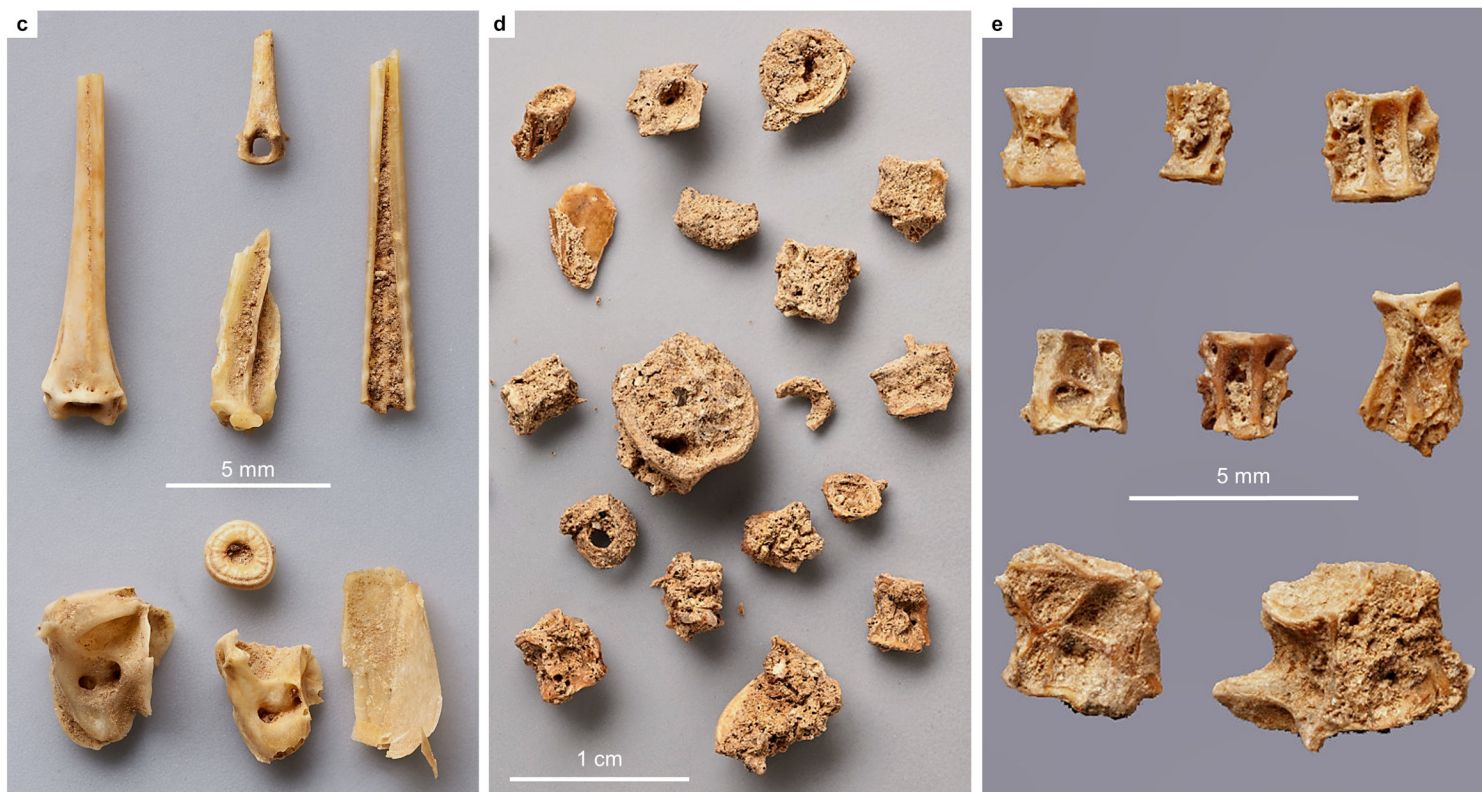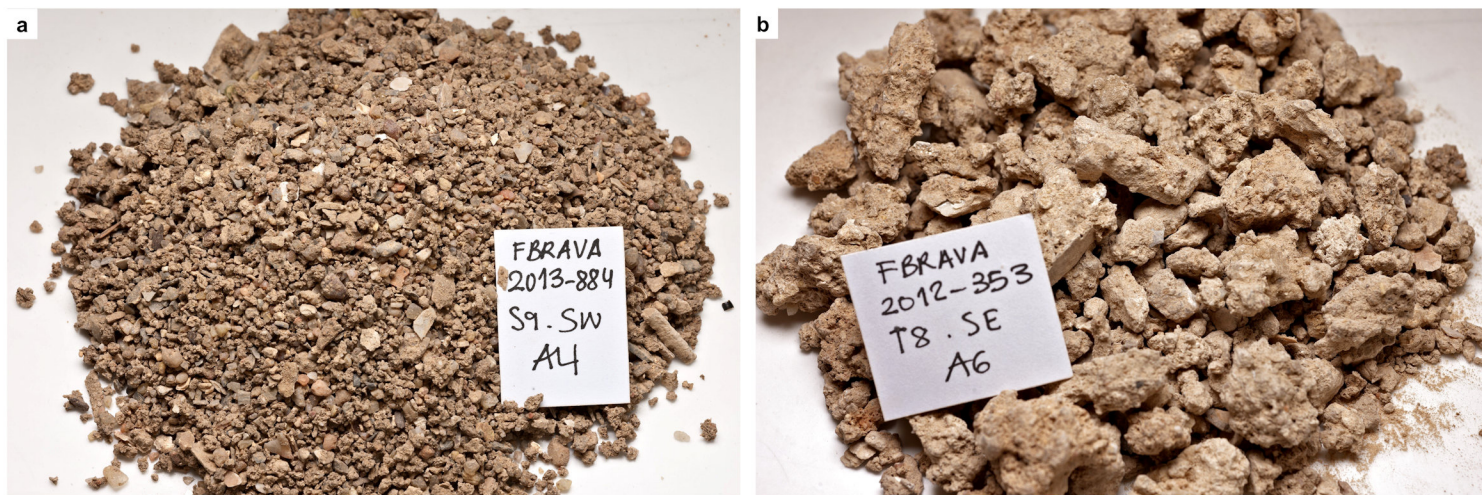
Fig. S29. The fish remains. a-b. Bulk sediment from units IH4 and IH8, washed and dried, prior to sorting. **c.** Fresh, clean fish remains from a burrow that penetrated into unit IH4. **d.** Vertebrae, and vertebral fragments sorted from unit IH6. **e.** Eel vertebrae from unit IH6, during (lower row) and after (upper and middle rows) manual removal, with stitching pins, of the cemented sediment that cached them. **f.** Representation of the main taxonomic groups in the Holocene, reworked, and MIS 5 levels; for each provenience, the NISP and the percentage of the NISP those five groups represent are indicated.
g-h. Skeletal part representation in the assemblage from Phase FB4 in the five main groups (**g**) and as a whole (**h**).
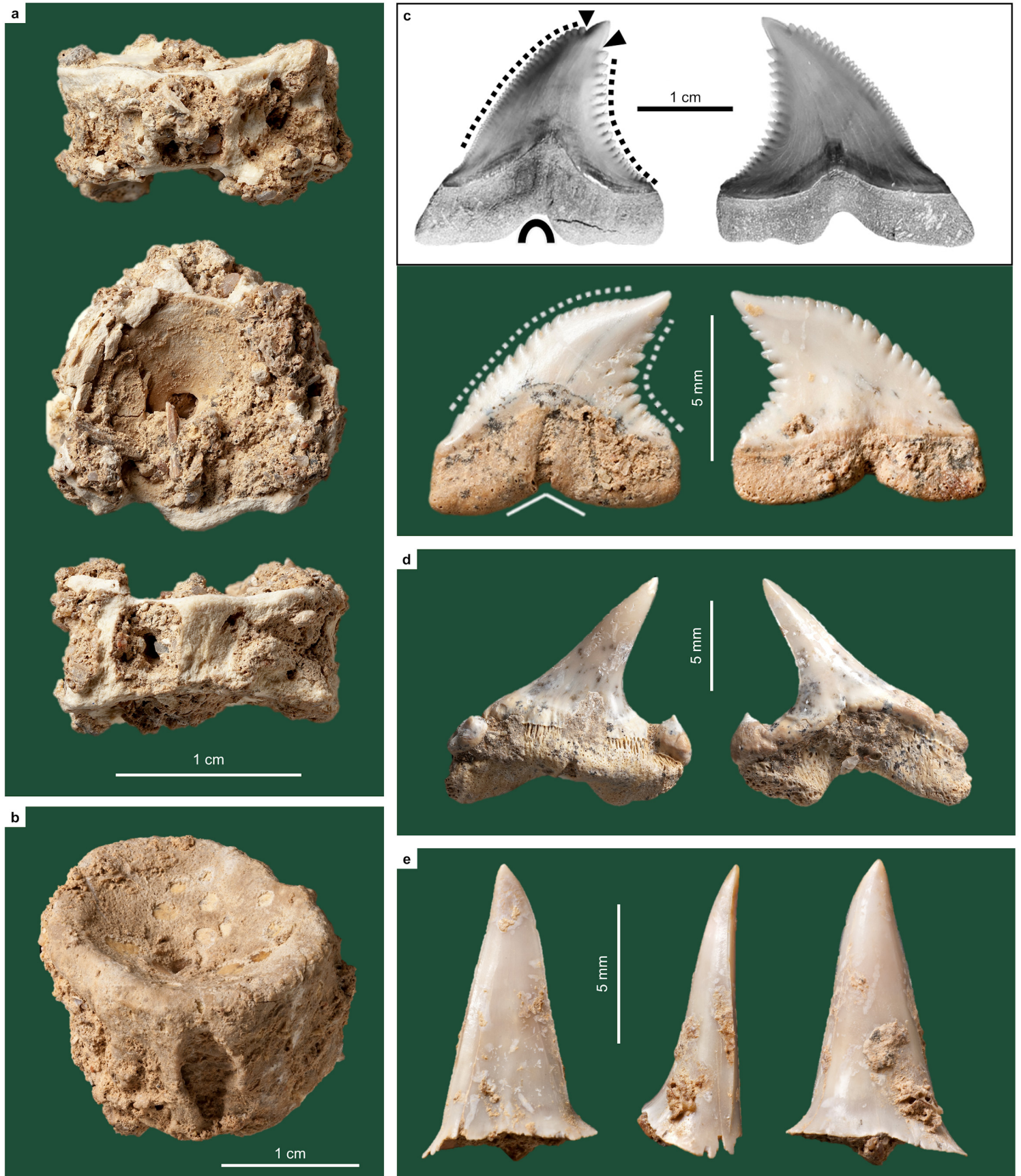
Fig. S30. The sharks from unit IH6. a. Vertebra from sieved sediment. **b.** Piece-plotted vertebra (possibly Carcharhiniformes). **c.** tooth of cf. *Prionace glauca* (blue shark) (below) compared with a tooth of *Hemipristis serra* (weasel shark) from the Miocene (above); note the differences in the shape of the basal notch and in the outline of the serrated edges. **d.** tooth of cf. *Lamna nasus* (porbeagle) after chemically-aided cleaning of the coating concretions. **e.** Anterolateral element of the dentition (cf. *Isurus oxyrinchus*, shortfin mako). Photo credits: J. P. Ruas and Carrillo-Briceño *et al*.

104
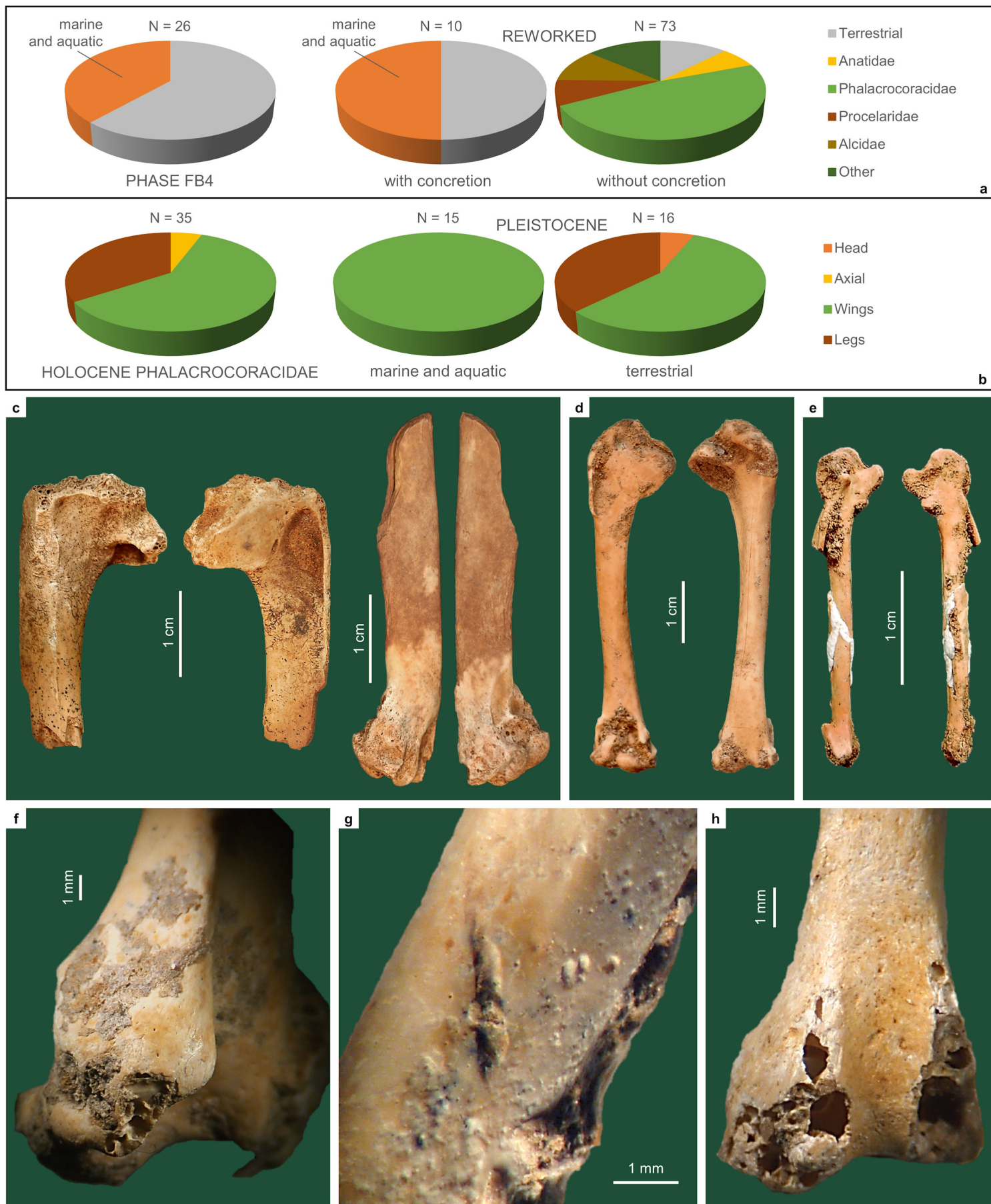
Fig. S31. The birds. a. Proportion and taxonomic composition of the marine bird bone assemblages found *in situ* and in reworked units of provenience. **b.** Skeletal part representation of the Pleistocene bird assemblage (Phase FB4 plus concreted bones from reworked sediment) compared with the non-concreted (Holocene) Phalacrocoracidae from reworked sediment. **c.** Pleistocene *Pinguinus impennis* (great auk) humeri (from reworked sediment, but with carbonate concretions). **d.** *Scolopax rusticola* (woodcock) humerus from unit IH6. **e.** *Athene noctua* (little owl) left carpometacarpus from unit IH6. **f.** possible squashing and notching on right distal humerus of *Anas* cf. *platyrhyncos* (mallard) from unit IH8; **g.** possible cut mark on right distal shaft of *Corvus* cf. *corax* (raven) from unit IH8. **h.** distal femur of an indeterminate bird from units IH2-IH3, punctured (by a small carnivore?).
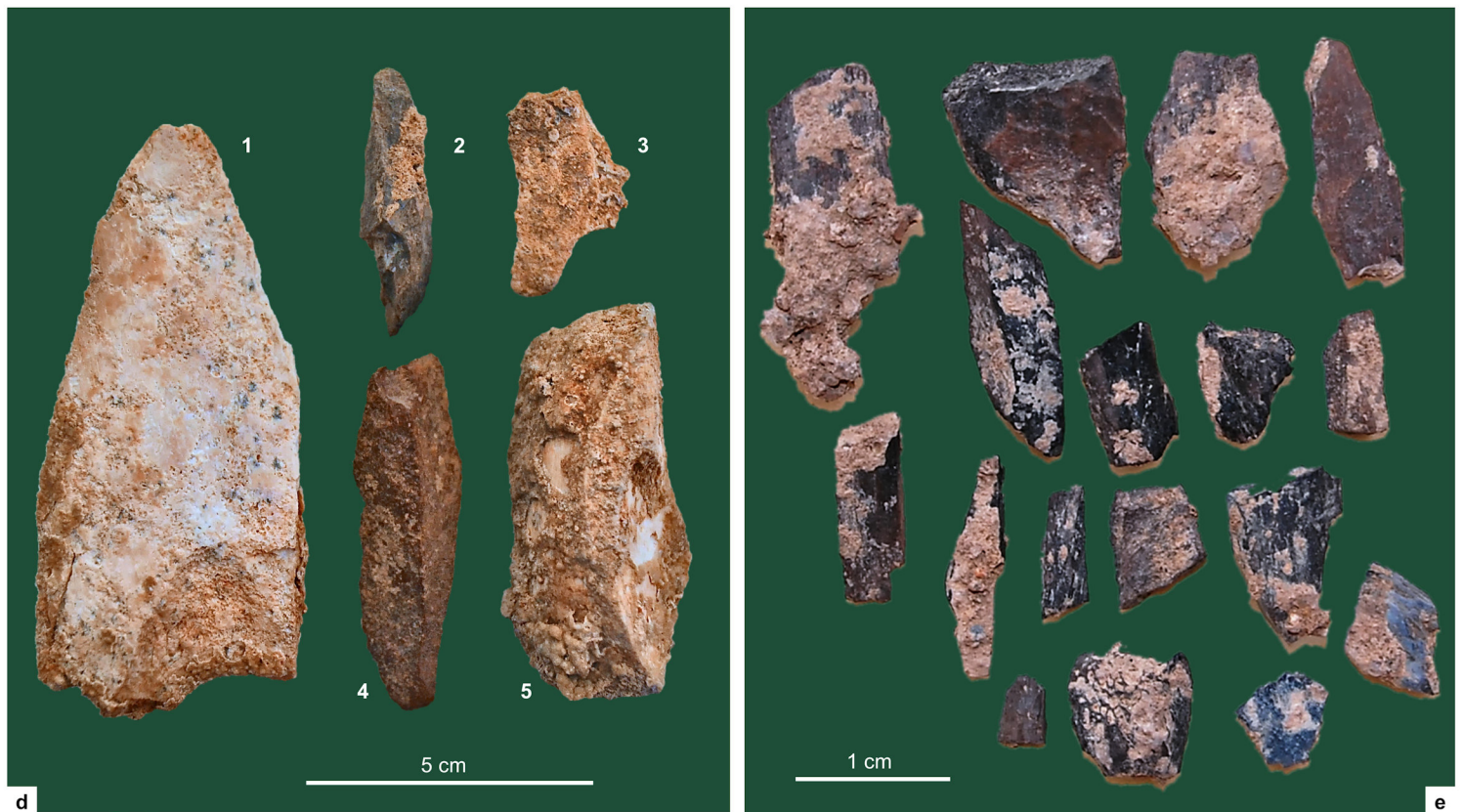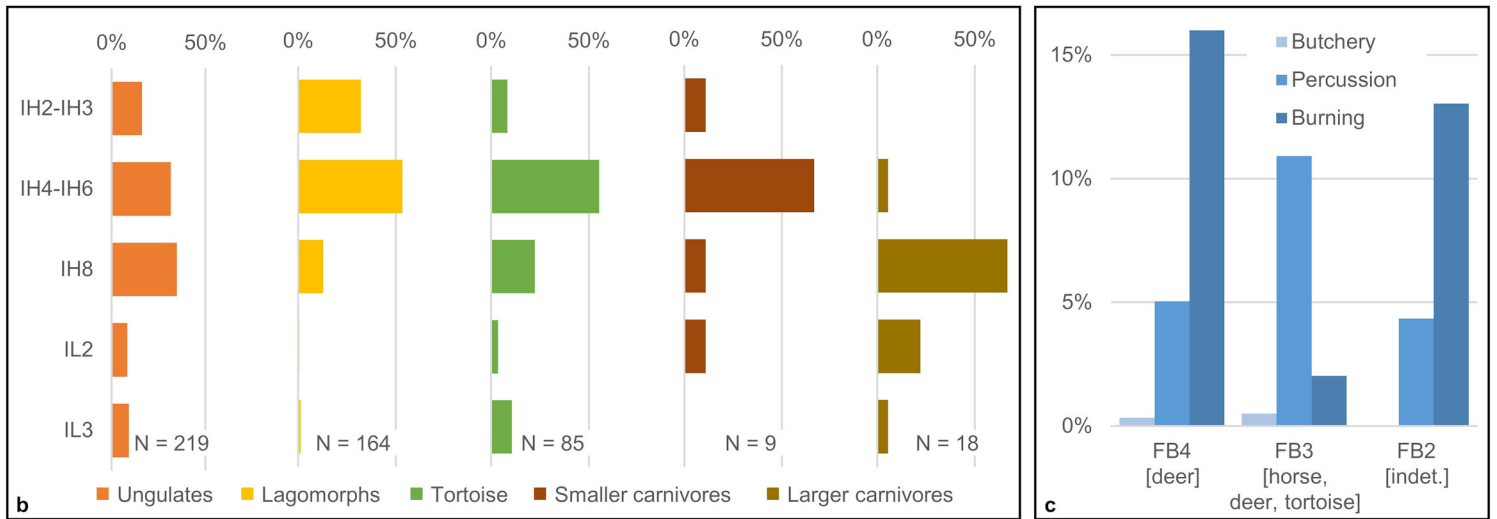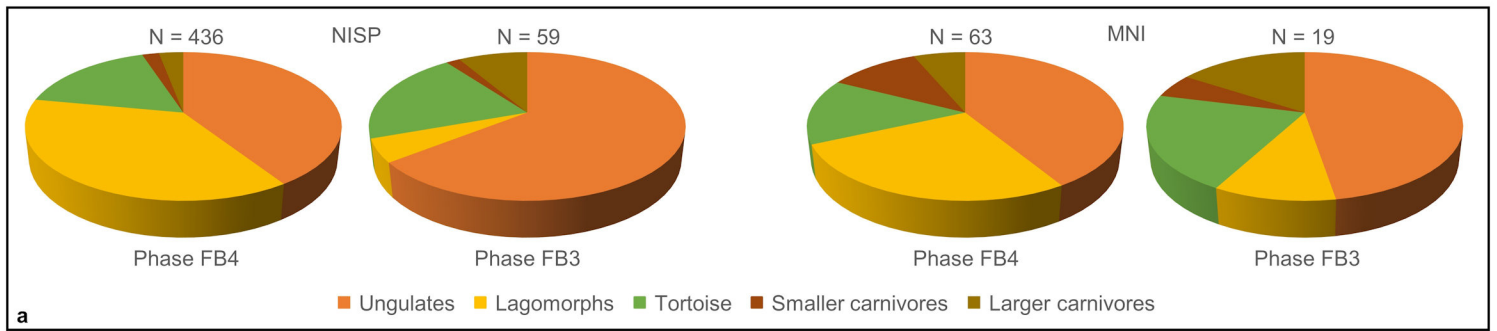
Fig. S32. Mammals and reptiles. a. Taxonomic composition per phase. **b.** vertical distribution, in the Area F trench and per stratigraphic unit, of the main groups (*in situ* Pleistocene levels only). **c.** Anthropogenic modification across occupation phases (% of NISP); the taxa identified among the modified remains are indicated. **d.** Bone percussion flakes (**1.** unit IL2; **2-3.** reworked unit IT0; **4.** unit IH6; **5.** unit IH8). **e.** Burnt bone fragments from unit IH6. Ungulates = horse, aurochs, deer, ibex, boar. Larger carnivores = bear, hyena, wolf. Smaller carnivores = fox, lynx, cat.
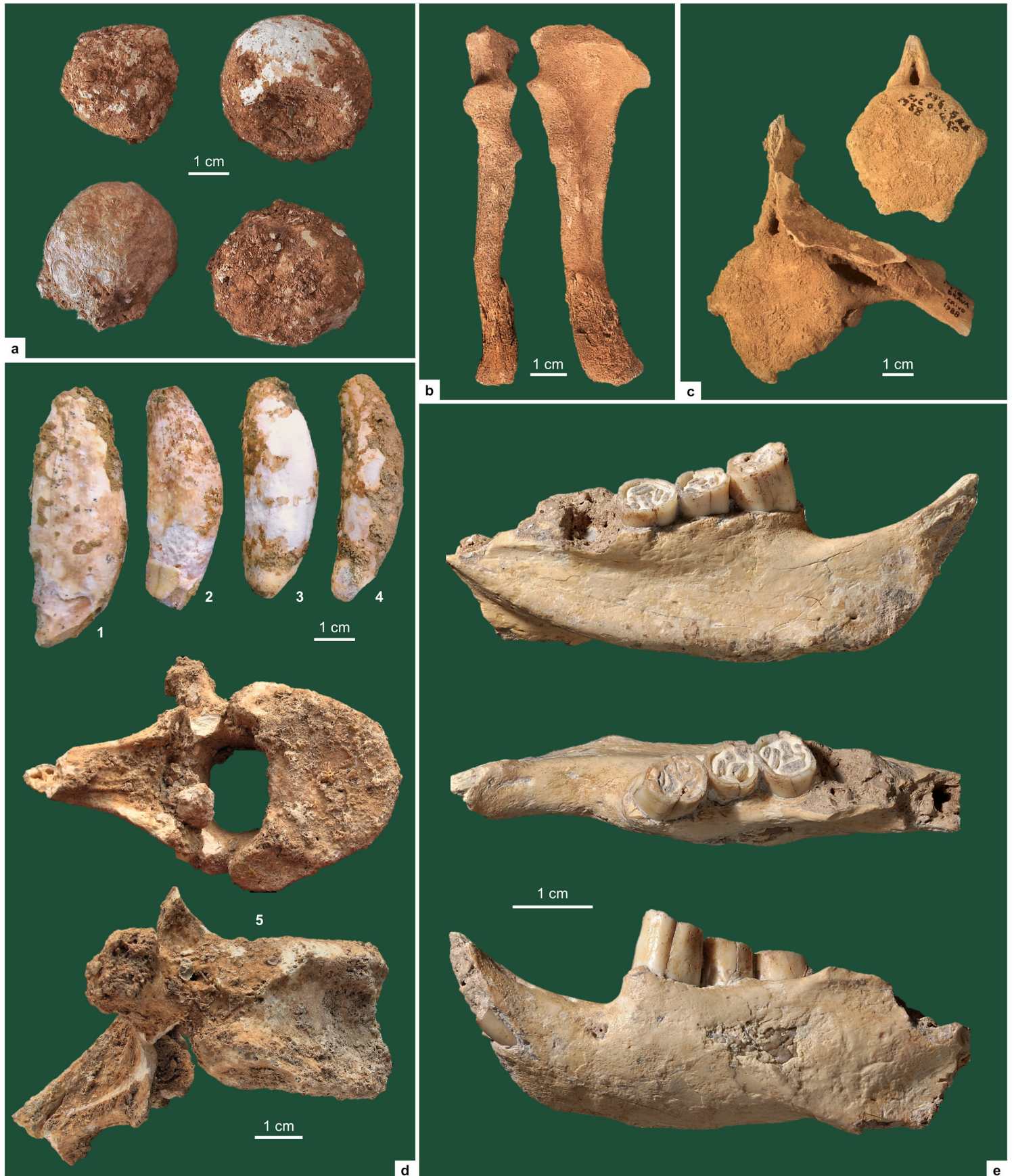
Fig. S33. Carnivores, cave dwellers and marine mammals. a. Coprolites (Area F, unit IH4). **b.** Right ulna of ringed seal (*Pusa hispida*; Area C, 1986-89 excavations). **c.** Vertebrae of short-beaked common dolphin (*Delphinus delphis*; Area C, 1986-89 excavations). **d.** Canines and thoracic vertebra of brown bear (*Ursus arctos*; Area F; **1.** unit IL3; **2.** top of unit IL2; **3-5.** unit IH8). **e.** Left mandible of porcupine (*Hystrix* sp.; Area F, unit IH8), after preparation.
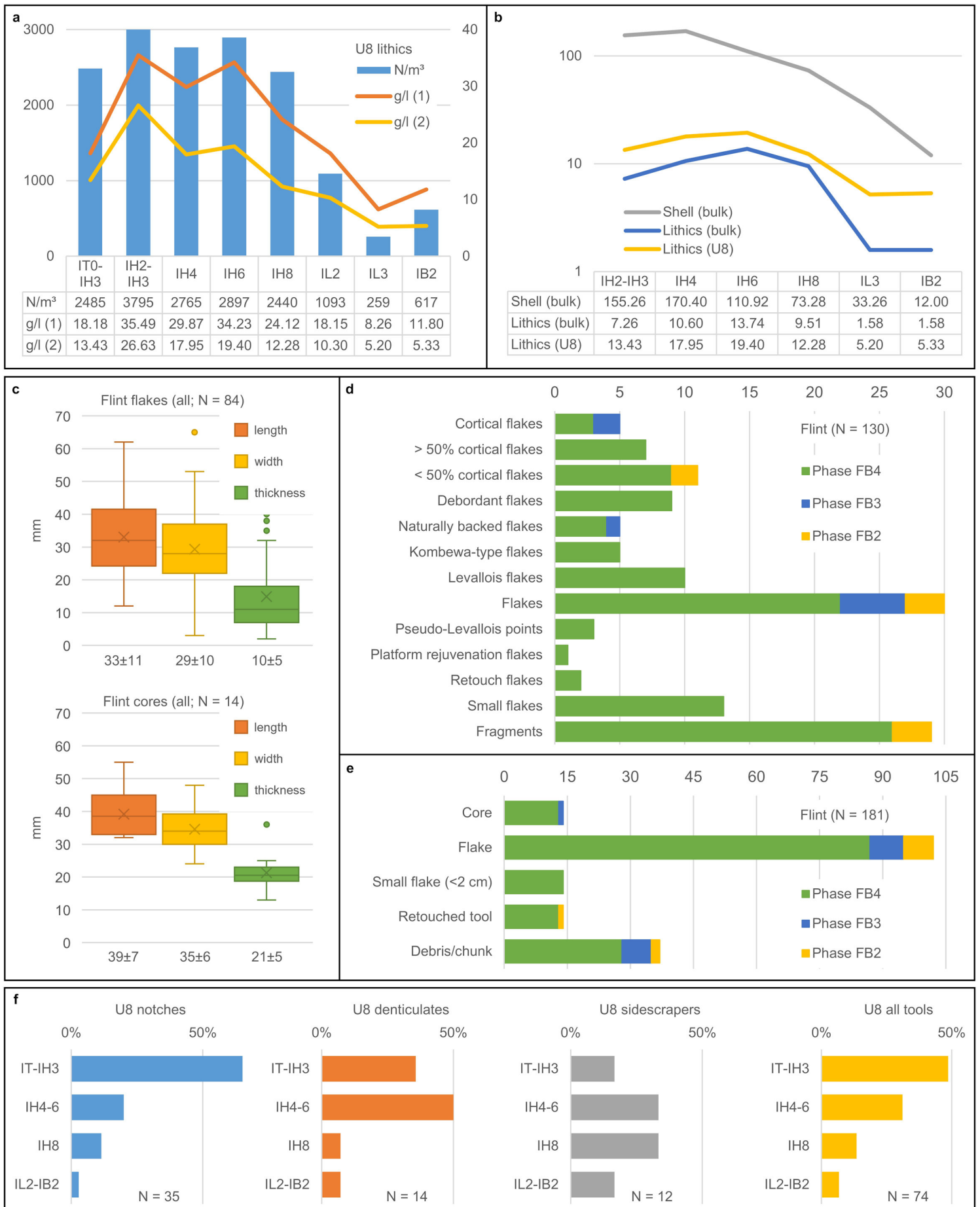
Fig. S34. Stone tools. a-b. Density data for the lithics in square U8, and comparison with Area F's bulk sample data for lithics and invertebrate shell; in (**a**), the density is calculated with [g/l (1)], and without [g/l (2)], manuports, hammerstones and chunks; in (**b**), U8 uses g/l (2), the IH2-IH3 lithics count subsumes IT0, and the logarithmic scale emphasizes the curves' similar trends. **c-e.** The flint assemblage: box-and-whisker plots and average size of flakes and cores (all units combined) (**c**), technological (**d**), and techno-economic (**e**) categories. **f.** Distribution of retouched tools across the U8 sequence.
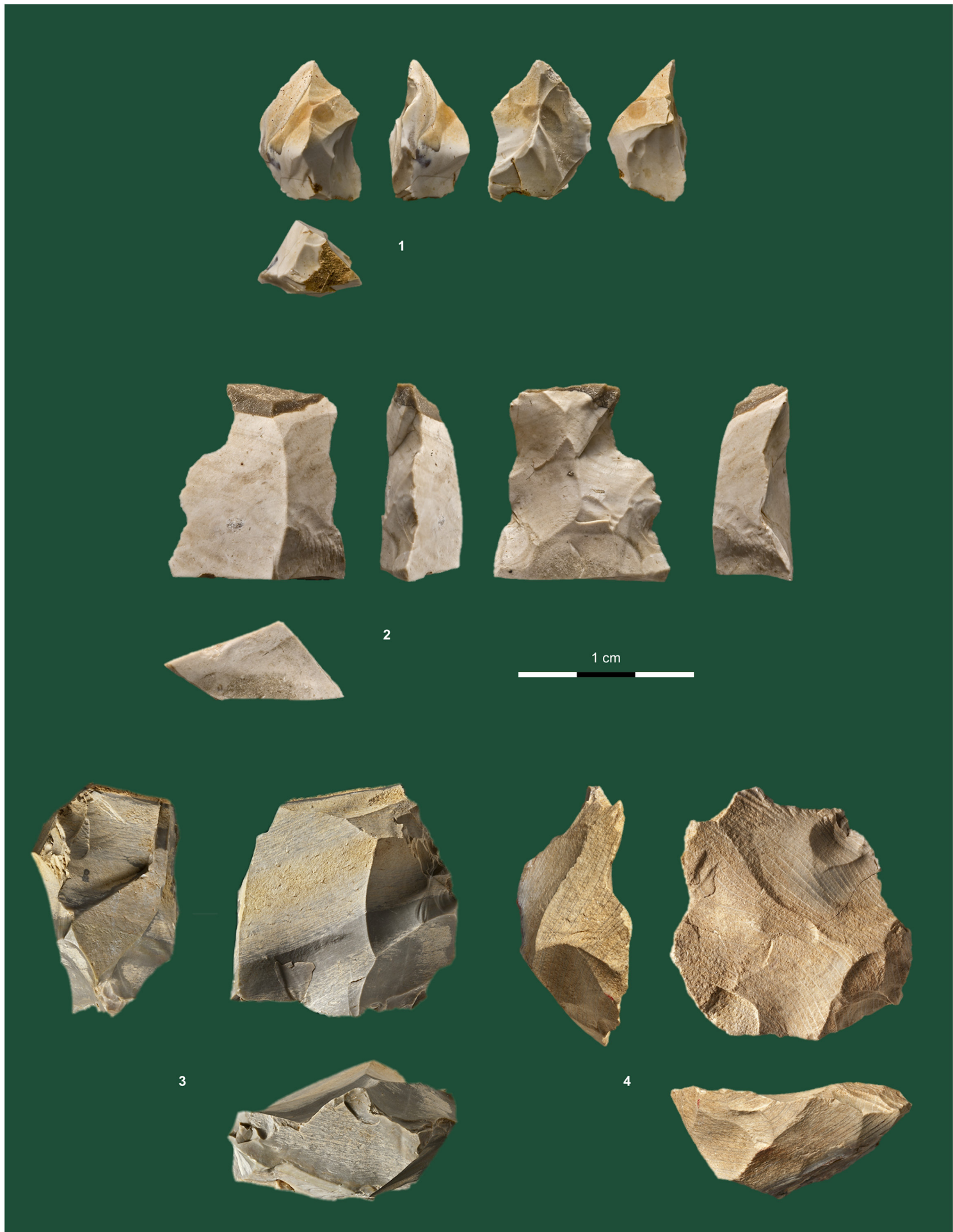
Fig. S35. Flint cores. 1. Fragment (units IH2-IH3). **2.** Core on flake (unit IT0). **3.** Levallois core (units IH2-IH3). **4.** Levallois core (unit IH4).

Fig. S36. Flint tools. 1. Denticulate (unit IH8). **2.** Denticulate (units IH2-IH3). **3.** Sidescraper (unit IH4). **4.** Preferential Levallois laminary flake (unit IH4). **5.** Preferential Levallois laminary flake (unit IH6) **6.** Notch (units IH2-IH3).
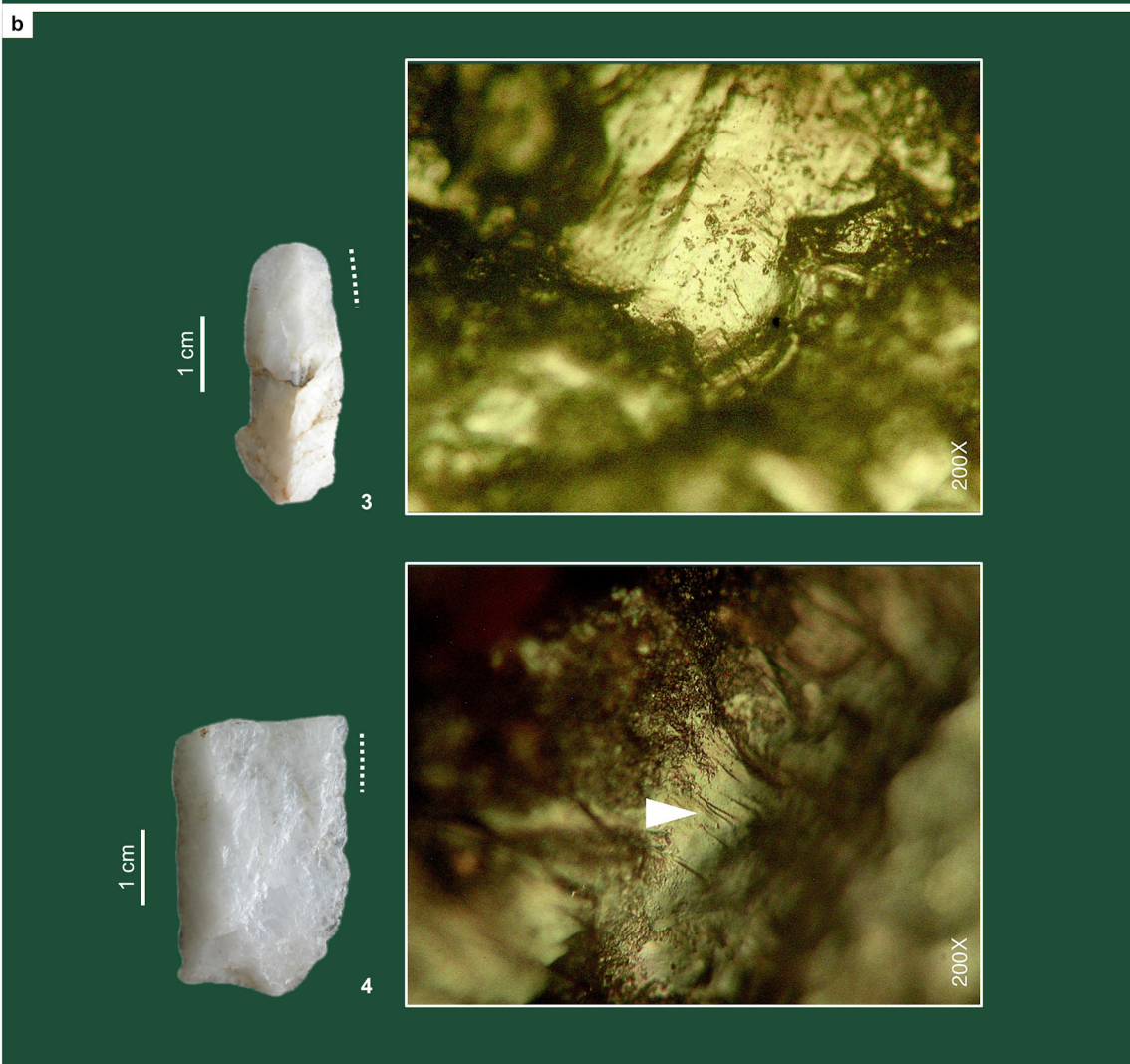
Fig. S37. Quartz tools. a. Examples made on coarser-grained varieties b. Use-wear on finer-grained blanks. 1. Core (units IH2-IH3). 2. Notched piece (units IH2-IH3). 3. Unretouched bladelet used to cut animal-soft material (unit IH6); 4. Retouched laminary flake/blade used to scrape a hard material (unit IH6). The white arrow points to parallel micro-striations typical of the motion involved.

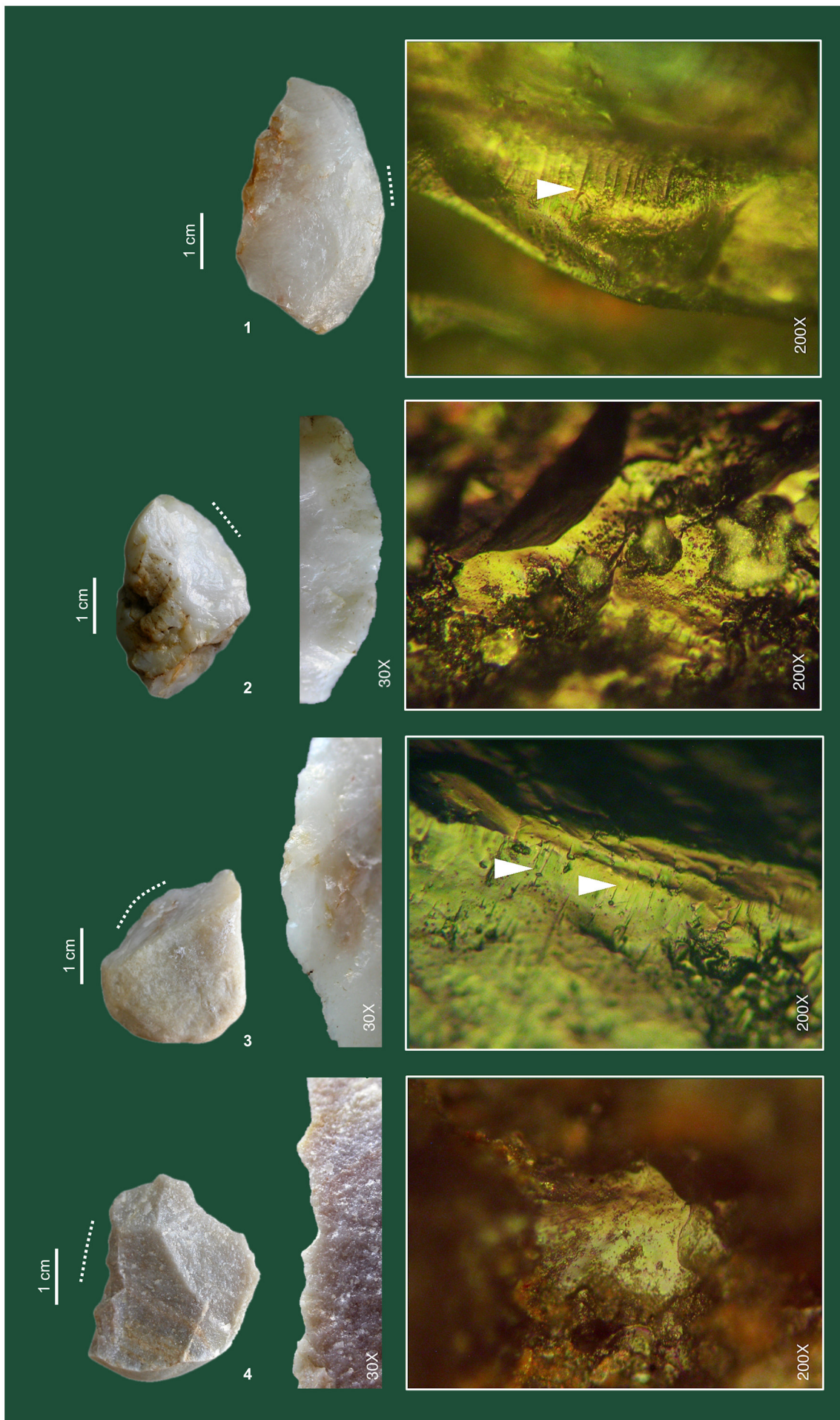**Fig. S38. Use-wear on quartz tools. 1**. Scraper used to scrape wood. **2-4.** Unretouched flakes used to cut wood. The arrows point to parallel micro-striations typical of the motions involved. **1.** unit IL3; **2.** unit IH4; **3-4.** units IH2-IH3.
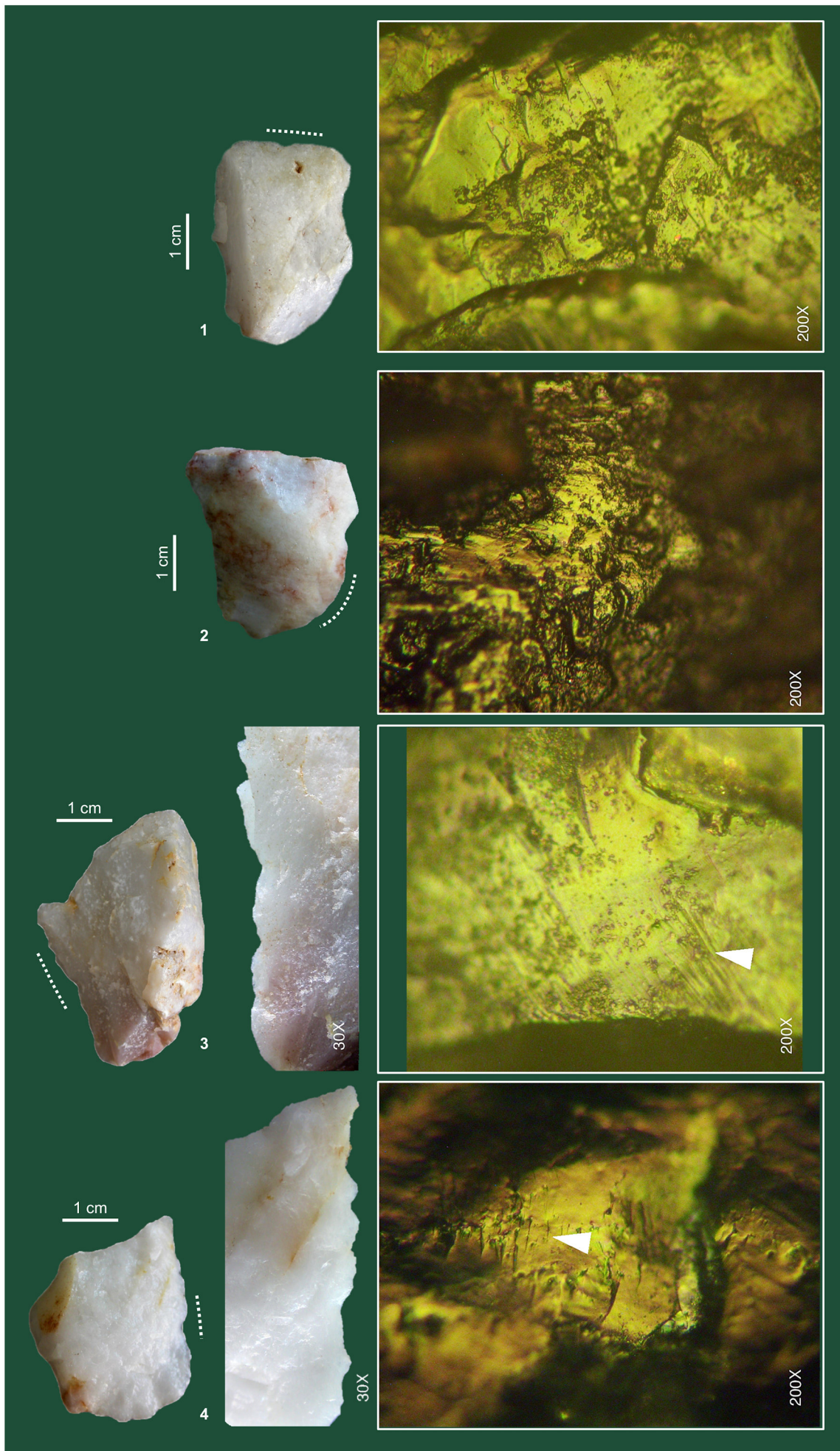
Fig. S39. Use-wear on quartz tools. 1. Nucleiform piece used to scrape a hard material. **2**. Denticulate used on a hard material in cutting motion. **3-4.** Denticulates used to scrape wood. The arrows point to parallel micro-striations typical of the motions involved. **1.** unit IH6; **2.** unit IH4; **3-4.** unit IH6.

Fig. S40. Sedimentary microfacies of shell-rich archeological deposits. Figueira Brava compared to the Late Mesolithic shell-midden of Cabeço da Amoreira (Muge, Tagus valley). The FB1002 thin section displays a succession of the 1b (interconnected shells with calcitic matrix), 3 (horizontally oriented components), and 2a (heterogeneous coarse sands and shells) microfacies (mF) as defined in the Mesolithic shell-midden..

114

Pinnacle Point 13B: MB-04-3A (XPL) Truncation Fill (MIS 3)

0.5 mm

Pinnacle Point 13B: MB-04-3B (XPL) Shelly Brown Sand (MIS 5c)

0.5 mm

Figueira Brava: FB1002-01 (XPL) unit MC5 (MIS 5c)

0.5 mm

Pinnacle Point 5-6: Shelly Ashy Brown Sand (MIS 5a)

1 mm

Figueira Brava: TS FB1002 (PPL scan) unit MC5 (MIS 5c)

1 mm

1 cm

Pinnacle Point 5-6: Shelly Ashy Brown Sand
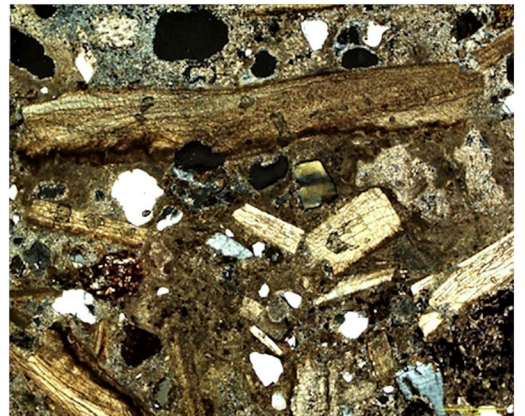
Figueira Brava: Entrance 3, Cut E (units MC4-MC5)
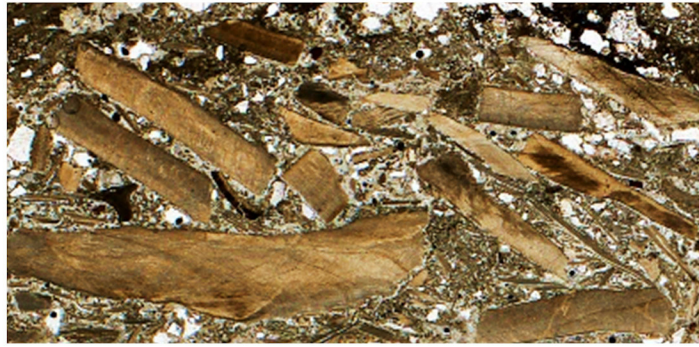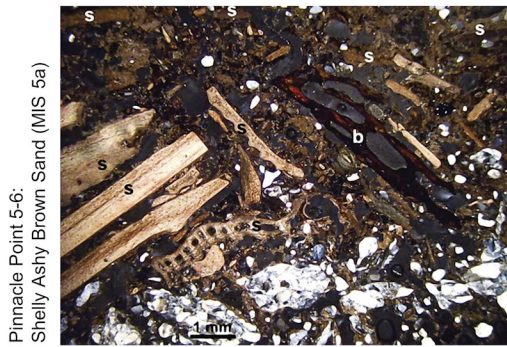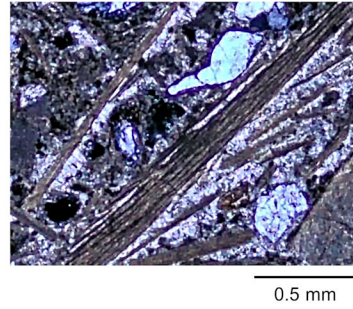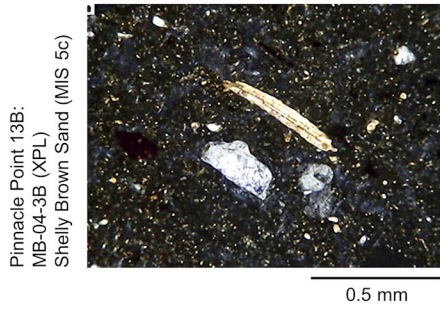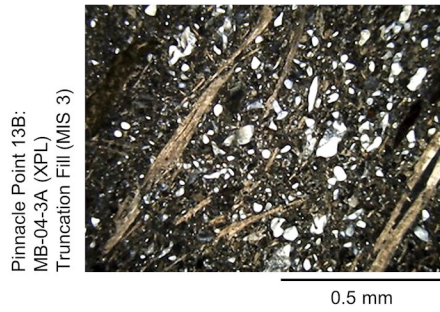
Fig. S41. Sedimentary microfacies of shell-rich archeological deposits. Top. Figueira Brava compared to Pinnacle Point 13B on thin-section microphotographs showing the density of shell in the groundmass. **Middle and Bottom.** Figueira Brava compared to the Shelly Ashy Brown Sand stratigraphic aggregate of Pinnacle Point 5-6, of MIS 5a age, using thin-section microphotographs that show the shell-supported nature of accumulation lenses and macrophotographs of sectioned stratigraphic exposures (jacketed in plaster, then resinated and sliced by diamond saw in the Pinnacle Point 5-6 case; raw surface, as cut in the field, in the Figueira Brava case) that show the alternation between shell-rich and shell-poor lenses

115
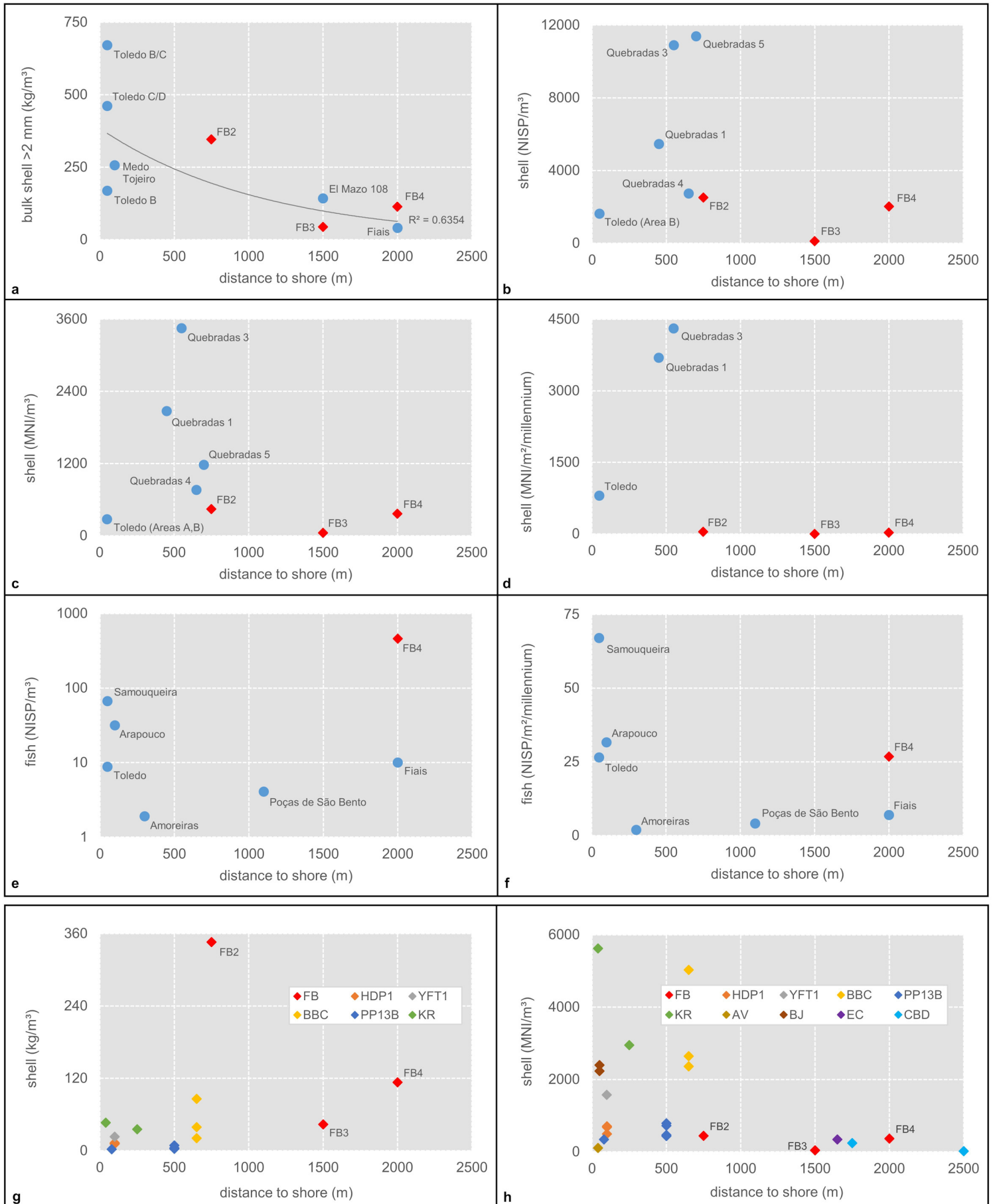
Fig. S42. Density of fish and marine invertebrate remains at Mesolithic and Last Interglacial sites of Iberia, the Maghreb and South Africa. Plot of the density proxies in Table S42 against distance to shore for Figueira Brava, the Mesolithic (**a-f**), and the Last Interglacial (**g-h**) sites. When Blombos is excluded, the R² for the exponential distribution seen in **h** is 0.4595. Site acronyms: FB = Figueira Brava; HDP1 = Hoedjiespunt 1; YFT1 = Ysterfontein 1 (average); BBC = Blombos; PP13B = Pinnacle Point 13B; KR = Klasies River; AV = Aviones; BJ = Bajondillo; EC = El Cuco; CBD = Contrebandiers.

Supplementary Tables

Table S1. Radiocarbon dating. Sample provenience

Collection	Lab #	Sample #	Species	Spatial provenience	Stratigraphic position
Area C					
17/09/1987	OxA-19978	FigBrav 1	*Patella depressa*	Area C, 8.6-12.6 m to datum	Layer 2
18/09/1987	OxA-19979	FigBrav 2	*Patella vulgata*	Area C, 4.6-6.6 m to datum	Layer 2, 60 cm below 1st bone bed
1988	OxA-19980	FigBrav 4	*Patella vulgata*	–	Layer 2
17/09/1987	OxA-19981	FigBrav 5	*Patella vulgata*	Area C, 4.6-6.6 m to datum	Layer 2
17/09/1987	OxA-19982	FigBrav 6	*Patella vulgata*	Area C, 6.6-8.6 m to datum	Layer 2
Area F					
23/07/2010	OxA-24055	FB1030a	*Patella vulgata*	grid unit T9, SW quadrate	spit A1, unit IT0
10/05/2013	OS-114170	FB-2013-234	*Littorina obtusata*	grid unit T9, SW quadrate	spit A1, unit IT0
Entrance 3					
20/07/2010	OxA-24051	FB1011	*Patella* sp.	Entrance 3, Cut D	unit MC2, 6.705 m asl
20/07/2010	OxA-24052	FB1012	*Patella vulgata*	Entrance 3, Cut D	unit MC2, 6.576 m asl
20/07/2010	OxA-24053	FB1023	*Glycymeris* sp.	Entrance 3, Cut G	unit MC2, 5.914 m asl
20/07/2010	OxA-24054	FB1024a	*Glycymeris* sp.	Entrance 3, Cut F	unit MC2, 5.784 m asl
20/07/2010	OxA-X-2446-7	FB1024b	*Mytilus* sp.	Entrance 3, Cut F	unit MC2, 5.784 m asl
20/07/2010	OxA-24050	FB1003	*Patella* sp.	Entrance 3, Cut E	unit MC3, 5.464 m asl
20/07/2010	OxA-X-2442-10	FB1004	*Mytilus* sp.	Entrance 3, Cut G	unit LC1, 4.918 m asl

Table S2. Radiocarbon dating. Age of the dated samples (a)

Lab #	Used	Yield	%Yld	%C	δ^{13}C (‰)	Date BP	Observations
Area C							
OxA-19978	29.8	3.3	10.9	94.6	2.8	2677±28	complete
OxA-19979	30.9	3.4	11.0	99.9	2.0	36420±240	top missing
OxA-19980	31.7	3.1	9.6	91.5	1.0	39750±400	complete
OxA-19981	27.7	3.1	11.1	94.5	1.5	40380±340	almost complete, broken in 3 pieces, hole on the top
OxA-19982	30.0	3.3	11.1	95.6	1.0	44900±500	almost complete, broken in 3 pieces, hole on the top
Area F							
OxA-24055	46.0	4.5	9.8	99.6	-0.5	12880±45	almost complete, minor edge break
OS-114170	–	–	–	–	-6.9	7390±25	perforated
Entrance 3							
OxA-24051	55.0	7.5	13.6	95.0	1.6	44050±450	complete, in rock-grade breccia
OxA-24052	53.0	5.4	10.2	107.3	1.4	41890±360	complete, in rock-grade breccia
OxA-24053	62.9	6.4	10.2	99.9	0.3	23120±90	small ventral margin fragment, in rock-grade breccia
OxA-24054	59.0	6.4	10.8	111.9	0.2	36530±230	large valve fragment, in rock-grade breccia
OxA-X-2446-7	32.3	3.3	10.2	92.3	0.5	32250±180	small valve fragment, in rock-grade breccia
OxA-24050	49.0	4.3	8.8	96.8	1.3	36420±230	broken, in rock-grade breccia
OxA-X-2442-10	85.9	9.4	10.9	97.5	-1.9	13720±50	valve fragments, in rock-grade breccia

(a) yield and amount of sample used are in mg; the quoted **δ^{13}C** values are measured independently on a stable isotope mass spectrometer

Table S3. U-series dating. Sample provenience (a)

Collection	Field #	Sample #	Square	Stratigraphy	x	y	z	Description
Area C								
22/07/2010		FB-1025		Surface			6.36	Capping flowstone, SE side
27/05/2011		FB-1107		Surface				Capping flowstone, NW side
Area E								
08/05/2012		FB-1200		Surface				Active stalagmite
Area F								
04/05/2011		FB-1101		Surface				Stalagmite (base missing)
04/05/2011		FB-1102		Surface				Stalagmite (base missing)
04/05/2011		FB-1103		Surface				Stalagmite (base missing)
04/05/2011		FB-1104		Surface				Stalagmite (base missing)
04/05/2011		FB-1105		Surface				Stalagmite (base missing)
10/05/2013	2013-229	FB-1303	T9	Surface	71	73	7.50	Stalagmite with its base of capping flowstone
10/05/2013	2013-245	FB-1304	T9	Surface	60	50	7.47	Stalagmite with its base of capping flowstone
23/05/2013	2013-825	FB-1305	S9	Surface	90	90	7.46	Stalagmite with its base of capping flowstone
10/05/2012	2012-13	FB-1207	T8	Surface	5	25	7.46	Stalagmite with its base of capping flowstone
22/07/2010		FB-1028	T9SW	Surface			7.42	Capping flowstone
15/05/2012	2012-225	FB-1208	T8	IH5	56	60	7.09	Stalagmite, *in situ* at the IH4/IH6 stratigraphic interface
20/05/2011	2011-330	FB-1106	U8	IH7	37	42	6.97	Stalagmite, tumbled, grown over encrusted surface of IH8
08/05/2013	2013-46	FB-1301	T7	IH8	37	23	6.95	Stalagmite, grown within IH8
08/05/2013	2013-95	FB-1302	T7	IH8	38	51	6.91	Stalagmite, grown within IH8
21/05/2012	2012-497	FB-1209	T8	IL1	15	30	6.87	Stalagmite, *in situ* at IH8/IL2 stratigraphic interface
30/05/2013	2013-1021	FB-1306	T8	IB1	40	0	6.60	Flowstone at stratigraphic IL3/IB2 stratigraphic interface
Entrance 2								
01/11/2014		FB-1406		Surface				Flowstone adhering to roof, inside the extant overhang
01/11/2014		FB-1407		Surface				Flowstone above wall next to seaward scarp
Entrance 3								
01/11/2014		FB-1401		Surface				Outer layer of stal capping fill between Entrances 2 and 3
01/11/2014		FB-1402		Surface				Outer layer of stal capping fill between Entrances 2 and 3
01/11/2014		FB-1405		Surface				Flowstone adhering to roof, inside the extant overhang
22/07/2010		FB-1026		Surface			7.99	Capping flowstone in Cut A
01/11/2014		FB-1404		Surface				Column against north wall, over disconnected remnant
01/11/2014		FB-1403		Surface				Stalagmite on bedrock, in seaward escarpment
22/07/2010		FB-1027		UC or MC			6.77	Stalagmite base of column hanging above Cut F
22/07/2010		FB-1029		↔ IB1				Bedrock-to-roof column between Area F and Entrance 3

(a) (x,y) are intra-grid unit coordinates, in cm; z are elevations asl, in m; for stalagmites, the elevation of the base is given.

Table S4. U-series dating. Age of interior speleothems capping the excavated deposit

FB sample	Lab #	^{238}U (ng/g)	^{232}Th (ng/g)	[^{230}Th/^{232}Th] activity ratio	(^{230}Th/^{238}U) activity ratio	(^{234}U/^{238}U) activity ratio	age (ka) uncorrected	age (ka) corrected	(^{234}U/^{238}U)$_{initial}$ activity ratio corrected	Stratigraphic significance
AREA C										
1025-9 (top)	UEVA 1737	46.566±0.920	3.225±0.065	12.711±0.229	0.288±0.005	1.358±0.008	25.752±0.569	24.308±0.873	1.391±0.009	Samples from the flowstone capping the Area C Pleistocene deposit, for which FB1025-1 provides a minimum age of 51.6 ka.
1025-1 (base)	UEVA 1731	71.601±0.719	0.138±0.002	663.645±7.707	0.419±0.004	1.096±0.004	52.244±0.618	52.194±0.618	1.111±0.005	
1107-1 (top)	UTO 436	42.044±0.516	4.962±0.105	7.638±0.421	0.295±0.019	1.270±0.011	28.590±2.085	25.945±2.428	1.299±0.013	
1107-2 (base)	UTO 437	65.200±0.570	2.248±0.034	43.441±0.740	0.490±0.009	1.277±0.006	51.872±1.195	51.123±1.236	1.322±0.007	
AREA F										
1028-2 (middle)	UTO 209	38.950±0.152	1.794±0.017	31.300±0.407	0.472±0.006	1.124±0.003	58.750±0.947	57.595±1.085	1.148±0.004	Samples from stalagmites and flowstone capping the Area F Pleistocene deposit, for which FB1207-6 implies a minimum age of 76.9 ka. Based on the lower limit of the range for sub-sample 1304-3, FB1304 provides a maximum age of 16.6 ka for the IT2 black lens, which laterally abutted (and, in certain areas, infiltrated) it.
1028-1 (base)	UTO 208	53.584±0.217	1.200±0.013	67.595±1.026	0.495±0.008	1.142±0.004	61.218±1.284	60.669±1.308	1.170±0.005	
1101-2 (top)	UTO 428	56.328±0.521	1.108±0.035	96.456±1.599	0.621±0.010	1.315±0.008	67.718±1.595	63.653±2.261	1.397±0.014	
1101-1 (base)	UTO 427	151.260±1.256	1.152±0.023	244.94±2.679	0.611±0.005	1.309±0.005	66.643±0.776	66.484±0.778	1.373±0.005	
1102-1 (top)	UTO 431	58.431±0.677	0.851±0.037	88.515±1.697	0.422±0.010	1.185±0.010	47.461±1.538	47.117±1.545	1.212±0.012	
1102-2 (base)	UTO 432	90.395±0.910	1.112±0.018	133.976±1.353	0.539±0.004	1.155±0.006	67.591±0.889	67.294±0.897	1.188±0.007	
1103-1 (top)	UTO 770	49.593±0.558	0.625±0.007	61.634±0.991	0.254±0.004	1.089±0.004	28.902±0.577	28.574±0.599	1.097±0.005	
1103-2 (base)	UTO 771	56.630±0.585	1.582±0.017	44.876±0.444	0.410±0.004	1.061±0.004	53.076±0.738	52.329±0.821	1.071±0.005	
1104-2 (top)	UTO 426	54.604±0.412	0.360±0.022	270.211±5.000	0.582±0.007	1.317±0.008	61.990±1.040	61.853±1.041	1.379±0.009	
1104-1 (base)	UTO 425	119.288±1.171	0.466±0.029	477.932±6.519	0.610±0.006	1.332±0.006	64.953±0.957	64.873±0.957	1.400±0.007	
1105-1 (top)	UTO-433	206.102±2.013	17.152±0.264	3.431±0.061	0.089±0.002	1.251±0.004	8.047±0.149	6.226±0.918	1.261±0.005	
1105-3 (base)	UEVA 417	107.624±1.160	0.103±0.005	1859.035±35.562	0.582±0.008	1.303±0.004	62.911±1.240	62.890±1.240	1.362±0.005	
1207-4 (middle)	UTO 777	64.908±1.057	2.990±0.056	26.516±0.380	0.400±0.006	1.093±0.005	49.357±0.923	48.162±1.084	1.108±0.006	
1207-6 (base)	UTO 776	89.406±1.246	14.821±0.217	11.124±0.134	0.603±0.008	1.115±0.004	83.615±1.665	79.400±2.511	1.150±0.006	
1303-3 (top)	UEVA 1390	59.848±0.516	0.123±0.002	626.607±7.472	0.423±0.003	1.147±0.003	49.658±0.526	49.608±0.526	1.169±0.004	
1303-1 (bottom)	UEVA 1384	51.535±0.585	0.966±0.012	80.562±0.807	0.494±0.005	1.165±0.005	59.302±0.839	58.851±0.862	1.196±0.006	
1304-5 (IT1top)	UEVA 1724	70.797±1.517	18.630±0.435	2.574±0.044	0.222±0.004	1.120±0.005	23.981±0.496	17.072±3.530	1.135±0.008	
1304-4 (IT1base)	UEVA 1723	138.890±3.062	38.471±0.876	2.458±0.043	0.223±0.004	1.140±0.004	23.631±0.452	16.487±3.637	1.159±0.008	
1304-3 (IH1top)	dlh 1211	53.535±0.787	2.789±0.048	9.595±0.296	0.164±0.005	1.126±0.005	17.086±0.566	15.764±0.863	1.134±0.006	
1304-1 (IH1base)	dlh 1029	38.282±0.352	0.292±0.004	105.342±2.224	0.262±0.005	1.116±0.007	29.134±0.724	28.941±0.730	1.126±0.007	
1305-9 (top)	dlh 1213	141.523±1.446	0.367±0.006	553.674±6.631	0.470±0.003	1.161±0.003	55.862±0.551	55.800±0.552	1.189±0.003	
1305-1 (base)	dlh 1212	92.973±0.584	0.846±0.009	181.723±1.899	0.541±0.005	1.136±0.003	69.455±0.921	69.232±0.926	1.166±0.004	

Table S5. U-series dating. Age of Area F interstratified speleothems (except for 1106-2 to -6, sub-samples are in internal order, from top to bottom)

FB sample	Lab #	^{238}U (ng/g)	^{232}Th (ng/g)	[^{230}Th/^{232}Th] activity ratio	(^{230}Th/^{238}U) activity ratio	(^{234}U/^{238}U) activity ratio	age (ka) uncorrected	age (ka) corrected	(^{234}U/^{238}U)$_{initial}$ activity ratio corrected	Stratigraphic significance
1208-5	UEVA 1729	230.459±2.088	10.130±0.082	46.090±0.164	0.663±0.003	1.171±0.003	88.731±0.637	87.693±0.762	1.222±0.003	Corresponds to unit IH5, an episode of calcite precipitation for which sub-samples 1208-5 and 1208-1 provide, respectively, minimum and maximum ages.
1208-4	UEVA 1728	212.152±1.920	1.501±0.014	283.705±1.698	0.657±0.003	1.165±0.003	88.304±0.739	88.137±0.742	1.212±0.003	
1208-3	UEVA 1727	243.392±1.740	3.310±0.025	148.937±0.533	0.663±0.003	1.176±0.003	88.116±0.636	87.797±0.649	1.226±0.003	
1208-2	UEVA 1726	247.903±1.390	10.308±0.056	49.068±0.130	0.668±0.002	1.170±0.002	89.907±0.563	88.924±0.688	1.221±0.003	
1208-1	UEVA 1725	230.340±1.759	1.913±0.016	240.840±1.293	0.654±0.003	1.165±0.002	87.756±0.621	87.559±0.626	1.212±0.003	
1106-2 (top)	dlh 1326	101.762±1.350	4.205±0.066	48.776±0.504	0.659±0.006	1.150±0.007	90.759±1.594	89.766±1.643	1.196±0.009	Corresponds to unit IH7, an episode of calcite precipitation for which the isochron date and sub-sample 1106-1 provide, respectively, minimum and maximum ages.
1106-3 (top)	dlh 1327	136.272±1.812	4.409±0.066	61.644±0.523	0.653±0.005	1.154±0.005	88.818±1.197	88.044±1.237	1.199±0.006	
1106-4 (top)	dlh 1328	158.441±2.081	1.752±0.025	177.730±1.643	0.643±0.005	1.153±0.004	87.029±1.073	86.765±1.078	1.196±0.005	
1106-5 (top)	dlh 1329	112.964±1.836	16.399±0.274	14.472±0.165	0.687±0.008	1.148±0.004	97.118±1.813	93.590±2.320	1.200±0.007	
1106-6 (top)	dlh 1330	104.092±1.559	17.191±0.271	12.548±0.138	0.678±0.008	1.144±0.004	95.607±1.807	91.563±2.467	1.195±0.007	
1106-top isochron								87.000±1.600		
1106-1 (base)	dlh 1325	108.898±1.100	4.906±0.060	44.346±0.415	0.654±0.005	1.149±0.004	89.756±1.073	88.670±1.162	1.194±0.005	
1301-7	UEVA 1713	128.149±1.030	4.888±0.037	52.341±0.268	0.653±0.004	1.158±0.003	88.496±0.833	87.582±0.913	1.204±0.004	Formed during the deposition of unit IH8 (FB-1301 at a slightly higher elevation than FB-1302, in agreement with the results obtained).
1301-6	UEVA 1712	144.737±1.208	32.446±0.254	9.717±0.045	0.713±0.003	1.160±0.003	101.057±0.873	95.614±2.368	1.222±0.008	
1301-5	UEVA 1711	141.175±0.752	8.284±0.042	34.157±0.124	0.656±0.003	1.159±0.002	88.851±0.651	87.444±0.870	1.207±0.003	
1301-4	UEVA 1710	133.128±0.787	18.809±0.110	14.545±0.055	0.672±0.003	1.153±0.002	93.074±0.726	89.641±1.592	1.205±0.005	
1301-3	UEVA 1709	118.631±0.911	13.077±0.101	18.498±0.116	0.667±0.004	1.160±0.003	91.128±0.969	88.475±1.457	1.211±0.005	
1301-2	UEVA 1708	114.495±1.123	4.527±0.044	49.914±0.301	0.646±0.003	1.157±0.003	87.042±0.780	86.094±0.871	1.203±0.004	
1301-1	UEVA 1707	124.685±1.027	5.287±0.047	46.804±0.254	0.649±0.004	1.154±0.003	88.215±0.885	87.194±0.979	1.199±0.004	
1302-3	UEVA 1705	66.016±0.635	18.838±0.180	7.214±0.069	0.674±0.006	1.131±0.004	96.483±1.528	89.260±3.459	1.183±0.009	
1302-2	UEVA 1704	63.279±0.444	6.997±0.050	18.096±0.115	0.655±0.004	1.122±0.004	93.589±1.115	90.818±1.625	1.163±0.005	
1302-1	UEVA 1703	66.419±0.405	5.547±0.032	23.721±0.145	0.648±0.005	1.120±0.004	92.435±1.120	90.343±1.432	1.159±0.005	
1209-3	UEVA 1389	68.814±1.761	20.145±0.552	7.129±0.087	0.683±0.009	1.111±0.006	101.908±2.431	94.326±4.102	1.157±0.011	Corresponds to unit IL1 and is a stalagmite for which sub-samples 1209-3 and -4 provide a minimum age and sub-sample 1209-5 provides a maximum age.
1209-4	UEVA 1701	104.913±1.115	2.314±0.025	88.660±0.572	0.640±0.004	1.114±0.003	91.428±0.939	90.875±0.968	1.149±0.004	
1209-5	UEVA 1702	89.507±1.039	1.433±0.017	123.236±1.007	0.646±0.004	1.116±0.004	92.512±1.122	92.113±1.134	1.151±0.005	
1306-1 (top)	dlh 1206	46.186±0.998	1.370±0.028	66.938±1.258	0.650±0.013	1.029±0.008	108.178±3.913	107.361±3.929	1.040±0.010	Corresponds to unit IB1, an episode of flowstone formation constrained by sub-samples 1306-1 (minimum age) and 1306-2 (maximum age).
1306-3 (basal)	dlh 1208	74.724±0.302	1.382±0.008	126.710±0.616	0.767±0.004	1.046±0.002	142.009±1.573	141.513±1.588	1.068±0.003	
1306-2 (bottom)	dlh 1207	65.085±0.237	1.234±0.008	125.927±0.725	0.781±0.004	1.037±0.003	150.683±2.060	150.169±2.072	1.057±0.004	

Table S6. U-series dating. Age of exterior speleothems (except for 1026 and 1027, sub-samples are in internal order, from top to bottom)

FB sample	Lab #	^{238}U (ng/g)	^{232}Th (ng/g)	[^{230}Th/^{232}Th] activity ratio	(^{230}Th/^{238}U) activity ratio	(^{234}U/^{238}U) activity ratio	age (ka) uncorrected	age (ka) corrected	(^{234}U/^{238}U)$_{initial}$ activity ratio corrected	Stratigraphic significance
ENTRANCE 2										
1406-4 (top)	UEVA 993	73.300±0.490	0.828±0.007	91.538±0.838	0.338±0.003	1.076±0.003	41.041±0.475	40.742±0.496	1.086±0.004	Both document flowstone formation across the whole area, with sub-sample 1406-1 providing a minimum age of 45.0 ka for the underlying, eroded sedimentary fill.
1406-1 (base)	UEVA 990	66.177±0.333	2.233±0.018	33.864±0.289	0.374±0.003	1.073±0.003	46.546±0.434	45.649±0.613	1.084±0.003	
1407-5 (top)	UEVA 1025	259.603±3.946	165.578±2.464	1.736±0.017	0.362±0.004	1.055±0.003	45.719±0.580	26.965±10.083	1.072±0.009	
1407-1 (base)	UEVA 1021	232.757±4.937	479.017±9.105	1.187±0.008	0.799±0.006	1.042±0.003	156.316±2.712	78.212±52.273	1.114±0.073	
ENTRANCE 3										
1026-1a	UEVA 1823	98.041±1.028	44.350±0.517	3.455±0.033	0.511±0.005	1.080±0.004	69.366±0.994	56.835±6.317	1.107±0.009	All three samples document flowstone formation across the whole area, with sub-sample 1402-1 providing a minimum age of 57.3 ka for the underlying, eroded sedimentary fill. The sub-samples from sample 1026 are for a single calcite lamina from the flowstone (unit UC1) capping a remnant of the UC complex.
1026-1b	UEVA 1824	93.800±1.060	36.913±0.443	4.008±0.036	0.516±0.005	1.079±0.004	70.349±0.990	59.524±5.425	1.104±0.008	
1026-1c	UEVA 1825	92.173±0.746	40.841±0.301	3.671±0.026	0.532±0.004	1.079±0.003	73.435±0.889	61.180±6.123	1.107±0.009	
1402-1	UEVA 1051	127.559±2.117	39.643±0.651	4.950±0.044	0.503±0.005	1.053±0.004	70.533±1.095	61.816±4.478	1.068±0.006	
1402-2	UEVA 1052	141.162±2.274	68.565±1.007	3.370±0.029	0.536±0.005	1.050±0.003	77.336±1.102	63.355±7.217	1.069±0.008	
1405-1 (top)	UEVA 987	111.902±0.549	130.384±0.621	1.604±0.008	0.611±0.003	1.180±0.002	77.887±0.641	46.184±16.162	1.296±0.065	
1405-3 (base)	UEVA 989	127.274±0.937	125.164±0.950	1.804±0.011	0.581±0.004	1.179±0.003	72.549±0.702	46.360±13.105	1.275±0.048	
1027-1	UTO 264	281.174±2.312	88.986±0.694	6.216±0.026	0.644±0.004	1.158±0.005	86.477±0.926	78.666±3.482	1.216±0.011	Dates a single calcite lamina taken along the outer rind of a stalagmite hanging from the roof above the erosionally truncated sedimentary fill. The isochron date provides a minimum age (75.0 ka) for the underlying sequence and a maximum age (87.0 ka) for the deposition of the sediments of the UC complex that eventually buried the speleothem.
1027-2	UTO 265	238.563±1.982	197.502±1.239	2.691±0.015	0.729±0.006	1.155±0.008	105.566±1.970	83.866±9.771	1.251±0.036	
1027-3	UTO 266	385.360±2.146	63.082±0.355	12.073±0.037	0.647±0.002	1.169±0.002	85.773±0.533	81.850±1.717	1.223±0.006	
1027-4	UEVA 1821	340.652±2.503	121.004±0.887	5.793±0.020	0.673±0.003	1.174±0.002	90.511±0.663	81.841±3.697	1.242±0.013	
1027-5	UEVA 1822	266.495±2.469	101.267±0.943	5.515±0.025	0.686±0.004	1.169±0.002	93.786±0.804	84.445±3.997	1.238±0.013	
1027 isochron								81.000±6.000		
1029-2	UEVA 1820	90.896±1.262	12.761±0.184	13.544±0.111	0.622±0.006	1.050±0.004	97.005±1.544	93.162±2.382	1.068±0.006	From the rind of the column separating Area F from Entrance 3, constrains the deposition of the UC complex to <91.0 ka
1029-1	UEVA 1819	77.699±1.260	3.164±0.054	44.931±0.367	0.599±0.005	1.055±0.005	90.669±1.300	89.573±1.395	1.071±0.006	

Table S7. Luminescence dating. Single-aliquot regenerative-dose (SAR) procedures used for dose-recovery measurements and D_e determination. Each of these SAR measurement cycles was repeated for the natural dose, 5 different sized regenerative doses and a 0 Gy regenerative-dose (to measure OSL signal recuperation). Both the smallest and largest non-zero regenerative-dose cycles were repeated at the end of the SAR procedure to assess the suitability of the test-dose sensitivity correction. In the case of the single-grain OSL SAR procedure, the smallest regenerative-dose cycle was also repeated a second time with the inclusion of step 2 to check for the presence of feldspar contaminants using the OSL IR depletion ratio of Duller (*188*). L_x = regenerative dose signal response; L_n = natural dose signal response; T_x = test dose signal response for a laboratory dose cycle T_n = test dose signal response for the natural dose cycle

Multi-grain aliquot OSL SAR procedure

Step	Treatment	Symbol
1	Dose (Natural or laboratory)	N or D
2	IRSL stimulation (50°C for 60 s)	–
3	Preheat 1 (x°C for 10 s)	PH_1
4	OSL stimulation (125ºC for 60 s)	L_n or L_x
5	Test dose (20 Gy)	T_d
6	IRSL stimulation (50ºC for 60 s)	–
7	Preheat 2 (x°C for 10 s)	PH_2
8	OSL stimulation (125°C for 60 s)	T_n or T_x
9	Repeat measurement cycle for different sized regenerative doses	–

Single-grain OSL SAR procedure

Step	Treatment	Symbol
1	Dose (Natural or laboratory)	N or D
2[a]	IRSL stimulation (50°C for 60 s)	–
3	Preheat 1 (x°C for 10 s)	PH_1
4	Single-grain OSL stimulation (125°C for 2 s)	L_n or L_x
5	Test dose (20 Gy)	T_d
6	Preheat 2 (x°C for 10 s)	PH_2
7	Single-grain OSL stimulation (125°C for 2 s)	T_n or T_x
8	Repeat measurement cycle for different sized regenerative doses	–

[a] Step 2 is only included in the single-grain SAR procedure when measuring the OSL IR depletion ratio (*188*).

Table S8. Luminescence dating. Single-grain OSL classification statistics. The proportion of grains that were rejected from final D_e estimation after applying the various SAR quality assurance criteria are shown in rows 5-13. The quality assurance criteria were applied to each single-grain measurement in the order shown in the left-hand column. T_n = natural test dose signal response; L_n/T_n = sensitivity-corrected natural signal response; L_x/T_x = sensitivity-corrected regenerative-dose signal response. DRT = dose-recovery test.

	12-5		12-6		12-3		12-2		12-1		12-1 DRT		12-4	
	n	%	*n*	%	*n*	%	*n*	%	*n*	%	*n*	%	*n*	%
Total measured grains	1100	100	900	100	1300	100	1900	100	1400	100	600	100	1200	100
SAR rejection criteria:														
1. T_n <3σ background	549	50	469	52	542	42	1199	63	850	60	367	61	706	58
2. Low-dose recycling ratio ≠ 1 at ±2σ	168	15	108	12	211	16	155	8	134	10	55	9	116	10
3. High-dose recycling ratio ≠ 1 at ±2σ	86	8	50	6	107	8	84	4	67	5	12	2	58	5
4. OSL-IR depletion ratios <1 at ±2σ	44	4	42	5	57	4	131	7	80	6	43	7	73	6
5. 0 Gy L_x/T_x >5% L_n/T_n	17	2	11	1	34	3	15	1	11	1	10	2	11	1
6. Non-intersecting grains [a]	10	1	8	1	7	1	15	1	10	1	6	1	8	1
7. Saturated grains [b]	10	1	14	1	2	–	18	1	19	–	10	2	14	1
8. Extrapolated grains [c]	–	–	–	–	11	1	2	–	–	1	0	–	1	–
9. Anomalous dose response / unable to perform Monte Carlo fit [d]	93	8	99	11	89	7	171	9	121	8	37	6	94	8
Sum of rejected grains	977	89	801	89	1060	82	1790	94	1292	92	540	90	1081	90
Sum of accepted grains	123	11	99	11	240	18	110	6	108	8	60	10	119	10

[a] L_n/T_n > the I_{max} saturation limit of the dose response curve at 2σ.

[b] L_n/T_n ≈ the I_{max} saturation limit of the dose response curve at 2σ.

[c] L_n/T_n values lying more than 2σ beyond the L_x/T_x value of the largest regenerative-dose administered in the SAR protocol.

[d] Includes grains displaying zero or negative response with increasing dose, and grains with very scattered L_x/T_x values that could not be fitted with the Monte Carlo D_e estimation procedure.

Table S9. Luminescence dating. Dose rate data, single-grain equivalent doses and quartz OSL ages

FB sample	Unit	Sample depth (cm)	Grain size (μm)	Water content [a]	Environmental dose rate (Gy/ka)				Equivalent dose (D$_e$) data				OSL age (ka) [g,l]
					Beta dose rate [b,c,d]	Gamma dose rate [d,e]	Cosmic dose rate [f]	Total dose rate [d,g,h]	No. of grains [i]	Over-dispersion (%) [j]	Age model [k]	D$_e$ (Gy) [g]	
Area F trench													
12-5	IH6	33	212-250	12±2	0.79±0.03	0.31±0.01	0.02±0.01	1.16±0.06	123/1100	17±2	CAM	110±2	95.0±5.3
12-6	IH6	34	212-250	14±3	0.61±0.03	0.34±0.02	0.02±0.01	1.01±0.05	99/900	14±2	CAM	94±2	93.9±5.6
Entrance 3 trench													
12-3	MC2	80	212-250	12±2	0.30±0.01	0.21±0.01	0.02±0.01	0.56±0.03	240/1300	32±2	MAM-4	55±2	97.8±6.0
Area C trench													
12-1	Layer 2	70	212-250	13±3	0.72±0.03	0.43±0.02	0.02±0.01	1.20±0.06	108/1400	28±3	MAM-3	104±6	86.1±6.8
12-2	Layer 2	55	212-250	13±3	1.22±0.05	0.55±0.02	0.02±0.01	1.83±0.09	110/1900	28±4	MAM-4	163±8	89.3±6.4
12-4	Layer 4	100	212-250	13±3	0.47±0.03	0.29±0.01	0.02±0.01	0.81±0.04	119/1200	39±3	MAM-3	89±4	110.2±8.3

[a] Long-term water content, expressed as % of dry mass of mineral fraction, with an assigned relative uncertainty of ±20%. Present-day water contents of samples FB12-5 and FB12-6 are taken to be representative of those prevailing throughout the sample burial periods, as the natural hydrological conditions remain undisturbed in the deeper, interior area of the cave. Long-term water contents of all other samples were calculated as being equivalent to 40% of the present-day saturated water values, based on proportional saturation assessments made on samples FB12-5 and FB12-6 from the deeper cave interior.

[b] Beta dose rates of all samples except FB12-4 were calculated on dried and powdered sediment samples using a Risø GM-25-5 low-level beta counter (*87*), after making allowance for beta dose attenuation due to grain-size effects and HF etching (*89*).

[c] Beta and gamma dose rates of sample FB12-4 were calculated from parental ^{238}U, ^{232}Th and ^{40}K concentrations determined using high-resolution gamma-ray spectrometry.

[d] Specific activities and radionuclide concentrations have been converted to dose rates using the conversion factors given in Guérin *et al.* (*97*), making allowance for beta-dose attenuation (*89, 98*).

[e] Gamma dose rates of all samples except FB12-4 were calculated from *in situ* measurements made at each sample position with a NaI:Tl detector, using the 'energy windows' approach (e.g., *86*).

[f] Cosmic-ray dose rates were calculated using the approach of Prescott and Hutton (1994) and assigned a relative uncertainty of ±10%.

[g] Mean ± total uncertainty (68% confidence interval), calculated as the quadratic sum of the random and systematic uncertainties.

[h] Includes an internal dose rate of 0.03 Gy/ka with an assigned relative uncertainty of ±30%, based on intrinsic ^{238}U and ^{232}Th contents published by Mejdahl (*92*), Bowler *et al.* (*93*), Jacobs *et al.* (*84*) and Pawley *et al.* (*94*), and an *a*-value of 0.04 ± 0.01 (*95, 96*).

[i] Number of D$_e$ measurements that passed the SAR rejection criteria and were used for D$_e$ determination / total number of grains analyzed.

[j] Relative spread in the D$_e$ dataset beyond that associated with the measurement uncertainties of individual D$_e$ values, calculated using the central age model (CAM) of Galbraith *et al.* (*124*).

[k] Age model used to calculate the sample-averaged D$_e$ value for each sample. MAM-3 = 3-parameter minimum age model of Galbraith *et al.* (*124*). MAM-4 = 4-parameter minimum age model of Galbraith *et al.* (*124*). MAM-3 and MAM-4 D$_e$ estimates were calculated after adding, in quadrature, a relative error of 15% to each individual D$_e$ measurement error to approximate the underlying dose overdispersion observed in 'ideal' (well-bleached and unmixed) sedimentary samples (e.g., FB12-5 and FB12-6; see also synthesis by Arnold and Roberts (*116*).

[l] Total uncertainty includes a systematic component of ±2% associated with laboratory beta-source calibration.

Table S10. Luminescence dating. High-resolution gamma spectrometry results and daughter-to-parent isotopic ratios for selected samples

FB sample	Unit	Sample depth (cm)	Radionuclide specific activities (Bq/kg) [a, b]						Beta dose rate (Gy / ka) [c, d]	Daughter: parent isotopic ratio		
			^{238}U	^{226}Ra	^{210}Pb	^{228}Ra	^{228}Th	^{40}K		^{226}Ra:^{238}U	^{210}Pb:^{226}Ra	^{228}Th:^{228}Ra
Area F trench												
12-5	IH6	33	25.9±2.2	23.3±0.5	23.1±0.6	11.9±0.4	10.7±0.9	282±10	0.82±0.04	0.90±0.08	0.99±0.03	0.90±0.08
Entrance 3 trench												
12-3	MC2	80	5.5±1.3	5.7±0.5	5.8±0.7	6.3±0.6	6.2±0.5	123±4	0.32±0.02	1.04±0.25	1.01±0.15	0.97±0.12
Area C trench												
12-1	Layer 2	70	15.3±1.6	17.4±0.4	17.2±0.5	9.8±0.4	9.8±0.2	281±10	0.73±0.03	1.13±0.12	0.99±0.04	1.00±0.05
12-4	Layer 4	100	14.9±2.9	12.6±1.1	13.0±1.2	8.2±0.8	7.3±0.6	162±6	0.47±0.03	0.85±0.18	1.03±0.13	0.88±0.11

[a] Measurements made on dried and powdered sediment sub-samples of ~120 g.

[b] Mean ± total uncertainty (68% confidence interval), calculated as the quadratic sum of the random and systematic uncertainties.

[c] Radionuclide concentrations and specific activities have been converted to dose rates using the conversion factors given in Guérin *et al.* (*97*).

[d] Beta dose rates are shown for comparison with the results obtained on the same bulk sediment samples using low-level beta counting (shown in Table S9). The beta dose rate estimates have been calculated for the 212-250 μm quartz fractions used for OSL dating, making allowance for beta dose attenuation due to sediment moisture content (see Table S9), grain-size effects and HF etching (*89, 98*).

Table S11. The 2010 geoarcheological work in Entrance 3. Stratigraphic provenience of the soil micromorphology samples

Sample	Cut A		Cut B				Cut C			Cut D				Cut F	Cut E		Cut G	
Field number	1009	1010	1008	1007	1005	1006	1018	1019	1020	1013	1014	1015	1016	1017	1001	1002	1022	1021
Stratigraphic unit	UC2	UC4	UC5		UC6		MC1	MC2							MC4	MC4-MC5	LC2	LC3

Table S12. Overall stratigraphic correlation scheme. Equivalence between excavation spits and stratigraphic units of the different areas, available dating evidence, position of the sequence in the global Pleistocene record (MIS = Marine Isotope Stage), and archeological phasing (a)

AREA C [layer]	U-Th (top)	U-Th (base)	OSL	AREA F [unit]	[spit]	ENTRANCE 3 [unit]	[spit]	U-Th (top)	U-Th (base)	OSL	CHRONO-STRATIGRAPHIC AGE	HUMAN OCCUPATION
2a				IT0	A1-A2						Reworked	
0				IT2	A0b (black lens)	—					Holocene	—
				IT1	Flowstone			13.5-20.6	14.9-16.6		MIS 2 - MIS 5a	
1	23.4-25.2	51.6-52.8		IH1	Flowstone	UC1	Unexcavated	26.4-28.7	76.9-81.9			
2			74.5-100.9	IH2	A3	UC2-UC6					MIS 5b	Phase FB4
				IH3								
				IH4	A4							
				IH5	Flowstone			86.9-88.5	86.9-88.1			
				IH6	A5					82.7-105.6		
				IH7	Flowstone			85.4-88.6	87.5-89.8			
				IH8	A6			86.7-88.5	85.8-92.7			
3				IL1	Flowstone	MC0		90.2-98.4	91.0-93.2		MIS 5c	Phase FB3
				IL2	A7	MC1-MC2	A49			85.8-109.8		
				IL3	A8							
				—	—	MC3-MC5	A50-A53					Phase FB2
4			93.6-126.8			LC1-LC3						Phase FB1
5				IB1	Flowstone	CO	Unexcavated	103.5-111.3	148.1-152.3		MIS 5c - MIS 6	—
—				IB2	A9	—	—				MIS 6 or older	

(a) The U-Th ages are bracketed by the upper and lower limits of the 95.4% probability intervals of the results obtained, respectively, for the uppermost and lowermost sample or sub-sample measured in any given stratigraphic unit; the OSL range for unit IH6 is given by the younger upper limit and the older lower limit of the 95.4% probability intervals obtained for the two available dates. Even though it can be observed below unit IT1 in profile views, unit IT2 in fact abuts it, filling-in voids that post-Pleistocene processes of differential erosion created at the interface between IT1 and IH1. The archeological content of unit IB2 is intrusive from overlying unit IL3 and, therefore, relates to Phase FB3; likewise, the stone tool component of unit IT0 is entirely derived from underlying units IH2-IH3 and, therefore, relates to Phase FB4

Table S13. The excavation. Volume of sediment removed (m³), per area of the site and excavation unit, during the 2010-13 field seasons. The estimates are derived from excavation records (décapage plans and stratigraphic profiles)

Stratigraphic unit / Excavation unit (spit)	IT0 A1-A2	IH2-IH3 A3	IH4 A4	IH6 A5	IH8 A6	Phase FB4	IL2 A7	IL3 A8	IB2 A9	MC1-MC2 A49	Phase FB3	MC3 A50	MC4-MC5 A51	A52	A53	Phase FB2
Area F (a)	0.638	0.319	0.326	0.326	0.403	**1.374**	0.150	0.440	0.350	–	**0.940**	–	–	–	–	**–**
Area F (fishes) (b)	–	0.319	0.326	0.326	0.256	**1.227**	–	–	–	–	**–**	–	–	–	–	**–**
Area F (U8 lithics)	0.200		0.068	0.068	0.084	**0.420**	0.075	0.220	0.175	–	**0.470**	–	–	–	–	**–**
Entrance 3 (SEx trench)	–	–	–	–	–	**–**	–	–	–	0.370	**0.370**	0.090	0.050	0.050	0.050	**0.240**

(a)   Based on the field log's record of sediment-for-sieve bags, the volume of reworked sediment was calculated as ⅔ of the combined volume of spits A1-A3
(b)   Excluding the estimated volume of seven ¼ m² units from spit A6/unit IH8 that remain to be processed and sorted

Table S14. Soil micromorphology thin sections. Main characteristics (groundmass and pedofeatures)

Thin section	Unit	Coarse/ Fine-related distribution pattern	b-fabric	Pedofeatures and sedimentary features
1009	UC2	porphyric (mostly single-spaced)	crystallitic	mass cementation by micrite (strong); micrite intercalations, infillings
1010	UC4?	porphyric (mostly single-spaced)	undifferentiated	moderate mass cementation by micrite; common sparry calcite coatings, rare infillings and nodules
1018	MC1	close to single-spaced porphyric	undifferentiated	mass cementation by micrite; micrite intercalations, coatings and infillings
1019 up	MC2	close to single-spaced porphyric	undifferentiated	mass cementation by micrite; micrite intercalations, coatings and infillings
1019 low	MC2	close to single-spaced porphyric	undifferentiated	as above, plus bedding/lamination dipping ~40°
1014	MC2	close to single-spaced porphyric	undifferentiated	mass cementation by micrite (strong); micrite intercalations and infillings; few loose, discontinuous biogenic infillings in chambers
1016	MC2	close to single-spaced porphyric	undifferentiated	mass cementation by micrite (strong); micrite intercalations and infillings; few loose, discontinuous biogenic infillings in chambers and channels
1017	MC2	close to single-spaced porphyric	undifferentiated	mass cementation by micrite; micrite intercalations; few loose, discontinuous biogenic infillings in chambers and channels
1001,1002	MC4	single-to-double-spaced porphyric	undifferentiated	mass cementation by micrite (strong); micrite intercalations and infillings; scarce loose, discontinuous and complete biogenic infillings in chambers and channels; passage features in 1002
1002	MC5	single-to-double-spaced porphyric	undifferentiated	mass cementation by micrite (strong); micrite intercalations and infillings; scarce loose, discontinuous and complete biogenic infillings in chambers and channels
1022	LC2	close porphyric	crystallitic	mass cementation by micrite (strong); few loose, discontinuous biogenic infillings in channels; large sparite nodule
1021	LC3	close porphyric	crystallitic	mass cementation by micrite (strong); few loose, discontinuous biogenic infillings in channels

Table S15. Soil micromorphology thin sections. Main characteristics (microstructure and components)

Thin section	Unit	Aggregation	Porosity	Coarse components (a)	Fine material
1009	UC2	–	very low	SIL dominant (but mainly quartz), LST scarce, CRB scarce, SHELL very rare, BONE absent	micrite
1010	UC4?	apedal (channels/chambers)	moderate; common channels, few chambers	SIL frequent, LST scarce, CRB very rare, SHELL very rare, BONE rare	brown to strong brown; speckled
1018	MC1	moderately developed, sub-angular blocky, mm-sized	low; scarce channels and chambers, few planes		yellowish brown; dotted
1019 up	MC2	well-developed, angular to sub-angular, blocky	low; chambers, planes, fine	SIL frequent, LST scarce, CRB rare, SHELL rare, BONE rare	reddish brown; speckled
1019 low	MC2	apedal	low: scarce channels and chambers; rare, fine vughs	SIL frequent, LST scarce, CRB rare, SHELL and BONE scarce (common in top part of unit); rare fragments of burnt vegetal organic matter and charcoal	reddish brown; speckled
1014	MC2	poorly developed, sub-angular, blocky	low (due to carbonate accumulation); few chambers and fine vughs	SIL frequent, LST scarce, CRB rare, SHELL and BONE scarce; rare fragments of burnt vegetal organic matter	reddish brown; speckled
1016	MC2	apedal	moderate; chambers, channels and fine vughs	SIL frequent, LST scarce, CRB rare, SHELL and BONE rare; rare fragments of burnt vegetal organic matter	reddish brown; speckled
1017	MC2	apedal	moderate; chambers, channels and fine vughs	SIL frequent, LST scarce, CRB rare, SHELL scarce, BONE rare; rare fragments of burnt vegetal organic matter	reddish brown; speckled
1001,1002	MC4	apedal	moderate to high; channels and chambers, fine vughs	SIL frequent, LST scarce, CRB rare, SHELL scarce, BONE scarce; rare fragments of burnt vegetal organic matter	brown; speckled
1002	MC5	apedal	moderate; channels and chambers, fine vughs	SIL scarce, LST rare, CRB rare, SHELL common, BONE rare; rare fragments of burnt vegetal organic matter	brown; speckled
1022	LC2	apedal	moderate; chambers, channels, few fine vughs	SIL scarce, LST rare, CRB rare, SHELL and BONE scarce	yellowish brown
1021	LC3	chambers	high; chambers, channels, few fine vughs	SIL scarce, LST rare, CRB rare, SHELL common, BONE scarce	yellowish brown

(a) SIL – siliciclastic fraction; LST – limestone fragments (mainly from bedrock); SHELL – non-fossil shells and fragments of shells; CRB – other carbonate components; BONE – bones and bone fragments

Table S16. Bayesian model of the dated sequence. Outlier Analysis results

Result	Prior	Posterior	Model	Type
1207.6	5	5	General	t
1027 isochron.	5	4	General	t
1208.5	5	14	General	t
1208.4	5	10	General	t
1208.3	5	4	General	t
1208.2	5	60	General	t
1208.1	5	2	General	t
12-6	5	5	General	t
12-5	5	5	General	t
1106 isochron	5	3	General	t
1106.1	5	1	General	t
1301.7	5	4	General	t
1301.6	5	100	General	t
1301.5	5	27	General	t
1301.4	5	2	General	t
1301.3	5	2	General	t
1301.2	5	100	General	t
1301.1	5	97	General	t
1302.3	5	1	General	t
1302.2	5	1	General	t
1302.1	5	3	General	t
1209.3	5	5	General	t
1209.4	5	6	General	t
1209.5	5	4	General	t
12-3	5	4	General	t
12-4	5	5	General	t
1306.1	5	5	General	t
1306.3	5	4	General	t
1306.2	5	4	General	t

Table S17. Bayesian model of the dated sequence. Results flagged as outliers were excluded from the modelling.

	Unmodelled			Modelled			A*	C**
	From	To	%	From	To	%		
FINAL				69232	81956	95.4		90.3
IH1 span				0	5640	95.4		99.5
Final IH1				75989	82140	95.4		98.7
1207.6 (79400,1256)	76893	81906	95.4	77328	82015	95.4	101.9	99.5
1027 isochron (81000,3000)	75014	86985	95.4	77627	82743	95.4	125.7	99.5
Initial IH1				77685	83930	95.4		98.8
Boundary between IH1 and IH2-IH3				78572	86880	95.4		97.6
IH2-IH3 span				–	–	–		–
Boundary between IH2-IH3 and IH4				82838	88062	95.4		99.0
IH4 span				–	–	–		–
Estimate (88000,250)	87500	88500	95.4	87320	87997	95.4	64.1	99.8
Boundary between IH4 and IH5				87461	88097	95.4		99.8
IH5 span				0	240	95.4		99.9
Final IH5				87547	88134	95.4		99.8
1208.5 (87693,381)	86932	88453	95.4	87564	88142	95.4	122.5	99.8
1208.4 (88137,371)	87396	88877	95.4	87579	88154	95.4	104.4	99.8
1208.3 (87797,325)	87147	88447	95.4	87590	88168	95.4	126.0	99.8
1208.1 (87559,313)	86934	88184	95.4	87596	88184	95.4	81.3	99.8
Initial IH5				87599	88206	95.4		99.7
Boundary between IH5 and IH6				87613	88403	95.4		99.8
IH6 span				0	382	95.4		100.0
12-6 (93900,5600)	82725	105075	95.4	87701	88658	95.4	83.5	99.9
12-5 (95000,5300)	84425	105575	95.4	87703	88660	95.4	61.4	99.9
Boundary between IH6 and IH7				87778	88894	95.4		99.8
IH7 span				0	637	95.4		100.0
Final IH7				87889	89000	95.4		99.8
1106 isochron (87000,800)	85404	88596	95.4	87939	89052	95.4	29.4	99.8
1106.1 (88670,581)	87510	89830	95.4	87977	89131	95.4	123.2	99.8
Initial IH7				87991	89251	95.4		99.6
Boundary between IH7 and IH8				88048	89585	95.4		99.7
IH8.1 span				0	974	95.4		99.9
Final IH8.1				88314	89830	95.4		99.7
1301.4 (89641,796)	88052	91230	95.4	88421	89897	95.4	109.6	99.8
1301.3 (88475,729)	87020	89930	95.4	88489	90002	95.4	81.6	99.8
Initial IH8.1				88522	90201	95.4		99.6
Boundary between IH8.1 and IH8.2				88692	90769	95.4		99.6
IH8.2 span				0	1158	95.4		99.8
Final IH8.2				89239	91001	95.4		99.6
1302.3 (90343,716)	88914	91772	95.4	89394	91034	95.4	120.8	99.8
1302.2 (90818,813)	89195	92440	95.4	89486	91107	95.4	107.2	99.8
1302.1 (89260,1730)	85807	92712	95.4	89539	91210	95.4	113.0	99.8
Initial IH8.2				89564	91343	95.4		99.6
Boundary between IH8.2 and [IL1 ↔ MC0]				89755	91738	95.4		99.7
IL1 span				0	2561	95.4		99.7
Final IL1				90299	91996	95.4		99.7
1209.4 (90875,484)	89909	91841	95.4	90624	92067	95.4	83.7	99.8
1209.5 (92113,567)	90981	93245	95.4	90801	92563	95.4	88.5	99.8
Initial IL1				90730	93535	95.4		99.6
Boundary between [IL1 ↔ MC0] and [IL2-IL3 ↔ MC1-MC2]				90773	96661	95.4		99.1
IL2-IL3 ↔ MC1-MC2 span				–	–	–		–
12-3 (97800,6000)	85827	109773	95.4	91291	100108	95.4	119.1	99.3
Boundary between [IL2-IL3 ↔ MC1-MC2] and MC3-MC5				91717	103274	95.4		98.3
MC3-MC5 span				–	–	–		–
Boundary between MC3-MC5 and [LC1-LC3 ↔ Layer 4]				94244	107221	95.4		97.8
LC1-LC3 ↔ Layer 4 span				–	–	–		–
12-4 (110200,8300)	93638	126762	95.4	96413	108638	95.4	92.9	98.9
Boundary between [LC1-LC3 ↔ Layer 4] and IB1				97869	110026	95.4		98.4
IB1 span				38484	50869	95.4		99.2
Final IB1				101268	111788	95.4		99.2
1306.1 (107361,1965)	103441	111281	95.4	105211	112768	95.4	86.0	98.1
1306.3 (141513,794)	139928	143098	95.4	139926	143090	95.4	100.0	99.2
1306.2 (150169,1036)	148102	152236	95.4	147632	151640	95.4	94.7	99.0
Initial IB1				148436	154486	95.4		99.5
INITIAL				150088	155646	95.4		99.3

* Agreement Indices: A_{model} = 62.7; $A_{overall}$ = 69.5

** C = convergence

130

Table S18. Site-to-shore distances. Estimates of sea level elevation relative to present through the accumulation of the deposit, and approximate distances (as the crow flies) to the nearest shore line

	Phases FB1-FB2 (early MIS 5c)	Phase FB3 (late MIS 5c)	Phase FB4 (MIS 5b)
Global sea level (m)			
mean elevation below present	25	35	45
extremes of uncertainty intervals	8 - 40	15 - 55	25 - 60
Site to shore (m)			
distance based on mean elevation	750	1500	2000
minimum to maximum distance	250 to 2000	500 to >2000	750 to >2000

Table S19. Foraminifera. Provenience, patina and identification

Provenience		Whitish, relatively fresh	Yellowish, heavily eroded	
Unit	**N**	**Benthic**	**Benthic**	**Planktonic**
IT2	3	–	*Elphidium* spp.	unidentified
IH2-to-IL3	–	–	–	–
MC5	14	*Elphidium* spp.; *Cibicides refulgens*	*Quinqueloculina* sp.; *Ammonia* (?) sp.	*Globigerina* sp.; *Orbulina suturalis*
IB2	8	*Elphidium crispum, Elphidium fichtellianum Elphidium macellum; Cibicides refulgens*	–	–

Table S20. Carbonized plant remains. Counts per stratigraphic unit and taxon

		Phase FB4				Phase FB3		Phase FB2		
TAXON	IT2	IH2-IH3	IH4	IH6	IH8	IL2	IL3	MC3	MC4-MC5	**TOTAL**
Pinus pinea	24	10	28	33	46	–	2	3	15	**161**
Pinus sp.	3	26	39	23	77	–	3	10	9	**190**
cone bract	–	80	177	163	252	–	16	50	110	**848**
nut shell	–	2	9	1	11	–	–	28	144	**195**
needle	–	–	–	2	–	–	1	–	–	**3**
Juniperus sp.	1	–	3	–	–	–	–	2	–	**6**
Conifer	–	5	22	13	21	3	14	2	5	**85**
Fabaceae	8	–	1	–	–	–	–	1	–	**10**
Olea europaea	28	4	3	3	–	–	1	4	–	**43**
Quercus sp. deciduous	–	–	–	–	–	–	–	10	–	**10**
Quercus sp. evergreen	3	–	–	–	–	–	–	7	–	**10**
Quercus sp.	3	3	–	1	–	–	–	14	–	**21**
Prunus sp.	4	1	–	–	–	–	–	–	–	**5**
Rhamnus-Phillyrea	23	–	4	–	–	–	–	2	1	**30**
Ficus carica	–	–	1	–	–	–	–	17	–	**18**
Salix-Populus	–	–	–	–	–	–	–	1	–	**1**
Vitis vinifera	–	–	–	–	1	–	–	–	–	**1**
Angiosperma	27	3	6	5	1	1	2	9	4	**58**
Arbutus unedo	6	–	–	–	–	–	–	–	–	**6**
Pistacia sp.	4	–	–	–	–	–	–	–	–	**4**
bark	–	1	–	–	–	–	–	1	1	**3**
Ficus carica (uncharred seed)	9	–	–	–	–	–	–	–	–	**9**
Olea europaea (uncharred seed)	1	–	–	–	–	–	–	–	–	**1**
Rubus sp. (uncharred seed)	2	–	–	–	–	–	–	–	–	**2**
Chenopodium album (uncharred seed)	8	–	–	–	–	–	–	–	–	**8**
TOTAL	**154**	**135**	**293**	**244**	**409**	**4**	**39**	**161**	**289**	**1728**

Table S21. Composition analysis of bulk samples. Component weights per stratigraphic unit (a)

Sample provenience	Sample weight (g)	Matrix (g)	Matrix (%)	Lithics (g)	Lithics (%)	Bone (g)	Bone (%)	Shell (g)	Shell (%)
>4 mm									
Figueira Brava IH2-IH3	55.24	46.69	84.52	0.17	0.31	1.66	3.01	6.72	12.17
Figueira Brava IH4	52.14	40.15	77.00	0.52	1.00	4.28	8.21	7.19	13.79
Figueira Brava IH6	57.17	50.42	88.19	0.71	1.24	1.00	1.75	5.04	8.82
Figueira Brava IH8	37.35	33.01	88.38	0.47	1.26	1.14	3.05	2.73	7.31
Figueira Brava IL3	58.88	56.27	95.57	0.06	0.10	1.28	2.17	1.27	2.16
Figueira Brava IB2	78.02	77.38	99.18	0.08	0.10	0.01	0.01	0.55	0.70
Figueira Brava MC5	95.27	65.11	68.34	5.27	5.53	–	–	24.89	26.13
Toledo B	29.34	23.67	80.67	–	–	–	–	5.67	19.33
Toledo B/C	13.06	3.00	22.97	–	–	–	–	10.06	77.03
Toledo C/D	3.79	0.41	10.82	–	–	–	–	3.38	89.18
[2-4] mm									
Figueira Brava IH2-IH3	25.56	20.95	81.96	0.34	1.33	0.84	3.29	3.43	13.42
Figueira Brava IH4	23.72	18.99	80.06	0.17	0.72	1.41	5.94	3.15	13.28
Figueira Brava IH6	19.00	15.74	82.84	0.20	1.05	1.19	6.26	1.87	9.84
Figueira Brava IH8	35.39	32.60	92.12	0.17	0.48	1.16	3.28	1.46	4.13
Figueira Brava IL3	25.62	22.80	88.99	0.05	0.20	1.95	7.61	0.82	3.20
Figueira Brava IB2	18.73	18.36	98.02	0.03	0.16	0.11	0.59	0.23	1.23
Figueira Brava MC5	18.27	12.21	66.83	0.05	0.27	0.38	2.08	5.63	30.82
Toledo B	23.84	19.47	81.67	–	–	–	–	4.37	18.33
Toledo B/C	12.60	1.55	12.30	–	–	0.05	0.40	11.00	87.30
Toledo C/D	7.28	1.42	19.51	0.06	0.82	0.00	0.00	5.80	79.67
[1-2] mm									
Figueira Brava IH2-IH3	25.01	22.97	91.84	0.02	0.08	0.84	3.36	1.18	4.72
Figueira Brava IH4	25.40	22.67	89.25	0.05	0.20	1.12	4.41	1.56	6.14
Figueira Brava IH6	22.00	20.81	94.59	0.02	0.09	0.57	2.59	0.60	2.73
Figueira Brava IH8	26.39	24.80	93.97	0.01	0.04	0.76	2.88	0.82	3.11
Figueira Brava IL3	25.35	24.51	96.69	0.01	0.04	0.40	1.58	0.43	1.70
Figueira Brava IB2	13.19	13.01	98.64	0.01	0.08	0.04	0.30	0.13	0.99
Figueira Brava MC5	14.34	11.84	82.57	–	–	0.33	2.30	2.17	15.13
Toledo B	33.19	30.62	92.26	–	–	0.01	0.03	2.56	7.71
Toledo B/C	19.86	12.58	63.34	–	–	0.03	0.15	7.25	36.51
Toledo C/D	17.79	13.99	78.64	–	–	–	–	3.80	21.36
All meshes									
Figueira Brava IH2-IH3	105.81	90.61	85.63	0.53	0.50	3.34	3.16	11.33	10.71
Figueira Brava IH4	101.26	81.81	80.79	0.74	0.73	6.81	6.73	11.90	11.75
Figueira Brava IH6	98.17	86.97	88.59	0.93	0.95	2.76	2.81	7.51	7.65
Figueira Brava IH8	99.13	90.41	91.20	0.65	0.66	3.06	3.09	5.01	5.05
Figueira Brava IL3	109.85	103.58	94.29	0.12	0.11	3.63	3.30	2.52	2.29
Figueira Brava IB2	109.94	108.75	98.92	0.12	0.11	0.16	0.15	0.91	0.83
Figueira Brava MC5	127.88	89.16	69.72	5.32	4.16	0.71	0.56	32.69	25.56
Toledo B	86.37	73.76	85.40	–	–	0.01	0.01	12.60	14.59
Toledo B/C	45.52	17.13	37.63	–	–	0.08	0.18	28.31	62.19
Toledo C/D	28.86	15.82	54.82	0.06	0.21	–	–	12.98	44.98

(a) Figueira Brava sample provenience: U9-NW (for units IH2-IH8), T7-SE (for units IL3-IB2), and SEx trench (for unit MC5). Lithics were defined as all products and byproducts of stone tool production, mostly quartz debris whose angularity, or presence of bulb or butt, clearly distinguished them from the quartz grains of the matrix (mature, well-rounded). The shell category includes all fragments of the invertebrates' exoskeleton. All skeletal fragments of vertebrates, including teeth and carapace, are counted in the bone category. Unit IL2 is not represented because, due to its heavily indurated nature across the Area F trench, no sample could be obtained. For the same reasons, only the basal level of the SEx trench could be analyzed.

Table S22. Density variation across units MC1-MC5 (SEx trench, Entrance 3). Marine invertebrate shell and stone tools per volume unit of excavation spit

Unit	Spit	Volume (m³)	Lithics (trench + sieve)			Shell (trench + sieve)			
			N	N/m³	kg/m³	NISP	NISP/m³	MNI	MNI/m³
MC1-MC2 (Phase FB3)	**A49**	0.370	187	505	3.041	54	146	8	22
MC3-MC5 (Phase FB2)	**A50**	0.090	290	3222	11.856	324	3600	50	556
	A51	0.050	121	2420	12.640	101	2020	13	260
	A52	0.050	100	2000	10.200	69	1380	17	340
	A53	0.050	88	1760	12.060	108	2160	26	520

Table S23. Marine gastropods. Counts per taxon and occupation phase

	Phase FB4		Phase FB3		Phase FB2		Reworked		TOTAL	
TAXON	NISP	MNI	NISP	MNI	NISP	MNI	NISP	MNI	NISP	MNI
PATELLIDAE										
Patella vulgata	414	193	20	15	6	6	16	9	456	223
Patella ulyssiponensis	35	20	4	3	1	1	4	4	44	28
Patella depressa	127	73	6	4	1	1	22	21	156	99
Patella rustica	2	2	–	–	–	–	1	1	3	3
Patella sp.	668	136	46	22	2	2	30	10	746	170
TROCHIDAE										
Phorcus lineatus	3	2	–	–	–	–	3	2	6	4
Steromphala cineraria	–	–	–	–	–	–	3	3	3	3
Steromphala umbilicalis	1	1	–	–	–	–	1	1	2	2
Steromphala sp.	4	3	–	–	1	1	2	2	7	6
LITTORINIDAE										
Littorina obtusata	1	1	–	–	–	–	1	1	2	2
Littorina littorea	–	–	–	–	–	–	1	1	1	1
Littorina saxatilis	–	–	–	–	–	–	1	1	1	1
Littorina sp.	3	2	–	–	–	–	1	1	4	3
Melarhaphe neritoides	–	–	–	–	–	–	1	1	1	1
CERITHIIDAE										
Bittium reticulatum	1	1	–	–	1	1	–	–	2	2
RANELLIDAE										
Charonia lampas	–	–	–	–	–	–	1	1	1	1
cf. *Charonia lampas*	–	–	–	–	–	–	1	1	1	1
MURICIDAE										
Nucella lapillus	2	2	1	1	–	–	–	–	3	3
Ocenebra erinaceus	–	–	–	–	–	–	3	2	3	2
NASSARIIDAE										
Tritia reticulata	–	–	–	–	3	3	–	–	3	3
NATICIDAE										
Euspira guilleminii	–	–	–	–	–	–	1	1	1	1
INDETERMINATE										
Indeterminate	6	–	–	–	–	–	9	–	15	–
TOTAL	**1267**	**436**	**77**	**45**	**15**	**15**	**102**	**63**	**1461**	**559**

Table S24. Marine bivalves. Counts per taxon and occupation phase

TAXON	Phase FB4		Phase FB3		Phase FB2		Reworked		TOTAL	
	NISP	MNI	NISP	MNI	NISP	MNI	NISP	MNI	NISP	MNI
GLYCYMERIDIDAE										
Glycymeris glycymeris	11	4	–	–	5	2	2	2	18	8
Glycymeris sp.	–	–	–	–	4	1	–	–	4	1
MYTILIDAE										
Mytillus galloprovincialis	1095	19	39	5	276	50	273	45	1683	119
OSTREIDAE										
Ostrea edulis	19	4	1	1	–	–	1	1	21	6
PECTINIDAE										
Pecten maximus	3	3	1	1	–	–	–	–	4	4
Pectinidae	4	3	–	–	–	–	2	2	6	5
ANOMIIDAE										
Anomia ephippium	8	3	1	1	–	–	1	1	10	5
CARDIIDAE										
Laevicardium crassum	1	1	–	–	7	2	–	–	8	3
Cerastoderma edule	–	–	–	–	1	1	3	2	4	3
Cardiidae	6	4	1	1	10	2	–	–	17	7
VENERIDAE										
Callista chione	18	4	1	1	10	3	1	1	30	9
Ruditapes decussatus	164	16	26	3	263	26	3	3	456	48
Veneridae	121	4	3	2	9	3	3	2	136	11
MACTRIDAE										
Lutraria lutraria	–	–	–	–	1	1	–	–	1	1
Spisula solida	–	–	–	–	–	–	1	1	1	1
Mactridae	11	1	–	–	–	–	1	1	12	2
SCROBICULARIIDAE										
Scrobicularia plana	–	–	–	–	–	–	4	2	4	2
SEMELIDAE										
Ervilia castanea	–	–	–	–	–	–	4	3	4	3
SOLENIDAE										
Solen marginatus	1	1	–	–	–	–	4	2	5	3
INDETERMINATE										
Indeterminate	45	–	1	–	–	–	13	–	59	–
TOTAL	**1507**	**67**	**74**	**15**	**586**	**91**	**316**	**68**	**2483**	**241**

Table S25. Crustaceans. Counts per taxon and occupation phase (w/C and n/C: number of crab specimens in the reworked assemblage with or without concretion, respectively)

TAXON	Phase FB4 NISP	Phase FB4 MNI	Phase FB3 NISP	Phase FB3 MNI	Phase FB2 NISP	Phase FB2 MNI	Reworked NISP	Reworked MNI	Reworked w/C	Reworked n/C	TOTAL NISP	TOTAL MNI
MALACOSTRACA												
Cancer pagurus (brown crab)	324	29	2	1	–	–	44	6	30	14	370	36
Maja squinado (spider crab)	29	6	–	–	–	–	13	2	2	11	42	8
Carcinus maenas (green crab)	1	1	–	–	–	–	4	2	–	4	5	3
Pachygrapsus marmoratus (marbled crab)	–	–	–	–	–	–	40	6	–	40	40	6
Eriphia verrucosa (yellow crab)	–	–	–	–	–	–	2	2	–	2	2	2
Indeterminate	311	4	–	–	–	–	39	2	8	31	350	6
MAXILLIPODA												
Perforatus perforatus (barnacle)	75	33	–	–	1	1	54	26			130	60
Cirripedia	23	13	–	–	–	–	7	3			30	16
TOTAL	**763**	**86**	**2**	**1**	**1**	**1**	**203**	**49**			**969**	**137**

Table S26. Crabs. NISP per taxon and stratigraphic unit in the *in situ* Pleistocene sequence of Area F

Phase	Unit	*Cancer pagurus* (brown crab)	*Maja squinado* (spider crab)	*Carcinus maenas* (green crab)	Indeterminate	TOTAL
FB4	**IH2-IH3**	51	–	–	33	84
	IH4	88	3	–	76	167
	IH6	110	8	–	126	244
	IH8	75	18	1	76	170
FB3	**IL2**	2	–	–	–	2
	TOTAL	**326**	**29**	**1**	**311**	**667**

Table S27. Fishes. NISP counts for recent-Holocene unit IT2 and for reworked sediment

TAXON	IT2	IT0	TOTAL
CHONDRICHTHYES – Cartilaginous fishes			
SQUATINIDAE			
Squatina squatina (angelshark)	–	1	1
TELEOSTEI – Teleost fishes			
CLUPEIDAE (herrings, shads, sardines)			
Alosa sp.(shads)	4	–	4
cf. *Sardina pilchardus* (sardine)	–	57	57
ANGUILLIDAE (eels)			
Anguilla anguilla (European eel)	–	3	3
MURAENIDAE (moray eels)			
Muraena helena (moray eel)	–	1	1
ANGUILLIFORMES (eels and morays)			
cf. Anguilliforms	–	3	3
GADIFORMES (cods)			
cf. Gadiformes	–	3	3
SERRANIDAE (sea basses and groupers)			
cf. Serranidae	–	1	1
MORONIDAE (basses)			
Dicentrarchus labrax (European bass)	–	1	1
cf. Moronidae	–	8	8
SPARIDAE (sea breams and porgies)			
cf. *Dentex* sp.	–	2	2
Diplodus vulgaris (two-banded seabream)	–	3	3
Diplodus sp. (porgies)	–	1	1
Pagrus sp. (porgies)	–	2	2
cf. *Sarpa salpa* (dreamfish)	–	1	1
Sparus aurata / cf. *S.aurata* (gilt-head seabream)	–	16	16
cf. *Spondyliosoma cantharus* (black seabream)	2	–	2
cf. Sparidae	35	57	92
LABRIDAE (wrasses)			
cf. Labridae	–	9	9
SCOMBRIDAE (mackerels, tunas and bonitos)			
Scomber scombrus (Atlantic mackerel)	–	1	1
cf. Scombridae	–	7	7
MUGILIDAE (mullets)			
cf. Mugilidae	–	7	7
PERISTEDIIDAE (armored searobins)			
cf. Peristediidae	–	4	4
PLEURONECTIFORMES (flatfishes)			
cf. Pleuronectiformes	–	1	1
UNIDENTIFIED			
Unidentified Chondrichthyes	1	17	18
Unidentified Teleostei	–	366	366
Unidentified Fish	–	217	217
TOTAL	**42**	**789**	**831**

Table S28. Fishes. NISP and MNI counts per taxon and stratigraphic unit (Phase FB4)

TAXON	IH2-IH3 NISP	IH2-IH3 MNI	IH4 NISP	IH4 MNI	IH6 NISP	IH6 MNI	IH8 NISP	IH8 MNI	TOTAL NISP	TOTAL MNI
CHONDRICHTHYES – Cartilaginous fishes										
LAMNIDAE (mackerel or white sharks)										
cf. Lamnidae *Lamna nasus* (porbeagle)	–	–	–	–	1	1	–	–	1	1
cf. *Isurus oxyrinhus* (shortfin mako)	–	–	–	–	1	1	–	–	1	1
CARCHARHINIDAE (requiem sharks)										
cf. *Prionace glauca* (blue shark)	–	–	3	2	5	2	1	1	9	2
Chondrichthyes	–	–	2	+	4	+	–	–	6	1
TELEOSTEI – Teleost fishes										
CLUPEIDAE (herrings, shads, sardines)										
cf. *Sardina pilchardus* (sardine)	6	1	–	–	–	–	–	–	6	1
ANGUILLIDAE										
Anguilla (European eel)	–	–	10	3	1	1	–	–	11	3
cf. *Anguilla anguilla*	–	–	7	+	14	+	1	1	22	+
CONGRIDAE (conger and garden eels)										
Conger conger (Conger eel)	–	–	–	–	1	1	–	–	1	1
cf. *Conger conger*	–	–	–	–	1	+	1	1	2	+
cf. Congridae	–	–	–	–	1	+	–	–	1	+
ANGUILLIFORMES (eels and morays)										
Anguilliformes	–	–	9	+	41	+	6	+	56	+
SPARIDAE (sea breams and porgies)										
cf. *Sparus aurata* (gilt-head seabream)	1	1	2	1	1	1	–	–	4	2
Sparidae / cf. Sparidae	5	+	–	–	2	+	–	–	7	+
***SCOMBRIDAE** (mackerels, tunas and bonitos)										
Scombridae	1	1	–	–	–	–	–	–	1	1
MUGILIDAE (mullets)										
Mugilidae	–	–	–	–	1	1	–	–	1	1
cf. Mugilidae	1	1	20	1	8	+	1	1	30	+
UNIDENTIFIED										
Unidentified fish	98		191		110		4		403	98
TOTAL	**112**		**244**		**192**		**14**		**562**	

Table S29. Fishes. Skeletal part frequency (Phase FB4) (a)

TAXON	Cranium and head bones						Pectoral skeleton	Vertebrae	Appendicular	Other				TOTAL
	AR	Q	OP	HMD	Cr	BASI	PTP	V	Fin	T	O. sag	S	Unidentified	TOTAL
cf. *Lamna nasus*	–	–	–	–	–	–	–	–	–	1	–	–	–	1
cf. *Isurus oxyrinhus*	–	–	–	–	–	–	–	–	–	1	–	–	–	1
cf. *Prionace glauca*	–	–	–	–	–	–	–	–	–	9	–	–	–	9
cf. Carcharinidae	–	–	–	–	–	–	–	1	–	–	–	–	–	1
Chondrichthyes	–	–	–	–	–	–	–	5	–	–	–	–	–	5
cf. *Sardina pilchardus*	–	–	–	–	–	–	–	5	–	–	1	–	–	6
Anguilla anguilla	–	–	–	–	–	3	–	8	–	–	–	–	–	11
cf. *Anguilla anguilla*	–	–	–	–	–	–	–	22	–	–	–	–	–	22
Conger conger	–	–	–	–	–	–	–	1	–	–	–	–	–	1
cf. *Conger conger*	–	–	–	–	–	–	–	2	–	–	–	–	–	2
cf. Congridae	–	–	–	–	–	–	–	1	–	–	–	–	–	1
Anguilliformes	–	–	–	–	–	–	–	56	–	–	–	–	–	56
cf. *Sparus aurata*	–	–	–	–	–	–	–	–	–	4	–	–	–	4
cf. Sparidae	–	–	–	–	–	–	–	2	–	5	–	–	–	7
Scombridae	–	–	–	–	–	–	–	1	–	–	–	–	–	1
cf. Mugilidae	–	–	–	–	–	1	–	30	–	–	–	–	–	31
Unidentified	2	2	7	1	66	–	1	175	108	4	–	15	22	403
TOTAL (N)	**2**	**2**	**7**	**1**	**66**	**4**	**1**	**309**	**108**	**24**	**1**	**15**	**22**	**562**
TOTAL (%)	0.36	0.36	1.25	0.18	11.74	0.71	0.18	54.98	19.22	4.27	0.18	2.67	3.91	100.00

(a) AR - Articular; Q - quadrate; OP - Opercular series; HMD - Hyomandibular; Cr - Cranium; BSI - Basioccipital; PTP - Postemporal; V - Vertebrae; Fin - bones of the fin skeleton; T - loose teeth; O. sag - Otolith (sagitta); S - scales

Table S30. Aquatic and marine birds. NISP counts (w/C and n/C: number of specimens in the reworked assemblage with or without concretion, respectively)

TAXON	Phase FB4	Phase FB3	IT0 w/C	IT0 n/C	TOTAL
ANATIDAE					
Anas sp.	1	–	–	–	1
Anas cf. *platyrhynchos* (cf. mallard)	3	–	–	–	3
cf. *Anser* sp. (cf. grey goose)	–	–	1	–	1
cf. *Melanitta nigra* (cf. scoter)	–	–	–	2	2
Anatidae	–	–	–	3	3
PHALACROCORACIDAE					
Phalacrocorax aristotelis (shag)	–	–	–	6	6
Phalacrocorax cf. *aristotelis* (cf. shag)	2	–	–	13	15
Phalacrocorax carbo (cormorant)	–	–	–	3	3
Phalacrocorax cf. *carbo*	–	–	–	1	1
Phalacrocorax sp.	–	–	–	6	6
cf. *Phalacrocorax* sp.	–	–	–	6	6
SULIDAE					
Morus bassanus (gannet)	1	–	–	1	2
PROCELLARIIDAE					
Puffinus cf. *puffinus* (cf. shearwater)	–	–	–	2	2
Puffinus sp.	–	–	–	3	3
Procellariidae	–	–	–	1	1
SCOLOPACIDAE					
Calidris sp. (sandpiper)	1	–	–	2	3
LARIDAE					
Larus cf. *canus* (seagull)	–	–	–	1	1
Larus sp.	–	1	–	–	1
Laridae	–	–	–	1	1
ALCIDAE					
Pinguinus impennis (great auk)	–	–	2	–	2
Alca torda (razorbill)	–	–	–	2	2
cf. *Alca torda*	–	–	–	5	5
cf. *Alca torda* / *Uria aalge* (cf. razorbill / common murre)	1	–	–	1	2
cf. *Cepphus grylle* / *Fratercula arctica* (cf. common guillemot / puffin)	–	–	2	–	2
STERNIDAE					
Sterna hirundo (common tern)	–	–	–	1	1
cf. *Sterna hirundo*	–	–	–	1	1
ARDEIDAE					
cf. *Egretta garzetta* (cf. little egret)	–	–	–	3	3
GAVIIDAE					
Gavia stellata (red-throated diver)	–	1	–	–	1
Gavia sp.	1	–	–	–	1
TOTAL	**10**	**2**	**5**	**64**	**81**

Table S31. Terrestrial birds. NISP counts (w/C and n/C: number of specimens in the reworked assemblage with or without concretion, respectively)

TAXON	Phase FB4	IT0 w/C	IT0 n/C	TOTAL
PHASIANIDAE				
Alectoris rufa (partridge)	–	1	2	3
cf. *Alectoris rufa*	–	1	–	1
cf. *Alectoris rufa* / *Perdix perdix* (partridge or hun)	1	–	–	1
PASSERIFORME				
Passeriforme	1	–	6	7
CUCULIDAE				
cf. *Cuculus canorus* (cuckoo)	1	–	–	1
CORVIDAE				
Corvus cf. *corax* (cf. raven)	1	–	–	1
Corvus cf. *corone* (cf. carrion crow)	2	–	–	2
Corvus sp.	2	–	–	2
cf. *Corvus* sp.	–	–	1	1
Pyrrhocorax pyrrhocorax (red-billed chough)	–	1	–	1
SCOLOPACIDAE				
Scolopax rusticola (woodpecker)	3	–	–	3
ACCIPITRIDAE				
cf. *Accipiter nisus* (cf. sparrowhawk)	1	–	–	1
Milvus cf. *migrans* (kite, cf. black kite)	–	1	–	1
cf. *Milvus migrans*	1	–	–	1
cf. *Gyps* sp. (cf. griffon)	1	–	–	1
Accipitridae	1	–	–	1
STRIGIDAE				
Athene noctua (little owl)	1	–	–	1
cf. *Athene noctua*	–	1	–	1
TOTAL	**16**	**5**	**9**	**30**

Table S32. Migratory marine and aquatic birds. Present-day European distribution, seasonality in Portugal, habitat and behavior of the Pleistocene taxa

Species	European distribution	In Portugal	Habitat and behavior
Shag	Western and southern Europe	Resident and wintering	Feeds at sea, nests on rocky coasts using ledges, crevices and small caves; very gregarious, forms large breeding colonies
Auks	Cold North Atlantic waters	Wintering and migrating-through (until the 20th century, Europe's southernmost colony of breeding murres)	Feed at sea or in larger estuaries with lower salinity levels, and come to land only to breed in large colonies
Red-throated diver	Northern Eurasia	Wintering (rare)	Breeds primarily in coastal tundra, often on very small lakes; can form large concentrations when wintering in southern Europe
Goose	Temperate and subarctic	Wintering and migrating-through	Lives in moorlands, marshes, lakes, and coastal islands; migratory and gregarious, forming flocks of varying sizes
Gannet	Coasts of north-western Europe	Wintering and migrating-through	Feeds at sea; found on land, in islands or rocky cliffs, when breeding in colonies
Sandpipers	Arctic coasts	Wintering and migrating-through	Arctic-breeding, form large flocks when wintering on coastal and estuarine areas of southern Europe

Table S33. Birds. Skeletal part frequency data

PROVENIENCE	Mandible	Sternum	Synsacrum	Coracoid	Scapula	Humerus	Ulna	Radius	Carpometacarpus	Femur	Fibula	Tibiotarsus	Tarsometatarsus	TOTAL
Holocene-intruded, marine														
PHALACROCORACIDAE	–	1	1	4	2	8	3	3	1	5	1	3	3	35
Reworked with concretion, aquatic and marine														
ANATIDAE	–	–	–	–	–	1	–	–	–	–	–	–	–	1
ALCIDAE	–	–	–	–	–	3	1	–	–	–	–	–	–	4
Phase FB4, aquatic and marine														
ANATIDAE	–	–	–	1	1	2	–	–	–	–	–	–	–	4
SULIDAE	–	–	–	–	–	–	–	1	–	–	–	–	–	1
PHALACROCORACIDAE	–	–	–	–	–	1	1	–	–	–	–	–	–	2
SCOLOPACIDAE	–	–	–	–	–	1	–	–	–	–	–	–	–	1
ALCIDAE	–	–	–	–	1	–	–	–	–	–	–	–	–	1
GAVIDAE	–	–	–	–	–	1	–	–	–	–	–	–	–	1
Phase FB4, terrestrial														
PHASIANIDAE	–	–	–	–	–	–	–	–	–	–	–	–	1	1
PASSERIFORME	–	–	–	–	–	1	–	–	–	–	–	–	–	1
CUCULIDAE	–	–	–	–	–	–	–	–	–	1	–	–	–	1
CORVIDAE	–	–	–	–	–	1	–	–	1	–	–	2	1	5
SCOLOPACIDAE	–	–	–	1	–	1	1	–	–	–	–	–	–	3
ACCIPITRIDAE	1	–	–	–	–	1	1	–	–	–	–	1	–	4
STRIGIDAE	–	–	–	–	–	–	–	–	1	–	–	–	–	1

Table S34. Carnivore-damaged bones. Birds vs. mammals

PROVENIENCE	Birds (aquatic)	Birds (terrestrial)	Birds (indeterminate)	Lagomorphs	cf. Lagomorphs (a)	Larger mammals	TOTAL
Reworked							
Crenulated edge	2	1	2	–	–	–	5
Pit	4	–	2	9	1	–	16
Puncture	3	–	3	12	3	–	21
Score	–	–	–	–	1	–	1
Phase FB4							
Crenulated edge	–	–	–	–	–	–	–
Pit	–	1	–	–	–	–	1
Puncture	–	2	1	1	–	–	4
Score	–	–	–	–	–	–	–
TOTAL	**9**	**4**	**8**	**22**	**5**	**–**	**48**

(a) Indeterminate Very Small Macro-mammals

Table S35. Macro-mammals and tortoise. Counts per taxon and phase

TAXON	Phase FB4 NISP	Phase FB4 MNI	Phase FB3 NISP	Phase FB3 MNI	Phase FB2 NISP	Phase FB2 MNI	IT0 NISP	IT0 MNI	TOTAL NISP	TOTAL MNI
LARGE MACRO-MAMMALS										
Equus caballus (horse)	1	1	–	–	–	–	–	–	1	1
Equus sp.	14	4	2	2	–	–	–	–	16	6
Bos sp.(aurochs)	6	3	–	–	–	–	1	1	7	4
Herbivore	6	–	5	–	2	–	1	–	14	–
Ursus arctos (brown bear)	9	2	4	2	–	–	–	–	13	4
Indeterminate	36	–	19	–	–	–	1	–	56	–
MEDIUM MACRO-MAMMALS										
Cervus elaphus (red deer)	53	7	18	2	–	–	2	1	73	10
Cervidae	42	4	5	2	1	1	4	2	52	9
Herbivore	10	–	–	–	–	–	1	–	11	–
Indeterminate	81	–	8	–	4	–	2	–	95	–
SMALL MACRO-MAMMALS										
Caprinae (ibex or chamois)	58	5	12	2	–	–	11	2	81	9
Herbivore	3	–	–	–	–	–	4	–	7	–
Sus sp. (wild boar)	4	2	1	1	–	–	–	–	5	3
Hyaenidae (hyena)	3	1	1	1	–	–	–	–	4	2
Canis lupus (wolf)	1	1	–	–	–	–	–	–	1	1
Martes sp. (marten)	–	–	–	–	–	–	1	1	1	1
Carnivore	33	–	3	–	–	–	1	–	37	–
Indeterminate	165	–	21	–	3	–	31	–	220	–
LARGER THAN VERY SMALL MACRO-MAMMALS										
Herbivore	24	–	4	–	–	–	3	–	31	–
Indeterminate	542	–	142	–	12	–	73	–	769	–
VERY SMALL MACRO-MAMMALS										
Hystrix sp. (porcupine)	1	1	–	–	–	–	–	–	1	1
Oryctolagus cuniculus (rabbit)	2	2	–	–	–	–	5	3	7	5
Lepus sp. (hare)	3	2	–	–	–	–	–	–	3	2
Leporidae	157	13	3	2	–	–	290	26	450	41
Erinaceus europaeus (hedgehog)	–	–	–	–	–	–	2	1	2	1
Felis silvestris (wild cat)	7	5	1	1	–	–	2	1	10	7
Lynx pardinus (Iberian lynx)	1	1	–	–	–	–	–	–	1	1
Vulpes vulpes (fox)	1	1	–	–	–	–	–	–	1	1
cf. *Vulpes vulpes*	–	–	–	–	–	–	1	1	1	1
Carnivore	–	–	–	–	–	–	2	–	2	–
Indeterminate	480	–	28	–	–	–	344	–	852	–
INDETERMINATE MACRO-MAMMALS										
Indeterminate	1989	–	105	–	1	–	304	–	2399	–
TESTUDINAE										
Testudo hermanni (Hermann's tortoise)	1	1	1	1	–	–	1	1	3	3
Testudo sp.	65	4	8	2	–	–	4	2	77	8
cf. *Testudo* sp.	8	4	3	1	–	–	–	–	11	5
TOTAL	**3806**	**64**	**394**	**19**	**23**	**1**	**1091**	**42**	**5314**	**126**

Table S36. Macro-mammals and tortoise. Vertical distribution per stratigraphic unit in Area F (NISP)

TAXON	Phase FB4				Phase FB3		TOTAL
	IH2-IH3	IH4	IH6	IH8	IL2	IL3	
UNGULATES							
Aurochs	3	–	2	1	–	–	6
Horse	7	2	2	4	1	1	17
Deer	16	27	20	32	9	14	118
Caprine	9	1	13	35	8	4	70
Boar	–	1	–	3	–	1	5
LAGOMORPHS							
Hare or rabbit	53	38	50	21	1	2	165
TORTOISE							
Testudo	7	16	31	19	3	9	85
LARGER CARNIVORES							
Bear	–	–	1	8	3	1	13
Hyena	–	–	–	3	1	–	4
Wolf	–	–	–	1	–	–	1
SMALLER CARNIVORES							
Lynx	–	–	–	1	–	–	1
Wild cat	1	–	6	–	1	–	8

Table S37. Macro-mammals and tortoise. Anthropogenic marks per phase, and frequency relative to total NISP

MARK TYPE	Phase FB4 (N=3806)	Phase FB3 (N=394)	Phase FB2 (N=23)	TOTAL (N=4223)
BUTCHERY				
Chops	1	–	–	1
Cuts	11	2	–	13
Scrapes	1	–	–	1
TOTAL	13	2	–	15
Frequency	**0.34%**	**0.51%**	–	**0.36%**
PERCUSSION				
Impact Flake	144	31	1	176
Adhering Flake	13	1	–	14
Percussion Notch	29	9	–	38
Percussion Pit	6	2	–	8
TOTAL	192	43	1	236
Frequency	**5.04%**	**10.91%**	4.35%	**5.59%**
BURNING				
Brown	131	1	–	128
Black	456	7	3	466
Grey	17	–	–	17
White	7	–	–	7
TOTAL	611	8	3	622
Frequency	**16.05%**	**2.03%**	**13.04%**	**14.73%**

Table S38. Stone tools. Square U8 counts per raw-material, techno-economic category and stratigraphic aggregate

RAW-MATERIAL	Core		Flake		Flake fragment		Small flake		Blade		Bladelet		Debris		Chunk		Tool		Hammerstone		Manuport		TOTAL	
	N	W (g)	N	W (g)	N	W (g)	N	W (g)	N	W (g)	N	W (g)	N	W (g)	N	W (g)	N	W (g)	N	W (g)	N	W (g)	N	W (g)
Phase FB4, units IT0 and IH2-IH3 (approximate volume = 0.200 m³; N/m³ = 2485)																								
Quartz	18	547	76	863	–	–	46	80	–	–	–	–	235	155	37	474	35	376	–	–	9	475	456	2970
Quartzite	2	59	6	231	3	35	–	–	–	–	–	–	1	1	–	–	1	28	–	–	–	–	13	353
Flint	4	113	5	95	6	20	–	–	–	–	–	–	7	3	–	–	–	–	–	–	–	–	22	231
Limestone	1	66	–	–	–	–	1	3	–	–	–	–	3	1	–	–	–	–	–	–	–	–	5	70
Other	–	–	1	12	–	–	–	–	–	–	–	–	–	–	–	–	–	–	–	–	–	–	1	12
TOTAL	25	785	88	1201	9	55	47	83	–	–	–	–	246	160	37	474	36	403	–	–	9	475	497	3636
Phase FB4, units IH4 and IH6 (approximate volume = 0.136 m³; N/m³ = 2831)																								
Quartz	24	820	78	898	–	–	51	123	1	3	–	–	113	138	42	450	21	245	1	62	19	975	350	3713
Quartzite	–	–	5	69	4	53	–	–	–	–	–	–	1	3	–	–	–	–	–	–	2	95	12	220
Flint	–	–	3	47	3	8	–	–	–	–	–	–	3	4	1	22	2	26	–	–	–	–	12	108
Limestone	1	44	1	9	1	12	–	–	–	–	–	–	1	3	–	–	–	–	–	–	4	205	8	273
Other	–	–	1	21	1	14	–	–	–	–	–	–	–	–	–	–	–	–	–	–	1	11	3	45
TOTAL	25	864	88	1044	9	87	51	123	1	3	–	–	118	148	43	472	23	271	1	62	26	1285	385	4359
Phase FB4, unit IH8 (approximate volume = 0.084 m³; N/m³ = 2440)																								
Quartz	12	347	40	360	–	–	25	53	–	–	–	–	55	54	46	442	10	1–9	1	202	5	298	194	1864
Quartzite	–	–	1	48	1	2	1	2	–	–	–	–	1	–	–	–	–	–	–	–	–	–	4	52
Flint	–	–	–	–	1	8	3	5	–	–	–	–	–	–	–	–	–	–	–	–	–	–	4	13
Limestone	–	–	–	–	–	–	–	–	–	–	–	–	–	–	1	4	–	–	–	–	1	49	2	53
Other	1	44	–	–	–	–	–	–	–	–	–	–	–	–	–	–	–	–	–	–	–	–	1	44
TOTAL	13	391	41	408	2	1–	29	60	–	–	–	–	56	54	47	445	10	1–9	1	202	6	347	205	2026
Phase FB3, units IL2-IB2 (approximate volume = 0.470 m³; N/m³ = 526)																								
Quartz	27	1602	47	681	–	–	13	31	–	–	–	–	63	92	54	746	4	33	–	–	17	1070	225	4255
Quartzite	3	187	–	–	2	54	1	10	–	–	–	–	1	2	–	–	–	–	–	–	2	434	9	686
Flint	–	–	5	84	–	–	–	–	–	–	–	–	1	1	–	–	–	–	–	–	–	–	6	85
Limestone	–	–	1	13	–	–	–	–	–	–	–	–	–	–	–	–	–	–	–	–	3	145	4	158
Other	1	34	1	16	–	–	–	–	–	–	–	–	–	–	–	–	1	10	–	–	–	–	3	60
TOTAL	31	1823	54	793	2	54	14	41	–	–	–	–	65	95	54	746	5	43	–	–	22	1649	247	5243

Table S39. Stone tools. Square U8 typological counts per stratigraphic aggregate (a)

	Phase FB4			Phase FB3	
TYPE	IT0-IH3	IH4+IH6	IH8	IL2-IB2	TOTAL
Notch	23	7	4	1	35
Denticulate	5	7	1	1	14
Sidescraper (b)	2	4	4	2	12
Naturally backed knife (c)	3	1	–	1	5
Unretouched Levallois blade / laminary flake (d)	–	1	–	–	1
Continuously, marginally retouched flake (use-worn?)	–	1	1	–	2
Retouched tool fragment	3	2	–	–	5
TOTAL	36	23	10	5	74

(a) quartz, except where indicated; (b) one in IH4 is flint; (c) one in IH2-IH3 is quartzite, one in IL2 is "other;" (d) flint

Table S40. Flint. Technological data for Area F and Entrance 3 items per occupation phase

	Phase FB4		Phase FB3		Phase FB2		TOTAL	
TECHNO-ECONOMIC CATEGORY	N	%	N	%	N	%	N	%
Core	13	8.39	1	6.25	–	–	14	7.73
Flake	87	56.13	8	50.00	7	70.00	102	56.35
Small flake (<2 cm)	14	9.03	–	–	–	–	14	7.73
Retouched tool	13	8.39	–	–	1	10.00	14	7.73
Debris /chunk	28	18.06	7	43.75	2	20.00	37	20.44
TOTAL	155		16		10		181	
TECHNOLOGICAL CATEGORY	N	%	N	%	N	%	N	%
Cortical flakes	3	2.63	2	25.00	–	–	5	3.85
> 50% cortical flakes	7	6.14	–	–	–	–	7	5.38
< 50% cortical flakes	9	7.89	–	–	2	25.00	11	8.46
Debordant flakes	9	7.89	–	–	–	–	9	6.92
Naturally backed flakes	4	3.51	1	12.50	–	–	5	3.85
Kombewa-type flakes	5	4.39	–	–	–	–	5	3.85
Levallois blanks (flakes, blades, laminary flakes)	10	8.77	–	–	–	–	10	7.69
Flakes	22	19.30	5	62.50	3	37.50	30	23.08
Pseudo-Levallois points	3	2.63	–	–	–	–	3	2.31
Platform rejuvenation flakes	1	0.88	–	–	–	–	1	0.77
Retouch flakes	2	1.75	–	–	–	–	2	1.54
Small flakes	13	11.40	–	–	–	–	13	10.00
Indeterminate flake fragments	26	22.81	–	–	3	37.50	29	22.31
TOTAL	114		8		8		130	

Table S41. Quartz. Use-wear of Area F artefacts (one Phase FB3 scraper excepted, all from Phase FB4)

		Preservation			Longitudinal (e.g. cutting)			Transversal (e.g. scraping)	
CATEGORY	N	good	weathered	with wear	animal soft	wood	hard	hard	wood
Unretouched flake	36	25	11	8	–	3	–	5	–
Denticulate	9	9	–	9	1	–	4	–	4
Scraper	2	2	–	2	–	–	1	–	1
Laminary blank	1	1	–	1	–	–	1	–	–
Bladelet-like blank	1	1	–	1	1	–	–	–	–
Nucleiform piece	1	1	–	1	–	–	–	1	–
TOTAL	50	39	11	22	2	3	6	6	5

Table S42. Density of marine/estuarine mollusk and fish remains. Proxy data for Holocene and Last Interglacial sites of Iberia, the Maghreb and South Africa

Site	Provenience (sample/unit/phase/trench)	Age	Distance to shore (m)	Occupation length (years)	Sampled deposit Area (m²)	Sampled deposit Volume (m³)	Shell density (kg/m³)	Shell in bulk samples >1 mm (kg/m³)	>2 mm (kg/m³)	>4 mm (kg/m³)	2-4 mm (kg/m³)	Marine mollusk remains NISP (/m³)	NISP (/m²/10³y)	MNI (/m³)	MNI (/m²/10³y)	Fish remains NISP (/m³)	NISP (/m²/10³y)	Sources
Figueira Brava (FB)	FB4	MIS 5b	2000	4000	5.25	1.374	–	131.81	116.47	79.94	36.54	2018	132	366	24	458	27	this work
	FB3	MIS 5c	1500	4000	5.25	3.000	–	22.63	43.57	27.75	15.82	115	7	46	3	–	–	
	FB2	MIS 5c	750	4000	0.63	0.240	–	370.66	346.06	282.22	63.84	2504	240	442	42	–	–	
El Cuco (EC)	VII-XIII	MIS 5 (?)	350	–	2.00	2.600	–	–	–	–	–	–	–	344	–	–	–	(44, 45)
Aviones (AV)	I-IV	MIS 5d	40	4000	6.50	4.000	–	–	–	–	–	205	50	106	27	–	–	(27, 28, 189)
Bajondillo (BJ)	Bj/18	MIS 5e	50	–	0.29	0.008	–	–	–	–	–	69,198	–	2400	–	–	–	(190-192)
	Bj/19		50	–	0.12	0.017	–	–	–	–	–	77,297	–	2234	–	–	–	
Contrebandiers (CBD)	Aterian	MIS 5c	1750	–	–	7.455	–	–	–	–	–	773	–	243	–	4	–	(50)
	Mousterian	MIS 5d	2500	–	–	8.954	–	–	–	–	–	95	–	20	–	1	–	
Hoedjiespunt 1 (HDP1)	AH-I	MIS 5e	100	–	–	0.672	12.05	–	–	–	–	–	–	496	–	–	–	(32, 177)
	AH-II		100	–	–	0.253	11.46	–	–	–	–	–	–	708	–	–	–	
	AH-III		100	–	–	0.479	13.15	–	–	–	–	–	–	685	–	–	–	
Ysterfontein 1 (YFT1)	Group 7	MIS 5e	100	–	2.50	0.500	69.37	–	–	–	–	–	–	–	–	–	–	(177, 193)
	Group 13		100	–	2.00	1.000	10.88	–	–	–	–	–	–	–	–	–	–	
	all groups average		100	–	–	–	23.33	–	–	–	–	–	–	1571	–	–	–	
Blombos (BBC)	M1	MIS 5a	650	–	3.00	1.210	20.74	–	–	–	–	–	–	2647	–	64	–	(51, 53, 56)
	M2		650	–	3.00	0.620	39.12	–	–	–	–	–	–	5029	–	67	–	
	M3		650	–	3.00	1.140	86.14	–	–	–	–	–	–	2361	–	47	–	
Pinnacle Point 13B (PP13B)	Shelly Brown Sand	MIS 5c	500	–	–	0.095	8.66	–	–	–	–	–	–	726	–	–	–	(51, 54)
	Upper Roof Spall		500	–	–	0.518	4.54	–	–	–	–	–	–	463	–	–	–	
	Lower Roof Spall		500	–	–	0.548	3.77	–	–	–	–	–	–	438	–	–	–	
	LC-MSA Upper	MIS 5d	500	–	–	0.047	3.32	–	–	–	–	–	–	787	–	–	–	
	LC-MSA Middle	MIS 5e	80	–	–	0.172	2.32	–	–	–	–	–	–	343	–	–	–	
Klasies River (KR)	MSA II (Cave 1A)	MIS 5c	250	–	5.00	1.580	35.50	–	–	–	–	–	–	2947	–	–	–	(19, 51, 53)
	MSA I (Caves 1-1B)	MIS 5e	40	–	3.00	1.170	46.40	–	–	–	–	–	–	5621	–	–	–	
El Mazo	108	Early Mesolithic	1500	50	0.50	0.022	–	–	142.42	–	–	876,318	771	91,455	80,480	–	–	(173, 174)
Barranco das Quebradas	Locality 1		450	600	2.00	2.000	6.62	–	–	–	–	5464	9106	2073	3454	–	–	(172)
	Locality 3		550	400	5.00	2.500	3.41	–	–	–	–	10,896	13,621	3447	4309	–	–	
	Locality 4		650	–	11.00	5.500	3.42	–	–	–	–	2736	–	761	–	–	–	
	Locality 5		700	–	9.00	4.500	6.17	–	–	–	–	11,382	–	1178	–	–	–	
Toledo (layers B-C)	sample B		50	200	–	–	–	211.53	168.55	95.19	73.36	–	–	–	–	–	–	(67, 151)
	sample B/C		50	200	–	–	–	901.79	670.85	320.45	350.40	–	–	–	–	–	–	
	sample C/D		50	200	–	–	–	652.15	461.23	169.82	291.41	–	–	–	–	–	–	
	Area B		50	200	8.00	4.800	–	–	–	–	–	1624	4872	–	–	–	–	
	Areas A-B		50	200	24.00	14.400	–	–	–	–	–	–	–	276	827	–	–	
	all areas		50	200	27.00	16.200	–	–	–	–	–	–	–	–	–	9	26	
Arapouco	1960s trench	Late Mesolithic	100	500	120.00	60.000	–	–	–	–	–	–	–	–	–	32	32	(151, 194)
Amoreiras	1985-86 trench		300	500	22.00	11.000	–	–	–	–	–	–	–	–	–	2	2	(151, 194)
Poças de São Bento	1987-88 trench		1100	500	26.00	13.000	–	–	–	–	–	–	–	–	–	4	4	(151, 194, 195)
Samouqueira I	1984 trench		50	750	18.00	13.500	–	–	–	–	–	–	–	–	–	67	67	(48, 49, 151)
Medo Tojeiro	1984 trench		100	–	10.00	6.500	–	–	256.42	–	–	–	–	–	–	–	–	(48, 49, 196)
Fiais	1986 trench		2000	750	12.00	6.000	–	–	40.20	–	–	–	–	–	–	10	7	(151, 196)

Table S43. Holocene coastal sites of Iberia. Criteria used to estimate age and distance to shoreline, and to calculate proxy indexes for the importance of aquatic foods

Sites	Type, location	Observations
El Mazo	Rock-shelter Llanes, Asturias Spain	Unit 108 is a dense midden lens at the base of the stratigraphic sequence. Duration is based on the one-sigma standard deviation of a ^{14}C date on bone: 8022±39 BP (OxA-28411). The sample comes from an area of 0.5 m² and represents a volume of 22 l that was floated, sorted and weighed using a sieve column with meshes of 4, 2 and 1 mm. Based on Leorri *et al.* (*197*), the distance to shoreline is the closest to sea that the site would have been during the interval indicated by the calibrated age range. Immediately overlying units 114 and 115 are statistically of the same age but lack weight/volume density data.
Toledo	Open air Lourinhã Portugal	Area-excavated 1995-98, the site is in the inner paleo-estuary of River Alcabrichel, slightly above the edge of the floodplain, here taken to be the nearest point for the procurement of the brackish water taxa that make up most of the mollusk shell assemblage. The rocky taxa are found in the cliffs around the river mouth, ~4 km away. The occupation span is based on the difference between the mid-point of ^{14}C dates on securely provenanced samples. The designations "B", "B/C" and "C /D" concern the samples for composition analysis. The specimen counts for mollusks concern layers B and C of the sequence. The sieve fraction (>2 mm) was counted in only seven of the 24 squares of Areas A and B that have been studied (there are no NISP counts for Area A). The fish data concern all areas of the site.
Arapouco Amoreiras Poças de São Bento	Open air Sado valley Portugal	The sites are in the inner paleo-estuary of River Sado. Distances to the present river mouth range between ~40 km, for Arapouco, and ~55 km, for Amoreiras. The fish and shellfish taxa found at these sites could all have been procured in the brackish waters of the paleo-estuary, so distance to the shore is the shortest path to the edge of the floodplain. In the absence of quantitative studies for the shellfish, density estimates are calculated for fish only. In the case of Arapouco, area and volume estimates are derived from the plans and profiles of the 1960s excavations, which, based on the size and abundance of the remains found in the collection, were systematically sieved with a fine mesh. For Amoreiras and Poças de São Bento, the data derive from the 1980s work, during which sediments were sieved with a fine mesh (2-3 mm). The occupation span of 500 years is based on the length of the interval during which, based on the direct radiocarbon dating of human skeletons, Amoreiras was used as a burial site coevally with the accumulation of the midden remains.
Samouqueira I Medo Tojeiro	Open air Alentejo coast Portugal	Both sites are at the beach or atop the adjacent cliffs. The data derive from the mid-1980s excavations. For Medo Tojeiro, shell weight per volume unit of sediment comes from the >2 mm fraction of 31 one-liter bulk samples collected across the site's vertical and horizontal extent. For Samouqueira, similar bulk samples were collected but only the results of their geochemical analysis have been published. The density values for the Samouqueira fish remains are calculated from the size of the excavated area, and the average thickness of the deposit (but all fish remains come from the 14 m² of the site's Sector XII, none were found in the four 1 m² test trenches open in other sectors). The span of Samouqueira's occupation is derived from the difference between the two reliable radiocarbon dates available for the site. The dating of Medo Tojeiro remains unresolved. Lubell *et al.* (*49*) convincingly argue that the shell-midden is entirely of Late Mesolithic age and the few Neolithic potsherds found in the uppermost levels reflect post-depositional intrusion.
Fiais	Open air Odemira Portugal	The site is in the inner part of the paleo-estuary of River Mira. Distance to the present river mouth is ~20 km, but the fish and shellfish taxa found at the site could all have been procured in the brackish waters of the paleo-estuary, so distance to the shore is the shortest path to the edge of the floodplain. The span of the occupation is derived from the range of radiocarbon dates available for the site. Shell weight per volume unit of sediment comes from the >2 mm fraction of one-liter bulk samples collected across the site's vertical and horizontal extent (40 in total; Lubell, personal communication). The fish data come from the analysis of five 1 m² excavation units and the density of fish remains has therefore been calculated against their area and volume only.
Barranco das Quebradas	Open air Sagres Portugal	Of this string of localities, two (1 and 3) may correspond to collapsed rock-shelters. All are found in the last few hundred meters of a narrow, 1300 m-long gorge that drains the adjacent plateau to the Praia do Telheiro sandy beach. Given the time of occupation, ~8-10 ka, a sea level lowered by 10-15 m relative to present is to be expected, but such a difference of elevation is of little consequence for the estimation of distance to shore because this is a rocky coast of vertical cliffs. The evidence comes from small-scale testing, undertaken 2002-04, and is based on specimen counts that include field-collected and sieve-sorted material (a 3 mm mesh was used). The duration of site use can only be estimated for localities 1 and 3, which have radiocarbon dates spanning the stratigraphic sequence.

Table S44. Last Interglacial coastal sites of Iberia and the Maghreb. Criteria used to estimate age and distance to shoreline, and to calculate proxy indexes for the importance of aquatic foods

Sites	Type, location	Observations
El Cuco (EC)	Rock-shelter Cantabria Spain	Once considered Aurignacian, the basal layers of the sequence (VII-XIII) lay below a thick carbonated crust and contain Middle Paleolithic stone tools. They have been dated by radiocarbon using limpet shells: three results, two for layer X (OxA-27115 and OxA-27196) and one for layer XIII (OxA-30851), yielded finite ages ranging between 42,350±700 and 46,400±800 BP, while the result for layer XII is an infinite date, >43,500 BP (Beta- 382681). As was eventually shown to be the case at Aviones and Figueira Brava, these dates must be minimum ages only and, given the abundance of marine mollusk remains, it is quite likely that the El Cuco deposit is of Last Interglacial age too. A rough estimate of distance to shore can be obtained by adding the current distances from the site to the coastline (350 m) and to the -20 m isobath (1300 m). The shell assemblage combines the excavated and water-sieved finds (fine mesh; size not given, probably in the 2-4 mm range). The deposit's volume is estimated from published plans and profiles.
Aviones (AV)	Cave Cartagena Bay Spain	It is not until after 120 ka that a lowered sea level would have allowed the accumulation of the archeological deposit overlying the Last Interglacial beachrock, and the capping flowstone dates to 114 ka, so a duration of four millennia is estimated. In front of the cave, 20 m and 50 m offshore, the sea bottom lies at -4 m and -15 m (the latter being the average low stand found ~115 ka), so an average site-to-shore distance of 40 m throughout is posited. Sieving of the excavated sediments with a fine mesh (~3 mm) is demonstrated by photographic evidence and the size ranges represented in the museum-stored finds. The number of individuals per taxon reported in Montes (*189*) is interpreted as the assemblage's MNI, while the NISP corresponds to Zilhão *et al.*'s (*28*) specimen counts (which, however, were not exhaustive). The area and volume data are based on published plans and the original field notes.
Bajondillo (BJ)	Rock-shelter Malaga Bay Spain	Published reports assign levels 18 and 19 to MIS 5e (~118 ka) and MIS 6 (~166 ka), respectively. The latter is based on U-series bone dates of 151.2±14.6 and 149.4±9.6 ka calculated under a specific LU (Linear Uptake) assumption. However, under EU (Early Uptake) and different LU assumptions, the results are much younger (65.6±3.6 to 76.1±7.2 ka). The underlying stalagmitic crust (level 20) dates to 139.9/+33.0/-26.0 ka, flowstone is a reliable material for U-Th dating (unlike bone) and, despite its imprecision, this result can confidently be used as a *terminus post quem* that, combined with the thermophilous pollen assemblage, places levels 18 and 19 in the Last Interglacial, probably MIS 5e. At that time, the site would have stood ~10 m above a shoreline located ~50 m away. The total excavated volume of levels 18 and 19 (~60 l) comes from a length and an average thickness of 5 m and 14 cm, for level 18, and 2 m and 17 cm for level 19, respectively. These numbers imply that the sampled sediment represents the cutting back of ~6 cm of a profile. The density values for level 19 derive from the total sample (all shell from the entire volume of excavated deposit, ~17 l), and those for level 18 derive from a sub-sample of 7.5 l. Both are based on counting all shell fragments >0.5 mm.
Contrebandiers	Cave Témara Morocco	The data come from the 2007-11 excavations, during which the sediment was wet screened at the site through 1 cm and 2 mm meshes. Above beachrock and under the Holocene and Iberomaurusian levels, mostly removed during earlier phases of excavation, the stratigraphic succession features Last Interglacial occupations. In the CEA (Central Excavation Area) sector, this deposit is ~3 m-thick and features a sequence of Aterian (layer 4) over Mousterian (layers 5-6) phases. The uncertainty intervals associated with the OSL, TL and ESR dates are large, but are considered to show that the Mousterian in layer 5 is of MIS 5c-5d age and the Aterian in layer 4 is of MIS 5c age. Here, given the much higher abundance of shells in the Aterian, it has been assumed that the Mousterian occupation falls in MIS 5d (but note that, within each phase, significant difference exists between individual stratigraphic units). Distances to shoreline of 2500 m for the Mousterian and 1750 m for the Aterian are rough estimates based on the distance between the site and the -30 m and -20 m isobaths off Témara, assumed to represent the average position of the coastline during MIS 5d and 5c, respectively. In this stretch of the Moroccan coast, contour lines are very close and regularly spaced, and the depth of -50 m is found ~4 km off the Contrebandiers beach; therefore, considering the minor sea level oscillations that occurred within MIS 5d and MIS 5c would impact those distance estimates minimally. Shell counts use the piece-plotted material plus that retrieved from 1 cm screens.

Table S45. Last Interglacial coastal sites of South Africa. Criteria used to estimate age and distance to shoreline, and to calculate proxy indexes for the importance of aquatic foods

Sites	Type, location	Observations
Hoedjiespunt 1 (HDP1)	Open air Saldanha Bay South Africa	The site lies directly on the coastline at +15 m, and its dating to MIS 5e is consistent with a distance to the shoreline like at the present time. The area, volume and density values in kg/m³ derive from Will *et al.* (*32*) and concern the field-collected and sieve-sorted material of the 2011 excavations, when a 2 mm mesh was used. Jerardino (*177*) uses the volume information in Will *et al.* but would seem to have calculated MNI/m³ values from the MNI provided in Kyriacou *et al.* (*198*). In the latter, however, the shellfish remains from 2011 are pooled with those from the older, 1993-1998 field seasons and with those from a surface collection at HDP3, located a few kilometers away. Even though reproduced here, Jerardino's MNI/m³ values are therefore overestimated, probably by a significant margin.
Ysterfontein 1 (YFT1)	Rock-shelter Saldanha Bay South Africa	The site's bedrock lies at +7 m, and the OSL dates for the richest parts of the sedimentary fill (Middle and Lower, Groups 4-13) range between 120.6±6.6 ka (for Group 6) and 127.5±8.8 ka (for Group 13). This evidence suggests occupation towards the end of MIS 5e, when modelled sea level off South Africa was like present (-1.16 to +2.20 m between 119.0 and 121.4 ka) and, consequently, so were distances to the shore. Published shell weight data concern the field-collected and sieve-sorted material (a 1.5 mm mesh was used) but subsume ostrich egg-shell, whose proportion is negligible only in Groups 7 and 13, in the Lower part of the deposit. These two groups were therefore selected for tabulation (Group 7 is the richest in the sequence; it yielded 35.7 kg of marine shell remains). The volume of the deposit was calculated from grid plan and profile data. For comparison, Jerardino's (*177*) overall site averages, in NISP/m³ and MNI/m³, are included.
Blombos (BBC)	Cave Mossel Bay South Africa	Fisher *et al.*'s (2010) model of sea level off Blombos returns a constant minimum distance to the shoreline of 1450 m for phase M3, corresponding to sea levels of -5.70 to -14.85 m. For the M2 and M1 phases, the minimum distances can be much higher (>7000 m at 72.5 ka) but are the same most of the time. However, Cawthra *et al.* (*56*) find that within only 650-810 m from the extant shore a depth of 12 m can be reached and that at ~1 km and a depth of 24 m there is an outcrop of foreshore deposits, Unit 18, dated to 93.9±5 ka, during a stillstand-to-regressive phase towards the end of MIS 5c. Based on Jacobs *et al.* (*179*), phases M1 and M2 and the shellfish-rich upper part of M3 are of MIS 5a age, when sea level was at its highest since the end of MIS 5e and therefore closer-by than during the formation of Cawthra *et al.*'s (*56*) Unit 18. Assuming that most shellfish would have been collected when the sea was closer, the distance to shore was posited at 650 m throughout. The shellfish counts concern the field-collected and sieve-sorted material (a 3 mm mesh was used), but only the three richest squares were analyzed.
Pinnacle Point 13B (PP13B)	Rock-shelter Mossel Bay South Africa	Only the richest stratigraphic units are tabulated. Dating follows the assignment to sub-stages of MIS 5 given by Marean (*54*). Sea level models for the region indicate elevations of -11.42 to -44.72 m for the 104-116 ka interval, and of -5.45 to +6.30 m for the 117.5-128.8 ka interval. Considering bathymetry, these elevations translate into average distances to shoreline of 500-2870 m during MIS 5c and of 80 m through MIS 5e. Under the reasonable assumption that most shellfish accumulation happened when the shoreline was closest, the 500 m distance was retained as typical for the MIS 5c occupations. The shellfish counts concern the field-collected and sieve-sorted material (a 3 mm mesh was used). The volume information used for the MNI/m³ calculation is derived from Jerardino and Marean (*199: Table 3*).
Klasies River (KR)	Caves (1, 1A, 1B) Tsitsikamma coast South Africa	The sources use Thackeray's (*55*) density numbers (based on the material from Deacon's work, during which sieving was carried out with a 3 mm mesh) with the updates required by subsequent revision of the site's culture-stratigraphic groupings. Distances to shoreline are based on Feathers' (*200*) OSL dates and on Wurz *et al.*'s (*201*) U-series age constraints for the base of the SAS member; they halve those for the MIS 5e and MIS 5c of Pinnacle Point because the latter is situated ~200 km to the west, where the continental platform is twice as wide. Fish remains were retrieved through the sequence, but taphonomic analysis concluded that most represent natural accumulations.

References

1. S. C. Cunnane, M. A. Crawford, Energetic and nutritional constraints on infant brain development: implications for brain expansion during human evolution. *Journal of Human Evolution* **77**, 88-98 (2014).

2. J. C. Joordens, R. S. Kuipers, J. H. Wanink, F. A. Muskiet, A fish is not a fish: patterns in fatty acid composition of aquatic food may have had implications for hominin evolution. *Journal of Human Evolution* **77**, 107-116 (2014).

3. K. Kyriacou, J. E. Parkington, A. D. Marais, D. R. Braun, Nutrition, modernity and the archaeological record: coastal resources and nutrition among Middle Stone Age hunter-gatherers on the Western Cape coast of South Africa. *Journal of Human Evolution* **77**, 64-73 (2014).

4. M. C. Stiner, Thirty years on the "Broad Spectrum Revolution" and paleolithic demography. *Proceedings of the National Academy of Sciences* **98**, 6993-69936 (2001).

5. M. A. Zeder, The Broad Spectrum Revolution at 40: Resource diversity, intensification, and an alternative to optimal foraging explanations. *Journal of Anthropological Archaeology* **31**, 241-264 (2012).

6. P. Mellars, K. C. Gori, M. Carr, P. A. Soares, M. B. Richards, Genetic and archaeological perspectives on the initial modern human colonization of southern Asia. *Proceedings of the National Academy of Sciences* **110**, 10699-10704 (2013).

7. S. Oppenheimer, The great arc of dispersal of modern humans: Africa to Australia. *Quaternary International* **202**, 2-13 (2009).

8. C. W. Marean, The origins and significance of coastal resource use in Africa and Western Eurasia. *Journal of Human Evolution* **77**, 17-40 (2014).

9. C. W. Marean, The transition to foraging for dense and predictable resources and its impact on the evolution of modern humans. *Philosophical Transactions of the Royal Society B: Biological Sciences* **371**, 20150239 (2016).

10. M. Will, A. W. Kandel, N. J. Conard, Midden or Molehill: The Role of Coastal Adaptations in Human Evolution and Dispersal. *Journal of World Prehistory* **32**, 33-72 (2019).

11. R. G. Klein, D. W. Bird, Shellfishing and human evolution. *Journal of Anthropological Archaeology* **44**, 198-205 (2016).

12. E. Trinkaus, M. Samsel, S. Villotte, External auditory exostoses among western Eurasian late Middle and Late Pleistocene humans. *PLoS ONE* **14**, e0220464 (2019).

13. A. C. Colonese *et al.*, Marine mollusc exploitation in Mediterranean prehistory: An overview. *Quaternary International* **239**, 86-103 (2011).

14. K. Douka, E. E. Spinapolice, Neanderthal Shell Tool Production: Evidence from Middle Palaeolithic Italy and Greece. *Journal of World Prehistory* **25**, 45-79 (2012).

15. F. Romagnoli, J. Baena, L. Sarti, Neanderthal retouched shell tools and Quina economic and technical strategies: An integrated behaviour. *Quaternary International* **407**, 29-44 (2016).

16. M. A. Mannino *et al.*, Origin and Diet of the Prehistoric Hunter-Gatherers on the Mediterranean Island of Favignana (Ègadi Islands, Sicily). *PLoS ONE* **7**, e49802 (2012).

17. M. A. Mannino *et al.*, Upper Palaeolithic hunter-gatherer subsistence in Mediterranean coastal environments: an isotopic study of the diets of the earliest directly-dated humans from Sicily. *Journal of Archaeological Science* **38**, 3094-3100 (2011).

18. A. Chakroun *et al.*, The Pleistocene of Rabat (Morocco): Mollusks, Coastal Environments and Human Behavior. *African Archaeological Review* **34**, 493-510 (2017).

19. G. L. Dusseldorp, G. H. J. Langejans, Carry that weight: coastal foraging and transport of marine resources during the South African Middle Stone Age. *Southern African Humanities* **25**, 105-135 (2013).

20. K. Hardy *et al.*, Shellfishing and shell midden construction in the Saloum Delta, Senegal. *Journal of Anthropological Archaeology* **41**, 19-32 (2016).

21. L. G. Straus, *Iberia before the Iberians*. (University of New Mexico Press, Albuquerque, 1992).

22. J. E. Arnaud, in *The Mesolithic in Europe. Papers presented at the Third International Symposium,* C. Bonsall, Ed. (John Donald, Edinburgh, 1989), pp. 614-631.

23. M. T. Antunes, Ed., *Últimos Neandertais em Portugal. Evidência, odontológica e outra*, (Academia das Ciências, Lisboa, 2000).

24. P. Brito, Thesis, University of Lisbon, (2009).

25. E. Badal, in *Las culturas del Pleistoceno superior en Andalucía,* J. L. Sanchidrián, M. D. Simón, Eds. (Patronato de la Cueva de Nerja, Málaga, 1998), pp. 287-300.

26. D. E. Bar-Yosef Mayer, B. Vandermeersch, O. Bar-Yosef, Shells and ochre in Middle Paleolithic Qafzeh Cave, Israel: indications for modern behavior. *Journal of Human Evolution* **56**, 307-314 (2009).

27. D. L. Hoffmann, D. E. Angelucci, V. Villaverde, J. Zapata, J. Zilhão, Symbolic use of marine shells and mineral pigments by Iberian Neandertals 115,000 years ago. *Science Advances* **4**, eaar5255 (2018).

28. J. Zilhão *et al.*, Symbolic use of marine shells and mineral pigments by Iberian Neandertals. *Proceedings of the National Academy of Sciences* **107**, 1023-1028 (2010).

29. M. Nabais, J. Zilhão, The consumption of tortoise among Last Interglacial Iberian Neanderthals. *Quaternary Science Reviews* **217**, 225-246 (2019).

30. E. J. Guiry, M. Hillier, M. P. Richards, Mesolithic Dietary Heterogeneity on the European Atlantic Coastline. Stable Isotope Insights into Hunter-Gatherer Diet and Subsistence in the Sado Valley, Portugal. *Current Anthropology* **56**, 460-470 (2015).

31. D. Lubell, M. Jackes, H. Schwarcz, M. Knyf, C. Meiklejohn, The Mesolithic-Neolithic Transition in Portugal: Isotopic and Dental Evidence of Diet. *Journal of Archaeological Science* **21**, 201-216 (1994).

32. M. Will, A. W. Kandel, N. J. Conard, in *Settlement Dynamics of the Middle Paleolithic and Middle Stone Age,* N. J. Conard, A. Delagnes, Eds. (Kerns Verlag, Tübingen, 2015), vol. IV, chap. 4, pp. 47-75.

33. M. J. Brenner, S. Wurz, A high-resolution perspective on MIS 5c-d lithic assemblages from Klasies River main site Cave 1. *Journal of Archaeological Science: Reports* **26**, 101891 (2019).

34. F. E. Grine, S. Wurz, C. W. Marean, The Middle Stone Age human fossil record from Klasies River Main Site. *Journal of Human Evolution* **103**, 53-78 (2017).

35. C. Henshilwood *et al.*, An abstract drawing from the 73,000-year-old levels at Blombos Cave, South Africa. *Nature* **562**, 115-118 (2018).

36. C. Henshilwood, F. d'Errico, M. Vanhaeren, K. van Niekerk, Z. Jacobs, Middle Stone Age Shell Beads from South Africa. *Science* **304**, 404 (2004).

37. C. S. Henshilwood *et al.*, A 100,000-Year-Old Ochre-Processing Workshop at Blombos Cave, South Africa. *Science* **334**, 219-222 (2011).

38. C. S. Henshilwood *et al.*, Emergence of Modern Human Behavior: Middle Stone Age Engravings from South Africa. *Science* **295**, 1278-1280 (2002).

39. H. J. Deacon, V. B. Geleijnse, The Stratigraphy and Sedimentology of the Main Site Sequence, Klasies River, South Africa. *The South African Archaeological Bulletin* **43**, 5-14 (1988).

40. P. Karkanas, K. S. Brown, E. C. Fisher, Z. Jacobs, C. W. Marean, Interpreting human behavior from depositional rates and combustion features through the study of sedimentary microfacies at site Pinnacle Point 5-6, South Africa. *Journal of Human Evolution* **85**, 1-21 (2015).

41. C. W. Marean *et al.*, The stratigraphy of the Middle Stone Age sediments at Pinnacle Point Cave 13B (Mossel Bay, Western Cape Province, South Africa). *Journal of Human Evolution* **59**, 234-255 (2010).

42. N. Barton, in *Neanderthals on the edge: 150th anniversary conference of the Forbes' Quarry discovery, Gibraltar,* C. Stringer, R. N. E. Barton, C. Finlayson, Eds. (Oxbow Books, Oxford, 2000), chap. 23, pp. 211-220.

43. R. I. Macphail, P. Goldberg, in *Neanderthals on the edge: 150th anniversary conference of the Forbes' Quarry discovery, Gibraltar,* C. B. Stringer, R. N. E. Barton, C. Finlayson, Eds. (Oxbow Books, Oxford, 2000), chap. 20, pp. 182-200.

44. I. Gutiérrez-Zugasti *et al.*, The role of shellfish in hunter–gatherer societies during the Early Upper Palaeolithic: A view from El Cuco rockshelter, northern Spain. *Journal of Anthropological Archaeology* **32**, 242-256 (2013).

45. I. Gutiérrez-Zugasti *et al.*, A chrono-cultural reassessment of the levels VI–XIV from El Cuco rock-shelter: A new sequence for the Late Middle Paleolithic in the Cantabrian region (northern Iberia). *Quaternary International* **474**, 44-55 (2018).

46. K. Jaouen *et al.*, Exceptionally high δ^{15}N values in collagen single amino acids confirm Neandertals as high-trophic level carnivores. *Proceedings of the National Academy of Sciences* **116**, 4928-4933 (2019).

47. D. L. Hoffmann *et al.*, U-Th dating of carbonate crusts reveals Neandertal origin of Iberian cave art. *Science* **359**, 912-915 (2018).

48. D. Lubell, M. Jackes, in *Actas da I Reunião do Quaternário Ibérico*. (Grupo de Trabalho Português para o Estudo do Quaternário, Lisboa, 1985), vol. 2, pp. 113-133.

49. D. Lubell, M. Jackes, P. Sheppard, P. Rowley-Conwy, in *From the Mediterranean basin to the Portuguese Atlantic Shore: Papers in Honor of Anthony Marks,* N. Bicho, Ed. (Universidade do Algarve, Faro, 2007), pp. 119-139.

50. H. L. Dibble *et al.*, New Excavations at the Site of Contrebandiers Cave, Morocco. *Paleoanthropology* **2012**, 145–201 (2012).

51. E. C. Fisher, M. Bar-Matthews, A. Jerardino, C. W. Marean, Middle and Late Pleistocene paleoscape modeling along the southern coast of South Africa. *Quaternary Science Reviews* **29**, 1382-1398 (2010).

52. C. S. Henshilwood *et al.*, Blombos Cave, Southern Cape, South Africa: Preliminary Report on the 1992–1999 Excavations of the Middle Stone Age Levels. *Journal of Archaeological Science* **28**, 421-448 (2001).

53. G. H. J. Langejans, K. L. van Niekerk, G. L. Dusseldorp, J. F. Thackeray, Middle Stone Age shellfish exploitation: Potential indications for mass collecting and resource intensification at Blombos Cave and Klasies River, South Africa. *Quaternary International* **270**, 80-94 (2012).

54. C. W. Marean, Pinnacle Point Cave 13B (Western Cape Province, South Africa) in context: The Cape Floral kingdom, shellfish, and modern human origins. *Journal of Human Evolution* **59**, 425-443 (2010).

55. J. F. Thackeray, Molluscan Fauna from Klasies River, South Africa. *The South African Archaeological Bulletin* **43**, 27-32 (1988).

56. H. C. Cawthra *et al.*, Depositional and sea-level history from MIS 6 (Termination II) to MIS 3 on the southern continental shelf of South Africa. *Quaternary Science Reviews* **181**, 156-172 (2018).

57. A. Ribeiro, M. C. Kullberg, J. C. Kullberg, G. Manuppella, S. Phipps, A review of Alpine tectonics in Portugal: Foreland detachment in basement and cover rocks. *Tectonophysics* **184**, 357-366 (1990).

58. A. F. Fonseca, J. L. Zêzere, M. Neves, Geomorphology of the Arrábida Chain (Portugal). *Journal of Maps* **10**, 103-108 (2014).

59. M. J. Alcoforado *et al.*, in *Geografia Física em Regiões de Montanha: A Ilha da Madeira e as Serras da Arrábida e da Estrela. Homenagem a Orlando Ribeiro,* C. Mora, Ed. (Centro de Estudos Geográficos, Lisboa, 2014), pp. 11-50.

60. J. C. Kullberg, P. Terrinha, J. Pais, R. P. Reis, L. P., in *Geologia de Portugal no contexto da Ibéria,* R. Dias, A. Araújo, P. Terrinha, J. C. Kullberg, Eds. (Universidade de Évora, Évora, 2006), pp. 369-396.

61. G. Manuppella, Ed., *Notícia explicativa da folha 38-B Setúbal, esc. 1:50 000,* (Instituto Geológico e Mineiro, Lisboa, 1999).

62. H. Breuil, G. Zbyszewski, Contribution à I'étude des industries paléolithiques du Portugal et leurs rapports avec la géologie du Quaternaire. Les principaux gisements des plages quaternaires du littoral d'Estremadura et des terrasses fluviales de la basse vallée du Tage. *Comunicações dos Serviços Geológicos de Portugal* **XXVII**, 1-678 (1945).

63. C. T. Silva, J. Soares, *Arqueologia da Arrábida*. (Serviço Nacional de Parques, Reservas e Conservação de Natureza, Lisboa, 1986).

64. G. Cuenca-Bescós *et al.*, Pleistocene history of *Iberomys*, an endangered endemic rodent from southwestern Europe. *Integrative Zoology* **9**, 481-497 (2014).

65. P. Bullock *et al.*, *Handbook for soil thin section description*. (Waine Research, Albrighton, Wolverhampton, 1985).

66. G. Stoops, Ed., *Guidelines for Analysis and Description of Soil and Regolith Thin Sections*, (Soil Science Society of America, Madison, 2003).

67. A. C. Araújo, Ed., *O concheiro de Toledo no contexto do Mesolítico Inicial do litoral da Estremadura*, (Instituto de Gestão do Património Arquitectónico e Arqueológico, Lisboa, 2011), pp. 255.

68. F. Brock, T. Higham, P. Ditchfield, C. B. Ramsey, Current Pretreatment Methods for AMS Radiocarbon Dating at the Oxford Radiocarbon Accelerator Unit (ORAU). *Radiocarbon* **52**, 103-112 (2010).

69. P. J. Reimer *et al.*, IntCal13 and Marine13 Radiocarbon Age Calibration Curves 0–50,000 Years cal BP. *Radiocarbon* **55**, 1869-1887 (2016).

70. D. L. Hoffmann, A. W. G. Pike, M. García-Diez, P. B. Pettitt, J. Zilhão, Methods for U-series dating of $CaCO_3$ crusts associated with Palaeolithic cave art and application to Iberian sites. *Quaternary Geochronology* **36**, 104-119 (2016).

71. D. L. Hoffmann *et al.*, Procedures for accurate U and Th isotope measurements by high precision MC-ICPMS. *International Journal of Mass Spectrometry* **264**, 97-109 (2007).

72. A. H. Jaffey, K. F. Flynn, L. E. Glendenin, W. C. Bentley, A. M. Essling, Precision Measurement of Half-Lives and Specific Activities of ^{235}U and ^{238}U. *Physical Review C* **4**, 1889-1906 (1971).

73. H. Cheng *et al.*, The half-lives of uranium-234 and thorium-230. *Chemical Geology* **169**, 17-33 (2000).

74. N. E. Holden, Total Half-Lives for Selected Nuclides. *Pure and Applied Chemistry* **62**, 941-958 (1990).

75. K. H. Wedepohl, The Composition of the Continental-Crust. *Geochimica et Cosmochimica Acta* **59**, 1217-1232 (1995).

76. K. R. Ludwig, D. M. Titterington, Calculation of ^{230}ThU isochrons, ages, and errors. *Geochimica et Cosmochimica Acta* **58**, 5031-5042 (1994).

77. M. Demuro, L. J. Arnold, D. G. Froese, R. G. Roberts, OSL dating of loess deposits bracketing Sheep Creek tephra beds, northwest Canada: Dim and problematic single-grain OSL characteristics and their effect on multi-grain age estimates. *Quaternary Geochronology* **15**, 67-87 (2013).

78. L. J. Arnold, M. Demuro, M. Navazo, A. Benito Calvo, A. Pérez-González, OSL dating of the Middle Paleolithic Hotel California site, Sierra de Atapuerca, north-central Spain. *Boreas* **42**, 285-305 (2013).

79. L. J. Arnold *et al.*, OSL dating of individual quartz 'supergrains' from the Ancient Middle Palaeolithic site of Cuesta de la Bajada, Spain. *Quaternary Geochronology* **36**, 78-101 (2016).

80. V. Hansen, A. Murray, J.-P. Buylaert, E.-Y. Yeo, K. Thomsen, A new irradiated quartz for beta source calibration. *Radiation Measurements* **81**, 123-127 (2015).

81. L. J. Arnold, M. Demuro, M. N. Ruiz, Empirical insights into multi-grain averaging effects from 'pseudo' single-grain OSL measurements. *Radiation Measurements* **47**, 652-658 (2012).

82. A. S. Murray, A. G. Wintle, Luminescence dating of quartz using an improved single-aliquot regenerative-dose protocol. *Radiation Measurements* **32**, 57-73 (2000).

83. R. Galbraith, A note on the variance of a background-corrected OSL. *Ancient TL* **20**, 49-51 (2002).

84. Z. Jacobs, G. Duller, A. G. Wintle, Interpretation of single grain De distributions and calculation of De. *Radiation Measurements* **41**, 264-277 (2006).

85. G. A. T. Duller, Assessing the error on equivalent dose estimates derived from single aliquot regenerative dose measurements. *Ancient TL* **25**, 15-24 (2007).

86. L. J. Arnold, M. Duval, C. Falguères, J. J. Bahain, M. Demuro, Portable gamma spectrometry with cerium-doped lanthanum bromide scintillators: Suitability assessments for luminescence and electron spin resonance dating applications. *Radiation Measurements* **47**, 6-18 (2012).

87. L. Bøtter-Jensen, V. Mejdahl, Assessment of beta dose-rate using a GM multicounter system. *International Journal of Radiation Applications and Instrumentation. Part D. Nuclear Tracks and Radiation Measurements* **14**, 187-191 (1988).

88. P. J. Potts, M. Thompson, S. R. N. Chenery, P. C. Webb, H. U. Kasper, "Geopt13 - An International Proficiency Test for Analytical Geochemistry Laboratories - Report on Round 13 / July 2003 (Köln Loess)," (2003).

89. B. J. Brennan, Beta doses to spherical grains. *Radiation Measurements* **37**, 299-303 (2003).

90. C. Lesley, Analysing environmental radioactivity in soils and sediments using high-purity germanium gamma detectors at CSIRO Land and Water: Procedures and Protocols. *CSIRO Land and Water Science Report series* **12/09**, (2009).

91. J. R. Prescott, J. T. Hutton, Cosmic ray contributions to dose rates for luminescence and ESR dating: Large depths and long-term time variations. *Radiation Measurements* **23**, 497-500 (1994).

92. V. Mejdahl, Internal radioactivity in quartz and feldspar grains. *Ancient TL* **5**, 10-17 (1987).

93. J. Bowler *et al.*, New ages for human occupation and climatic change at Lake Mungo, Australia. *Nature* **421**, 837-840 (2003).

94. S. M. Pawley *et al.*, Age limits on Middle Pleistocene glacial sediments from OSL dating, north Norfolk, UK. *Quaternary Science Reviews* **27**, 1363-1377 (2008).

95. J. Rees-Jones, M. S. Tite, Optical Dating Results for British Archaeological Sediments. *Archaeometry* **39**, 177-187 (1997).

96. J. Rees-Jones, Optical dating of young sediments using fine-grain quartz. *Ancient TL* **13**, 9-14 (1995).

97. G. Guérin, N. Mercier, G. Adamiec, Dose-rate conversion factors: Update. *Ancient TL* **29**, 5-8 (2011).

98. V. Mejdahl, Thermoluminescence dating: beta-dose attenuation in quartz grains. *Archaeometry* **21**, 61-72 (1979).

99. M. J. Aitken, *Thermoluminescence Dating*. (Academic Press, London, 1985).

100. E. Badal, V. Villaverde, J. Zilhão, in *Wood and charcoal. Evidence for human and natural History,* E. Badal, Y. Carrión, M. Macías, M. Ntinou, Eds. (Universitat de València, València, 2012), pp. 13-24.

101. F. H. Schweingruber, *Anatomie europäischer Hölzer. Ein Atlas zur Bestimmung europäischer Baum-, Strauch- und Zwergstrauchhölzer*, Feddes Repertorium (Eidgenössische Forschungsanstalt für Wald, Schnee und Landschaft; Haupt, Birmensdorf; Bern, 1990), pp. 800.

102. C. Dupont, *La malacofaune de sites mésolithiques et néolithiques de la façade atlantique de la France: contribution à l'économie et à l'identité culturelle des groupes concernés*. British Archaeological Reports British Series (Archaeopress, Oxford, 2006), pp. 438.

103. I. Gutiérrez-Zugasti, *La explotación de moluscos y otros recursos litorales en la región cantábrica durante el Pleistoceno final y el Holoceno inicial*. (Ediciones de la Universidad de Cantabria, Santander, 2009), pp. 539.

104. M. Igreja, in *200 séculos da história do Vale do Côa: incursões na vida quotidiana dos caçadores-recolectores do Paleolítico,* T. Aubry, Ed. (IGESPAR, IP Lisboa, 2009), pp. 235-247.

105. M. Igreja, M. Moreno-García, C. Pimenta, Um exemplo de abordagem experimental de interface Traceologia lítica/Arqueozoologia: esquartejamento e tratamento da pele de um corço (*Capreolus capreolus*) com artefactos de pedra lascada. *Revista Portuguesa de Arqueologia* **10**, 17-34 (2007).

106. T. Aubry, M. Igreja, in *Recent functional studies on non-flint stone tools: Methodological improvements and archaeological inferences. Proceedings of the workshop,* M. Igreja, I. Clemente-Conte, Eds. (2009).

107. J. Pais, P. Legoinha, in *Últimos Neandertais em Portugal. Evidência, odontológica e outra,* M. T. Antunes, Ed. (Academia das Ciências, Lisboa, 2000), pp. 69-80.

108. A. M. M. Soares, J. M. A. Dias, Coastal Upwelling and Radiocarbon—Evidence for Temporal Fluctuations in Ocean Reservoir Effect off Portugal During the Holocene. *Radiocarbon* **48**, 45-60 (2006).

109. R. Soares, Thesis, University of Lisbon, (2012).

110. F. S. Busschers *et al.*, Radiocarbon Dating of Late Pleistocene Marine Shells from the Southern North Sea. *Radiocarbon* **56**, 1151-1166 (2014).

111. A. W. G. Pike *et al.*, U-Series Dating of Paleolithic Art in 11 Caves in Spain. *Science* **336**, 1409-1413 (2012).

112. L. J. Arnold, M. Demuro, Insights into TT-OSL signal stability from single-grain analyses of known-age deposits at Atapuerca, Spain. *Quaternary Geochronology* **30**, 472-478 (2015).

113. H. Yoshida, R. G. Roberts, J. M. Olley, G. M. Laslett, R. F. Galbraith, Extending the age range of optical dating using single 'supergrains' of quartz. *Radiation Measurements* **32**, 439-446 (2000).

114. Z. Jacobs, A. G. Wintle, R. G. Roberts, G. Duller, Equivalent dose distributions from single grains of quartz at Sibudu, South Africa: Context, causes and consequences for optical dating of archaeological deposits. *Journal of Archaeological Science* **35**, 1808-1820 (2008).

115. L. J. Arnold *et al.*, Paper II - Dirt, dates and DNA: OSL and radiocarbon chronologies of perennially frozen sediments in Siberia, and their implications for sedimentary ancient DNA studies. *Boreas* **40**, 417-445 (2011).

116. L. J. Arnold, R. G. Roberts, Stochastic modelling of multi-grain equivalent dose (De) distributions: Implications for OSL dating of sediment mixtures. *Quaternary Geochronology* **4**, 204-230 (2009).

117. J. M. Olley, T. Pietsch, R. G. Roberts, Optical dating of Holocene sediments from a variety of geomorphic settings using single grains of quartz. *Geomorphology* **60**, 337-358 (2004).

118. L. J. Arnold, R. G. Roberts, R. F. Galbraith, S. B. DeLong, A revised burial dose estimation procedure for optical dating of young and modern-age sediments. *Quaternary Geochronology* **4**, 306-325 (2009).

119. L. J. Arnold, R. M. Bailey, G. E. Tucker, Statistical treatment of fluvial dose distributions from southern Colorado arroyo deposits. *Quaternary Geochronology* **2**, 162-167 (2007).

120. R. Roberts *et al.*, Optical and radiocarbon dating at Jinmium rock shelter in northern Australia. *Nature* **393**, 358-362 (1998).

121. J. M. Olley, R. G. Roberts, A. S. Murray, Disequilibria in the uranium decay series in sedimentary deposits at Allen's cave, nullarbor plain, Australia: Implications for dose rate determinations. *Radiation Measurements* **27**, 433-443 (1997).

122. R. P. Nathan, P. J. Thomas, M. Jain, A. S. Murray, E. J. Rhodes, Environmental dose rate heterogeneity of beta radiation and its implications for luminescence dating: Monte Carlo modelling and experimental validation. *Radiation Measurements* **37**, 305-313 (2003).

123. L. J. Arnold *et al.*, Luminescence dating and palaeomagnetic age constraint on hominins from Sima de los Huesos, Atapuerca, Spain. *Journal of Human Evolution* **67**, 85-107 (2014).

124. R. F. Galbraith, R. G. Roberts, G. M. Laslett, H. Yoshida, J. M. Olley, Optical dating of single and multiple grains of quartz from Jinmium rock shelter, northern Australia: Part I, Experimental design and statistical models. *Archaeometry* **41**, 339-364 (1999).

125. J. M. Olley, G. G. Caitcheon, R. G. Roberts, The origin of dose distributions in fluvial sediments, and the prospect of dating single grains from fluvial deposits using optically stimulated luminescence. *Radiation Measurements* **30**, 207-217 (1999).

126. R. M. Bailey, L. J. Arnold, Statistical modelling of single grain quartz De distributions and an assessment of procedures for estimating burial dose. *Quaternary Science Reviews* **25**, 2475-2502 (2006).

127. L. J. Arnold *et al.*, Optical dating of perennially frozen deposits associated with preserved ancient plant and animal DNA in north-central Siberia. *Quaternary Geochronology* **3**, 114-136 (2008).

128. N. R. Jankowski, G. A. Gully, Z. Jacobs, R. G. Roberts, G. J. Prideaux, A late Quaternary vertebrate deposit in Kudjal Yolgah Cave, south-western Australia: refining regional late Pleistocene extinctions. *Journal of Quaternary Science* **31**, 538-550 (2016).

129. G. J. Prideaux *et al.*, Timing and dynamics of Late Pleistocene mammal extinctions in southwestern Australia. *Proceedings of the National Academy of Sciences* **107**, 22157-22162 (2010).

130. R. G. Roberts *et al.*, Preliminary Luminescence Dates for Archaeological Sediments on the Nullarbor Plain, South Australia. *Australian Archaeology* **42**, 7-16 (1996).

131. P. Goldberg, S. C. Sherwood, Deciphering human prehistory through the geoarcheological study of cave sediments. *Evolutionary Anthropology: Issues, News, and Reviews* **15**, 20-36 (2006).

132. J. Benjamin *et al.*, Late Quaternary sea-level changes and early human societies in the central and eastern Mediterranean Basin: An interdisciplinary review. *Quaternary International* **449**, 29-57 (2017).

133. L. Lisiecki, J. V. Stern, Regional and global benthic δ^{18}O stacks for the last glacial cycle: Last Glacial Cycle Benthic δ^{18}O. *Paleoceanography* **31**, 1368-1394 (2016).

134. S. O. Rasmussen *et al.*, A stratigraphic framework for abrupt climatic changes during the Last Glacial period based on three synchronized Greenland ice-core records: refining and extending the INTIMATE event stratigraphy. *Quaternary Science Reviews* **106**, 14-28 (2014).

135. C. Bronk Ramsey, Bayesian Analysis of Radiocarbon Dates. *Radiocarbon* **51**, 337-360 (2016).

136. J. A. Dorale *et al.*, Sea-level highstand 81,000 years ago in Mallorca. *Science* **327**, 860-863 (2010).

137. P. Figueiredo, Thesis, University of Lisbon, (2015).

138. J. M. Montoya, Ed., *El pino piñonero*, (Mundi-Prensa, Madrid, 1990), pp. 98.

139. C. Nergiz, İ. Dönmez, Chemical composition and nutritive value of *Pinus pinea* L. seeds. *Food Chemistry* **86**, 365-368 (2004).

140. S. M. Kidwell, in *Taphonomy: releasing the data locked in the fossil record,* A. P., D. Briggs, Eds. (Plenum Press, New York, 1991), pp. 211-290.

141. S. F. López, in *Tratado de Paleontología,* B. Meléndez, Ed. (Consejo Superior de Investigaciones Científicas, Madrid, 1999), pp. 51-107.

142. J. Haig, J. Pantin, H. Salomonsen, M. J. Kaiser, "Size at maturity of the edible crab (*Cancer pagurus*) in Welsh waters," *Fisheries & Conservation Science report No. 51* (Bangor University, 2015).

143. A. K. Woll, *The edible crab: biology, grading and handling live crabs*. (Møreforsking Marine, 2006).

144. J. M. Erlandson, M. L. Moss, Shellfish Feeders, Carrion Eaters, and the Archaeology of Aquatic Adaptations. *American Antiquity* **66**, 413-432 (2001).

145. A. C. F. Silva, S. J. Hawkins, D. M. Boaventura, E. Brewster, R. C. Thompson, Use of the intertidal zone by mobile predators: influence of wave exposure, tidal phase and elevation on abundance and diet. *Marine Ecology Progress Series* **406**, 197-210 (2010).

146. A. F. Ainis, R. L. Vellanoweth, Q. G. Lapeña, C. S. Thornber, Using non-dietary gastropods in coastal shell middens to infer kelp and seagrass harvesting and paleoenvironmental conditions. *Journal of Archaeological Science* **49**, 343-360 (2014).

147. F.-X. Chauvière, Industries et parures sur matières dures animales du Paléolithique supérieur de la grotte de Caldeirão (Tomar, Portugal). *Revista Portuguesa de Arqueologia* **5**, 5-28 (2002).

148. J. Zilhão *et al.*, Precise dating of the Middle-to-Upper Paleolithic transition in Murcia (Spain) supports late Neandertal persistence in Iberia. *Heliyon* **3**, e00435 (2017).

149. T. E. Steele, E. Álvarez-Fernández, E. Hallett-Desguez, Special issue: Personal ornaments in early Prehistory - A Review of Shells as Personal Ornamentation during the African Middle Stone Age. *Paleoanthropology* **2019**, 24-51 (2019).

150. F. d'Errico *et al.*, Additional evidence on the use of personal ornaments in the Middle Paleolithic of North Africa. *Proceedings of the National Academy of Sciences* **106**, 16051-16056 (2009).

151. S. Gabriel, Thesis, Autonomous University of Madrid, (2015).

152. J. D. Carrillo-Briceño, E. Maxwell, O. A. Aguilera, R. Sánchez, M. R. Sánchez-Villagra, Sawfishes and Other Elasmobranch Assemblages from the Mio-Pliocene of the South Caribbean (Urumaco Sequence, Northwestern Venezuela). *PLoS ONE* **10**, e0139230 (2015).

153. D. Jacoby, M. Gollock, in *The IUCN Red List of Threatened Species 2014*. (2014), pp. e.T60344A45833138.

154. J. P. Granadeiro, T. Catry, P. Catry, S. Pereira, A. Campos, "Distribuição e impacto do Corvo-marinho-de-faces-brancas sobre as comunidades ictiológicas do estuário do Sado," (Tróia-Natura S.A., 2013).

155. J. Zilhão *et al.*, Cueva Antón: A multi-proxy MIS 3 to MIS 5a paleoenvironmental record for SE Iberia. *Quaternary Science Reviews* **146**, 251-273 (2016).

156. A. Meirinho *et al.*, *Atlas das Aves Marinhas de Portugal. Sociedade Portuguesa para o Estudo das Aves*. (Sociedade Portuguesa para o Estudo das Aves, 2014).

157. D. Serjeantson, *Birds*. Cambridge Manuals in Archaeology (Cambridge University Press, Cambridge, 2009).

158. M. Peresani, I. Fiore, M. Gala, M. Romandini, A. Tagliacozzo, Late Neandertals and the intentional removal of feathers as evidenced from bird bone taphonomy at Fumane Cave 44 ky B.P., Italy. *Proceedings of the National Academy of Sciences* **108**, 3888-3893 (2011).

159. C. Finlayson *et al.*, Birds of a Feather: Neanderthal Exploitation of Raptors and Corvids. *PLoS ONE* **7**, e45927 (2012).

160. C. Pimenta, S. Figueiredo, M. Moreno-García, Novo registo de Pinguim (*Pinguinus impennis*) no Plistocénico de Portugal. *Revista Portuguesa de Arqueologia* **11**, 361-370 (2008).

161. F. d'Errico, Birds of the Grotte Cosquer: the Great Auk and Palaeolithic prehistory. *Antiquity* **11**, 47-57 (1994).

162. J. L. Cardoso, *Contribuição para o conhecimento dos grandes mamíferos do Plistocénico Superior de Portugal*. (Câmara Municipal de Oeiras, Oeiras, 1993).

163. J. L. Cardoso, F. T. Regala, Sobre a presença de mamute, *Mammuthus primigenius* (Blumembach, 1799) em Portugal: descoberta de uma lamela dentária em depósitos plistocénicos do fundo do estuário do Tejo (Cruz Quebrada, Oeiras). *Estudos Arqueológicos de Oeiras* **10**, 39-47 (2001-2002).

164. M. Nabais, in *Actas das IV Jornadas de Jovens em Investigação Arqueológica (Faro, 11 a 14 de Maio de 2011),* J. Cascalheira, C. Gonçalves, Eds. (Universidade do Algarve, Faro, 2012), vol. 1, pp. 381-385.

165. C. Tavares da Silva, J. Soares, *Arqueologia da Arrábida*. (Serviço Nacional de Parques, Reservas e Conservação de Natureza, Lisboa, 1986).

166. N. Pimentel, D. Nukushina, M. Diniz, P. Arias, in *Muge 150th: The 150th Anniversary of the Discovery of Mesolithic Shellmiddens,* N. Bicho, C. Detry, T. D. Price, E. Cunha, Eds. (Cambridge Scholars Publishing, Newcastle upon Tyne, 2015), vol. 1, chap. 23, pp. 321-332.

167. E. Leitão *et al.*, in *Extrair e produzir... Dos primeiros artefactos à industrialização,* J. C. Senna-Martinez, A. C. Martins, A. Caessa, A. Marques, I. Cameira, Eds. (Centro de Arqueologia de Lisboa, Lisboa, 2019), pp. 35-44.

168. N. Bicho *et al.*, Resilience, replacement and acculturation in the Mesolithic/Neolithic transition: The case of Muge, central Portugal. *Quaternary International* **446**, 31-42 (2017).

169. V. Aldeias, N. Bicho, Embedded Behavior: Human Activities and the Construction of the Mesolithic Shellmound of Cabeço da Amoreira, Muge, Portugal. *Geoarchaeology* **31**, 530-549 (2016).

170. N. Bicho *et al.*, Chronology of the Mesolithic occupation of the Muge valley, central Portugal: The case of Cabeço da Amoreira. *Quaternary International* **308-309**, 130-139 (2013).

171. C. Duarte, E. Iriarte, M. Diniz, P. Arias, The microstratigraphic record of human activities and formation processes at the Mesolithic shell midden of Poças de São Bento (Sado Valley, Portugal). *Archaeological and Anthropological Sciences* **11**, 483–509 (2019).

172. M. J. Valente, O Barranco das Quebradas (Vila do Bispo) no contexto dos concheiros mesolíticos no Sudoeste português. *Xelb* **10**, 16-38 (2010).

173. A. García-Escárzaga, I. Gutiérrez-Zugasti, M. R. González-Morales, in *La Investigación Arqueomalacológica en la Península Ibérica: Nuevas Aportaciones,* I. Gutiérrez Zugasti, D. Cuenca Solana, M. R. González Morales, Eds. (Nadir Ediciones, Santander, 2015), pp. 77-89.

174. A. García-Escárzaga, I. Gutiérrez-Zugasti, M. R. González-Morales, A. Cobo-García, Shells and Humans: Molluscs and Other Coastal Resources from the Earliest Human Occupations at the Mesolithic Shell Midden of El Mazo (Asturias, Northern Spain). *Papers from the Institute of Archaeology* **27**, 1-17 (2017).

175. J. D. Taylor, M. Layman, The mechanical properties of bivalve (Mollusca) shell structures. *Palaeontology* **15**, 73-87 (1972).

176. E. Muñoz-Fernández, P. Rasines del Río, S. Santamaría-Santamaría, J. M. Morlote-Expósito, in *Intervenciones arqueológicas en Castro Urdiales, tomo III. Arqueología y arte rupestre paleolítico en las cavidades de El Cuco o Sobera y La Lastrilla,* E. Muñoz-Fernández, R. Montes Barquín, Eds. (Excmo. Ayuntamiento de Castro Urdiales. Concejalía de Medio Ambiente y Patrimonio Arqueológico, Castro Urdiales, 2007), pp. 15-160.

177. A. Jerardino, On the origins and significance of Pleistocene coastal resource use in southern Africa with particular reference to shellfish gathering. *Journal of Anthropological Archaeology* **41**, 213-230 (2016).

178. K. L. van Niekerk, Thesis, University of Cape Town, (2011).

179. Z. Jacobs, B. G. Jones, H. C. Cawthra, C. S. Henshilwood, R. G. Roberts, The chronological, sedimentary and environmental context for the archaeological deposits at Blombos Cave, South Africa. *Quaternary Science Reviews*, 105850 (2019).

180. P. Karkanas, P. Goldberg, Site formation processes at Pinnacle Point Cave 13B (Mossel Bay, Western Cape Province, South Africa): Resolving stratigraphic and depositional complexities with micromorphology. *Journal of Human Evolution* **59**, 256-273 (2010).

181. E. I. Smith *et al.*, Humans thrived in South Africa through the Toba eruption about 74,000 years ago. *Nature* **555**, 511-515 (2018).

182. M. Aubert, A. Brumm, J. Huntley, Early dates for 'Neanderthal cave art' may be wrong. *Journal of Human Evolution* **125**, 215-217 (2018).

183. D. L. Hoffmann *et al.*, Response to Comment on "U-Th dating of carbonate crusts reveals Neandertal origin of Iberian cave art". *Science* **362**, eaau1736 (2018).

184. D. L. Hoffmann *et al.*, Dates for Neanderthal art and symbolic behaviour are reliable. *Nature Ecology & Evolution* **2**, 1044-1045 (2018).

185. D. L. Hoffmann *et al.*, Response to Aubert et al.'s reply 'Early dates for 'Neanderthal cave art' may be wrong' [J. Hum. Evol. 125 (2018), 215–217]. *Journal of Human Evolution* **135**, article 102644 (2019).

186. D. G. Pearce, A. Bonneau, Trouble on the dating scene. *Nature Ecology & Evolution* **2**, 925-926 (2018).

187. L. Slimak, J. Fietzke, J.-M. Geneste, R. Ontañón, Comment on "U-Th dating of carbonate crusts reveals Neandertal origin of Iberian cave art". *Science* **361**, eaau1371 (2018).

188. G. A. T. Duller, Distinguishing quartz and feldspar in single grain luminescence measurements. *Radiation Measurements* **37**, 161-165 (2003).

189. R. Montes, La Cueva de los Aviones. Un yacimiento del Paleolítico Medio (Cartagena, España). *Memorias de Arqueología de la Región de Murcia* **2**, 35-58 (1991).

190. M. Cortés-Sánchez *et al.*, Shellfish collection on the westernmost Mediterranean, Bajondillo cave (~160-35 cal kyr BP): A case of behavioral convergence? *Quaternary Science Reviews* **217**, 284-296 (2019).

191. M. Cortés-Sánchez *et al.*, Earliest Known Use of Marine Resources by Neanderthals. *PLoS ONE* **6**, e24026 (2011).

192. M. Cortés-Sánchez, *El Paleolítico Medio y Superior en el sector central de Andalucía (Córdoba y Málaga)*. Monografías Museo de Altamira (Ministerio de Cultura, Madrid, 2007), pp. 197.

193. G. Avery *et al.*, The Ysterfontein 1 Middle Stone Age rock shelter and the evolution of coastal foraging. *South African Archaeological Society Goodwin Series* **10**, 66-89 (2008).

194. R. Peyroteo, *On Death in the Mesolithic or the Mortuary Practices of the Last Hunter-Gatherers of the South-Western Iberian Peninsula, 7th–6th Millennium BCE*. Occasional Papers in Archaeology (Uppsala Universitet, Uppsala, 2016).

195. A. C. Araújo, A indústria lítica do concheiro de Poças de São Bento (vale do Sado) no seu contexto regional. *O Arqueólogo Português* **IV-13/15**, 87-159 (1995-1997).

196. C. T. Silva, J. Soares, C. Penalva, Para o estudo das comunidades neolíticas do Alentejo litoral: o concheiro do Medo Tojeiro. *Arqueologia* **11**, 5-15 (1985).

197. E. Leorri, A. Cearreta, G. Milne, Field observations and modelling of Holocene sea-level changes in the southern Bay of Biscay: implication for understanding current rates of relative sea-level change and vertical land motion along the Atlantic coast of SW Europe. *Quaternary Science Reviews* **42**, 59-73 (2012).

198. K. Kyriacou, J. E. Parkington, M. Will, A. W. Kandel, N. J. Conard, Middle and Later Stone Age shellfish exploitation strategies and coastal foraging at Hoedjiespunt and Lynch Point, Saldanha Bay, South Africa. *Journal of Archaeological Science* **57**, 197-206 (2015).

199. A. Jerardino, C. W. Marean, Shellfish gathering, marine paleoecology and modern human behavior: Perspectives from cave PP13B, Pinnacle Point, South Africa. *Journal of Human Evolution* **59**, 412-424 (2010).

200. J. K. Feathers, Luminescence Dating in Less Than Ideal Conditions: Case Studies from Klasies River Main Site and Duinefontein, South Africa. *Journal of Archaeological Science* **29**, 177-194 (2002).

201. S. Wurz *et al.*, Connections, culture and environments around 100 000 years ago at Klasies River main site. *Quaternary International* **495**, 102-115 (2018).